THE EFFECT OF STELLAR MULTIPLICITY ON EXOPLANETARY SYSTEMS

EDITED BY: Steve B. Howell, Rachel Matson and Francesco Marzari
PUBLISHED IN: Frontiers in Astronomy and Space Sciences

frontiers Research Topics

frontiers

ISSN 1664-8714
ISBN 978-2-88971-516-9
DOI 10.3389/978-2-88971-516-9

About Frontiers

Frontiers is more than just an open-access publisher of scholarly articles: it is a pioneering approach to the world of academia, radically improving the way scholarly research is managed. The grand vision of Frontiers is a world where all people have an equal opportunity to seek, share and generate knowledge. Frontiers provides immediate and permanent online open access to all its publications, but this alone is not enough to realize our grand goals.

Frontiers Journal Series

The Frontiers Journal Series is a multi-tier and interdisciplinary set of open-access, online journals, promising a paradigm shift from the current review, selection and dissemination processes in academic publishing. All Frontiers journals are driven by researchers for researchers; therefore, they constitute a service to the scholarly community. At the same time, the Frontiers Journal Series operates on a revolutionary invention, the tiered publishing system, initially addressing specific communities of scholars, and gradually climbing up to broader public understanding, thus serving the interests of the lay society, too.

Dedication to Quality

Each Frontiers article is a landmark of the highest quality, thanks to genuinely collaborative interactions between authors and review editors, who include some of the world's best academicians. Research must be certified by peers before entering a stream of knowledge that may eventually reach the public - and shape society; therefore, Frontiers only applies the most rigorous and unbiased reviews.
Frontiers revolutionizes research publishing by freely delivering the most outstanding research, evaluated with no bias from both the academic and social point of view. By applying the most advanced information technologies, Frontiers is catapulting scholarly publishing into a new generation.

What are Frontiers Research Topics?

Frontiers Research Topics are very popular trademarks of the Frontiers Journals Series: they are collections of at least ten articles, all centered on a particular subject. With their unique mix of varied contributions from Original Research to Review Articles, Frontiers Research Topics unify the most influential researchers, the latest key findings and historical advances in a hot research area! Find out more on how to host your own Frontiers Research Topic or contribute to one as an author by contacting the Frontiers Editorial Office: frontiersin.org/about/contact

THE EFFECT OF STELLAR MULTIPLICITY ON EXOPLANETARY SYSTEMS

Topic Editors:
Steve B. Howell, Ames Research Center, National Aeronautics and Space Administration (NASA), United States
Rachel Matson, United States Naval Observatory (USNO), United States
Francesco Marzari, University of Padua, Italy

Citation: Howell, S. B., Matson, R., Marzari, F., eds. (2022). The Effect of Stellar Multiplicity on Exoplanetary Systems. Lausanne: Frontiers Media SA.
doi: 10.3389/978-2-88971-516-9

Table of Contents

frontiers in Astronomy and Space Sciences

EDITORIAL
published: 14 February 2022
doi: 10.3389/fspas.2021.830980

Editorial: The Effect of Stellar Multiplicity on Exoplanetary Systems

Steve B. Howell[1]*, *Rachel A. Matson*[2] *and Francesco Marzari*[3]

[1]NASA Ames Research Center, Moffett Field, CA, United States, [2]U.S. Naval Observatory, Washington, DC, United States, [3]Astronomy Department, University of Padua, Padua, Italy

Keywords: binary stars, exoplanets, multiple stars, circumbinary planets, habitability, occurrence rates

Editorial on the Research Topic

The Effect of Stellar Multiplicity on Exoplanetary Systems

Exoplanet discovery is a recent endeavor, being only about a generation old. Characterization of exoplanetary systems is well underway and one of the most exciting findings is that planets can form and survive in binary star systems. Binary systems provide unique environments and planetary architectures, as well as presenting special observational challenges and research opportunities. Current work on observation, formation, dynamics and evolution of exoplanets residing in binary star systems forms a large research arena. Planning for future exoplanet studies, both from large aperture ground-based telescopes and focused "search for life" 6-m space telescopes, requires both insight into the nature of such complex systems as well as a full understanding of the best exoplanet candidates. Additionally, proper telescope and instrument design need to build on such information in order to deliver successful future observations.

Given that about half of all exoplanet systems exist in multiple star systems, it seems timely and appropriate to put together this Research Topic. Observational as well as theoretical work on the formation and evolution of exoplanetary systems and their stars, current and future searches for habitable worlds, and near-future work on direct imaging and terrestrial planet atmospheric spectra, will need to take multiple stellar hosts into account. Furthermore, to infer the true distribution of planetary properties and exoplanetary occurrence rates, a proper treatment of multiple stellar hosts is required.

Many bright and nearby stars, some visible to the naked eye, are now known to host exoplanets, leading to a stronger connection of the night sky to the age-old question "Are we alone?". In this Research Topic, the above ideas and current investigations from theory modeling, and observation are collected together to provide insights into this field of study. Transit searches, especially those being conducted from space (e.g., Kepler, TESS, CHEOPS), are finding thousands of candidate exoplanets all in need to detailed follow-up, characterization, theoretical modelling and study.

Observational Studies and High-Resolution Imaging: High-resolution imaging in both the IR and the optical band-passes has matured into one of the mainstays of exoplanet validation and characterization. Large ground-based programs, such as those undertaken by NASA, observe and provide to the exoplanet community many hundreds of observations each year. These surveys contribute to the Exoplanet Follow-up Observing Program (ExoFOP) archive which includes a broad range of follow-up studies of targets observed by TESS, K2, and Kepler plus a number of other exoplanet search programs. High-resolution imaging allows the elimination of possible contamination from blends, such as bound and background sources, in the near vicinity (< a few arcsec) of the exoplanet host star. This is an important step to assess host star multiplicity and increase the statistics of exoplanet occurrence rates in multiple systems. High-resolution imaging also yields a more precise determination of the planet radius yielding confirmation of small planets beyond the reach of PRV (Precise Radial Velocity) measurements (such as those terrestrial planets in

OPEN ACCESS

Edited and reviewed by:
Daniel Angerhausen,
ETH Zurich, Switzerland

***Correspondence:**
Steve B. Howell
steve.b.howell@nasa.gov

Specialty section:
This article was submitted to Exoplanets, a section of the journal Frontiers in Astronomy and Space Sciences

Received: *07 December 2021*
Accepted: *17 December 2021*
Published: *14 February 2022*

Citation:
Howell SB, Matson RA and Marzari F (2022) Editorial: The Effect of Stellar Multiplicity on Exoplanetary Systems. Front. Astron. Space Sci. 8:830980. doi: 10.3389/fspas.2021.830980

the habitable zone) as well as planets that orbit fainter stars. The precise knowledge of the physical parameters of exoplanets, and their hosts stars, are an important step to give robust information about the planet formation process and possible differences between formation and evolution of planetary systems in binary and single stars.

In their paper, Schlieder et al. discuss some results of their multi-year campaign to observe candidate exoplanet host stars using Keck NIRC2 AO imaging. In the optical, Howell et al. and Ziegler et al. use ROBO-AO and speckle interferometric techniques to perform surveys of exoplanet host stars in order to assess their multiplicity fraction and provide needed "third-light" corrections to both the stellar and planetary parameters. Observations of many hundreds of exoplanet host stars have allowed studies of the statistical properties of binary exoplanet host stars, revealing a number of intriguing properties. Binary hosts have, in general, wider spatial separations, possible planer alignment between the binary plane and the known planetary orbits, and serious observational biases in the detection of small, Earth-size planets. Theoretical work is needed to refine the current models of binary and exoplanet formation and to reconcile them with the recently available observational results.

Gaia Contributions: While observational evidence has shown close stellar companions, such as those detected with high-resolution imaging, affect planet formation, the role of companions at intermediate separations ($\sim 100-300$ AU) is still uncertain. At angular separations greater than about one arcsecond stellar companions can be resolved as individual point sources, however, as the separation between the stars increases it becomes increasingly difficult to distinguishing between physically bound stars and optical alignments. The position, proper motion, and parallax data of more than a billion stars provided by Gaia has enabled the detection of stellar companions consistent with being gravitationally bound over a wide range of separations.

The papers by Michel and Mugrauer and Fontanive and Bardalez Gagliuffi use Gaia DR2 to search for co-moving stellar companions to exoplanet host stars. As part of an ongoing multiplicity survey, Michel & Mugrauer detected 61 companions (47 stars, 1 white dwarf, and 13 brown dwarfs) to 289 exoplanet host stars within 500pc of the Sun for a multiplicity rate of 16%. The detected companions have masses of $0.06-1.66 M_{\odot}$ with projected separations of $52-10,000$ AU.

Fontanive and Bardalez Gagliuffi use Gaia DR2 and existing literature to find 218 companions to 938 exoplanet (and brown dwarf) host stars within 200pc, yielding a multiplicity rate of 23%. The detected companions have masses between $\sim 0.07-2.37 M_{\odot}$ and projected separations of $0.5-20,000$ AU. However, they find that small planets ($< 0.1 M_{\rm Jup}$) have a lower binary rate than more massive Jovian planets. Fontanive and Bardalez Gagliuffi also explore trends between multiplicity and the properties of the planetary companions in their sample, finding that high-mass ($> 0.1 M_{\rm Jup}$), small-separation planets have a different distribution of planet properties than planets in single star systems.

Such studies of wide companions to exoplanet host stars confirm the wider binary separations seen in high-resolution studies, as compared to field stars, with the Fontanive and Bardalez Gagliuffi paper finding a peak around 600 AU. While stellar companions at separations of thousands of AU appear to have no impact on planetary populations, the different trends for high-mass, small-separation planets as a function of multiplicity found by Fontanive and Bardalez Gagliuffi suggest that stellar binary companions likely affect the formation and/or migration of such objects. Further studies of exoplanet host stars with stellar companions within tens to hundreds of AU will be key to unraveling the impact stellar binaries have on planet formation.

Circumbinary Planets and Habitability: A challanging problem in binaries is assessing the habitability of terrestrial planets either on circumstellar (S–type) or circumbinary orbits (P–type). The scenario may be further complicated by the presence of a giant planet on an outer orbit. The combination of the binary and exterior planet perturbations may destabilize the habitable zone or produce large variations in the orbital elements which may jeopardize the habitability of an Earth–size planet. Giant planets on outer orbits have indeed been found in a significant fractions of exoplanets in S–type orbits (like 94 Cet or HD 169 885) and in P–type orbits (Kepler–35 or Kepler–39). When dealing with P–type configurations it is necessary to account also for the two close sources of radiation, possibly of different spectral type which may also affect the habitability of a planet.

In their paper, Georgakarakos et al. compute the location of the habitable zones for circumbinary terrestrial planets perturbed by an external giant planet. In this study, they adopt the concept of "dynamically informed habitable zones" (DIHZ) which accounts not only for the orbital evolution of the planet, which affects its distance from the binary, but also for the climate inertia defined as the time it takes climate parameters, such as the mean surface temperature, to react to radiative forcing.

In order to calculate DIHZ borders for circumbinary systems it is necessary to determine whether or not the dynamical configuration is stable, how the orbital evolution of the system affects the amount of radiation the planet receives, and how the star light influences the climate of a potentially habitable world.

Georgakarakos et al. apply their analytical formulations for the computation of the limits of the DIHZ to a sample of circumbinary systems where a known giant planet is on a circumbinary orbit. By applying their methodology, they prove that the presence of the additional known planet in the majority of cases does not prevent the existence of habitable words such as in the case of Kepler-35, Kepler-38, and Kepler-64.

For planets in S–type orbits, the combined perturbations of the binary companion and an external giant planet are more complex due to the presence of secular resonances. Pilat-Lohinger and Bazsó in their paper explore this peculiar dynamical environment and they describe the main features of the algorithm SHaDoS (Secular perturbations in Habitable zones of Double Stars), accessible at https://www.univie.ac.at/adg/shados/index.html, which determines the location of secular resonances in the habitable zone around the primary star. This algorithm allows, for given initial conditions concerning the binary and exterior planet orbital elements and masses, to compute the stable areas

within the habitable zone of the system for putative terrestrial planets. Applications of SHaDoS to the wide binary star HD106515 AB and the tight system HD41004 AB reveal a quiet HZ for both systems.

AUTHOR CONTRIBUTIONS

All authors listed have made a substantial, direct and intellectual contribution to the work, and approved it for publication.

ACKNOWLEDGMENTS

The Editors wish to thank all the authors and reviewers of the papers submitted to this research topic for their time, their careful work, and their patience. We gratefully acknowledge the assistance of the staff in the Editorial Office of Frontiers, especially Elena Fedulova, Alicia Fallows and Mathew Williams.

Conflict of Interest: The authors declare that the research was conducted in the absence of any commercial or financial relationships that could be construed as a potential conflict of interest.

Publisher's Note: All claims expressed in this article are solely those of the authors and do not necessarily represent those of their affiliated organizations, or those of the publisher, the editors and the reviewers. Any product that may be evaluated in this article, or claim that may be made by its manufacturer, is not guaranteed or endorsed by the publisher.

frontiers in Astronomy and Space Sciences

ORIGINAL RESEARCH
published: 05 March 2021
doi: 10.3389/fspas.2021.635864

The NASA High-Resolution Speckle Interferometric Imaging Program: Validation and Characterization of Exoplanets and Their Stellar Hosts

Steve B. Howell[1], Nicholas J. Scott[1], Rachel A. Matson[2], Mark E. Everett[3], Elise Furlan[4], Crystal L. Gnilka[1], David R. Ciardi[4] and Kathryn V. Lester[1]*

[1]NASA Ames Research Center, Moffet Field, CA, United States, [2]U.S. Naval Observatory, Washington, DC, United States, [3]NSF's National Optical-Infrared Astronomy Research Laboratory, Tucson, AZ, United States, [4]NASA Exoplanet Science Institute, Caltech/IPAC, Pasadena, CA, United States

Starting in 2008, NASA has provided the exoplanet community an observational program aimed at obtaining the highest resolution imaging available as part of its mission to validate and characterize exoplanets, as well as their stellar environments, in search of life in the Universe. Our current program uses speckle interferometry in the optical (320–1,000 nm) with new instruments on the 3.5-m WIYN and both 8-m Gemini telescopes. Starting with Kepler and K2 follow-up, we now support TESS and other space- and ground-based exoplanet related discovery and characterization projects. The importance of high-resolution imaging for exoplanet research comes via identification of nearby stellar companions that can dilute the transit signal and confound derived exoplanet and stellar parameters. Our observations therefore provide crucial information allowing accurate planet and stellar properties to be determined. Our community program obtains high-resolution imagery, reduces the data, and provides all final data products, without any exclusive use period, to the community via the Exoplanet Follow-Up Observation Program (ExoFOP) website maintained by the NASA Exoplanet Science Institute. This paper describes the need for high-resolution imaging and gives details of the speckle imaging program, highlighting some of the major scientific discoveries made along the way.

Keywords: exoplanets, high-resolution imaging, speckle interferometry, binary stars, exoplanet demographics

OPEN ACCESS

Edited by:
Susan Elizabeth Mullally, Space Telescope Science Institute (NASA), United States

Reviewed by:
Ji Wang, The Ohio State University, United States
Ramses Mario Ramirez, Tokyo Institute of Technology, Japan

****Correspondence:***
Steve B. Howell
steve.b.howell@nasa.gov

Specialty section:
This article was submitted to Exoplanets, a section of the journal Frontiers in Astronomy and Space Sciences

Received: *30 November 2020*
Accepted: *20 January 2021*
Published: *05 March 2021*

Citation:
Howell SB, Scott NJ, Matson RA, Everett ME, Furlan E, Gnilka CL, Ciardi DR and Lester KV (2021) The NASA High-Resolution Speckle Interferometric Imaging Program: Validation and Characterization of Exoplanets and Their Stellar Hosts. Front. Astron. Space Sci. 8:635864. doi: 10.3389/fspas.2021.635864

1 INTRODUCTION

The study of exoplanets is one of the most important topics in astrophysics today. Starting over a decade ago, in support of the NASA Kepler mission, a program providing follow-up observations began. It became clear as Kepler was nearing launch, that the 4 arcsec pixels (Borucki et al., 2010) as well as the many possible confounding events which could imitate exoplanet transit events (e.g., Brown et al., 2011; Santerne et al., 2013) would require follow-up observations from ground-based telescopes in order to validate and characterize any discovered transit candidates. In addition, for transit observations it is crucial to know the stellar properties well, since the planet radius depends directly on the stellar radius. Also, given the relatively large pixels and multi-pixel photometric apertures, it is possible that more than one star is measured, and thus the transit measurement becomes even more uncertain or unreliable.

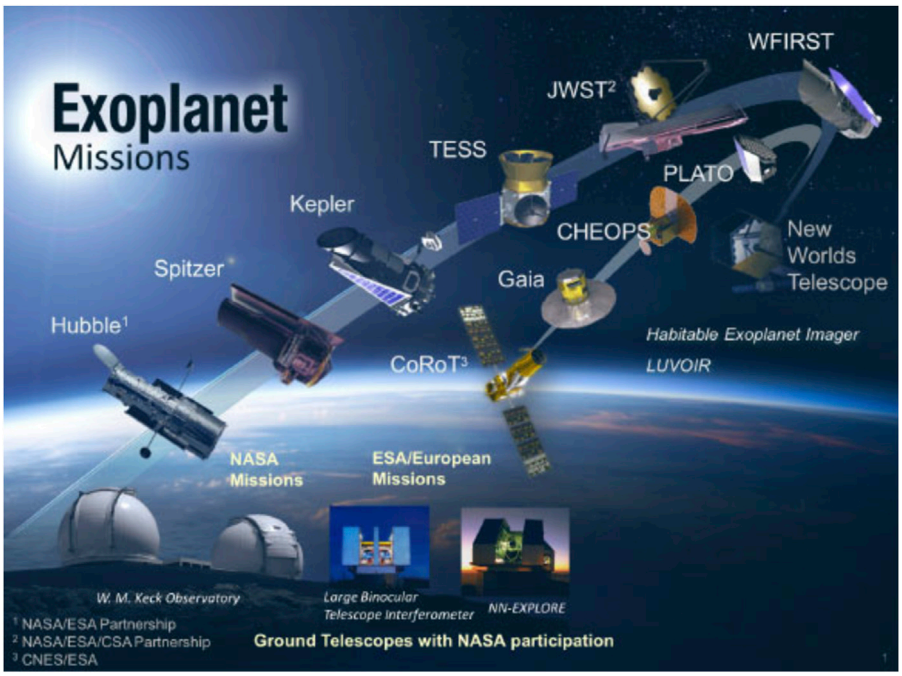

FIGURE 1 | A schematic timeline of NASA and ESA exoplanet related space missions and the ground-based follow-up telescopes NASA directly participates in. Image Credit: NASA/JPL-Caltech.

To support exoplanet discovery, spectroscopic follow-up observations consisted of medium- and high-resolution work using reconnaissance spectra at the start and then large telescope efforts once specific validation steps were passed (Furlan et al., 2018). Likewise, imaging observations were performed ranging from standard native seeing CCD imaging and lucky imaging to high-resolution observations (Furlan et al., 2017). These latter consisted of both Infrared Adaptive Optics (IR/AO) observations using Lick, Palomar, and Keck and optical speckle interferometric imaging using WIYN and Gemini telescopes.

As new exoplanet transit missions such as K2 (Howell et al., 2014), and the currently operating missions TESS (Ricker et al., 2015) and CHEOPS (Benz et al., 2020) come along, follow-up high-resolution (sub-arcsecond) imaging continues to be needed and in larger amounts than before. While Gaia can resolve companions down to near 1.0 arcsec and a bit closer using additional observations over time, e.g., EDR3; (Fabricius et al., 2016), it does not reach the spatial resolution of speckle imaging. Additionally, other exoplanet search techniques such as radial velocity (Kane et al., 2019) and ground-based small telescope transit surveys (Bakos et al., 2007) also benefit from speckle imaging of any candidate systems. Finally, the next wave of exoplanet space telescope missions will soon be upon us (**Figure 1**); missions covering larger and deeper sky areas such as PLATO (transits), and those hoping to obtain detailed exoplanet science such as the James Webb Space Telescope (JWST; transit spectroscopy, emission spectroscopy, direct imaging of exoplanets) and the Nancy Grace Roman Space Telescope (formally the Wide Field Infrared Survey Telescope [WFIRST]; direct imaging and microlensing planets), as well as

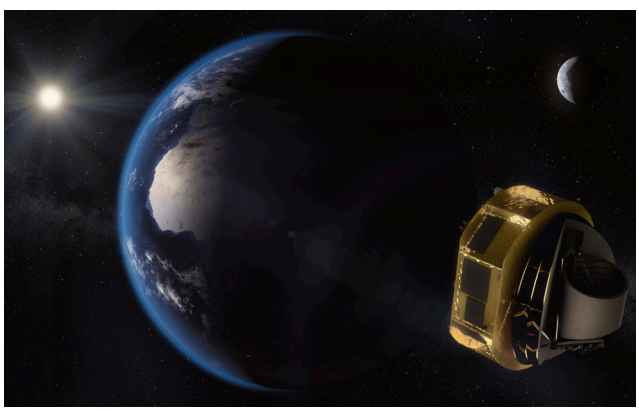

FIGURE 2 | Artist concept of the Ariel space telescope. Image Credit: ESA/STFC RAL Space/UCL/Europlanet-Science Office.

complete spectroscopic characterization of exoplanet atmospheres with Ariel (**Figure 2**). Anywhere high-resolution imaging is needed, including for future missions such as LUVOIR, HabEX, or OST, our speckle program will be valuable. By that time, it is hoped that speckle imaging will be an integral part of the 30-m ground-based telescope system, providing angular resolutions near 5 mas.

For JWST, our program will provide high resolution imaging in support of targeted exoplanets and their host stars. Roman will make use of speckle imaging to support exoplanet research in two main ways: First, to vet and fully characterize direct exoplanet imaging targets in order to assess their multiplicity, and secondly,

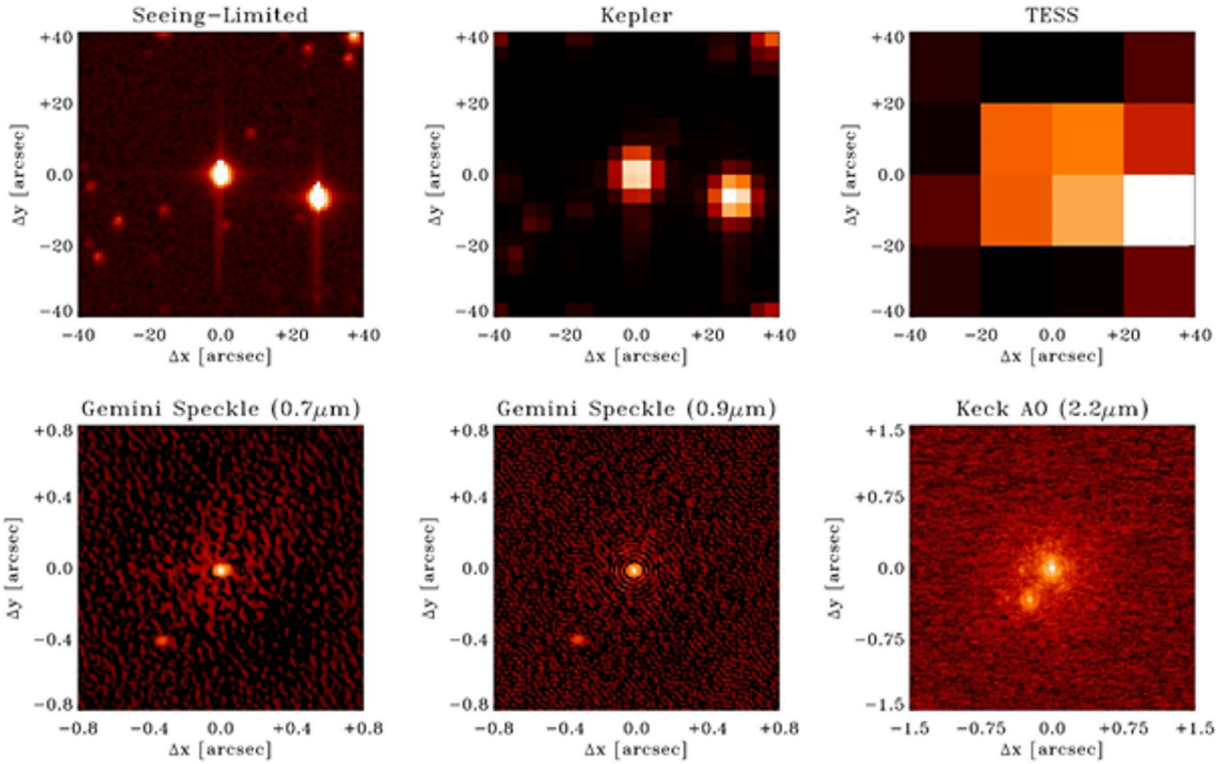

FIGURE 3 | (Top row) Ground-based seeing-limited image of KOI-1002 (star at center) obtained from the Palomar Observatory Sky Survey (POSS). The image shows the local star field which contains two bright stars. The Kepler image is from the standard 30-minute postage stamp images downloaded from the spacecraft and the TESS "image" was produced (before TESS had observed the Kepler FOV) by convolving the Kepler image with the TESS 20 arcsec pixel size kernel. **(Bottom row)** Here the much smaller spatial dimension boxes are centered on the bright central star in the top row and it is revealed in the high-resolution images that the star is a binary system with a separation of about 0.5 arcsec. The Keck AO image shows the central 3 arcsec box. The speckle images took a total time of 5 min (3 min on source) and reached a contrast of 6.5 magnitudes while the IR/AO image required 15 min total time (~ 1.5 min on source) and reached a contrast limit of 9.2 magnitudes. The inner working angle for the speckle and IR/AO observations was ~ 20 and ~ 80 mas respectively.

imaging of microlens sources to aid in the characterization of the source and lens stars.

This paper provides an overview of the NASA high resolution speckle imaging program. Exoplanet transit and radial velocity studies mainly focus on (A) F to M stars, however, our speckle imaging techniques have been used for research programs related to stars of all spectral and luminosity classes, extended objects, and Solar System bodies. These applications are not discussed further in this report. **Section 2** discusses the need for high-resolution imaging, §3 presents the NASA mechanism to engage the exoplanet community, §4 and §5 give an overview of the instrumentation used, the community program, and data produced in this program, §6 lists some of the major scientific discoveries the speckle program has made in relation to exoplanet host star multiplicity, and finally we summarize in §7.

2 The Need for High-Resolution Imaging

Survey telescopes, such as Kepler and TESS, cover a wide field of view, but have large pixels on the sky. Kepler (and K2) had 4 arcsec/pixel values in their focal plane and TESS has 20 arcsec/pixel. These large pixels gather all the light from any stars present within the extracted photometric apertures. If a transit-like event is detected, it is not immediately obvious which star in the pixel (or actually in the pixels) used for light curve construction is the cause of the event. Thus, the status as a real exoplanet transit candidate remains in question until some form of validation is carried out.

Telescopes such as Hubble have great spatial resolution, but they come at the cost of a small field of view and large over-subscription rates for observational proposals. While space has the advantage of stable observing conditions and no atmospheric effects, high-resolution imaging from the ground must make use of clever means to attempt to "remove" the blurring effects of the atmosphere. IR/AO uses (laser) guide stars and deformable mirrors while speckle interferometry freezes the atmospheric distortions using many short exposures and reconstructs these into diffraction limited images using specialized software techniques.

Figure 3 illustrates these points for the case of KOI-1002 imaged from a typical ground-based telescope, Kepler, and TESS. The two bright stars in the top row of the figure are approximately 25 arcsec apart. The two stars are still separate in the Kepler image but near enough to place scattered light or even be both captured in any aperture used to measure the photometry. In the TESS image, it is difficult to even understand the scene. A good ground-based image, such as the top left image, can be used to help

understand the star field imaged by TESS, but does not answer the question of which star had the transit-like event. The bottom row of **Figure 3** shows optical speckle results obtained at Gemini and an IR adaptive optics image obtained at Keck for the star at the center of the top panel. Note the factor of ~ 50 scale change in spatial dimension. We see that the speckle and the IR/AO images reveal that the central star is actually a binary system, thus while the transit-like event could be real, the properties of the planet and its host star would need revision due to the third-light of the close, likely bound companion.

These types of follow-up high-resolution images are key to understanding the light within the scene of an exoplanet host star candidate. This is an important step in exoplanet validation and characterization. If the star is indeed multiple, and we know that about 40–50% of exoplanet host stars have one or more stellar companions (Horch et al., 2014; Matson et al., 2018), then knowledge of the brightness and type of any companion stars are crucial in order to properly assess the exoplanet and host star properties.

Ciardi et al. (2015); Wang et al. (2015); Furlan and Howell (2017); Deacon et al. (2016) and Ziegler et al. (2018), for example, have shown that the presence of third-light will mean that the planet radius determined from the transit depth alone is incorrect, the planet will always be larger than estimated from the transit depth, at times so large as to lose planet status. Furlan and Howell (2017) noted that such third-light properties will also decrease the mean density of the planet, possibly turning a terrestrial exoplanet into an ice giant as well as causing atmospheric scale height calculations to be flawed. These same two authors (Furlan and Howell, 2020) also showed how the lack of knowledge of a companion star could cause measured stellar properties, such as metal content and log g, to be incorrectly derived from an analysis of the star's spectrum. Use of the knowledge of a companion (or not) allows a proper characterization of both the exoplanet and stellar properties. High resolution knowledge of the scene around host stars will remain an important diagnostic for future transit, direct imaging, microlens, and atmospheric spectroscopy exoplanet missions.

As an aside, Robo-AO is another high-resolution imaging technique used in the optical wavelength range. Ziegler et al. (2017) discuss their results using this method for exoplanet host stars. Unlike speckle imaging, Robo-AO uses the mechanical deformable mirror techniques of IR/AO and applies them to optical light. To date, this application has suffered from the use of small aperture telescopes (< 2-m) at sites providing modest native seeing (~ 1 arcsec) and only low-order AO corrections due to the very short wavefront coherence times available in the optical. As such, Robo-AO observations resolve roughly equal mass binaries at separations ≥ 0.8 arcsec with an increasing delta magnitude contrast from ~ 1 at 0.9 arcsec to ~ 3 at 1.4 arcsec.

3 THE SPECKLE IMAGING PROGRAM

Our speckle imaging program is set up under the auspices of NASA through the Exoplanet Exploration Office (ExEP) NN-EXPLORE program located at the Jet Propulsion Laboratory (JPL). The ExEP provides advocacy for the exoplanet community to NASA in terms of future mission science directions, needed technology, and exoplanet science critical to enable a full understanding of exoplanets, their environments, and the search for life. As an aid to establishing an open forum with the community, the ExEP maintains two "gap lists," one for technology[1] and one for science[2]. Each of these documents represent community vetted gaps, that is, areas which need additional understanding in the pursuit of exoplanet science. The ExEP science gap list contains twelve specific areas that the exoplanet community has agreed are in need of further, detailed understanding. Our speckle interferometry program directly addresses five of these science gaps and enables four additional ones.

Directly Addresses

- Science Gap 12 - Measurements of Accurate Transiting Planet Radii. Speckle imaging provides knowledge of companions, especially true bound companions and, if detected, the ability to correct the exoplanet radius and other properties for "third light".
- Science Gap 07 - Properties of Known Exoplanet Host Stars. Speckle imaging provides knowledge of the multiplicity of exoplanet host stars providing accurate stellar parameters and directly assessing the topics of exoplanet formation, migration, dynamics, and evolution.
- Science Gap 10 - Precursor Observations of Direct Imaging Targets. Speckle imaging provides exploratory observations of potential targets for future direct imaging and atmospheric observation missions, assessing their multiplicity and thus their potential as high-value targets.
- Science Gap 04 - Planetary System Architectures: Occurrence Rates for Exoplanets of all sizes. Speckle imaging allows the correct exoplanet and stellar properties to be determined. This in turn is used to derive robust occurrence rates for exoplanets orbiting stars in multiple star systems.
- Science Gap 05 - Occurrence Rates and Uncertainties for Temperate Rocky Planets (eta-Earth). Speckle imaging addresses exoplanet occurrence rates as described above and allows habitable zone locations in binary host star systems to be determined yielding eta-Earth rates for temperate planets.

Enables

- Science Gap 01—Spectral characterization of atmospheres of small exoplanets
- Science Gap 02—Modeling exoplanet atmospheres
- Science Gap 03—Spectral signature retrieval
- Science Gap 06—Yield estimation for exoplanet direct imaging missions.

[1]https://exoplanets.nasa.gov/exep/technology/gap-lists/
[2]https://exoplanets.nasa.gov/internal_resources/1547/

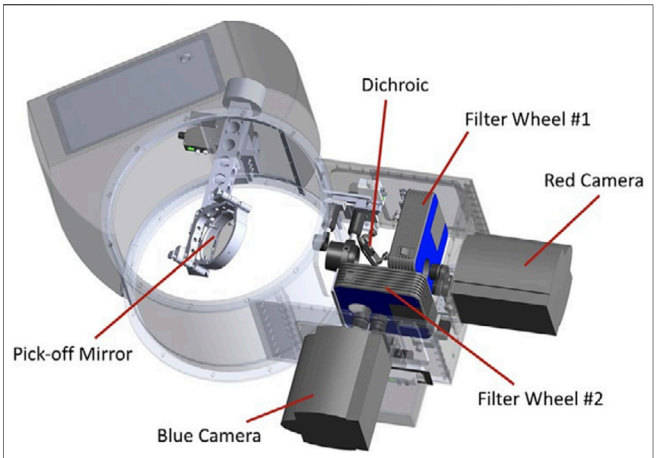

FIGURE 4 | Schematic CAD drawing of 'Alopeke or Zorro (they are identical), the speckle instruments residing at the twin Gemini 8-m telescopes. The compact design is illustrated along with the primary parts labeled. 'Alopeke and Zorro both mean fox in the language of the local people.

4 THE SPECKLE INSTRUMENTS

Just before the Kepler mission was launched, we began our speckle imaging work to support the NASA community. At that time, we used the Differential Speckle Survey Instrument (DSSI; Horch et al., 2009) on the 3.5-m WIYN telescope located on Kitt Peak in southern Arizona, United States. This instrument was a workhorse during the Kepler mission, providing high-resolution images of ~ 1,000 Kepler Objects of Interest (KOIs). Since that time, three new instruments of similar overall design but with increased functionality, larger and faster EMCCD imagers, and modernization in terms of automation, user interface, filter wheels, and remote operation have been built and deployed. The three new instruments are the NN-EXPLORE Exoplanet Star and Survey Imager (NESSI[3]; Scott et al., 2018) at the 3.5-m WIYN telescope, and 'Alopeke and Zorro[4], (Scott et al., 2021, in prep[5].) duplicate instruments at the twin Gemini 8-m telescopes in Hawaii and Chile.

Each of the new instruments provide simultaneous observations in two optical bands, determined by filters placed in each of two beams, split at 700 nm. **Figure 4** presents a schematic of the Gemini instruments with the major parts labeled and **Figure 5** shows one of the instruments being constructed in our optics lab at NASA Ames (left) and the completed instrument mounted on the Gemini telescope (middle and right). **Table 1** presents the general parameters of these new instruments with 'Alopeke and Zorro being identical therefore having identical parameters. The instruments have two field of view options user selectable in real-time; a narrow speckle imaging field and a wider more traditional imaging field of view. The angular resolution of these instruments provide inner working angle spatial resolutions for nearby exoplanet host stars (e.g., TESS) of < 10 au (Matson et al., 2019).

These instruments are fully integrated into the telescope control systems where they reside and the Gemini instruments are permanently mounted for use at any time during the year. 'Alopeke and Zorro are able to be operated remotely from the Gemini control room or anywhere internet is available via a secure connection to the observatory.

5 THE COMMUNITY OBSERVING PROGRAM

The NASA speckle imaging program is openly available to the world-wide exoplanet community. While we have built and deployed the speckle instruments, our observing protocol is a community-based program with targets and observing priorities set by the missions and the community.

Below, we discuss the observational program, the target selection methodology, the data reduction processes, and the archives which house the raw and reduced data products.

5.1 Observations

Proposals to use the speckle instruments, including proposals submitted by our team, are peer reviewed for each telescope by the relevant telescope allocation committee (TAC). Once the approved programs are known for a semester, we work with each observatory to set up block scheduled observation runs, once or twice each semester on each telescope. Each run consists of 6–10 nights depending on time demand.

All speckle targets are placed in a queue to be observed by our team during the observing block. Most targets are observed in the usual manner (Howell et al., 2011) that is, thousands of 40 to 60 msec images are simultaneously collected in two narrow band filters, one each in the blue and red regions of the optical bandpass. Here blue and red are defined by the dichroic in our instruments, splitting the optical light at 700 nm (See **Table 1**). Some observations may come with special requirements such as the use of specific filters, extended integration times, or specific time constraints.

5.2 Target Selection

Targets to observe are selected in three main ways. First, each space mission or ground-based exoplanet program has a team of scientists and staff designated to produce a priority list of targets to be observed. These targets, usually called "objects of interest" (e.g., Kepler objects of interest, KOIs or TESS objects of interest, TOIs) are listed in priority order and provided to our observing team ahead of each observation run. For example, the TESS Follow-up Observing Program Working Group as well as the TESS sub-group for high-resolution imaging (SG3) play roles in target ranking and selection. The priority order reflects target brightness, number, location or type of exoplanet candidates, or stellar properties. The list contains 100–200 targets at a time and gets updated throughout each observing season.

The second main way is direct communication with our group. If an exoplanet host star is in need of high-resolution

[3]https://www.wiyn.org/Instruments/wiynnessi.html

[4]https://www.gemini.edu/instrumentation/current-instruments/alopeke-zorro

[5]Scott, N. et al., 2021 is in preparation

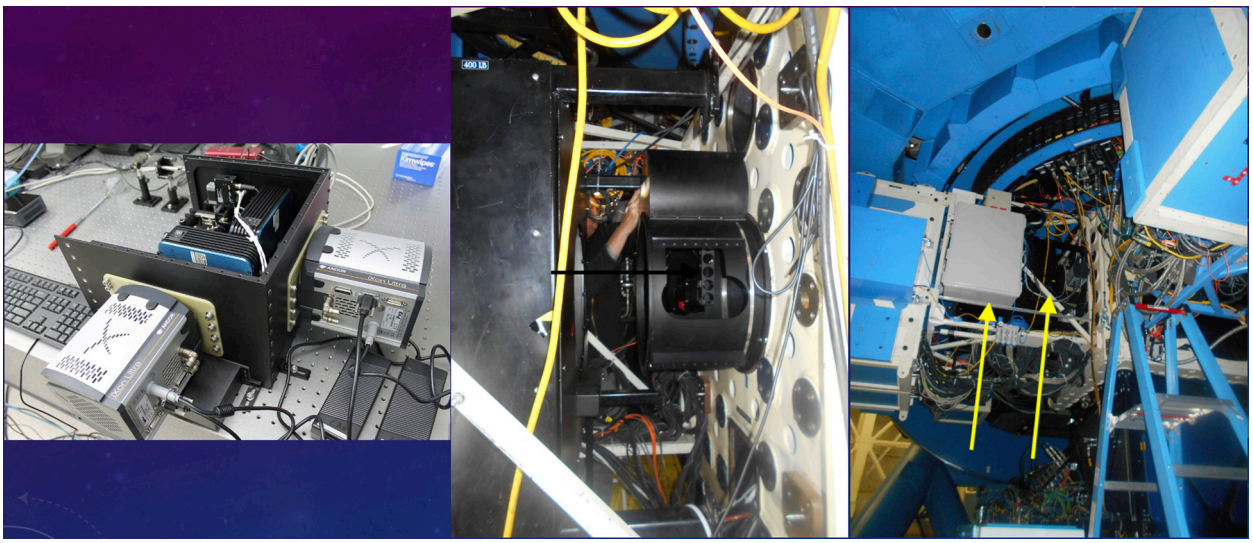

FIGURE 5 | (Left) One of the two identical speckle imagers under construction at the NASA Ames Research Center. The two grey boxes extending out of the black box are the two Andor EMCCD cameras. **(Middle)** A close-up view of the instrument mounted on Gemini at the GCAL port and **(Right)** a view of the instrument (black box) with the associated power supply, electronics, and computer unit (white box). See yellow arrows.

TABLE 1 | Speckle interferometers.

Instrument	Telescope	Detectors[a]	FOV(")[b]	"/pixel[b]	Filters[c]	Resolution (mas)	Limiting Mag (R)
NESSI	WIYN	EMCCD	19/83	0.02/0.08	SDSS ugriz + 4 narrow band	39 @550 nm/64 @880 nm	~ 13.2
'Alopeke	Gemini-North	EMCCD	6.7/60	0.01/0.1	SDSS ugriz + 4 narrow band	17 @562 nm/28 @832 nm	~ 18
Zorro	Gemini-South	EMCCD	6.7/60	0.01/0.1	SDSS ugriz + 4 narrow band	17 @562 nm/28 @832 nm	~ 18

[a]*Each instrument uses two Andor iXon Ultra 888 back-illuminated Electron Multiplying (1024 × 1024, 13 micron) pixel CCDs (EMCCDs).*
[b]*Values given are for the "speckle"/"wide-field" of view modes.*
[c]*Narrow band filters are centered at 466, 562, 716, and 832 nm.*

imaging, regardless of what space mission or ground-based telescope discovered it or who is currently studying the target, we will add it into our priority list and observe the target for the PI. This method usually involves 1 to a few targets of immediate interest to someone in the exoplanet community.

Finally, PIs can propose for telescope time themselves as each of our instruments at their associated telescopes have "open sky" policies, that is, proposals are accepted from anyone.

5.3 Data Reduction

Speckle interferometry produces diffraction-limited images over a small field of view (~ 1 arcsec) by using very short exposure times to "freeze" the atmosphere. Fourier or other techniques are then used to reconstruct these images and search for interference fringes that exist if two or more stars are within the narrow field of view (See **Figure 6**).

Speckle imaging has been used since the early 1970's but has been greatly upgraded since then, now using digital detectors, large telescopes, and advanced software techniques. For example, EMCCDs provide for electron multiplication in the output gain register, increasing the input signal by up to 1,000 times. Stars as faint as 19th magnitude can now be observed using our instruments at Gemini coupled with their EMCCD detectors.

Our standard data reduction pipeline and the data products available are described in Howell et al. (2011) with some additional reduced data products now provided (e.g., **Figure 7**). The following reduced data products are delivered to each PI: sensitivity curves, reconstructed images, and any binary fit parameters if a companion is detected.

5.4 Data Archives

Our raw data and reduced data products are archived at both the Gemini data archive[6] and the NASA Exoplanet Archive, Exoplanet Follow-up Program (ExoFOP) archive[7]. They are accessible to the public once the proprietary period has ended. All of our community observations, that is those observed within the NASA proposed program time, are available to the public with no proprietary period. Other PIs observing exoplanet targets can specify a proprietary period of up to 12 months, however, most PIs choose no proprietary period as well.

[6]https://archive.gemini.edu/searchform
[7]https://exoplanetarchive.ipac.caltech.edu

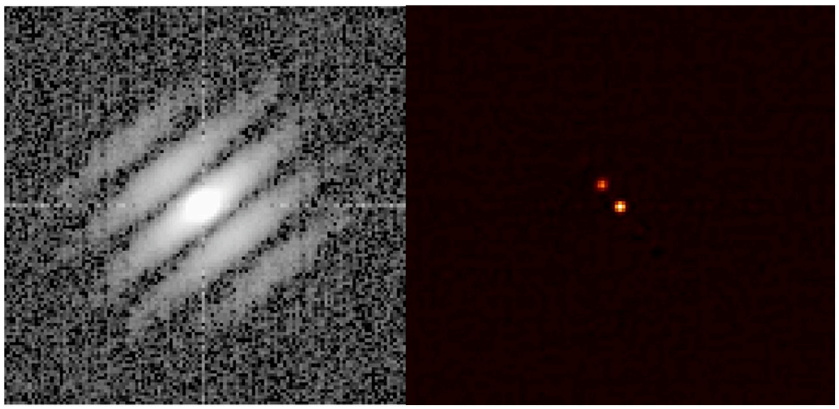

FIGURE 6 | Power spectrum of TOI-1356, an exoplanet hosting star, produced by our reduction pipeline using 2000 speckle images and obtained at the WIYN telescope. Note the interference fringes whose spacing, intensity, and orientation allow a reconstructed image **(right)** to be produced. From this image and the Fourier analysis, we can determine the separation, position angle, and magnitude difference of the two stars. In this case, the host star is a member of a close binary having a separation near 0.16 arcsec. The reconstructed image is 2 arcsec on a side.

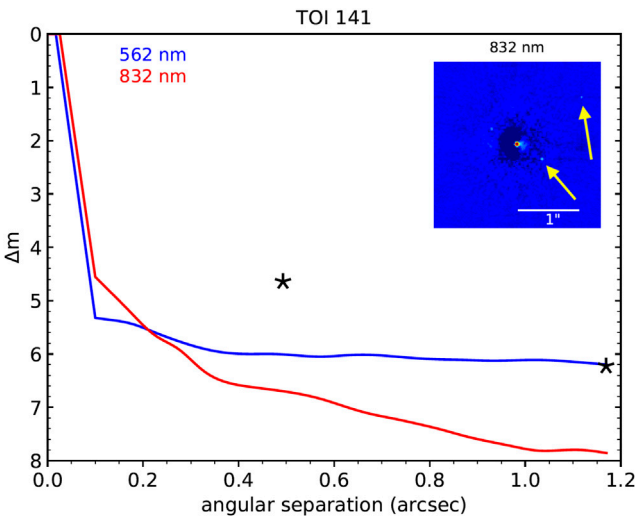

FIGURE 7 | One of our standard pipeline reduced data products. The plot shows our 5σ contrast curves in both filters as a function of the angular separation out to 1.2 arcsec, the end of speckle coherence. In addition, the inset shows the reconstructed 832 nm image with a 1 arcsec scale bar. This star, TOI 141, was found to have two close companions, one at 0.5 arcsec (PA = 240 degrees, Delta magnitude = 4.6) and one at 1.3 arcsec (PA = 307 degrees, Delta magnitude = 6.2). The yellow arrows mark the companions in the reconstructed image and the black stars mark the locations of the stars on the main plot, the 1.3 arcsec companion placed at 1.2″ to fit within the plot.

All observed targets are listed on the Exoplanet Follow-Up Observation Program website[8] within days of an observing run; in this way the community is informed about which exoplanet host stars have been imaged with our speckle instruments. Final data products from the reductions are also posted on ExoFOP; tags link them to the corresponding entries in the imaging observations tables. For targets observed as part of our community program, the reduced data products are posted on ExoFOP soon after an observing run ends and the reduction has been completed, typically within a few weeks. To date, we have observed over 1,000 exoplanet host stars from Kepler and K2 and more than 500 TESS mission TOIs, so far, for the community. These observations have been used to validate and characterize exoplanets in over 65 published papers in the past 1.5 years.

6 DISCOVERIES IN STELLAR MULTIPLICITY

In addition to validating and characterizing numerous exoplanet discoveries as contributions to the exoplanet community research, we have used the large samples of exoplanet host stars observed at high resolution to enable a number of overarching findings.

(1) *Percentage of binary exoplanet host stars:* For both the Kepler and K2 exoplanet host stars, and it seems true also for TESS, we have shown that for those stars hosting at least one exoplanet, 40–50% of them reside in binary or multiple star systems; See Horch et al. (2014); Matson et al. (2018) and the upcoming papers by Howell et al. (2021) and Lester et al. (2021)[9].

(2) *Binary host star properties:* Recent work (Howell et al., 2021) has shown that the mass ratio of exoplanet host star binaries follows that of field binaries, that is an excess of nearly equal mass systems. The orbital period distribution however does not. These authors find that exoplanet hosting binary stars show generally larger mean separations having a peak in their orbital separation near 100 au, not 40 au as for the field sample (Raghavan et al., 2010).

[8]https://exofop.ipac.caltech.edu/tess/

[9]Lester k, et al. (2021) is in preparation

Furlan and Howell (2017) and Furlan and Howell (2020) have shown that it is critical to fully understand the "scene" of light near an exoplanet host star. If a close companion is present, both the exoplanet and the stellar properties determined may be in error.

(3) *Bound vs. line of* sight *companions*: Using statistical modeling, Horch et al. (2014) and Matson et al. (2018) have shown that most stellar companions that reside within 0.4 arcsec (at Gemini) and 0.8 arcsec (at WIYN) of the primary star are true bound companions (at $\geq 90\%$ probability). These limits are important to note as stellar companions found to lie farther from the host star are most likely, but not exclusively, line of sigh companions, therefore not part of the formation, dynamical, and evolutionary processes of the exoplanetary system. However, they nonetheless cause transit dilution, and so their flux has to be taken into account when the transit depth and exoplanet properties are derived. Observational techniques such as lucky imaging or Robo-AO tend to only detect companion stars which are 0.75 arcsec or farther away. Even Gaia cuts off at direct companion detection near 1.0 arcsec. At such sub-arcsecond angular resolutions, speckle imaging provides inner working angles for many of the target stars of 1 to a few au. Everett et al. (2015) and Hirsch et al. (2017) also used model isochrones to provide evidence that companion stars around KOIs are bound or not. Finally, Colton et al. (2020) has begun to measure space and orbital motions for exoplanet host stars with stellar companions, a process that takes decades for the far away Kepler stars, but will only take a few years for some very close K2 and TESS binary host stars with separations of ≤ 10 au. These astrometric measurements have already begun to provide information on the formation, dynamics, and evolution of exoplanet systems.

(4) *Which star in a binary hosts the exoplanet:* Transit discoveries in binary host stars often leave open the question of which of the stars the exoplanet(s) actually orbit. If the planet orbits the primary, the transit depth may require only a modest correction due to a fainter secondary star. However, if the transit is due to something orbiting the secondary star or the two stars are nearly equal in brightness, it can be very unclear what the measured transit depth is really telling us. One way to solve this dilemma was employed by Howell et al. (2019) for the binary A star exoplanet host Kepler-13. Using simultaneous time-series speckle observations of both stars in the pair, it was shown that the transit occurs on Kepler-13A.

7 SUMMARY

We have summarized our continuing decade long NASA high resolution imaging work for exoplanet research. Using speckle interferometry, we carry out a community led observational program that supports space- and ground-based exoplanet efforts. Observations are obtained at the WIYN 3.5-m telescope in Arizona, and at both the Gemini-North and Gemini-South 8-m telescopes located in Chile and Hawaii. We have designed and built new instruments for these telescopes that are available to the community through peer review proposals under the NN-EXPLORE/NOIRLabs open-sky policies. All our observations and their fully reduced data products are made available via public data archives.

Sub-arcsec imaging, especially inside of 0.4 arcsec, is critical for our detailed understanding of exoplanets, their host stars, and the search for other life in the Universe. Exoplanet radii and mean densities, plus the stellar properties of their hosts, can be incorrectly determined without proper knowledge of the close-in light scene.

Our imaging program has supported many exoplanet validation and characterization studies for space missions and ground-based surveys, and radial velocity studies as well as made scientific findings itself along the way.

We plan to continue our community service program throughout the TESS extended mission and into the JWST and Roman missions and beyond.

DATA AVAILABILITY STATEMENT

The datasets presented in this study can be found in the online NASA Exoplanet archive: https://exoplanetarchive.ipac.caltech.edu.

AUTHOR CONTRIBUTIONS

SH—wrote the majority of the manuscript, leads the program NS, EF, RM—made substantial contributions to the manuscript ME, DC, KL, CG—Part of observation/instrument team.

ACKNOWLEDGMENTS

We thank Elliott Horch and William Sherry for their previous team work. Additionally, we thank the generous support and collaboration of the staff at the WIYN and Gemini Telescopes, they are indeed part of the Team. We appreciate the reviews by the referees which led to a better paper. Finally, we'd like to thank NASA headquarters and the Exoplanet Program Office at JPL, in particular, Doug Hudgins, Gary Blackwood, and John Callas, for their substantial support of the speckle imaging program over these many years. Facilities: WIYN: 3.5 m (NESSI), Gemini-North:8-m ('Alopeke), Gemini-South:8-m (Zorro).

REFERENCES

Bakos, G. Á., Kovács, G., Torres, G., Fischer, D. A., Latham, D. W., Noyes, R. W., et al. (2007). HD 147506b: a supermassive planet in an eccentric orbit transiting a bright star. *Acta Pathol. Jpn.* 670 (1), 826–832. doi:10.1086/521866

Benz, W., Broeg, C., Fortier, A., Rando, N., Beck, T., Beck, M., et al. (2020). The CHEOPS mission. *Exp. Astro.* 51, 109–151. doi:10.1007/s10686-020-09679-4

Borucki, W. J., Koch, D., Basri, G., Batalha, N., Brown, T., Caldwell, D., et al. (2010). Kepler planet-detection mission: introduction and First results. *Science* 327 (5968), 977. doi:10.1126/science.1185402

Brown, T. M., Latham, D. W., Everett, M. E., and Esquerdo, G. A. (2011). Keplerinput catalog: photometric calibration and stellar classification. *Astron. J.* 142 (4), 112. doi:10.1088/0004-6256/142/4/112

Ciardi, D. R., Beichman, C. A., Horch, E. P., and Howell, S. B. (2015). Understanding the effects of stellar multiplicity on the derived planet radii from transit surveys: implications for Kepler, K2, and Tess. *Acta Pathol. Jpn.* 805 (1), 16. doi:10.1088/0004-637x/805/1/16

Colton, N. M., Horch, E. P., Everett, M. E., Howell, S. B., Davidson, J. W. J., Baptista, B. J., et al. (2020). Identifying bound stellar companions to Kepler exoplanet host stars using speckle imaging. arXiv e-prints, arXiv: 2011.03903.

Deacon, N. R., Kraus, A. L., Mann, A. W., Magnier, E. A., Chambers, K. C., Wainscoat, R. J., et al. (2016). A Pan-STARRS 1 study of the relationship between wide binarity and planet occurrence in the Kepler field. *Mon. Not. Roy. Astron. Soc.* 455 (4), 4212–4230. doi:10.1093/mnras/stv2132

Everett, M. E., Barclay, T., Ciardi, D. R., Horch, E. P., Howell, S. B., Crepp, J. R., et al. (2015). High-resolution multi-band imaging for validation and characterization of small Kepler planets. *AJ* 149 (2), 55. doi:10.1088/0004-6256/149/2/55

Fabricius, C., Bastian, U., Portell, J., Castañeda, J., Davidson, M., Hambly, N. C., et al. (2016). Gaia Data Release 1. Pre-processing and source list creation. *arXiv* 595. doi:10.1051/0004-6361/201628643

Furlan, E., Ciardi, D. R., Cochran, W. D., Everett, M. E., Latham, D. W., Marcy, G. W., et al. (2018). The Kepler follow-up observation program. II. Stellar parameters from medium- and high-resolution spectroscopy. *Acta Pathol. Jpn.* 861 (2), 149. doi:10.3847/1538-4357/aaca34

Furlan, E., Ciardi, D. R., Everett, M. E., Saylors, M., Teske, J. K., Horch, E. P., et al. (2017). The Kepler follow-up observation program. I. A catalog of companions toKeplerstars from high-resolution imaging. *AJ* 153 (2), 71. doi:10.3847/1538-3881/153/2/71

Furlan, E., and Howell, S. B. (2017). The densities of planets in multiple stellar systems. *AJ* 154 (2), 66. doi:10.3847/1538-3881/aa7b70

Furlan, E., and Howell, S. B. (2020). Unresolved binary exoplanet host stars fit as single stars: effects on the stellar parameters. *Acta Pathol. Jpn.* 898 (1), 47. doi:10.3847/1538-4357/ab9c9c

Hirsch, L. A., Ciardi, D. R., Howard, A. W., Everett, M. E., Furlan, E., Saylors, M., et al. (2017). Assessing the effect of stellar companions from high-resolution imaging of Kepler objects of interest. *AJ* 153 (3), 117. doi:10.3847/1538-3881/153/3/117

Horch, E. P., Howell, S. B., Everett, M. E., and Ciardi, D. R. (2014). Most sub-arcsecond companions of Kepler exoplanet candidate host stars are gravitationally bound. *Acta Pathol. Jpn.* 795 (1), 60. doi:10.1088/0004-637x/795/1/60

Horch, E. P., Veillette, D. R., Baena Gallé, R., Shah, S. C., O'Rielly, G. V., and van Altena, W. F. (2009). Observations of binary stars with the differential speckle survey instrument. I. Instrument description and first results. *Astron. J.* 137 (6), 5057–5067. doi:10.1088/0004-6256/137/6/5057

Howell, S. B., Everett, M. E., Sherry, W., Horch, E., and Ciardi, D. R. (2011). Speckle camera observations for the NASA Kepler mission follow-up program. *Astron. J.* 142 (1), 19. doi:10.1088/0004-6256/142/1/19

Howell, S. B., Matson, R. A., Ciardi, D. R., Everett, M. E., Livingston, J. H., Scott, N. J., et al. (2021). Speckle observations of TESS exoplanet host stars: understanding the binary exoplanet host star orbital period distribution. *Astron. J.* [in press].

Howell, S. B., Scott, N. J., Matson, R. A., Horch, E. P., and Stephens, A. (2019). High-resolution imaging transit photometry of Kepler-13AB. *AJ* 158 (3), 113. doi:10.3847/1538-3881/ab2f7b

Howell, S. B., Sobeck, C., Haas, M., Still, M., Barclay, T., Mullally, F., et al. (2014). The K2 mission: characterization and early results. *Publ. Astron. Soc. Pac.* 126 (938), 398. doi:10.1086/676406

Kane, S. R., Dalba, P. A., Li, Z., Horch, E. P., Hirsch, L. A., Horner, J., et al. (2019). Detection of planetary and stellar companions to neighboring stars via a combination of radial velocity and direct imaging techniques. *AJ* 157 (6), 252. doi:10.3847/1538-3881/ab1ddf

Matson, R. A., Howell, S. B., and Ciardi, D. R. (2019). Detecting unresolved binaries in TESS data with speckle imaging. *AJ* 157 (5), 211. doi:10.3847/1538-3881/ab1755

Matson, R. A., Howell, S. B., Horch, E. P., and Everett, M. E. (2018). Stellar companions of exoplanet host stars in K2. *AJ* 156 (1), 31. doi:10.3847/1538-3881/aac778

Raghavan, D., McAlister, H. A., Henry, T. J., Latham, D. W., Marcy, G. W., Mason, B. D., et al. (2010). A survey of stellar families: multiplicity of solar-type stars. *APJs* 190 (1), 1–42. doi:10.1088/0067-0049/190/1/1

Ricker, G. R., Winn, J. N., Vanderspek, R., Latham, D. W., Bakos, G. Á., Bean, J. L., et al. (2015). Transiting exoplanet survey satellite (TESS). *J. Astronomical Telesc. Instrum. Syst.* 1, 014003. doi:10.1117/1.JATIS.1.1.014003

Santerne, A., Fressin, F., Díaz, R. F., Figueira, P., Almenara, J.-M., and Santos, N. C. (2013). The contribution of secondary eclipses as astrophysical false positives to exoplanet transit surveys. *AAP* 557, A139. doi:10.1051/0004-6361/201321475

Scott, N. J., Howell, S. B., Horch, E. P., and Everett, M. E. (2018). The NN-explore exoplanet stellar speckle imager: instrument description and preliminary results. *PASP* 130 (987), 054502. doi:10.1088/1538-3873/aab484

Wang, J., Fischer, D. A., Xie, J.-W., and Ciardi, D. R. (2015). Influence of stellar multiplicity on planet formation. Iv. Adaptive optics imaging of Kepler stars with multiple transiting planet candidates. *Acta Pathol. Jpn.* 813 (2), 130. doi:10.1088/0004-637x/813/2/130

Ziegler, C., Law, N. M., Baranec, C., Howard, W., Morton, T., Riddle, R., et al. (2018). Robo-AO Kepler Survey. V. The Effect of Physically Associated Stellar Companions on Planetary Systems. *AJ* 156 (2), 83. doi:10.3847/1538-3881/aace59

Ziegler, C., Law, N. M., Morton, T., Baranec, C., Riddle, R., Atkinson, D., et al. (2017). Robo-Ao Kepler planetary candidate survey. III. Adaptive optics imaging of 1629 Kepler exoplanet candidate host stars. *AJ* 153 (2), 66. doi:10.3847/1538-3881/153/2/66

Conflict of Interest: The authors declare that the discussion and research was conducted in the absence of any commercial or financial relationships that could be construed as a potential conflict of interest.

frontiers in Astronomy and Space Sciences

CORRECTION
published: 30 September 2021
doi: 10.3389/fspas.2021.696011

Corrigendum: The NASA High-Resolution Speckle Interferometric Imaging Program: Validation and Characterization of Exoplanets and Their Stellar Hosts

Steve B. Howell[1], Nicholas J. Scott[1], Rachel A. Matson[2], Mark E. Everett[3], Elise Furlan[4], Crystal L. Gnilka[1], David R. Ciardi[4] and Kathryn V. Lester[1]*

[1]NASA Ames Research Center, Moffett Field, CA, United States, [2]U.S. Naval Observatory, Washington, DC, United States, [3]NSFs National Optical-Infrared Astronomy Research Laboratory, Tucson, AZ, United States, [4]NASA Exoplanet Science Institute, Pasadena, CA, United States

Keywords: exoplanets, exoplanetary systems, binary host stars, speckle interferometry, high-resolution imaging

A Corrigendum on

The NASA High-Resolution Speckle Interferometric Imaging Program: Validation and Characterization of Exoplanets and Their Stellar Hosts
by Steve B. Howell, Nicholas J. Scott, Rachel A. Matson, Mark E. Everett, Elise Furlan, Crystal L. Gnilka, David R. Ciardi, Kathryn V. Lester. (2021). Front. Astron. Space Sci. 10:635864. doi: 10.3389/fspas.2021.635864

OPEN ACCESS

Edited and reviewed by:
Susan Elizabeth Mullally, Space Telescope Science Institute (NASA), United States

****Correspondence:***
Steve B. Howell
steve.b.howell@nasa.gov

Specialty section:
This article was submitted to Exoplanets, a section of the journal Frontiers in Astronomy and Space Sciences

Received: *30 April 2021*
Accepted: *07 May 2021*
Published: *30 September 2021*

Citation:
Howell SB, Scott NJ, Matson RA, Everett ME, Furlan E, Gnilka CL, Ciardi DR and Lester KV (2021) Corrigendum: The NASA High-Resolution Speckle Interferometric Imaging Program: Validation and Characterization of Exoplanets and Their Stellar Hosts. Front. Astron. Space Sci. 8:696011. doi: 10.3389/fspas.2021.696011

TEXT CORRECTION

In the original article, there were incorrect parameters listed in the **last paragraph of Section 2**.

A correction has been made to that paragraph as follows:

"As an aside, Robo-AO is another high-resolution imaging technique used in the optical wavelength range. Ziegler et al. (2017) discuss their results using this method for exoplanet host stars. Unlike speckle imaging, Robo-AO uses the mechanical deformable mirror techniques of IR/AO and applies them to optical light. See Ziegler et al. (2018) for details.

Ref is: @ARTICLE2018AJ....156...83Z, author = Ziegler, Carl and Law, Nicholas M. and Baranec, Christoph and Howard, Ward and Morton, Tim and Riddle, Reed and Duev, Dmitry A. and Salama, Ma¨ıssa and Jensen-Clem, Rebecca and Kulkarni, S. R., title = "Robo-AO Kepler Survey. V. The Effect of Physically Associated Stellar Companions on Planetary Systems", journal =, keywords = binaries: close, instrumentation: adaptive optics, methods: data analysis, methods: observational, planets and satellites: fundamental parameters, techniques: high angular resolution, Astrophysics - Earth and Planetary Astrophysics, year = 2018, month = aug, volume = 156, number = 2, eid = 83, pages = 83, doi = 10.3847/1538-3881/aace59, archivePrefix = arXiv, eprint = 1804.10208, primaryClass = astro-ph.EP, adsurl = https://ui.adsabs.harvard.edu/abs/2018AJ....156...83Z, adsnote = Provided by the SAO/NASA Astrophysics Data System."

The authors apologize for this error and state that this does not change the scientific conclusions of the article in any way. The original article has been updated.

REFERENCE

Ziegler, C., Law, N. M., Baranec, C., Howard, W., Morton, T., Riddle, R., et al. (2018). Robo-AO Kepler Survey. V. The Effect of Physically Associated Stellar Companions on Planetary Systems. *AJ* 156 (2), 83. doi:10.3847/1538-3881/aace59

frontiers in Astronomy and Space Sciences

ORIGINAL RESEARCH
published: 19 March 2021
doi: 10.3389/fspas.2021.625250

The Census of Exoplanets in Visual Binaries: Population Trends from a Volume-Limited Gaia DR2 and Literature Search

Clémence Fontanive[1]* *and Daniella Bardalez Gagliuffi*[2]

[1]Center for Space and Habitability, University of Bern, Bern, Switzerland, [2]American Museum of Natural History, New York, NY, United States

OPEN ACCESS

Edited by:
Steve B. Howell,
National Aeronautics and Space Administration (NASA), United States

Reviewed by:
Nuno C. Santos,
Instituto de Astrofísica e Ciências do Espaço (IA), Portugal
David Barrado,
Centro de Astrobiología (CSIC-INTA), Spain

***Correspondence:**
Clémence Fontanive
clemence.fontanive@csh.unibe.ch

Specialty section:
This article was submitted to Exoplanets, a section of the journal Frontiers in Astronomy and Space Sciences

Received: 02 November 2020
Accepted: 28 January 2021
Published: 19 March 2021

Citation:
Fontanive C and Bardalez Gagliuffi D (2021) The Census of Exoplanets in Visual Binaries: Population Trends from a Volume-Limited Gaia DR2 and Literature Search. Front. Astron. Space Sci. 8:625250. doi: 10.3389/fspas.2021.625250

We present results from an extensive search in the literature and Gaia DR2 for visual co-moving binary companions to stars hosting exoplanets and brown dwarfs within 200 pc. We found 218 planet hosts out of the 938 in our sample to be part of multiple-star systems, with 10 newly discovered binaries and 2 new tertiary stellar components. This represents an overall raw multiplicity rate of 23.2 ± 1.6 % for hosts to exoplanets across all spectral types, with multi-planet systems found to have a lower stellar duplicity frequency at the 2.2-σ level. We found that more massive hosts are more often in binary configurations, and that planet-bearing stars in multiple systems are predominantly observed to be the most massive component of stellar binaries. Investigations of the multiplicity of planetary systems as a function of planet mass and separation revealed that giant planets with masses above 0.1 M_{Jup} are more frequently seen in stellar binaries than small sub-Jovian planets with a 3.6-σ difference, a trend enhanced for the most massive (>7 M_{Jup}) short-period (<0.5 AU) planets and brown dwarf companions. Binarity was however found to have no significant effect on the demographics of low- mass planets (<0.1 M_{Jup}) or warm and cool gas giants (>0.5 AU). While stellar companion mass appears to have no impact on planet properties, binary separation seems to be an important factor in the resulting structure of planetary systems. Stellar companions on separations <1000 AU can play a role in the formation or evolution of massive, close-in planets, while planets in wider binaries show similar properties to planets orbiting single stars. Finally, our analyses indicate that numerous stellar companions on separations smaller than 1–3 arcsec likely remain undiscovered to this date. Continuous efforts to complete our knowledge of stellar multiplicity on separations of tens to hundreds of AU are essential to confirm the reported trends and further our understanding of the roles played by multiplicity on exoplanets.

Keywords: exoplanets, multiplicity, visual, binaries, companions, formation, demographics, statistics

1 INTRODUCTION

The architectures of stellar, sub-stellar, and planetary systems are relics of their formation and evolutionary processes. By studying the orbital parameters and configurations of hierarchical systems as an ensemble we can in principle trace back to the formation mechanisms that originated them. Planet formation is a direct consequence of star formation, yet it can be severely influenced by the presence of a stellar companion. The existence of planets in orbit around one or both components of binary systems are stringent probes of planet formation process. Radial velocity measurements estimate that 18 ± 1 % of FGK stars will have a giant planet within 20 AU (Cumming et al., 2008). About 44 % of FGK stars are found in multiple systems, with 33 % in binary systems, and 11 % in higher-order architectures (Raghavan et al., 2010). Hence roughly half of potential planet hosts are in multiple-star systems, arguing that the fraction of giant planets orbiting a stellar component of a binary system is likely not negligible.

A number of campaigns have thus searched for planets in and around stellar binaries, including radial velocity programs (e.g., Konacki et al., 2009), transit discoveries (e.g., Doyle et al., 2011) and direct imaging surveys (e.g., Asensio-Torres et al., 2018; Hagelberg et al., 2020), leading to the detection of a number of circumstellar (orbiting one star) and circumbinary (orbiting two stars) planets. Despite these efforts, most exoplanet searches routinely exclude stars in binary or multiple systems to avoid systematic errors in planet detection, and the first systems of this type were identified serendipitously (see e.g., Patience et al., 2002; Mugrauer et al., 2006). The distinct demographics of the first planets discovered in binary star systems hinted at the possibility that binary companions could dramatically reorient the orbital configuration of planetary systems (Zucker and Mazeh, 2002). Approaching the question from the opposite end, numerous high-resolution imaging studies have also searched for stellar companions to known planetary systems, either to validate or refine the nature of identified planets (Everett et al., 2015; Furlan et al., 2017; Hirsch et al., 2017), or to purposely investigate the effect of stellar duplicity on planetary populations (Horch et al., 2014; Wang et al., 2014; Matson et al., 2018; Colton et al., 2021).

Dedicated studies of circumstellar planets in binary systems rapidly revealed a lack of stellar companions within 20–50 AU (e.g., Bergfors et al., 2013; Kraus et al., 2016). Close stellar companions on this separation range are generally accepted to prevent planet formation, although early examples of giant planets in < 20 AU binaries (Queloz et al., 2000; Hatzes et al., 2003) demonstrated that such systems do exist. Consistent with the observed shortfall of planets of tight binaries, theoretical models predict that the presence of a very close binary companion can truncate a protoplanetary disk (Pichardo et al., 2005; Kraus et al., 2012), hence obstructing the formation of a planet by core accretion, or ejecting the planet in unstable systems (Kaib et al., 2013). Binary companions at large separations (beyond several hundreds to thousands of AU) from planet hosts, on the other hand, have been argued to have no impact on the formation and evolution of planets (White and Ghez, 2001; Desidera and Barbieri, 2007).

Meanwhile, the effects of binary companions at intermediate (around ~100–300 AU) separations are more debated. Such companions could truncate circumprimary disks by opening large gaps, hence redirecting the material to the primary stars' circumstellar disks and leaving the secondaries with no or depleted disks (Artymowicz and Lubow, 1994; Bate and Bonnell, 1997), consistent with observations of binary systems among T Tauri stars (Jensen and Akeson, 2003). Theoretical simulations also showed that perturbations from secondary stars may assist the formation and evolution of giant planets by enhancing mass accretion and orbital migration rates in circumstellar disks (Kley, 2001). The Kozai-Lidov mechanism (Kozai, 1962; Lidov, 1962) could also play a role in the inward migration and final orbital properties of planets through secular interactions induced by an outer stellar companion on such separations. This process has indeed been invoked to explain the formation of hot Jupiters (Fabrycky and Tremaine, 2007; Winn et al., 2010).

In this study, we present an overview of the current census of circumstellar exoplanets in visual binaries, with separations from tens of AU out to 20,000 AU, within a volume limited to 200 pc. The goal of this compilation is to gather information of stellar multiplicity for a large sample of exoplanets, which will hopefully serve in future investigations, rather than to perform a detailed statistical analysis of these populations. In particular, this work extends previous such studies of exoplanets orbiting one component of a binary system to all stellar spectral types and all types of extra-solar planets and brown dwarf companions. In Section 2, we describe the construction of our exoplanet sample (Section 2.1), followed by a search for co-moving companions to exoplanet hosts (Section 2.2) in the literature and in *Gaia*. Section 3 presents our results, in which we explore differences between the demographics of planets in binaries and around single stars (Section 3.2), as well as potential trends in planet properties based on binary separation and mass, for the population of planets in multiple-star systems (Section 3.3). Section 4 discusses the completeness of our sample and the observed effects of stellar duplicity on various exoplanetary populations. Our conclusions are presented in Section 5.

2 MATERIALS AND METHODS

We describe in this Section the construction of our studied exoplanet sample (Section 2.1) and the searches performed for wide binary companions to all selected planet hosts (Section 2.2). In the context of this work, we consider brown dwarfs and extra-solar planets orbiting stars as a unique population of sub-stellar companions. We thus make no distinction between companions below and above the deuterium burning limit (13 M_{Jup}), and will use the term sub-stellar companion to denote planetary and brown dwarf companions in general, unless otherwise specified. Similarly, double and multiple stellar systems will often be referred to as binaries throughout most of this work for conciseness. Finally, given the exoplanet-oriented approach of this study, the term host will always refer to the planet-bearing star in a system, independently of whether or not it is the higher-mass component of a multiple-star system.

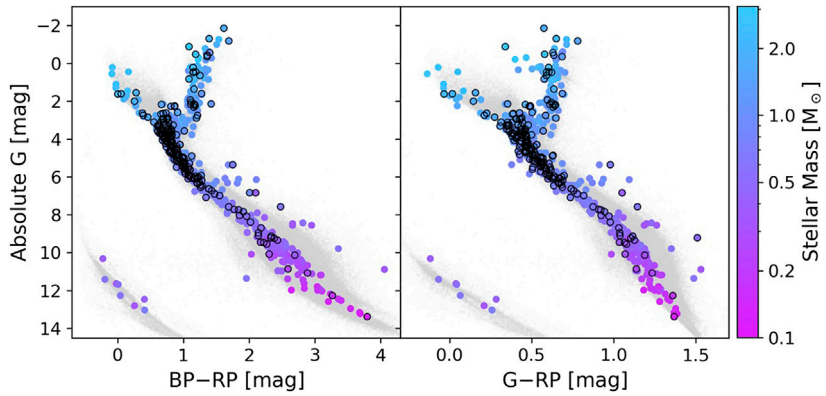

FIGURE 1 | *Gaia* color-magnitude diagrams of planet hosts stars, showing absolute *G* magnitudes against *BP-RP* colors **(left)** and *G-RP* **(right)**. Symbols plotted with black rings represent planet hosts found to be part of multiple-star systems. The colorbar indicates the mass of each planet host, using a logarithmic scale. The gray background population shows the 200-pc volume-limited cleaned sample from *Gaia* DR2.

2.1 Exoplanet Compilation

We gathered a sample of extra-solar planets and brown dwarfs from the NASA Exoplanet Archive[1], the Extrasolar Planets Encyclopaedia[2] (Schneider et al., 2011), the Exoplanet Orbit Database[3] (Han et al., 2014) and the Open Exoplanet Catalogue[4]. The data from these libraries were collected on June 23, 2020, and cross-matched to identify all systems with at least one planet or brown dwarf companion reported as confirmed in at least one of these databases. We gathered from these catalogs all available information about the sub-stellar companions and stellar hosts, and only kept systems with robust companion mass (or minimum mass) and semi-major axis measurements. We imposed a cut of 0.1 $M_{\odot}$ on the minimum mass of the host, based on primary masses supplied in the considered databases, in order to focus our study on stellar hosts only. We also removed all circumbinary (P-type) systems, orbiting both stars from a binary system, as our study concentrates on circumstellar (S-type) planets and brown dwarfs, found around a single component of a binary system.

We cross-matched the resulting sample with the *Gaia* Data Release 2 (DR2; Gaia Collaboration et al., 2016; Gaia Collaboration et al., 2018) catalog, obtaining positions, parallaxes, proper motions, *Gaia* magnitudes and effective temperatures for all hosts found in *Gaia* DR2. Astrometric information was taken from the SIMBAD Astronomical Database (Wenger et al., 2000) for the few targets that are not part of *Gaia* DR2 or do not have full astrometric solutions from the *Gaia* mission. Based on the obtained stellar parallaxes, we restricted our sample to systems with parallax measurements larger than 5 mas, corresponding to a maximum distance of 200 pc for our volume-limited investigation. This cut allows us to focus on relatively nearby stars, thus limiting the range of probed inner working angles around different targets when searching for stellar companions, while keeping a sufficiently large sample for a statistically significant study.

The final sample consists of 938 host stars, harboring a total of 1,316 exoplanets and brown dwarfs, and contains 693 single-planet systems and 245 multi-planetary systems. Stellar hosts have masses ranging from 0.1 to 3.09 $M_{\odot}$, with a median of 0.95 $M_{\odot}$. Most primaries are along the main sequence, covering spectral types from B to M, with 171 giants or sub-giants and 8 white dwarfs. We show in **Figure 1** the *Gaia* Hertzsprung-Russell diagrams for all primaries in our sample with *Gaia* DR2 parallaxes and *G*, *BP*, and *RP* magnitudes (926 stars), with the color scale indicating the host mass. Tables for the final samples are provided as supplementary material and are available online, with separate tables for the stellar hosts and sub-stellar companions.

2.2 Binary Search

In this work, we focus on co-moving visual binaries or higher-order hierarchical stellar systems, that is, systems with two or more stars confirmed to be moving together in the sky. The co-moving nature of two gravitationally-bound objects can be determined in two ways. The first approach is via proper motion (and parallax) measurements, where the components of a multiple system will show astrometric parameters consistent with one another. The second method consists in comparing images taken over a sufficiently-long time baseline to demonstrate that two sources show the same displacement over time compared to fixed background objects. Both approaches require the two (or more) stars to be spatially resolved in imaging observations, and such visual binaries are thus typically widely-separated systems. We place an outer limit of 20,000 AU on the projected separation in our search for multiple systems.

In the following sections, we describe the searches we performed for wide, co-moving visual companions to all stellar hosts from our gathered sample of exoplanetary systems. The full

[1]https://exoplanetarchive.ipac.caltech.edu
[2]http://exoplanet.eu
[3]http://exoplanets.org
[4]http://www.openexoplanetcatalogue.com

compilation of binary systems is provided as online supplementary material.

2.2.1 Binaries in Surveys and the Literature

The catalogs used to compile our studied sample contain some information about stellar binarity. We complemented the multiplicity data from these databases with the Catalogue of Exoplanets in Binary Star Systems[5] (Schwarz et al., 2016). We added to this all systems from published surveys searching for visual stellar companions to circumprimary planetary systems (Luhman and Jayawardhana, 2002; Patience et al., 2002; Udry et al., 2004; Mugrauer et al., 2006; Mugrauer et al., 2007a; Mugrauer et al., 2007b; Raghavan et al., 2006; Eggenberger et al., 2007, Eggenberger et al., 2011; Daemgen et al., 2009; Mugrauer and Neuhäuser, 2009; Adams et al., 2012; Adams et al., 2013; Ginski et al., 2012, Ginski et al., 2016; Ginski et al., 2020; Lillo-Box et al., 2012; Bergfors et al., 2013; Faedi et al., 2013; Lodieu et al., 2014; Wang et al., 2014; Mugrauer and Ginski, 2015; Wöllert et al., 2015; Deacon et al., 2016; Kraus et al., 2016; Ngo et al., 2016; Ngo et al., 2017; Furlan et al., 2017; Moutou et al., 2017; Coker et al., 2018; Dietrich and Ginski, 2018; Ziegler et al., 2018; Fontanive et al., 2019; Mugrauer, 2019; Bohn et al., 2020; Southworth et al., 2020) or reviews of planets in binaries (Bonavita and Desidera, 2007; Bonavita and Desidera, 2020; Desidera and Barbieri, 2007; Eggenberger and Udry, 2007; Eggenberger, 2010; Roell et al., 2012; Thebault and Haghighipour, 2015) that we could find, and finally any other serendipitous discovery we were aware of that may have been missing from the above compilations.

In parallel, we cross-matched our host star sample with large-scale catalogs of stellar multiplicity like the Washington Double Star Catalog (WDS; Mason et al., 2001), the Catalog of Components of Double and Multiple stars (CCDM; Dommanget and Nys, 2002), the Tycho Double Star Catalogue (TDSC; Fabricius et al., 2002) and the Updated Multiple Star Catalog (MSC; Tokovinin, 2018), as well as surveys for wide stellar binaries conducted with direct imaging (Deacon et al., 2014; Janson et al., 2012; Janson et al., 2014; Janson et al., 2017; Raghavan et al., 2010; Tokovinin and Lépine, 2012; Tokovinin, 2014a; Tokovinin, 2014b; Ward-Duong et al., 2015; Winters et al., 2019).

Each reported multiple system was then checked individually in the literature to ensure the S-type nature of the planets and brown dwarfs, and confirm that the binary or multiple system was indeed visual (with resolved components), and astrometrically confirmed to be co-moving, either via consistent relative astrometry in multi-epoch observations or through similar kinematics (as opposed to optical binaries with a probabilistic bound nature from the chance of alignment). A total of 184 stars in our sample were mentioned in the considered surveys to have at least one companion satisfying these criteria (excluding the recent *Gaia* search performed by Mugrauer, 2019; see Section 2.2.2). For all identified systems, we gathered, when available, binary separations, companion masses, and companion spectral types.

2.2.2 Companions in Gaia DR2

To complement the literature search performed above, we searched for bright companions in the *Gaia* DR2 catalog to all stars in our compilation. Using the collected positions, proper motions and parallaxes for the stellar hosts, we searched for *Gaia* sources within angular distances corresponding to separations of 20,000 AU from our primaries, and displaying consistent kinematics. Following the approach from Fontanive et al. (2019), we used thresholds of 20 % disparity in parallax, and offsets of < 20 % of the total proper motion in one direction and < 50 % in the other coordinate. These cuts allow to account for the fact the short-term astrometric measurements from *Gaia* DR2 may capture the reflex motion of binary systems, or may have spurious solutions for unresolved binaries (see Fontanive et al., 2019 for details).

For systems part of young moving groups, other members of the same association may appear nearby in the sky and display similar proper motions and parallaxes, consistent with the average moving group kinematics. To avoid the inclusion of unassociated close-by group members in our binary list, we checked that no more than one other astrometric match was found on angular separations up to 20 times the identified binary radius. We consider that a co-moving source within 20,000 AU projected separation is statistically unlikely to be an unrelated member of the same group if no other members are found within a 400-fold sky area. We thus regard such sources as bonafide bound companions for the purpose of this study. When one other match was found, we applied the same procedure centered on this outer source, with the same search radius, to establish whether other group members were found nearby, in which case all sources were taken to be unrelated moving group members. If no additional sources with consistent kinematics were found, we considered the outer source to be the tertiary component of a triple system. Finally, we checked that identified binary companions were different from the sub-stellar companions in our exoplanet list, as some young and bright brown dwarfs discovered with direct imaging on wide separations may be detected at the low-mass end of the *Gaia* DR2 completeness (Reylé, 2018).

This analysis yielded 175 companions around 172 hosts stars. For all identified systems, we measured the binary separation from the respective *Gaia* DR2 positions of co-moving components, and collected *Gaia* photometry for the companions. The majority (139) of identified *Gaia* companions were already known from the literature (excluding findings from Mugrauer, 2019) and were included in our compilation from Section 2.2.1. Based on our literature findings, 19 of the detected *Gaia* companions were in fact tight binaries themselves, unresolved in *Gaia*. Mugrauer (2019) recently performed a very similar search for wide companions to exoplanet host stars in *Gaia* DR2, which presents a useful comparison survey to validate our approach. We found that all binaries reported in that work and present in our sample list (121 systems) were also retrieved in our *Gaia* analysis. From these, 23

[5]https://www.univie.ac.at/adg/schwarz/multiple.html

TABLE 1 | New stellar companions to planet host stars identified in this work using the *Gaia* DR2 catalog. The new system components are marked in bold in the System column, which is only indicative of the overall system architecture, and do not represent proposed naming conventions. Following the approach in the main tables, component A systematically denotes the planet host irrespectively of the relative component masses, unless already named differently in the literature. Indices 1 in the stellar mass and spectral type columns refer to the planet hosts, and indices 2 refer to the considered stellar companions. This is a highlight of full tables available as **Supplementary Material**, which provide additional information about these systems, together with the rest of our compilation.

System	Parallax [mas]	Separation [arcsec]	Separation [AU]	SpT_1	Mass1 [$M_\odot$]	SpT_2	Mass2 [$M_\odot$]
New binary companions							
CoRoT-7 Abc + **B**	6.23	75.7	12160	K0V	0.93	M4	0.23
HD 13167 Ab + **B**	6.69	20.1	3,001	G3V	1.35	M4	0.21
HD 23472 Abc + **B**	25.59	9.6	374	K3.5V	0.75	M6	0.14
HIP 73990 Abc + **B**	9.03	47.3	5,234	F2IV	1.72	M2	0.50
K2-228 Ab + **B**	7.71	22.6	2933	K6	0.71	G3	1.08
L2 Pup Ab + **B**	15.61	32.8	1998	M5IIIe	0.66	M5	0.20
TOI-132 Ab + **B**	6.08	19.6	3,231	G8V	0.97	M4	0.17
WASP-189 Ab + **B**	10.00	9.4	942	A4/5IV/V	1.89	M2	0.45
WASP-29 Ab + **B**	11.39	125.2	10994	K4V	0.82	M3	0.38
WASP-59 Ab + **B**	8.60	81.8	9512	K5V	0.72	K7	0.62
New tertiary companions							
HIP 65 (Ab + B) + **C**	16.16	73.6	4557	K4V	0.78	M7.5	0.11
V 1298 Tau Ab-e + (B**C**)	9.21	117.0	14795	K1	1.10	K7	0.66

systems and a tertiary companion to the WASP-11 system (unresolved in *Gaia*) were never reported prior to that study. We however retrieved 51 additional *Gaia* systems missing from the Mugrauer (2019) compilation, which is likely due to different target samples between that study and ours. Finally, 10 of our identified *Gaia* co-moving systems were not found to have been previously reported in the literature (up to early September 2020): CoRoT-7, HD 13167, HD 23472, HIP 73990, K2-228, L2 Pup, TOI-132, WASP-189, WASP-29, WASP-59. In addition, new tertiary components were discovered around HIP 65A and V 1298 Tau. These companions are presented in **Table 1**, with additional information about the systems provided within the full catalogs available online.

For all new *Gaia* systems, we checked whether the wide stellar companions were known (seemingly single) objects in SIMBAD, and gathered additional mass and spectral type information from the literature for these components when available. In addition, for all components known from the literature but missing from our *Gaia* binary list, we searched for these wide companions in *Gaia* DR2 in case these stars were in the catalog but with no astrometric solutions, and thus not detectable as co-moving sources in our *Gaia* search. From these, 14 companions were recovered without *Gaia* DR2 astrometry, and available *Gaia* magnitudes and relative positions of components were added to our catalog for these additional companions.

2.2.3 Properties of Stellar Companions

As a number of literature systems (mostly from WDS) and *Gaia* binaries had no existing stellar classification or measured mass, we estimated these characteristics for all identified *Gaia* components based on their positions in the *Gaia* color-magnitude diagrams. Hertzsprung-Russell diagrams were made for all binary companions with measured magnitudes in the *G*, *BP* and *RP* bands, using the sources' parallaxes if available, and the astrometry from the associated planet hosts otherwise.

From these, six sources populated the white dwarf part of the parameter space, and were all found in the *Gaia* DR2 white dwarf study by Gentile Fusillo et al. (2019). The white dwarf classifications and masses were thus taken from this work for these companions.

All other companions appeared to fall along the main sequence. For these systems, we used the *TESS* Input Catalog (TIC; Stassun et al., 2018) to map the parameter space of the *Gaia* color-magnitude diagrams to stellar masses and spectral types, based on TIC stellar masses and queried SIMBAD spectral types for all sources from the catalog out to 200 pc. As clear and continuous trends in mass and spectral type were seen along the *Gaia* main sequences of the TIC sample (similar to our host sample in **Figure 1**), the masses and spectral types of wide companions could be inferred directly based on their location along these *Gaia* main sequences. Quantities were interpolated using the mean mass and spectral type from the TIC sample in a box of size 0.2 mag centered on the companion's absolute magnitude and color, provided that at least 10 sources were found in that box. For each detected *Gaia* companion, masses (rounded to 0.01 $M_\odot$) and spectral types (to 1 sub-type) were obtained from the TIC *BP–RP* and *G–RP* parameter spaces, and averaged for more robust final values. For sources characterized in this way from their colors and magnitudes, the average offset and scatter between literature values and our *Gaia*-derived estimates was $+0.3 \pm 1.5$ sub-type in spectral type, and $-0.01 \pm 0.05\,M_\odot$ in mass (removing known unresolved sources). We also validated this method by applying it to our main sequence host star sample, and observed comparably negligible offsets to values collected in the planet-host catalog.

For companions that fell outside the TIC main sequence due to unusual *Gaia* colors (14 objects), or for sources with no *BP* and *RP* magnitudes (16 objects), we used the median intersection of the absolute *G* magnitude with the TIC main sequences instead, assuming that these objects were single, main sequence stars, similar to the approach followed in the recent *Gaia* study by Mugrauer (2019). For companions classified from their absolute magnitudes alone, the average scatter was -0.4 ± 2.4 sub-types in spectral type and $-0.2 \pm 0.07\,M_\odot$ in mass for sources truly on the

main sequence, with very similar results in mass to Mugrauer (2019) for overlapping systems. Larger offsets were seen for known white dwarf companions with no *Gaia* colors, which were hence assimilated to M dwarfs on the main sequence based on their absolute *G*-band magnitudes.

Based on these results, we consider that our *Gaia*-inferred quantities are robust measurements for main sequence components. We adopt these as final values when no previous mass and spectral type estimates were available for the retrieved companions, and use existing literature estimates otherwise. The literature, *Gaia*, and final adopted values are all reported in our tables.

3 RESULTS

Many surveys looking for extra-solar planets, in particular with the radial velocity method, are affected by or biased against binaries with separation $\leq$2–6 arcsec, excluding known multiple systems in target selection processes (see e.g., Eggenberger, 2010; Ngo et al., 2017). As a result, measurements of multiplicity rates for exoplanetary systems are particularly challenging, as these selection biases are not trivial to quantify and correct for (see e.g., Moe and Kratter, 2019). This typically means that studies like ours, investigating the binarity of planetary systems discovered partly by such surveys, cannot be used to derive the true frequency of planets in binaries, nor to probe the existence of planets in very tight binaries. With this in mind, the goal of this work is thus to provide an overview the current census of sub-stellar companions in wide visual binaries, rather than to achieve robust statistical results, and we will therefore not attempt to account for these biases here.

Our studied sample of planetary systems was nonetheless compiled independently from the binary nature (known or unknown) of the systems. The gathered compilation should thus not be biased toward or against the existence of binary star systems beyond the intrinsic biases from exoplanet detection campaigns. Our *Gaia* search for wide companions is also homogeneous across the host star sample, limited only in inner working angle by the distance to each star, and by the inherent completeness of *Gaia* DR2. Our ability to recover stellar companions in *Gaia* is therefore, in principle, independent of the architecture of the planetary systems themselves. Similarly, the existing literature surveys considered spanned a large range of planet host stars and probed various distinct planetary populations. We thus consider that while strong biases remain in our binary list, which should be taken into account for detailed statistics and the derivation of absolute occurrence rates, our compilation does not strongly discriminate between different types of sub-stellar companions (i.e., planet or brown dwarf masses, separations or detection methods) in the potential to detect wide visual companions. Our compilation can hence be used to search for raw trends within the obtained sample of binaries and highlight potential correlations between multiplicity and the properties of planetary and sub-stellar companions.

3.1 Overall Compilation

From the compilation gathered in Section 2.2.1, combining an extensive literature search and a *Gaia* DR2 investigation, 218 planet hosts were found to have at least one visual co-moving stellar companion: 186 host stars were found to be in binary systems, and 32 host stars in higher-order hierarchical systems. From these, 4 binaries and 1 triple system are composed of 2 planet-hosting stars, organizing the 218 planet hosts into 213 unique multiple systems. The architecture of each planet-bearing multiple-star system is presented in **Figure 2**, which illustrates the relative separations and masses of sub-stellar and stellar companions within each system. **Figure 3** presents the distribution of spectral types among the planet hosts stars, showing relative numbers of single stars and planet hosts in multiple systems for each spectral type, and compared to the sample of detected stellar companions. Companion masses range from 2.37 $M_{\odot}$ down to the hydrogen-burning limit (~0.07 $M_{\odot}$). Binary projected separations extend from 0.85 AU (GJ 682) out to our 20,000 AU search limit, with a median value of 678 AU. A total of 19 binaries were found in the range 10–50 AU, and 27 systems were identified on separations shorter than 100 AU.

Table 2 summarizes the numbers and raw fractions of sub-stellar companions in single and multiple-star systems, where binaries and triples are counted similarly as hierarchical multiple systems. We emphasize once again that no completeness or selection bias corrections have been performed, and the quoted numbers simply provide an overview of the collected catalogs. From the 1,316 exoplanets and brown dwarfs in our compilation, 286 were found to be around one component of a multiple-star system (21.7 ± 1.3 %). In terms of individual planetary systems, 218 out of 938 planet host stars (23.2 ± 1.6 %) are part of multiple-star systems. Interestingly, a marginally higher fraction (2.2-σ) of single-planet systems are in hierarchical stellar systems (25.1 ± 1.9 %) compared to multi-planet systems (18.0 ± 2.7 %).

3.2 Multiplicity as a Function of Planet Properties

In this section, we explore the multiplicity of our planet host star sample as a function of planetary mass and separation. Unfortunately, other orbital elements (eccentricity, inclination) are not available for the full exoplanet sample. Investigations involving these parameters would thus be limited to planetary systems detected with specific methods and are not explored here. In **Figure 4**, we show the masses and semi-major axes of all planet and brown dwarfs in our compilation, with systems found to be in visual stellar binaries marked in magenta, and apparently single stars in blue.

Some previously-known trends associated with specific sub-populations of planets are visually apparent in **Figure 4**. One such feature is the lack of blue scatter points (single-star systems) for sub-stellar companions with semi-major axis in the range ~0.01–0.10 AU (orbital periods of ~0.5–10 days around a Sun-like star) and masses larger than $\sim 3\ M_{Jup}$. This part of the parameter space, representing massive hot Jupiters and brown dwarfs, is entirely filled with multiple-stars systems (magenta

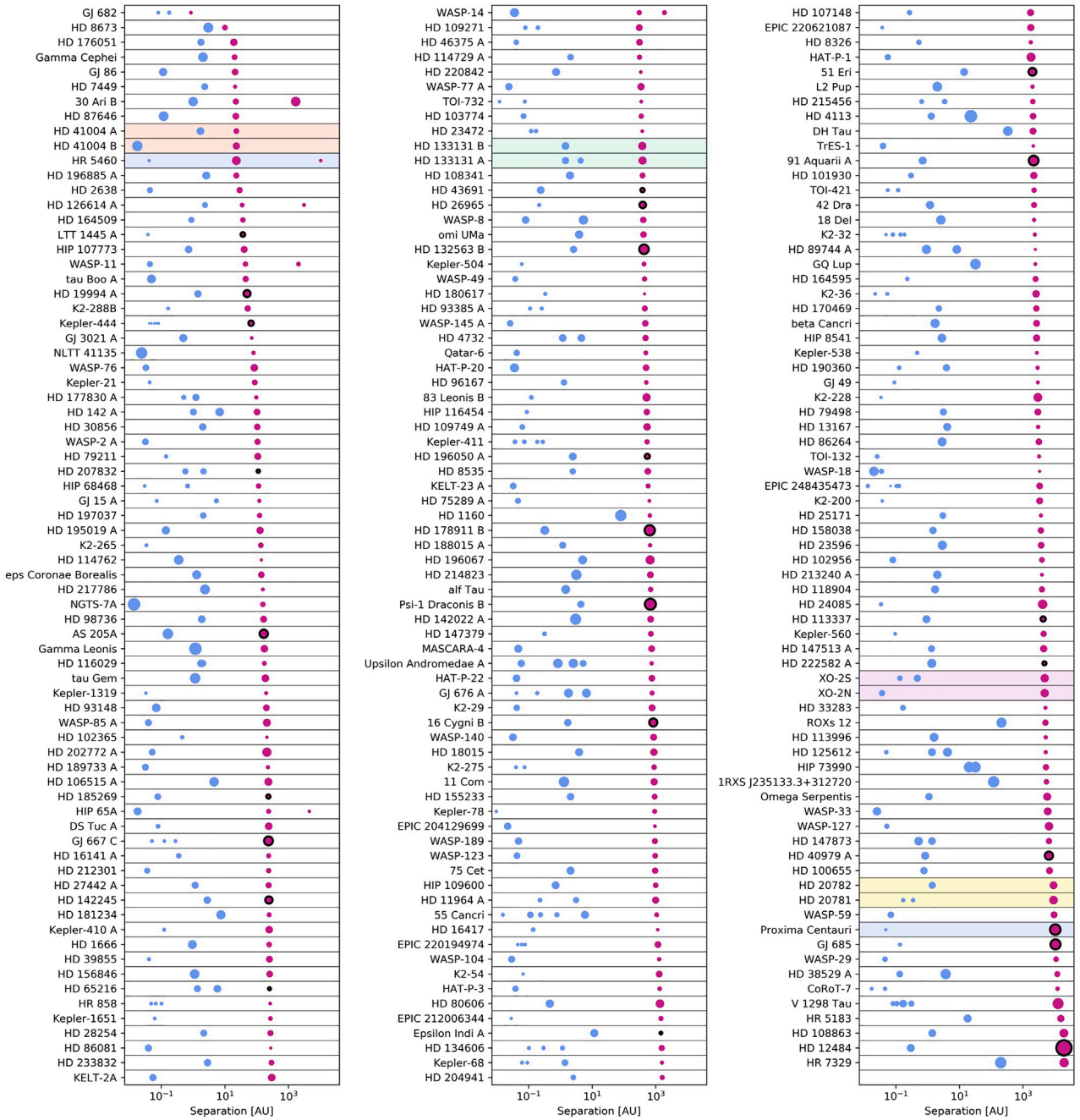

FIGURE 2 | Architectures of all exoplanetary systems identified to be in multiple-star configurations. The blue circles represent the inner brown dwarfs and planets, with symbol sizes proportional to their masses cubed. Magenta symbols show the positions of all confirmed wide stellar companions, with radii proportional to the mass of these outer companions. Stellar companions marked with black circles are themselves tight binaries, with the symbol sizes based on the combined mass of the two components. The five host stars in multiple systems containing two planet-bearing stars are color-coded accordingly. We note that separations for inner sub-stellar companions correspond are semi-major axes, while observed projected separations are displayed for the wide stellar companions.

scatter points), consistent with early observations that these planets and brown dwarfs are almost exclusively observed in binary stars (Zucker and Mazeh, 2002). A second notable attribute from **Figure 4** is the small group of brown dwarfs with even shorter orbital separations (<0.01 AU) identified around single stars (top left corner). These sub-stellar companions are all found to orbit white dwarfs, and correspond to most white dwarf hosts from our compilation. Such extreme systems are thought to result from the considerable mass loss stars undergo as they become white dwarfs. This post-main sequence process drastically changes the star-planet mass ratios, thus altering the dynamics and stability of brown dwarfs

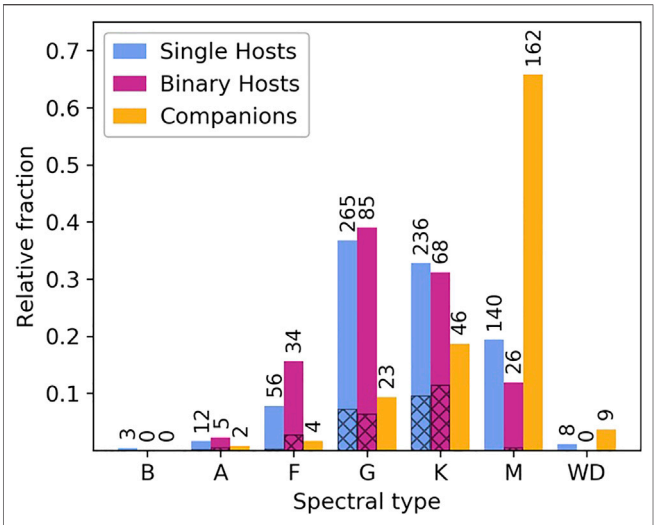

FIGURE 3 | Distribution of spectral types from B through M, plus white dwarfs, for single-star planet hosts (blue), multiple-star planet hosts (magenta) and stellar companions (yellow). Hatched sections of the plotted bars represents giants and sub-giants, with the remaining systems being on the main sequence. Each color-coded histogram is independently normalized so that the sum of the bars within each individual group adds up to 1.

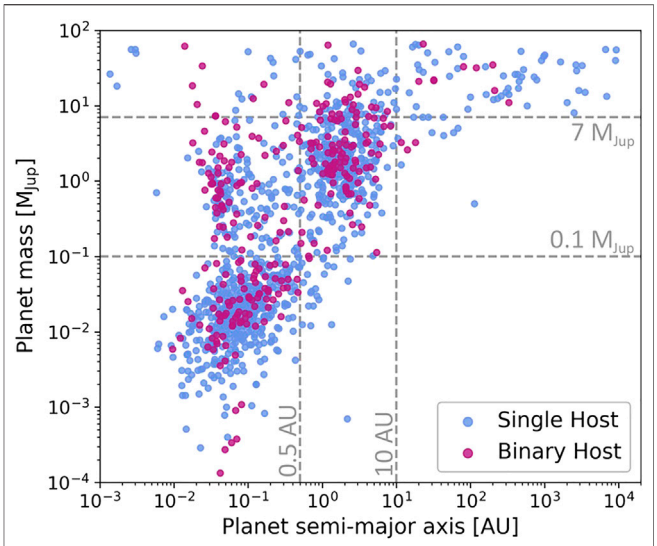

FIGURE 4 | Planet mass against semi-major axis for all sub-stellar companions in our exoplanet compilation. Planets identified to be part of multiple-star systems are shown in magenta, while planets orbiting single stars are plotted in blue. The dashed lines divide the parameter space into several bins detailed in the text.

TABLE 2 | Summary of results, providing the number of single and multiple (binary or higher-order) systems hosting various planetary sub-populations. Raw occurrence rates are given in parentheses with uncertainties computed as Poisson noise.

Planetary population	Total	Single-star systems	Multiple-star systems
All planets	1,316	1,030 (78.3 ± 2.4 %)	286 (21.7 ± 1.3 %)
All planetary systems	938	720 (76.8 ± 2.9 %)	218 (23.2 ± 1.6 %)
Single-planet systems	693	519 (74.9 ± 3.3 %)	174 (25.1 ± 1.9 %)
Multi-planet systems	245	201 (82.0 ± 5.8 %)	44 (18.0 ± 2.7 %)
$M_{pl} < 0.1\ M_{Jup}$	554	462 (83.4 ± 3.9 %)	92 (16.6 ± 1.7 %)
$M_{pl} = 0.1 - 7\ M_{Jup}$	597	444 (74.4 ± 3.5 %)	153 (25.6 ± 2.1 %)
$M_{pl} > 7\ M_{Jup}$	165	124 (75.2 ± 6.7 %)	41 (24.8 ± 3.9 %)
$a_{pl} < 0.5$ AU	766	603 (78.7 ± 3.2 %)	163 (21.3 ± 1.7 %)
$a_{pl} = 0.5 - 10$ AU	476	365 (76.7 ± 4.0 %)	111 (23.3 ± 2.2 %)
$a_{pl} > 10$ AU	74	62 (83.8 ± 10.6 %)	12 (16.2 ± 4.7 %)
$M_{pl} \geq 0.1\ M_{Jup}$, $a_{pl} \leq 10$ AU	688	506 (73.5 ± 3.3 %)	182 (26.5 ± 2.0 %)
$M_{pl} \geq 0.1\ M_{Jup}$, $a_{pl} \leq 0.5$ AU	236	164 (69.5 ± 5.4 %)	72 (30.5 ± 3.6 %)
$M_{pl} \geq 7\ M_{Jup}$, $a_{pl} \leq 10$ AU	106	73 (68.9 ± 8.1 %)	33 (31.1 ± 5.4 %)
$M_{pl} \geq 7\ M_{Jup}$, $a_{pl} \leq 0.5$ AU	28	19 (66.9 ± 15.6 %)	9 (32.1 ± 10.7 %)

and planets, in particular in multi-planet systems (e.g., Maldonado et al., 2020).

In order to investigate the effect of stellar multiplicity as a function of sub-stellar companion mass and separation, we divide the planetary parameter space into three bins in semi-major axis (a_{pl}) and three bins in mass (M_{pl}), delimited by the dashed lines in **Figure 4**. We chose arbitrary limits of 0.5 and 10 AU in semi-major axis, and 0.1 and 7 M_{Jup} in mass. The boundary at 0.5 AU corresponds to the observed dearth between two distinct peaks in the distribution of exoplanet orbital periods, representing the pile-up of hot planets, and the bulk population near the snow line (~1–3 AU), respectively (Udry et al., 2003). The 10-AU threshold corresponds roughly to the outer detection limit for the radial velocity method, and only massive, directly imaged companions are typically identified beyond 10 AU. The 0.1-M_{Jup} mass bound was adopted as the lower limit for the mass of Jovian planets (Mordasini, 2018), while 7 M_{Jup} was taken as the median transition between core accretion and gravitational instability giant planets (4–10 M_{Jup}; Schlaufman, 2018), a limit also advocated by Moe and Kratter (2019) (see also Santos et al. 2017).

Table 2 reports the relative numbers of sub-stellar companions in single and binary systems in each planetary semi-major axis and mass bin. Stars harboring low-mass, sub-Jovian planets ($M_{pl} < 0.1\ M_{Jup}$) appear to have a substantially lower stellar binary rate, with 16.6 ± 1.7 % of such planets being found in multiple-star systems. This compares to 25.5 ± 1.8 % for higher-mass planets and brown dwarfs, with a 3.6-σ difference in raw multiplicity frequency between planetary and sub-stellar companions below and above 0.1 M_{Jup}. A similar trend is seen with planet orbital distance, where sub-stellar companions with $a_{pl} > 10$-AU are less frequently found in stellar binaries, although the smaller number of such planetary companions reduces the significance of this tendency. This effect is most likely the result of an enhanced bias against the existence of wide binaries within 20,000 AU for systems with sub-stellar companions large orbital distances. Indeed, the presence of a planet or brown dwarf prevents the possibility of finding a binary companion on comparable or marginally larger separations than the sub-stellar companion semi-major axis, and binaries with separations of hundreds to thousands of AU are thus dynamically impossible for a sizable fraction of these planetary

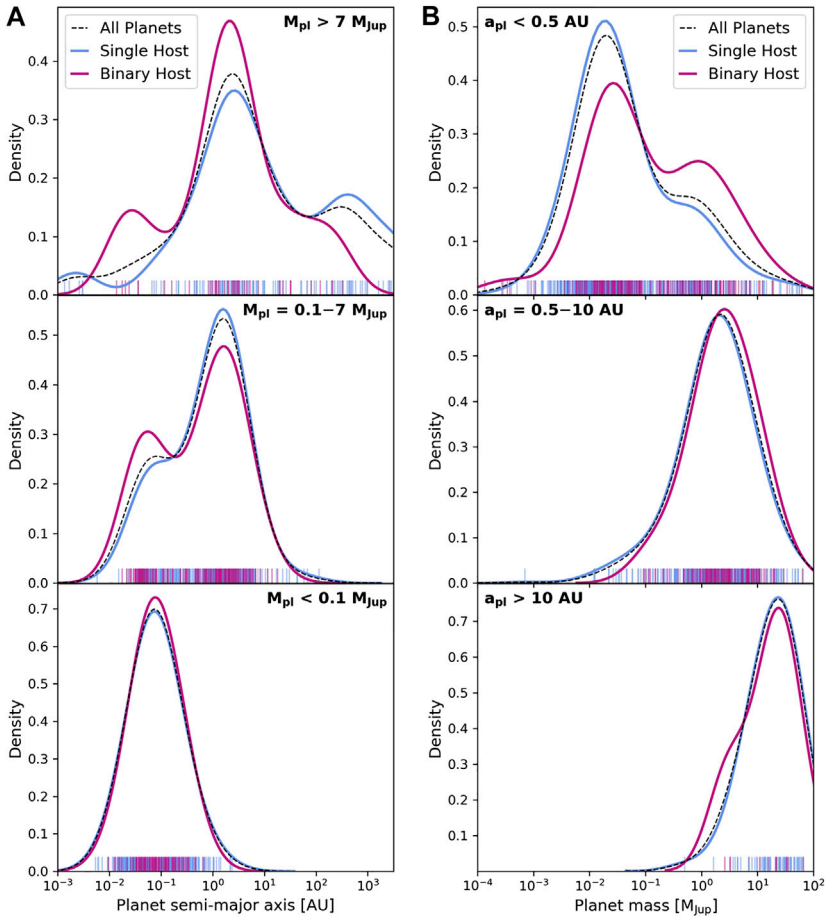

FIGURE 5 | KDEs of planet properties comparing planets in binaries (magenta) and planets around single stars (magenta), with the full planetary population shown in the dotted black lines. Panel **(A)** shows the distribution of planetary semi-major axis, divided between massive giant planets and brown dwarfs **(top)**, lower-mass giants **(middle)** and sub-Jovian planets **(bottom)**, following the cuts in parameter space shown in **Figure 4**. Panel **(B)** shows the distribution of planetary mass for close-in planets **(top)**, intermediate-separation planets **(middle)** and wide-orbit giant planets **(bottom)**.

systems. Given these results, we also report values at the end of **Table 2** focusing exclusively on the close-in ($a_{pl} < 10$ AU and < 0.5 AU) giant planet and brown dwarf populations. While the lower number of systems associated with these subsets decreases again the significance of observed trends, raw multiplicity rates seem to increase up to around 30 % for the very shortest-separation and most massive sub-stellar companions. We also note that the vast majority of sub-Jovian planets, with masses below 0.1 M_{Jup}, are found in orbits with semi-major axes shorter than 0.5 AU.

To better understand these tendencies and the effect of multiplicity with planet and brown dwarf properties, we explore the distributions of sub-stellar companions around single and binary stars in the various mass and separation bins considered. In **Figure 5**, we show kernel density estimates (KDE) of the distributions of planet semi-major axis (left panels) and mass (right panel), for the different regions of the parameter space described above. Planets and brown dwarfs in single-star systems are shown in blue, and those in hierarchical stellar systems in magenta. We use KDE bandwidths of 0.3 in all cases, and consider that such estimates of the probability density functions should provide good insights into potential underlying trends.

In terms of planet semi-major axis (**Figure 5A**), multiplicity appears to have no effect on the orbital separation of sub-Jovian planets ($M_{pl} < 0.1\ M_{Jup}$), illustrated by the perfectly consistent distributions for single and binary hosts in the bottom panel, both showing the same narrow peak in the semi-major axis distribution around 0.1 AU. As we enter the giant planet regime ($M_{pl} = 0.1$–$7\ M_{Jup}$; middle panel), the bulk of the planetary population shifts to separations of 1–3 AU, with a secondary peak at tighter separations ($a_{pl} < 0.1$ AU). The relative density of planets in this secondary sub-population seems to be marginally higher for binary-star systems. Looking at the most massive giant planets and brown dwarf companions ($M_{pl} > 7\ M_{Jup}$; top panel), a number of new features emerge in the plotted KDEs. While the core of this exoplanet population still lies at separations of a few AU, comparable to the lower-mass Jovian planets, a strong over-density of closer-in planets and brown dwarfs ($a_{pl} \sim 0.01$–0.1 AU) is seen among the sample of multiple-

star systems (magenta), corresponding to the population of massive, small-separation sub-stellar companions in binaries highlighted previously from **Figure 4**. The minor peak at even tighter separations around single hosts corresponds to the sample of extremely short-period brown dwarfs found around white dwarfs discussed previously. At larger orbital distances, the directly imaged population is subdued in the binary-star sample relative to closer-in planets and brown dwarfs, due to the effect explained above for systems with wide sub-stellar companions.

Regarding the distribution of planet masses (**Figure 5B**), stellar binarity again seems to have no significant effect on the resulting masses for giant planets and brown dwarfs with separations larger than 0.5 AU (middle and bottom panels). At small semi-major axes (top panel), two sub-populations are observed, composed of the sub-Jovian planets with masses below 0.1 M_{Jup} forming the primary peak in the mass distribution, and a broader secondary population of giant planets and brown dwarfs. Again, we observe a relative over-abundance of binaries among the more massive planetary population on small semi-major axes, consistent with the findings deduced from our analysis as a function of planet orbital separation, and with the values reported in **Table 2**.

3.3 Planet Properties as a Function of Binary Properties

Based on our results from Section 3.2, suggesting that stellar multiplicity impacts the existence or properties of Jovian giant planets and brown dwarfs ($M_{pl} > 0.1\ M_{Jup}$) on semi-major axes within 0.5 AU, we further investigate the properties of these sub-stellar companions as a function of binary properties and the statistical significance of these results. We will not look in more details at other planetary systems as the previous analyses revealed no significant effect of binarity on these planetary populations.

We assess the effect of binary separation by comparing the distribution of properties for close-in giant planets and brown dwarfs in binaries as a function of the orbital distance to outer stellar companions. Based on the size of this subset (66 sub-stellar companions), we arbitrarily define ranges of <250 AU, 250–1,000 AU and >1,000 AU in binary separation ρ_{bin}, dividing this sample into roughly evenly populated bins with 22, 24 and 20 systems, respectively. For hierarchical triple systems in which the planetary host star is in an inner tight binary, we only consider the close binary companion, as the outer tertiary component is unlikely to have a significant effect on the planetary system compared to the nearby stellar component. For triple systems with a planet host star widely separated from a closer binary, we count this outer binary as a single companion, using the mean separation between the planet host and the distant sub-system. Individual binary systems may be counted more than once, however, if several sub-stellar companions with masses larger than 0.1 M_{Jup} around found within 0.5 AU around the same star.

Figure 6 shows KDEs of the planet semi-major axes (**Figure 6A**) and mass (**Figure 6B**), comparing planets and brown dwarfs in the short (yellow), intermediate (magenta) and wide (blue) binary separation ranges to those around single stars (dashed black line). Despite the small sample size available for this restricted planetary population, clear trends are visible in these figures. In particular, the subset of sub-stellar companions in extremely widely-separated binaries ($\rho_{bin} > 1000$ AU) shows very similar distributions in planetary semi-major axis and mass to planets and brown dwarfs found in single-star systems. In contrast, sub-stellar companions found in tighter stellar binary systems appear to have smaller semi-major axes and higher masses. The previously-noted overabundance massive, close-in giant planets and brown dwarfs in binaries is hence primarily found in <100 AU binary systems. We highlight, in particular, that from the nine massive ($M_{pl} > 7\ M_{Jup}$), close-in ($a_{pl} < 0.5$ AU) giant planets and brown dwarfs found in binaries, eight are in binaries with separations <1,000 AU, from which 6 have binary separations <250 AU. While these rare sub-stellar companions only represent ~2% of the full exoplanet sample, these systems make up about 10 % of the 64 binaries with separations under 250 AU identified for the full catalog of planet hosts. We further assess the significance of these results by performing two-sided Kolmogorov-Smirnov tests comparing each sub-population of planets in binaries to the sample of planets around single stars (dashed black lines). We are thus testing the null hypothesis that the samples are drawn from the same distribution, and use a threshold of 0.05 on the resulting *p*-values. We found that the null hypothesis could be rejected for the distributions of planet masses and semi-major axes in short and intermediate-separation binaries ($\rho_{bin} < 1000$ AU; yellow and magenta curves), but not for sub-stellar companions in very wide binaries (blue), confirming that the above findings are statistically significant (p-values of 0.027 and 0.0003 for the planet semi-major axes in short and intermediate-separation binaries, respectively, compared to 0.842 for wider binaries; p-values of 0.005 and 0.013 for the planet masses in short and intermediate-separation binaries, and 0.470 for wide binaries). This result further suggests that close and intermediate-separation (< 1000 AU) binary companions have strong effects on the final semi-major axes of massive planets and brown dwarfs, whereas planetary systems in very wide (> 1000 AU) binaries are more likely to evolve as independent stars.

We also investigate potential trends of planet and brown dwarf properties as a function of binary companion mass, M_c. As for the binary separation, we divide the available sample into bins of $< 0.3\ M_\odot$, 0.3–0.6 $M_\odot$ and $> 0.6\ M_\odot$. Triple systems are treated similarly as in the previous analysis, using the total mass of the outer components in the case of tight binaries on wider separations from the planet hosts. **Figure 7** shows the resulting distributions of planet semi-major axis (**Figure 7A**) and mass (**Figure 7B**) for the various stellar companion mass bins, together with the overall distributions of single-star planetary systems (dashed black line). Unlike **Figure 6**, no clear trend is observed with binary companion mass. The only marginal tendency is a rather comparable distribution between the planet orbital distances of single-star systems and the binaries with the most massive companions (yellow). Kolmogorov-Smirnov tests performed on these sub-samples confirmed that

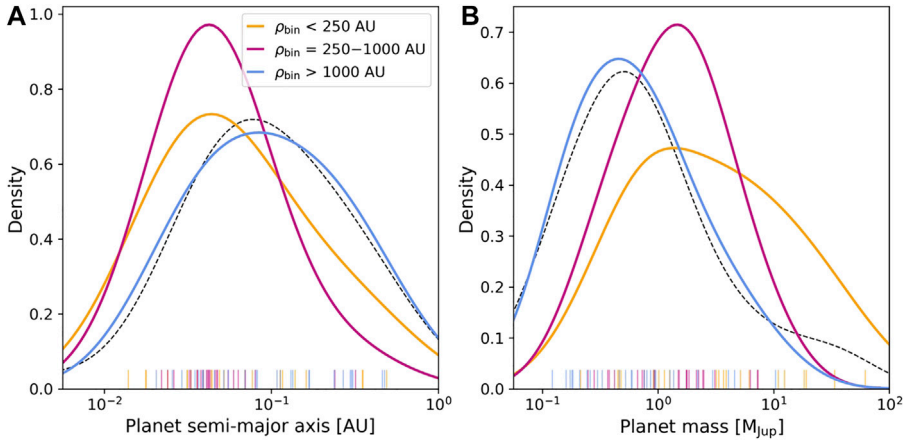

FIGURE 6 | Planet properties as a function of binary separation (ρ_{bin}) for all planets with masses above 0.1 M_{Jup} and semi-major axes within 0.5 AU, corresponding to the binary systems plotted in the magenta distribution in **Figure 10**. KDEs of planetary semi-major axis are shown in panel **(A)**, and distributions of planet masses are shown in panel **(B)**. The dashed black lines show the distributions for planets in the mass and semi-major axis ranges found to be orbiting single stars.

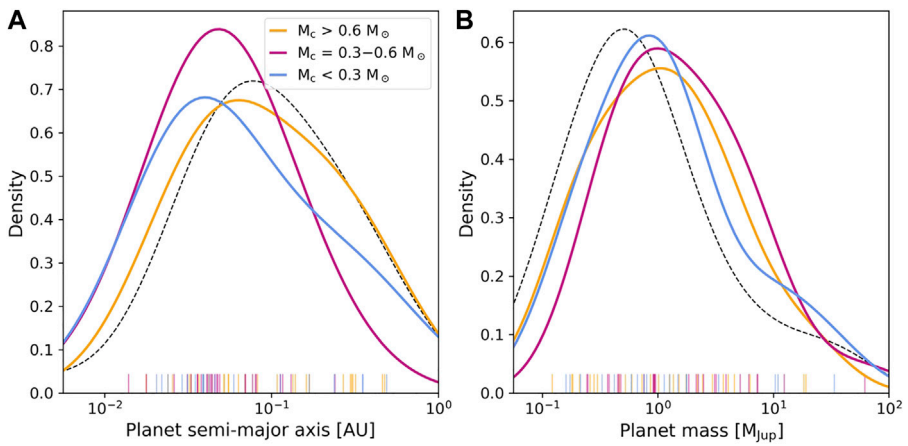

FIGURE 7 | Same as **Figure 6** dividing the sample of binary stars by companion mass (M_c). KDEs of planetary semi-major axis are shown in panel (A), and distributions of planet masses are shown in panel (B). For triple systems with a tight binary on a wide separation from the planet host, the total mass of the outer sub-system is considered. The dashed black lines show the distributions for planets in the mass and semi-major axis ranges found to be orbiting single stars.

the planet separation distribution was statistically different from the single-star planetary population for binary systems with companion masses below 0.6 $M_\odot$ (p-values of 0.001 and 0.021 for binary companions in the intermediate and low mass bins, respectively; p-value of 0.859 for high-mass binary companions). However, this effect is mostly due to the fact that most stellar companions in this bin are in fact very distant, two-component companions from triple systems, thus increasing the adopted companion mass, and correspond for the major part to the systems with separations >1,000 AU that were found to match the single-planet population. Kolmogorov-Smirnov tests could not reject the null hypothesis when comparing the masses of planets and brown dwarfs in various types of binaries to single-star systems, nor was any evidence found that sub-stellar companions in binaries with various stellar companion masses come from different populations (p-values > 0.15 in all cases). Overall, the excess of smaller-separation and higher-mass giant planets and brown dwarfs in binaries appears to be distributed across the different binary mass bins defined, with no robust trend with stellar companion mass.

4 DISCUSSION

In this work, we performed analyses of planetary populations as a function of multiplicity over all spectral types for hosts to exoplanets and brown dwarf companions. This section similarly presents discussions of our results across all types of stars, without distinguishing between massive stars, Sun-like stars and M dwarfs, or main sequence and evolved stars

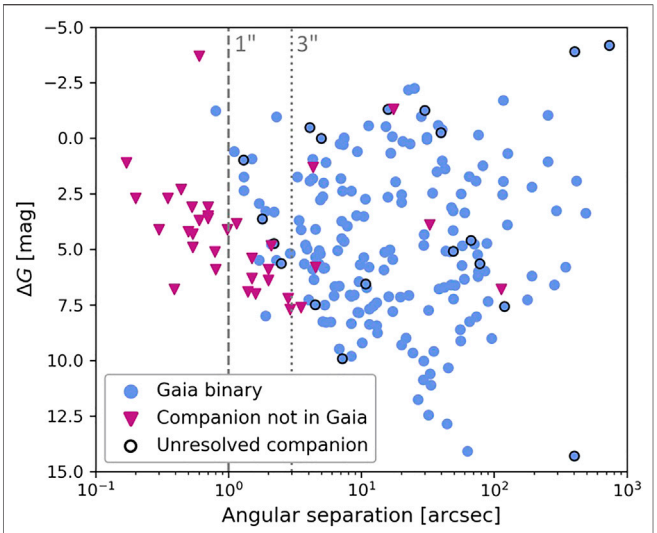

FIGURE 8 | Completeness of the *Gaia* DR2 binary search showing *G*-band magnitude differences against angular separations for all companions retrieved in *Gaia* (blue circles). Detected companions known to be themselves close binaries unresolved in*Gaia* are marked with black circles. Known companions not recovered in the *Gaia* DR2 catalog are shown in the magenta triangles, with plotted magnitude differences corresponding the lower limits in the *Gaia G*-band. The dashed and dotted gray lines show inner working angles of 1 arcsec and 3 arcsec, respectively.

(sub-giants, giants or white dwarfs), unless explicitly stated otherwise. We note however that only 28 of our stellar hosts (out of 938, i.e. < 3 %) are massive BA stars or white dwarfs, from which only 5 A stars were found to be in multiple systems (i.e. ~2 % of the binary sample). Excluding these systems would thus make little difference in the observed results and trends. While giants and sub-giants represent a more consequent fraction of the sample of host stars (~25 % of the FGK hosts), a sizable number of our host stars have no luminosity class (giant/sub-giant vs. main sequence) in the spectral types gathered from the considered exoplanet catalogs or Simbad (e.g. numerous Kepler/TESS/WASP targets). We are therefore not able to strictly discuss main sequence stars separately, and our conclusions include a range of stellar masses and a mixture of stellar evolutionary stages.

4.1 Stellar Mass Function and Multiplicity

Figure 3 shows the distribution of spectral types from our planet host sample, divided between those identified in visual binaries or multiples (magenta) and seemingly single stars (blue), and compared to the identified stellar companions (yellow). Absolute numbers are provided at the top of each bar. In addition, each color-coded histogram is normalized so that the sum of the bars in a given color add up to 1, i.e. the height of each bar on the y-axis gives the relative contribution from that spectral type toward to full considered sub-sample.

Comparing the single and binary stars from our planet hosts, the subset of binary hosts contains a larger relative fraction of massive A, F and G stars, with a smaller contribution from lower-mass K and M dwarfs, as demonstrated by the turnover in the relative heights of the magenta and blue bars from G to K spectral types. This is consistent with the well-known trend of decreasing binary rate with decreasing stellar mass, dropping from ~70% for B and A stars (Kouwenhoven et al., 2007) to around 50 % for Sun-like stars (Raghavan et al., 2010), and about 30% for M dwarfs (Janson et al., 2012; Ward-Duong et al., 2015; Winters et al., 2019). While our survey results were not corrected for incompleteness and additional binaries may be missing from our compilation (see Section 4.2), our ability to retrieve wide stellar companions for our sample can be assumed to be rather independent of the host spectral types. With raw binary fractions of 37.8 ± 6.5 %, 24.3 ± 2.6 %, 22.4 ± 2.7 % and 15.7 ± 3.1 % for F, G, K and M stars, respectively, these results thus suggest that the population of planet-bearing stars is representative of the relative multiplicity output of stellar formation across the stellar spectral sequence. However, without robust completeness corrections, we are not able to determine whether the differences between our observed raw fractions and overall stellar multiplicity rates are due to missing binaries in our samples or to the fact that stars hosting planets and brown dwarfs are truly less commonly found in binary-star systems.

The distribution of spectral types from companions, on the other hand, peaks strongly toward low-mass M dwarfs (yellow), which represented over 65% of our sample of stellar companions. In fact, this resembles closely the stellar initial mass function, with M dwarfs being the most abundant types of stars (Chabrier, 2003; Bochanski et al., 2010). This indicates that planet hosts in multiple systems are more often the most massive component of stellar binaries. The feature is partly due to a selection effect, as lower-mass stars are often too faint to be included in target samples for exoplanet campaigns (Eggenberger, 2010). Nonetheless, although Earth to Neptune-sized planets are more abundant around M dwarfs (Mulders et al., 2015), giant planet formation is thought to be more efficient around more massive stars (Mordasini, 2018), and giant planets are indeed observed to be more frequent around higher-mass stars (Bonfils et al., 2013; Vigan et al., 2020). Given that binary systems seem to preferentially host giant planets based on our results, it is not surprising that most planet hosts in multiple systems would be the most massive stellar component in these hierarchical systems.

4.2 Completeness and Survey Limitations

As mentioned previously, the (in)completeness of our multiplicity search was not accounted for in the results presented in Section 3, as corrections of observational biases are beyond the scope of this work. We may nonetheless look at the properties of our detected systems to understand what biases might lie in our gathered sample.

Figure 8 shows the angular separation and *Gaia G*-band magnitude difference for every visual companion, relative to the planet host star it is bound to. Blue circles represent companions successfully retrieved in *Gaia* DR2. Binary components which are themselves known to be unresolved binaries are marked with black rings. Magenta triangles correspond to companions known from the literature but undetected in *Gaia*. As a ΔG magnitude difference is unavailable for these systems, the plotted magnitudes

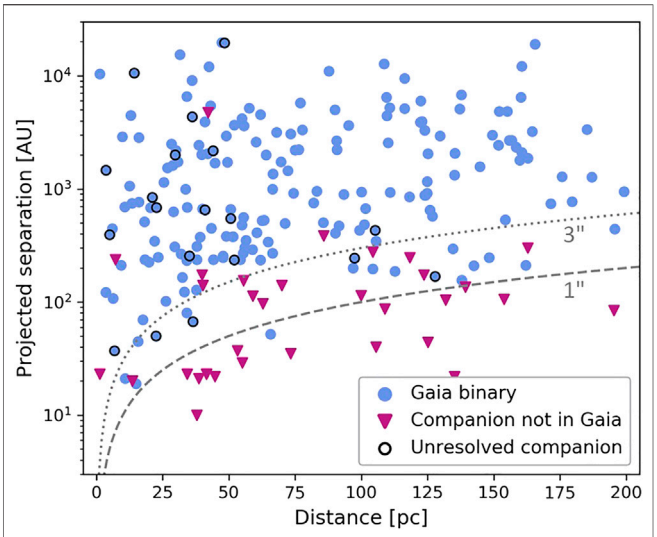

FIGURE 9 | Physical projected separations against distance all identified stellar companions, with the same symbols and color-codes as in **Figure 8**, highlighting the completeness of our *Gaia* binary search as a function of distance to the Sun. The dashed and dotted gray lines show inner working angles of 1 arcsec and 3 arcsec, respectively.

correspond to contrasts in various visual or infrared filters, and thus correspond to lower limits compared to the expected magnitude difference values in the *G*-band. Our observed recoverability for binaries is consistent with the estimated *Gaia* completeness to close binaries (Ziegler et al., 2018): near equal-brightness binaries ($\Delta G < 2$ mag) are consistently retrieved from separations of one arcsec (dashed line), binaries down to around $\Delta G = 6$ mag are typically recovered at separations of ~ three arcsec (dotted line), and wider systems are subject to *Gaia* DR2 completeness down to the limiting magnitude of $G \sim 21$ mag of the *Gaia* DR2 survey.

A significant number of known tight binaries with angular separation < 1 arcsec (magenta triangles) were not recovered in *Gaia*, only known thanks to high angular-resolution imaging campaigns. As only a small fraction of our hosts stars have been targeted by such dedicated imaging programs, these results indicate that additional unresolved sub-arcsecond systems may still be hidden among our exoplanet host sample. In particular, the 27 binaries for our sample with projected separations <100 AU have a median angular separation of 0.7 arcsec, and such systems are therefore for the most part not recoverable in *Gaia*. Studies like Kraus et al. (2016) or Furlan et al. (2017) have identified numerous optical candidate companions to Kepler hosts stars on small angular separations, but additional observational epochs are required to confirm or refute the bound nature of most of these candidates.

A shortfall of close binaries (<50–100 AU) among planet hosts has been vastly reported in observational surveys (Roell et al., 2012; Bergfors et al., 2013; Wang et al., 2014; Kraus et al., 2016; Moe and Kratter, 2019; Bonavita and Desidera, 2020). This feature is generally attributed to a hindrance of planet formation in very tight binaries, and is also predicted in theoretical models (Thebault and Haghighipour, 2015). However, our survey is highly incomplete out to separations of hundreds of AU and thus cannot be used to probe this feature. Indeed, the resolving limit of ~1–3 arcsec in our *Gaia* search corresponds to projected separations of 200–600 AU for the most distant stars in our study (200 pc). This effect is illustrated in of **Figure 9**, which plots the physical projected separation of all identified binaries as a function of distance from the Sun. Detection limits corresponding to inner working angles of one arcsec and three arcsec are marked with dashed and dotted lines, respectively. The figure clearly demonstrates that the range of probed binary separation is strongly affected by the distance to each star. Our compilation is only sensitive in *Gaia* to binary separations below 100 AU for targets out to 30 pc (~ 20 % of the sample), and only data from heterogeneous high-angular resolution programs have allowed the detection of such systems beyond 100 pc.

4.3 Impacts of Multiplicity on Exoplanets

4.3.1No Influence on Low-Mass Planets

We found that small planets with masses below 0.1 M_{Jup} have a significantly lower raw binary rate (16.6 ± 1.7 %) than more massive Jovian planets (25.5 ± 1.8 % for planets above 0.1 M_{Jup} throughout the brown dwarf mass range), an offset with a 3.6-σ significance. While these numbers certainly suffer from inherent and observational biases as discussed in Section 4.2, it is reasonable to assume that these biases do not affect hosts to different types of planets differently. Indeed, the transit and radial velocity surveys that yield the detection of these planets are partially subject to the same inherent selection biases as campaigns discovering more massive planets with the same methods. As a result, we consider that the observed trend of lower multiplicity fraction for sub-Jovian planets is a real feature. Furthermore, terrestrial and Neptunian planets are often found in tightly-packed multiple-planet systems (Mayor et al., 2011). The fact that such planets are less frequently seen in hierarchical star systems is thus also consistent with the observation that multi-planet systems are less commonly found in stellar binaries.

These results, however, may be a direct consequence of the lower binary frequency of M dwarfs compared to more massive stars. Since low-mass M stars host ~2–3 times more close, small planets than Sun-like stars (Howard et al., 2012; Mulders et al., 2015), and rarely harbor giant planets (Bonfils et al., 2013), the majority of small sub-Jovian planets and high-order multi-planet systems are therefore found around M dwarfs. The intrinsic lower stellar multiplicity rate of M dwarf could hence be responsible, at least partly, for the observed trends. Nonetheless, Moe and Kratter (2019) found that the biases from stellar companions against the detection of planets are higher for F and G stars than M dwarfs. This trend is rooted on the suppression of planet formation in close binaries and bright stellar companions preventing transit detections. This suggests that the observed differences in raw binary fractions between sub-Jovian and giant systems planet systems would likely be increased after accounting for these biases, and we conclude that low-mass planets and tightly-packed systems with multiple small planets are truly less commonly found in hierarchical stellar systems.

4.3.2 The Excess of Massive Close-In Planets and Brown Dwarfs in Binaries

The substantial prevalence of short-orbit massive planets and brown dwarfs around members of binary stars was first noted by Zucker and Mazeh (2002), and later confirmed by numerous observational studies (Eggenberger et al., 2004; Mugrauer et al., 2007b; Desidera and Barbieri, 2007). More recently, the Friends of Hot Jupiters survey reported an enhancement of binary frequency for stars hosting hot Jupiters, with a binary rate 3 times higher that for field stars over the separation range 50–2,000 AU (Ngo et al., 2016). Fontanive et al. (2019) established the continuity of this trend to the most massive giant planets and brown dwarfs (>7 M_{Jup}) found within ~1 AU, constraining the binary frequency of such systems to be around 80 % between 20 and 10,000 AU, a result further validated statistically in Moe and Kratter (2019). Results from these studies demonstrate that stellar companions play an important role in the formation and/or evolution of these rare planetary systems. These findings also suggest that the influence of binary companions is strengthened for higher-mass close-in exoplanets and sub-stellar companions, and that this effect may be magnified for sub-stellar companions on even tighter orbits.

While the work presented here did not allow us to place any such frequency constraints, the intrinsic tendencies with planet mass and separation observed in previous studies are confirmed in our compilation. Indeed, we observed a larger relative fraction of Jovian planets in binaries within 0.5 AU than for the bulk of the Jovian planet population around the snow line (~1–5 AU). This relative frequency was found to further increase when focusing exclusively on the most massive planets and brown dwarfs. These trends suggest that stellar multiplicity affects the orbital separation of massive giant planets. The presence of an outer wide companion would hence allow for the inner sub-stellar companion to reach closer-in semi-major axes than planets of similar masses orbiting single stars, onto an orbital separation regime where essentially no planets around single stars are observed (Fontanive et al., 2019).

The influence from outer stellar companions shows a possible dependence on binary separations. Stellar companions on separations of the order of thousands of AU seem to have no significant effect on the demographics of planetary systems, with similar distributions observed between the masses and semi-major axes of planets and brown dwarfs in such binaries and around single stars. In contrast, the most massive, close-in giant planets and brown dwarfs in binaries, in the most extreme planetary configurations, are all in rather tight binaries, with separations of tens to a few hundreds of AU compared to a mean ~600 AU for the full binary sample (likely a direct consequence of uncorrected incompleteness biases as discussed in Sections 4.2 and 4.3.4). This is consistent with the observed peak in binary separation from Fontanive et al. (2019) for such systems (~250 AU), and further supports the idea that additional binaries may remain undiscovered in our probed sample on this separation range.

On the other hand, no robust dependence of binary influence on stellar companion mass was seen in our results. This is not surprising since the gravitational pull from a companion scales with M_c/ρ_{bin}^2 (where M_c is the companion mass and ρ_{bin} the binary separation). As the companion masses span a range of about one order of magnitude, compared to over three orders of magnitude for the separation (which is then squared), binary separation is thus expected from physical arguments to have larger impact on the circumstellar planetary system.

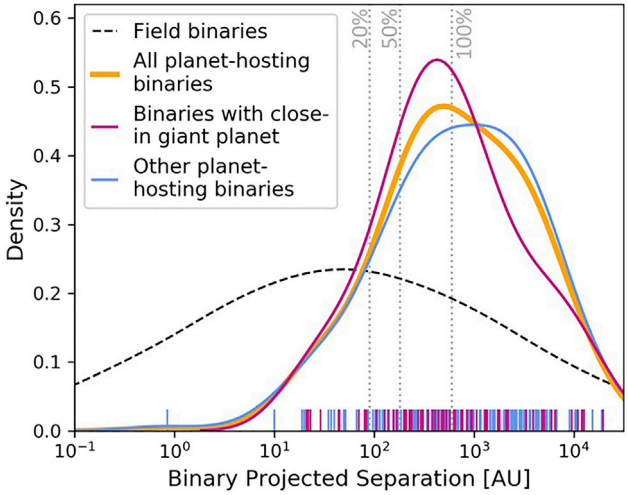

FIGURE 10 | Binary separation distribution comparing the full sample of planet-hosting binaries (thick blue line) to stellar binaries in the Solar-neighborhood (dashed black line) from Raghavan et al. (2010). The sample of planet-bearing multiples is further divided between systems hosting a giant planet of mass > 0.1 M_{Jup} within 0.5 AU (magenta) and all other systems (yellow). Multi-planet systems with planets falling into the two planetary categories are counted toward the close-in giant planet subset. Planet host stars in close binaries with an outer tertiary companion are plotted as the inner binary only. Triple systems composed of a planet host and a wide tighter binary are counted as a binary system using the mean separation to the distant sub-system. The dashed vertical gray lines show the projected separations probed for the closest 20, 50 and 100% of our sample for angular separations of 3 arcsec.

4.3.3 Very Close Binaries in Triple Systems

The vast majority of main sequence stars in spectroscopic binaries are known to be the inner binaries of hierarchical triple systems. Tokovinin et al. (2006) demonstrated that 96% of binaries with orbital periods below ~3 days have tertiary stellar companions. The occurrence of outer components for these systems is found to steadily decrease with inner binary period, falling to a rate of 34% triple systems for spectroscopic binaries with periods of 12–30 days. The excess of tertiary companions has been argued (Fabrycky and Tremaine, 2007; Naoz and Fabrycky, 2014) to allow for the migration of the inner companions via Kozai-Lidov oscillations in misaligned triples (Kozai, 1962; Lidov, 1962). Alternatively, these close binary companions have been suggested to form via disk fragmentation and migration within the circumstellar disk of the primary star (Moe and Kratter, 2018). The substantial mass required to form and drive inward such massive inner companions can simultaneously form additional tertiary companions, leading to

such systems being often in triple-star configurations. These outer components could then allow for more extreme migrations of the inner companions, leading to the observed negative correlation between inner binary period and triple architecture frequency (Moe and Kratter, 2019).

Fontanive et al. (2019) studied hosts to close giant planets and brown dwarf companions with masses of 7–60 M_{Jup}, inferring a tertiary companion fraction comparatively high to the spectroscopic binaries from Tokovinin et al. (2006). This population of sub-stellar companions corresponds to the most massive, short-separation systems found to be predominantly in hierarchical stellar structures in this work. Moe and Kratter (2019) further confirmed this excess of triple occurrence rate to be a statistical, real feature, as well as to be measurably higher than for genuine hot Jupiters (<4 M_{Jup}) surveyed by Ngo et al. (2016). The similar demographics between these brown dwarf desert systems and stellar spectroscopic binaries argues for a common origin for the inner companions from Tokovinin et al. (2006) and Fontanive et al. (2019), indicating that these inner giant planet and brown dwarf companions extent the population of triple stellar systems to sub-stellar masses for the secondary components of the inner binaries.

4.3.4 The Effect of Binary Separation

In **Figure 10**, we compare the distributions in projected separation of the planet-hosting wide binaries (solid yellow line) gathered in this work, and the Solar-type field binaries (dashed black line) from Raghavan et al. (2010). For multi-planet systems with planets or brown dwarfs falling into the two planetary categories considered (55 Cancri, HD 38529 A, Upsilon Andromedae A, WASP-8), we count the binaries only once, toward the close-in giant planet subset. Triple systems are accounted for in the same way as in Section 3.3.

The binary separations of the planet-bearing systems appears to peak at significantly larger values, with a peak around 600 AU compared to ~50 AU for field binaries. Field binaries also show a much broader distribution, with a log-width of 1.70 compared to 0.75 for planet-hosting multiples. A Kolmogorov-Smirnov test confirms that the raw observed distributions are indeed statistically different, with a p-value for the null hypothesis that they are drawn from the same distribution $< 10^{-5}$. These differences are primarily due to the incompleteness of our compilation on short binary separations as discussed in Section 4.2. Furthermore, the field binaries from Raghavan et al. (2010) include unresolved companions detected by spectroscopic techniques or proper motion accelerations. Such systems are not detectable with visual detection methods and a number of such tighter binaries could remain undetected in our studied sample.

The dashed lines in **Figure 10** show the projected separations probed for the closest 20%, 50% and 100% of our sample with angular separations of 3 arcsec, our adopted completeness limit for *Gaia*. Our observed peak in the separation distribution (600 pc) roughly coincides with our inner completeness limit for the full sample (see Section 4.2). This strongly suggests that a number of undiscovered binaries with separations of tens to hundreds of AU may still lie in our sample. For example, the planet host stars DMPP-3 A and HD 59686 from our exoplanet compilation were both found through significant radial velocity trends to have close stellar companions at 1.22 AU (Barnes et al., 2020) and 13.56 AU (Ortiz et al., 2016), respectively. These companions have never been resolved to this date, and these systems were thus counted as single in the context of this work, which only considered visual, astrometrically-confirmed systems. Current high-angular resolution efforts and complementary detection methods, probing smaller binary separation ranges, must thus be pursued to obtain a more complete picture of the multiplicity of exoplanet host stars, and understand the true effect of tight binary companions on the formation and evolution of extra-solar planets and brown dwarf companions.

Figure 10 also shows the distribution of binary separation, dividing the sample between binaries hosting a giant planet or brown dwarf within 0.5 AU (magenta) and the all other systems (blue). The sample of binaries hosting a short-period gas giant appears to be on somewhat smaller binary separations than the remaining planet-hosting multiples, with logarithmic means shifting from ~ 500 AU to ~700 AU between the two samples, and a slightly tighter distribution for the former subset. This is representative of our results from Section 3.3, which showed an enhanced relative fraction of shorter-separation binaries for systems with close-in planets, an effect that is further magnified for the most massive planets and brown dwarfs on very tight orbits. These results are in agreement with previous observations (Desidera and Barbieri, 2007) that found massive planets in short period orbits to be in most cases around the components of rather tight binaries. Finally, the larger relative number of very wide binaries (>1000 AU) for hosts to lower-mass and larger-separation planets is also consistent with the rest of our results. We indeed found that such widely-separated binaries generally do not impact the planet properties (see **Figure 6**), and observed small and wide-orbit planets to not be significantly affected by the presence of stellar companions, compatible with the idea that most such planets are only found in very wide binaries or around single stars. Desidera and Barbieri (2007) similarly concluded that the properties of exoplanets orbiting components of very wide binaries are compatible with those of planets orbiting single stars.

4.4 Implications for Formation Mechanisms

The final architectures of planetary systems around members of binary stars strongly depend on how the presence of a close massive body impacts standard formation and migration processes, through its efficiency to alter the local disk environment, accretion rates, or tidal interactions between planets and the host star. The population trends highlighted throughout this study might provide new clues and insights into the effects of stellar companions on planet and brown dwarf formation and evolution.

Our findings show that binarity has little effect on the distributions of planet mass and semi-major axis for the population of sub-Jovian planets found inside ~1 AU. The impact of stellar duplicity on short binary separations (<50 AU) remains to be fully understood theoretically and better constrained observationally, as such very tight binaries would be more amenable to influence disks inner regions crucial for small planet formation and stable orbital behaviors.

Nonetheless, our results demonstrate that sub-Jovian planets that form in binaries with separations of hundreds of AU are consistent with the population of single-star planets. This suggests that stellar multiplicity does not need to be extensively accounted for in order to reproduce the core of this population of small planets, either completely inhibiting the formation or survival of such planets, or having no visible effect on the demographics of successfully formed planets.

In contrast, we found that the populations of intermediate-mass giant planets (M_{pl} = 0.1–7 M_{Jup}) and high-mass sub-stellar companions ($M_{pl} > 7\ M_{Jup}$) show different statistical properties between single-star systems and hosts with stellar companions. Small-separation planets and brown dwarf companions within the snow line (<1–3 AU) were found to have somewhat larger masses and/or tighter separations when in binary stars. This trend is enhanced for the most massive and closest-separation sub-stellar companions, that also have inflated raw stellar multiplicity rates compared to lower-mass and wider planets, consistent with previous studies (Fontanive et al., 2019; Moe and Kratter, 2019). This strongly indicates that the identified stellar binary companions likely affect the formation and/or migration of these massive sub-stellar objects, either allowing for more massive planets to exist at similar separations than planets around single stars, or enabling similar-mass planets to form or migrate to shorter semi-major axes in stellar binaries.

Understanding the true nature and extend of these effects is a challenging task. Unfortunately, available data provide little insight at this stage into the details of the possible underlying processes, with few prospects to disentangle between planetary formation and evolution, and missing information about most orbital elements for binary orbits. Likewise, modeling the formation and evolution of planets in binaries requires to explore a very wide parameter space, including binary separations, mass ratios, inclinations and eccentricities. The large variety of possible binary configurations likely impacts the existence and properties of planetary systems differently for each combination of these key binary parameters, from detrimental to perturbing or even favorable effects.

For circumstellar planets, which represent the focus of this study, a nearby stellar companion is expected to primarily affect the outer parts of typical planet formation locations, where the gravitational influence from the stellar companions will be enhanced. The outskirts of protoplanetary disks are believed to predominantly harbor more massive planets, with mostly rare, cold Jovian planets predicted beyond a few tens of AU in the core accretion paradigm (Emsenhuber et al., 2020), and the formation of massive planets and brown dwarfs by gravitational disk fragmentation occurring preferentially in the cool outer regions of disks, from separations of several tens to hundreds of AU (Rafikov, 2005; Hall et al., 2017). Following this reasoning, giant planets and brown dwarfs forming at large orbital separations are thus more likely to be affected by the presence of an outer star in the system than small planets forming and accreting within a few AU from the host star. The observed population of wide-orbit (>10 AU) planets and brown dwarfs was found to have a lower raw binary rate than similar-mass sub-stellar companions on shorter orbits, and no significant differences were observed in planetary properties between single and multiple-star systems. The effect from outer companion stars would thus likely be in facilitating inward migration processes, bringing massive giant planets and brown dwarfs onto extremely tight orbits typically unreachable in single-star environments, via e.g. the Kozai-Lidov mechanism (Winn et al., 2010; Naoz and Fabrycky, 2014) or other triggered dynamical perturbations.

Alternately, binarity could impact separate planet formation channels differently, i.e., influencing the conditions for gravitational disk instability, but with little effect on the results of core accretion mechanisms if they proceed, thus affecting the very most massive planets and brown dwarfs only. For example, the presence of a nearby companion star within ~100–300 AU could tidally truncate protoplanetary disks (Kraus et al., 2012) and lead to faster disk dissipation rates (Müller and Kley, 2012). This effect would be particularly problematic for giant planet formation by core accretion, which requires significantly longer timescales to operate than disk fragmentation. Formation by core accretion would therefore only take place if the outer companion has little effect on the disk and forming planetary system, thus not significantly impacting the final planet properties compared to single star conditions. Similarly, binary companions have been suggested to be able to trigger instabilities in otherwise stable disks (Boss, 2006), hence favorably modifying formation environments for *in-situ* disk fragmentation, but inconsequential for core accretion. This idea is reconcilable with the high masses of the outlying population of sub-stellar companions observed to be predominantly in binaries, which seemingly formed differently from the population of lower-mass planets on similar orbits, most likely through gravitational disk fragmentation (Moe and Kratter, 2019).

Finally, our results regarding the separation distribution of binaries might help to narrow down the effect of at least one binary parameter. As mentioned previously, there is reliable observational evidence that close binarity (<50 AU) hinders planet formation around a host star (Wang et al., 2014; Kraus et al., 2016; Fontanive et al., 2019), although this feature could not be robustly investigated in the present work. We also found stellar multiplicity of very large separations (thousands of AU) to have no significant impact on observed planetary populations, suggesting that planet formation and evolutionary patterns in such systems behave similarly as around single stars. Intermediate separations, from several tens to a few hundreds of AU, therefore appear to be a key region of the parameter space to explore in order to further our perspective of exoplanets in stellar binaries. Examinations of physical quantities in these systems such as binding energy may be especially interesting to study for a better physical understanding of the processes in play, and we particularly advocate for investigations to be conducted in the theoretical context of gravitational disk instability based on our results.

5 SUMMARY

In this work, we have compiled a sample of 938 stars hosting a total of 1,316 extra-solar planets and brown dwarf companions, out to 200 pc. We searched for visual co-moving companions to

these systems via an extensive search in the literature and using the *Gaia* DR2 catalog to identify common proper motion sources. This analysis yielded a total of 218 planet hosts in multiple-star systems, including 186 binaries and 32 hierarchical triple systems, with 10 newly-discovered binary companions and 2 new tertiary components. From these, 4 binaries and 1 triple system contain 2 planet-bearing stars. Stellar companions have masses ranging from the brown dwarf/star boundary at 0.07 $M_{\odot}$ up to 2.27 $M_{\odot}$, with separations ranging from <1 AU to 20,000 AU with a median of ~600 AU.

Investigating our gathered sample of binaries, we found that:

1) More massive planet hosts are more often part of multiple-star systems, consistent with the population of planet-bearing stars following the overall relative multiplicity outcome of stellar formation.
2) Planet hosts in multiple systems were also predominantly observed to be the most massive component of stellar binaries.
3) A total of 27 binary systems have separations <100 AU, from which 20 have binary separations smaller than 50 AU, with 1 system in an extreme <1 AU configuration. Most of these close binaries, however, were only identified thanks to dedicated high-angular resolution campaigns, and could not, for the most part, be retrieved with the resolving limit of *Gaia* (1–3 arcsec), in particular for the most distant targets in our sample.
4) As only a small fraction of planet hosts have been targeted by such imaging programs, a significant number of sub-arcsecond binaries and companions on separations of a few arcseconds could still be missing from our catalog, further supported by the concurrence of our measured peak in binary separation and our estimated *Gaia* completeness limit.

Assuming that the selection and observational biases lying in and limiting our gathered compilation of stellar binaries affect various subsets of planetary populations and planet hosts in a reasonably homogeneous way, we investigated possible correlations between planet properties and the existence and properties of outer stellar companions. Our main results are:

1) From our identified sample of binary companions, we measured a raw multiplicity rate of 23.2 ± 1.6 % for planet hosts.
2) Multi-planet systems were found to have a somewhat lower stellar duplicity frequency (18.0 ± 2.7 %) compared to single-planet systems (25.1 ± 1.9 %) with a 2.2-σ significance.
3) Dividing the planet parameter space into various sub-populations, we found that giant planets and brown dwarfs with masses above 0.1 M_{Jup} have a substantially larger (3.6-σ) raw stellar multiplicity fraction (25.5 ± 1.8 %) than lower-mass planets (16.6 ± 1.7 %), consistent with the fact that these small sub-Jovian planets are typically organized in tightly-packed multi-planet systems.
4) This trend appears to further increase up to about ~30% for massive planet and brown dwarfs ($M_{pl} > 7\ M_{Jup}$) on very short orbital separations ($a_{pl} < 0.5$ AU), with the most massive and shortest-period sub-stellar companions almost exclusively observed in multiple-star systems. These results are consistent with previous studies of these populations (Fontanive et al., 2019; Moe and Kratter, 2019), which appear to follow the architectures of stellar spectroscopic binaries, systematically observed as part of hierarchical triple systems (Tokovinin et al., 2006).

In terms of planet properties, our results suggest that:

1) Stellar duplicity has no significant effect on the demographics of low-mass planets ($M_{pl} < 0.1\ M_{Jup}$) or the core population of warm giant exoplanets on separations neighboring the snow line ($a_{pl} > 0.5$ AU).
2) Only high-mass, small-separation planets were observed to have different distributions of planet properties between the subset of planets in binaries and single-star systems, with an over-density of planets and brown dwarfs of several Jupiter masses found on semi-major axes of ~0.01–0.1 AU identified in multiple-star systems.
3) These extreme planetary systems with few or no single-star analogues were predominantly found to be in rather tight binary configurations <1000 AU, and mostly on separations <250 AU for sub-stellar companions with masses >7 M_{Jup}. These systems represent a sizable fraction of such tight binaries in our compilation (~10%), despite the rarity of these planets and brown dwarfs in our overall exoplanet catalog (~2%).
4) In contrast, the subset of these planets in binaries with separations >1000 AU showed similar distributions in mass and semi-major axis to planets and brown dwarfs orbiting single stars. This indicates that short (<250 AU) or intermediate-separation (<1000 AU) binaries play a role the formation or evolution of these massive planets and brown dwarfs, but that very wide binaries do not influence the architectures of planetary systems.
5) Binary companion mass, on the other hand, was found to have no significant effect on planetary properties.

Between the upcoming generation of telescopes and future *Gaia* data releases, the next decade promises to lead to unprecedented discoveries and new characterization possibilities. These findings will arguably yield unparalleled information and new robust constraints on system architectures and population demographics, which will in turn provide key probes into formation histories and dynamical evolution processes. We hope that the gathered compilation of exoplanets in visual binaries will be useful to future studies in this constantly-growing research area, and will motivate the need to pursue existing campaigns searching for small-separation binary companions to known planetary systems. With a more comprehensive picture of stellar multiplicity on the separation ranges demonstrated here to remain highly incomplete, we will be able to confirm and better understand the tentative trends highlighted in this paper, and improve our fundamental understanding of stellar, sub-stellar and planetary formation and evolution.

DATA AVAILABILITY STATEMENT

The catalogs presented in this study are included in the article/ supplementary files. The compilations are also made publicly

available online at https://docs.google.com/spreadsheets/d/11b29RREm_rTWcpUGvh7M_-wOQgH8aTiyoxDPHieqXBo/edit?usp=sharing, in a catalog that we plan update regularly.

AUTHOR CONTRIBUTIONS

CF led this study, performing the catalog compilations and binary searches and leading the data analyses. DBG contributed to the search for trends within the obtained catalogs, scientific interpretation of results, and writing of the paper.

FUNDING

CF acknowledges support from the Center for Space and Habitability (CSH). This work has been carried out within the framework of the NCCR PlanetS supported by the Swiss National Science Foundation. DG acknowledges support from the NASA ADAP award No. 80NSSC19K0532.

ACKNOWLEDGMENTS

This research has made use of the NASA Exoplanet Archive, which is operated by the California Institute of Technology, under contract with the National Aeronautics and Space Administration under the Exoplanet Exploration Program. This research has made use of the Exoplanet Orbit Database and the Exoplanet Data Explorer at exoplanets.org. This work has made use of data from the European Space Agency (ESA) mission *Gaia* (https://www.cosmos.esa.int/gaia), processed by the *Gaia* Data Processing and Analysis Consortium (DPAC, https://www.cosmos.esa.int/web/gaia/dpac/consortium). This research has made use of the SIMBAD database and the VizieR catalogue access tool, operated at CDS, Strasbourg, France.

SUPPLEMENTARY MATERIAL

The Supplementary Material for this article can be found online at: https://www.frontiersin.org/articles/10.3389/fspas.2021.625250/full#supplementary-material.

REFERENCES

Adams, E. R., Ciardi, D. R., Dupree, A. K., Gautier, T. N., Kulesa, C., McCarthy, D., et al. (2012). Adaptive optics images ofkeplerobjects of interest. *AJ* 144, 42. doi:10.1088/0004-6256/144/2/42

Adams, E. R., Dupree, A. K., Kulesa, C., and McCarthy, D. (2013). Adaptive optics images. Ii. 12Keplerobjects of interest and 15 confirmed transiting planets. *AJ* 146, 9. doi:10.1088/0004-6256/146/1/9

Artymowicz, P., and Lubow, S. H. (1994). Dynamics of binary-disk interaction. 1: resonances and disk gap sizes. *APJ* 421, 651. doi:10.1086/173679

Asensio-Torres, R., Janson, M., Bonavita, M., Desidera, S., Thalmann, C., Kuzuhara, M., et al. (2018). SPOTS: the search for planets orbiting two stars. *A&A* 619, A43. doi:10.1051/0004-6361/201833349

Barnes, J. R., Haswell, C. A., Staab, D., Anglada-Escudé, G., Fossati, L., Doherty, J. P. J., et al. (2020). An ablating 2.6 M⊕ planet in an eccentric binary from the Dispersed Matter Planet Project. *Nat. Astron.* 4, 419–426. doi:10.1038/s41550-019-0972-z

Bate, M. R., and Bonnell, I. A. (1997). Accretion during binary star formation--II. Gaseous accretion and disc formation. *MNRAS* 285, 33–48. doi:10.1093/mnras/285.1.33

Bergfors, C., Brandner, W., Daemgen, S., Biller, B., Hippler, S., Janson, M., et al. (2013). Stellar companions to exoplanet host stars: lucky Imaging of transiting planet hosts★. *MNRAS* 428, 182–189. doi:10.1093/mnras/sts019

Bochanski, J. J., Hawley, S. L., Covey, K. R., West, A. A., Reid, I. N., Golimowski, D. A., et al. (2010). The luminosity and mass functions of low-mass stars in the galactic disk. II. The field. *AJ* 139, 2679–2699. doi:10.1088/0004-6256/139/6/2679

Bohn, A. J., Southworth, J., Ginski, C., Kenworthy, M. A., Maxted, P. F. L., and Evans, D. F. (2020). A multiplicity study of transiting exoplanet host stars. *A&A* 635, A73. doi:10.1051/0004-6361/201937127

Bonavita, M., and Desidera, S. (2007). The frequency of planets in multiple systems. *A&A* 468, 721–729. doi:10.1051/0004-6361:20066671

Bonavita, M., and Desidera, S. (2020). Frequency of planets in binaries. *Galaxies* 8, 16. doi:10.3390/galaxies8010016

Bonfils, X., Delfosse, X., Udry, S., Forveille, T., Mayor, M., Perrier, C., et al. (2013). The HARPS search for southern extra-solar planets. *A&A* 549, A109. doi:10.1051/0004-6361/201014704

Bouchy, A. P. (2006). Gas giant protoplanets formed by disk instability in binary star systems. *APJ* 641, 1148–1161. doi:10.1086/500530

Chabrier, G. (2003). Galactic stellar and substellar initial mass function. *Publ. Astron. Soc. Pac.* 115, 763–795. doi:10.1086/376392

Coker, C. T., Gaudi, B. S., Pogge, R. W., and Horch, E. (2018). A search for binary star companions to the KELT planet hosts and a comparison sample. I. Results of DSSI observations. *AJ* 155, 27. doi:10.3847/1538-3881/aa9f0e

Colton, N. M., Horch, E. P., Everett, M. E., Howell, S. B., Davidson, J., James, W., et al. (2021). Identifying bound stellar companions to kepler exoplanet host stars using speckle imaging. *AJ* 161, 21. doi:10.3847/1538-3881/abc9af

Cumming, A., Butler, R. P., Marcy, G. W., Vogt, S. S., Wright, J. T., and Fischer, D. A. (2008). The keck planet search: detectability and the minimum mass and orbital period distribution of extrasolar planets. *Publ. Astron. Soc. Pac.* 120, 531. doi:10.1086/588487

Daemgen, S., Hormuth, F., Brandner, W., Bergfors, C., Janson, M., Hippler, S., et al. (2009). Binarity of transit host stars. *A&A* 498, 567–574. doi:10.1051/0004-6361/200810988

Deacon, N. R., Liu, M. C., Magnier, E. A., Aller, K. M., Best, W. M. J., Dupuy, T., et al. (2014). Wide cool and ultracool companions to nearby stars from pan-STARRS 1. *APJ* 792, 119. doi:10.1088/0004-637X/792/2/119

Deacon, N. R., Kraus, A. L., Mann, A. W., Magnier, E. A., Chambers, K. C., Wainscoat, R. J., et al. (2016). A Pan-STARRS 1 study of the relationship between wide binarity and planet occurrence in theKeplerfield. *Mon. Not. R. Astron. Soc.* 455, 4212–4230. doi:10.1093/mnras/stv2132

Desidera, S., and Barbieri, M. (2007). Properties Properties of planets in binary systems. *A&A* 462, 345–353. doi:10.1051/0004-6361:20066319

Dietrich, J., and Ginski, C. (2018). Archival VLT/NaCo multiplicity investigation of exoplanet host stars. *A&A* 620, A102. doi:10.1051/0004-6361/201731341

Dommanget, J., and Nys, O. (2002). *VizieR online data catalog: CCDM (catalog of components of double & multiple stars) (Dommanget+ 2002)*: VizieR Online Data Catalog, I/274. Available at: https://ui.adsabs.harvard.edu/abs/2002yCat.1274....0D/abstract

Doyle, L. R., Carter, J. A., Fabrycky, D. C., Slawson, R. W., Howell, S. B., Winn, J. N., et al. (2011). Kepler-16: a transiting circumbinary planet. *Science* 333, 1602. doi:10.1126/science.1210923

Eggenberger, A., and Udry, S. (2007). Probing the impact of stellar duplicity on planet occurrence with spectroscopic and imaging observations. arXiv e-prints arXiv:0705.3173.

Eggenberger, A., Udry, S., and Mayor, M. (2004). Statistical properties of exoplanets. *A&A* 417, 353–360. doi:10.1051/0004-6361:20034164

Eggenberger, A., Udry, S., Chauvin, G., Beuzit, J. L., Lagrange, A. M., Ségransan, D., et al. (2007). The impact of stellar duplicity on planet occurrence and properties. *A&A* 474, 273–291. doi:10.1051/0004-6361:20077447

Eggenberger, A., Udry, S., Chauvin, G., Forveille, T., Beuzit, J.-L., Lagrange, A.-M., et al. (2011). "Probing the impact of stellar duplicity on the frequency of giant

planets: final results of our VLT/NACO survey," in *The astrophysics of planetary systems: formation, structure, and dynamical evolution*. Editors A. Sozzetti, M. G. Lattanzi, and A. P. Boss (Vienna, Austria: IAU Symposium), Vol. 276, 409–410. doi:10.1017/S1743921311020564

Eggenberger, A. (2010). "Detection and characterization of planets in binary and multiple systems," in *EAS publications series*. Editors K. Gożdziewski, A. Niedzielski, and J. Schneider Vol. 42 (Les Ulis (France): EAS Publications Series), 19–37. doi:10.1051/eas/1042002

Emsenhuber, A., Mordasini, C., Burn, R., Alibert, Y., Benz, W., and Asphaug, E. (2020). The New Generation Planetary Population Synthesis (NGPPS). II. Planetary population of solar-like stars and overview of statistical results. arXiv e-prints arXiv:2007.05562.

Everett, M. E., Barclay, T., Ciardi, D. R., Horch, E. P., Howell, S. B., Crepp, J. R., et al. (2015). High-resolution multi-band imaging for validation and characterization of smallkeplerplanets. *AJ* 149, 55. doi:10.1088/0004-6256/149/2/55

Fabricius, C., Hog, E., Makarov, V. V., Mason, B. D., Wycoff, G. L., and Urban, S. E. (2002). *VizieR online data catalog: A&A* 384, 180. doi:10.1051/0004-6361:20011822

Fabrycky, D., and Tremaine, S. (2007). Shrinking binary and planetary orbits by Kozai cycles with tidal friction. *APJ* 669, 1298–1315. doi:10.1086/521702

Faedi, F., Staley, T., Gómez Maqueo Chew, Y., Pollacco, D., Dhital, S., Barros, S. C. C., et al. (2013). Lucky imaging of transiting planet host stars with LuckyCam. *MNRAS* 433, 2097–2106. doi:10.1093/mnras/stt885

Fontanive, C., Rice, K., Bonavita, M., Lopez, E., Mužić, K., et al. (2019). A high binary fraction for the most massive close-in giant planets and brown dwarf desert members. *MNRAS* 485, 4967–4996. doi:10.1093/mnras/stz671

Furlan, E., Ciardi, D. R., Everett, M. E., Saylors, M., Teske, J. K., Horch, E. P., et al. (2017). Thekeplerfollow-up observation program. I. A catalog of companions tokeplerstars from high-resolution imaging. *AJ* 153, 71. doi:10.3847/1538-3881/153/2/71

Gaia CollaborationPrusti, T., de Bruijne, J. H. J., Brown, A. G. A., Vallenari, A., Babusiaux, C., et al. (2016). The Gaia mission. *A&A* 595, A1. doi:10.1051/0004-6361/201629272

Gaia CollaborationBrown, A. G. A., Vallenari, A., Prusti, T., de Bruijne, J. H. J., Babusiaux, C., et al. (2018). Gaia Data Release 2. Summary of the contents and survey properties. *A&A* 616, A1. doi:10.1051/0004-6361/201833051

Gentile Fusillo, N. P., Tremblay, P.-E., Gänsicke, B. T., Manser, C. J., Cunningham, T., Cukanovaite, E., et al. (2019). A Gaia Data Release 2 catalogue of white dwarfs and a comparison with SDSS. *MNRAS* 482, 4570–4591. doi:10.1093/mnras/sty3016

Ginski, C., Mugrauer, M., Seeliger, M., and Eisenbeiss, T. (2012). A lucky imaging multiplicity study of exoplanet host stars. *MNRAS* 421, 2498–2509. doi:10.1111/j.1365-2966.2012.20485.x

Ginski, C., Mugrauer, M., Seeliger, M., Buder, S., Errmann, R., Avenhaus, H., et al. (2016). A lucky imaging multiplicity study of exoplanet host stars - II. *Mon. Not. R. Astron. Soc.* 457, 2173–2191. doi:10.1093/mnras/stw049

Ginski, C., Mugrauer, M., Adam, C., Vogt, N., and van Holstein, R. (2020). How many suns are in the sky? A SPHERE multiplicity survey of exoplanet host stars I–Four new close stellar companions including a white dwarf. arXiv e-prints arXiv:2009.10363.

Hagelberg, J., Engler, N., Fontanive, C., Daemgen, S., Quanz, S. P., Kühn, J., et al. (2020). VIBES: visual binary exoplanet survey with SPHERE. *A&A* 643, A98. doi:10.1051/0004-6361/202039173

Hall, C., Forgan, D., and Rice, K. (2017). Identifying and analysing protostellar disc fragments in smoothed particle hydrodynamics simulations. *MNRAS* 470, 2517–2538. doi:10.1093/mnras/stx1244

Han, E., Wang, S. X., Wright, J. T., Feng, Y. K., Zhao, M., Fakhouri, O., et al. (2014). Exoplanet orbit database. II. Updates to Exoplanets.org. *Publications Astronomical Soc. Pac.* 126, 827. doi:10.1086/678447

Hatzes, A. P., Cochran, W. D., Endl, M., McArthur, B., Paulson, D. B., Walker, G. A. H., et al. (2003). A planetary companion to γ cephei A. *APJ* 599, 1383–1394. doi:10.1086/379281

Hirsch, L. A., Ciardi, D. R., Howard, A. W., Everett, M. E., Furlan, E., Saylors, M., et al. (2017). Assessing the effect of stellar companions from high-resolution imaging of kepler objects of interest. *AJ* 153, 117. doi:10.3847/1538-3881/153/3/117

Horch, E. P., Howell, S. B., Everett, M. E., and Ciardi, D. R. (2014). Most sub-arcsecond companions ofkeplerexoplanet candidate host stars are gravitationally bound. *APJ* 795, 60. doi:10.1088/0004-637X/795/1/60

Howard, A. W., Marcy, G. W., Bryson, S. T., Jenkins, J. M., Rowe, J. F., Batalha, N. M., et al. (2012). Planet occurrence within 0.25 AU of solar-type stars from kepler. *APJS* 201, 15. doi:10.1088/0067-0049/201/2/15

Janson, M., Hormuth, F., Bergfors, C., Brand ner, W., Hippler, S., Daemgen, S., et al. (2012). The AstraLux large M-dwarf multiplicity survey. *APJ* 754, 44. doi:10.1088/0004-637X/754/1/44

Janson, M., Bergfors, C., Brandner, W., Kudryavtseva, N., Hormuth, F., Hippler, S., et al. (2014). The AstraLux multiplicity survey: extension to late M-dwarfs. *APJ* 789, 102. doi:10.1088/0004-637X/789/2/102

Janson, M., Durkan, S., Hippler, S., Dai, X., Brandner, W., Schlieder, J., et al. (2017). Binaries among low-mass stars in nearby young moving groups. *A&A* 599, A70. doi:10.1051/0004-6361/201629945

Jensen, E. L. N., and Akeson, R. L. (2003). Protoplanetary disk mass distribution in young binaries. *APJ* 584, 875–881. doi:10.1086/345719

Kaib, N. A., Raymond, S. N., and Duncan, M. (2013). Planetary system disruption by Galactic perturbations to wide binary stars. *Nature* 493, 381–384. doi:10.1038/nature11780

Kley, W (2001). "planet formation in binary systems," in *the formation of binary stars*. Editors H. Zinnecker and R Mathieu, Vol. 200, 511.

Konacki, M., Muterspaugh, M. W., Kulkarni, S. R., and Hełminiak, K. G. (2009). The radial velocity tatooine search for circumbinary planets: planet detection limits for a sample of double-lined binary stars-initial results from keck I/hires, shane/cat/hamspec, and tng/sarg observations. *APJ* 704, 513–521. doi:10.1088/0004-637X/704/1/513

Kouwenhoven, M. B. N., Brown, A. G. A., Portegies Zwart, S. F., and Kaper, L. (2007). The primordial binary population. II. *A&A* 474, 77–104. doi:10.1051/0004-6361:20077719

Kozai, Y. (1962). Secular perturbations of asteroids with high inclination and eccentricity. *AJ* 67, 591–598. doi:10.1086/108790

Kraus, A. L., Ireland, M. J., Hillenbrand, L. A., and Martinache, F. (2012). The role of multiplicity in disk evolution and planet formation. *APJ* 745, 19. doi:10.1088/0004-637X/745/1/19

Kraus, A. L., Ireland, M. J., Huber, D., Mann, A. W., and Dupuy, T. J. (2016). The impact of stellar multiplicity on planetary systems. I. The ruinous influence of close binary companions. *AJ* 152, 8. doi:10.3847/0004-6256/152/1/8

Lidov, M. L. (1962). The evolution of orbits of artificial satellites of planets under the action of gravitational perturbations of external bodies. *Planet. Space Sci.* 9, 719–759. doi:10.1016/0032-0633(62)90129-0

Lillo-Box, J., Barrado, D., and Bouy, H. (2012). Multiplicity in transiting planet-host stars. *A&A* 546, A10. doi:10.1051/0004-6361/201219631

Lodieu, N., Pérez-Garrido, A., Béjar, V. J. S., Gauza, B., Ruiz, M. T., Rebolo, R., et al. (2014). Binary frequency of planet-host stars at wide separations. *A&A* 569, A120. doi:10.1051/0004-6361/201424210

Luhman, K. L., and Jayawardhana, R. (2002). An adaptive optics search for companions to stars with planets. *APJ* 566, 1132–1146. doi:10.1086/338338

Maldonado, R. F., Villaver, E., Mustill, A. J., Chavez, M., and Bertone, E. (2020). Understanding the origin of white dwarf atmospheric pollution by dynamical simulations based on detected three-planet systems. *MNRAS* 499, 1854–1869. doi:10.1093/mnras/staa2946

Mason, B. D., Wycoff, G. L., Hartkopf, W. I., Douglass, G. G., and Worley, C. E. (2001). The 2001 US naval observatory double star CD-ROM. I. The Washington double star catalog. *AJ* 122, 3466–3471. doi:10.1086/323920

Matson, R. A., Howell, S. B., Horch, E. P., and Everett, M. E. (2018). Stellar companions of exoplanet host stars in K2. *AJ* 156, 31. doi:10.3847/1538-3881/aac778

Mayor, M., Marmier, M., Lovis, C., Udry, S., Ségransan, D., Pepe, F., et al. (2011). The HARPS search for southern extra-solar planets XXXIV. Occurrence, mass distribution and orbital properties of super-Earths and Neptune-mass planets. arXiv e-prints arXiv:1109.2497.

Moe, M., and Kratter, K. M. (2018). Dynamical formation of close binaries during the pre-main-sequence phase. *APJ* 854, 44. doi:10.3847/1538-4357/aaa6d2

Moe, M., and Kratter, K. M. (2019). Impact of binary stars on planet statistics–I. Planet occurrence rates, trends with stellar mass, and wide companions to hot jupiter hosts. arXiv e-prints arXiv:1912.01699.

Mordasini, C. (2018). "Planetary population synthesis," in *Handbook of exoplanets*. Editors H. Deeg and J. Belmonte (Cham, Switzerland: Springer. doi:10.1007/978-3-319-55333-7_143

Moutou, C., Vigan, A., Mesa, D., Desidera, S., Thébault, P., Zurlo, A., et al. (2017). Eccentricity in planetary systems and the role of binarity. *A&A* 602, A87. doi:10.1051/0004-6361/201630173

Müller, T. W. A., and Kley, W. (2012). Circumstellar disks in binary star systems. *A&A* 539, A18. doi:10.1051/0004-6361/201118202

Mugrauer, M., and Ginski, C. (2015). High-contrast imaging search for stellar and substellar companions of exoplanet host stars. *MNRAS* 450, 3127–3136. doi:10.1093/mnras/stv771

Mugrauer, M., and Neuhäuser, R. (2009). The multiplicity of exoplanet host stars. *A&A* 494, 373–378. doi:10.1051/0004-6361:200810639

Mugrauer, M., Neuhäuser, R., Mazeh, T., Guenther, E., Fernández, M., and Broeg, C. (2006). A search for wide visual companions of exoplanet host stars: the Calar Alto Survey. *Astron. Nachr.* 327, 321. doi:10.1002/asna.200510528

Mugrauer, M., Neuhäuser, R., and Mazeh, T. (2007a). The multiplicity of exoplanet host stars. *A&A* 469, 755–770. doi:10.1051/0004-6361:20065883

Mugrauer, M., Seifahrt, A., and Neuhäuser, R. (2007b). The multiplicity of planet host stars - new low-mass companions to planet host stars. *Monthly Notices R. Astronomical Soc.* 378, 1328–1334. doi:10.1111/j.1365-2966.2007.11858.x

Mugrauer, M. (2019). Search for stellar companions of exoplanet host stars by exploring the second ESA-Gaia data release. *MNRAS* 490, 5088–5102. doi:10.1093/mnras/stz2673

Mulders, G. D., Pascucci, I., and Apai, D. (2015). A stellar-mass-dependent drop in planet occurrence rates. *APJ* 798, 112. doi:10.1088/0004-637X/798/2/112

Naoz, S., and Fabrycky, D. C. (2014). Mergers and obliquities in stellar triples. *APJ* 793, 137. doi:10.1088/0004-637X/793/2/137

Ngo, H., Knutson, H. A., Hinkley, S., Bryan, M., Crepp, J. R., Batygin, K., et al. (2016). Friends of hot jupiters. IV. stellar companions beyond 50 au might facilitate giant planet formation, but most are unlikely to cause kozai-lidov migration. *APJ* 827, 8. doi:10.3847/0004-637X/827/1/8

Ngo, H., Knutson, H. A., Bryan, M. L., Blunt, S., Nielsen, E. L., Batygin, K., et al. (2017). No difference in orbital parameters of rv-detected giant planets between 0.1 and 5 au in single versus multi-stellar systems. *AJ* 153, 242. doi:10.3847/1538-3881/aa6cac

Ortiz, M., Reffert, S., Trifonov, T., Quirrenbach, A., Mitchell, D. S., Nowak, G., et al. (2016). Precise radial velocities of giant stars. *A&A* 595, A55. doi:10.1051/0004-6361/201628791

Patience, J., White, R. J., Ghez, A. M., McCabe, C., McLean, I. S., Larkin, J. E., et al. (2002). Stellar companions to stars with planets. *APJ* 581, 654–665. doi:10.1086/342982

Pichardo, B., Sparke, L. S., and Aguilar, L. A. (2005). Circumstellar and circumbinary discs in eccentric stellar binaries. *Mon. Notices R. Astronomical Soc.* 359, 521–530. doi:10.1111/j.1365-2966.2005.08905.x

Queloz, D., Mayor, M., Weber, L., Blécha, A., Burnet, M., Confino, B., et al. (2000). The CORALIE survey for southern extra-solar planets. I. A planet orbiting the star Gliese 86. *A&A* 354, 99–102.

Rafikov, R. R. (2005). Can giant planets form by direct gravitational instability?. *APJ* 621, L69–L72. doi:10.1086/428899

Raghavan, D., Henry, T. J., Mason, B. D., Subasavage, J. P., Jao, W. C., Beaulieu, T. D., et al. (2006). Two suns in the sky: stellar multiplicity in exoplanet systems. *APJ* 646, 523–542. doi:10.1086/504823

Raghavan, D., McAlister, H. A., Henry, T. J., Latham, D. W., Marcy, G. W., Mason, B. D., et al. (2010). A survey of stellar families: multiplicity of solar-type stars. *APJS* 190, 1–42. doi:10.1088/0067-0049/190/1/1

Reylé, C. (2018). New ultra-cool and brown dwarf candidates in Gaia DR2. *A&A* 619, L8. doi:10.1051/0004-6361/201834082

Roell, T., Neuhäuser, R., Seifahrt, A., and Mugrauer, M. (2012). Extrasolar planets in stellar multiple systems. *A&A* 542, A92. doi:10.1051/0004-6361/201118051

Santos, N. C., Adibekyan, V., Figueira, P., Andreasen, D. T., Barros, S. C. C., Delgado-Mena, E., et al. (2017). Observational evidence for two distinct giant planet populations. *A&A* 603, A30. doi:10.1051/0004-6361/201730761

Schlaufman, K. C. (2018). Evidence of an upper bound on the masses of planets and its implications for giant planet formation. *APJ* 853, 37. doi:10.3847/1538-4357/aa961c

Schneider, J., Dedieu, C., Le Sidaner, P., Savalle, R., and Zolotukhin, I. (2011). Defining and cataloging exoplanets: the exoplanet.eu database. *A&A* 532, A79. doi:10.1051/0004-6361/201116713

Schwarz, R., Funk, B., Zechner, R., and Bazsó, Á. (2016). New prospects for observing and cataloguing exoplanets in well-detached binaries. *Mon. Not. R. Astron. Soc.* 460, 3598–3609. doi:10.1093/mnras/stw1218

Southworth, J., Bohn, A. J., Kenworthy, M. A., Ginski, C., and Mancini, L. (2020). A multiplicity study of transiting exoplanet host stars. *A&A* 635, A74. doi:10.1051/0004-6361/201937334

Stassun, K. G., Oelkers, R. J., Pepper, J., Paegert, M., Lee, N. D., Torres, G., et al. (2018). The TESS Input catalog and candidate target list. *AJ* 156, 102. doi:10.3847/1538-3881/aad050

Thebault, P., and Haghighipour, N. (2015). *Planet formation in binaries.* Berlin: Springer, 309–340.

Tokovinin, A., and Lépine, S. (2012). Wide companions tohipparcosstars within 67 pc of the Sun. *AJ* 144, 102. doi:10.1088/0004-6256/144/4/102

Tokovinin, A., Thomas, S., Sterzik, M., and Udry, S. (2006). Tertiary companions to close spectroscopic binaries. *A&A* 450, 681–693. doi:10.1051/0004-6361:20054427

Tokovinin, A. (2014a). From binaries to multiples. I. Data on F and G dwarfs within 67 pc of the Sun. *AJ* 147, 86. doi:10.1088/0004-6256/147/4/86

Tokovinin, A. (2014b). From binaries to multiples. II. Hierarchical multiplicity of F and G dwarfs. *AJ* 147, 87. doi:10.1088/0004-6256/147/4/87

Tokovinin, A. (2018). The updated multiple star catalog. *APJS* 235, 6. doi:10.3847/1538-4365/aaa1a5

Udry, S., Mayor, M., and Santos, N. C. (2003). Statistical properties of exoplanets. *A&A* 407, 369–376. doi:10.1051/0004-6361:20030843

Udry, S., Eggenberger, A., Beuzit, J. L., Lagrange, A. M., Mayor, M., and Chauvin, G. (2004). "The binarity status of stars with and without planets probed with VLT/NACO," in *Revista Mexicana de Astronomia y astrofisica conference series*. Editors C. Allen and C. Scarfe Vol. 21 (Buenos Aires, Argentina: Instituto de Astronomía), 215–216.

Vigan, A., Fontanive, C., Meyer, M., Biller, B., Bonavita, M., Feldt, M., et al. (2020). The SPHERE infrared survey for exoplanets (SHINE). III. The demographics of young giant exoplanets below 300 au with SPHERE. arXiv e-prints arXiv:2007.06573.

Wang, J., Xie, J.-W., Barclay, T., and Fischer, D. A. (2014). Influence of stellar multiplicity on planet formation. I. Evidence of suppressed planet formation due to stellar companions within 20 Au and validation of four planets from thekeplermultiple planet candidates. *APJ* 783, 4. doi:10.1088/0004-637X/783/1/4

Ward-Duong, K., Patience, J., De Rosa, R. J., Bulger, J., Rajan, A., Goodwin, S. P., et al. (2015). The M-dwarfs in Multiples (MinMs) survey-I. Stellar multiplicity among low-mass stars within 15 pc★. *MNRAS* 449, 2618–2637. doi:10.1093/mnras/stv384

Wenger, M., Ochsenbein, F., Egret, D., Dubois, P., Bonnarel, F., Borde, S., et al. (2000). The SIMBAD astronomical database. *Astron. Astrophys. Suppl. Ser.* 143, 9–22. doi:10.1051/aas:2000332

White, R. J., and Ghez, A. M. (2001). Observational constraints on the formation and evolution of binary stars. *APJ* 556, 265–295. doi:10.1086/321542

Winn, J. N., Fabrycky, D., Albrecht, S., and Johnson, J. A. (2010). Hot stars with hot Jupiters have high obliquities. *APJ* 718, L145–L149. doi:10.1088/2041-8205/718/2/L145

Winters, J. G., Henry, T. J., Jao, W.-C., Subasavage, J. P., Chatelain, J. P., Slatten, K., et al. (2019). The solar neighborhood. XLV. The stellar multiplicity rate of M dwarfs within 25 pc. *AJ* 157, 216. doi:10.3847/1538-3881/ab05dc

Wöllert, M., Brandner, W., Bergfors, C., and Henning, T. (2015). A Lucky Imaging search for stellar companions to transiting planet host stars. *A&A* 575, A23. doi:10.1051/0004-6361/201424091

Ziegler, C., Law, N. M., Baranec, C., Howard, W., Morton, T., Riddle, R., et al. (2018). Robo-AO kepler survey. V. The effect of physically associated stellar companions on planetary systems. *AJ* 156, 83. doi:10.3847/1538-3881/aace59

Zucker, S., and Mazeh, T. (2002). On the mass-period correlation of the extrasolar planets. *APJ* 568, L113–L116. doi:10.1086/340373

Conflict of Interest: The authors declare that the research was conducted in the absence of any commercial or financial relationships that could be construed as a potential conflict of interest.

frontiers in Astronomy and Space Sciences

ORIGINAL RESEARCH
published: 29 March 2021
doi: 10.3389/fspas.2021.624907

Search for (sub)stellar Companions of Exoplanet Hosts by Exploring the Second ESA-Gaia Data Release

K.-U. Michel and M. Mugrauer*

Astrophysikalisches Institut und Universitäts-Sternwarte Jena, Jena, Germany

We present the latest results of an ongoing multiplicity survey of exoplanet hosts, which was initiated at the Astrophysical Institute and University Observatory Jena, using data from the second data release of the ESA-Gaia mission. In this study the multiplicity of 289 targets was investigated, all located within a distance of about 500 pc from the Sun. In total, 41 binary, and five hierarchical triple star systems with exoplanets were detected in the course of this project, yielding a multiplicity rate of the exoplanet hosts of about 16%. A total of 61 companions (47 stars, a white dwarf, and 13 brown dwarfs) were detected around the targets, whose equidistance and common proper motion with the exoplanet hosts were proven with their precise Gaia DR2 astrometry, which also agrees with the gravitational stability of most of these systems. The detected companions exhibit masses from about 0.016 up to 1.66 $M_{\odot}$ and projected separations in the range between about 52 and 9,555 au.

Keywords: Multiple stars, white dwarfs, brown dwarfs, exoplanets, ESA-Gaia DR2

OPEN ACCESS

Edited by:
Rachel Matson, United States Naval Observatory (USNO), United States

Reviewed by:
Claudio Melo, European Southern Observatory, Chile
Robert De Rosa, European Southern Observatory, Chile

****Correspondence:***
K.-U. Michel
kai-uwe.michel@uni-jena.de

Specialty section:
This article was submitted to Exoplanets, a section of the journal Frontiers in Astronomy and Space Sciences

Received: *01 November 2020*
Accepted: *25 January 2021*
Published: *29 March 2021*

Citation:
Michel K-U and Mugrauer M (2021) Search for (sub)stellar Companions of Exoplanet Hosts by Exploring the Second ESA-Gaia Data Release. Front. Astron. Space Sci. 8:624907. doi: 10.3389/fspas.2021.624907

1 INTRODUCTION

Since the detection of the first planet orbiting a star other than the Sun, several thousands of these exoplanets have been discovered by various detection techniques. While the majority of stars are members of multiple star systems (Duchêne and Kraus, 2013), most of the exoplanet host stars are single stars. Nevertheless several multiple star systems hosting exoplanets, could already be revealed by previous multiplicity studies using seeing limited or high contrast AO imaging observations (see e.g. Mugrauer et al., 2014; Mugrauer and Ginski, 2015). In order to explore the effects of the presence of stellar companions on the formation process and orbital evolution of exoplanets, a survey was initiated at the Astrophysical Institute and University Observatory Jena (described in detail by Mugrauer, 2019) to identify and characterize companions of exoplanet host stars, detected in the second data release of the European Space Agency (ESA) Gaia mission (Gaia DR2 from hereon, Gaia Collaboration et al., 2018). Furthermore, in Mugrauer and Michel (2020) a comparable investigation was carried out among potential exoplanet host stars, identified by the TESS mission (Ricker et al., 2015). The study, whose results are presented here, is the third work in the context with Mugrauer (2019). The following section gives a detailed description of this study, and the detected companions and their derived properties are presented in the third section of this paper.

2 GAIA DR2 SEARCH FOR (SUB)STELLAR COMPANIONS OF EXOPLANET HOSTS

The Gaia DR2 is based on data taken by the Gaia spacecraft in the first 22 months of its mission and contains 1.7 billion detected sources up to a limiting magnitude of $G = 21$ mag. For 1.3 billion sources

a five parameter astrometric solution could be derived, i.e. beside their equatorial coordinates (α, δ), also the parallax π and proper motion ($\mu_\alpha \cos(\delta)$, μ_δ) of these sources were determined. Furthermore, for about 88 million detected objects estimates of their G-band extinction and effective temperature are listed in the Gaia DR2, determined by the Priam algorithm, which is part of the astrophysical parameters inference system (Apsis, see Bailer-Jones et al., 2013) in the Gaia data processing.

Using Gaia DR2 data Mugrauer (2019) already explored the multiplicity of all exoplanet host stars, whose exoplanets were detected either by photometric transit observations, radial-velocity (RV), or astrometric measurements, and were listed in the Extrasolar Planets Encyclopedia[1] (EPE from hereon, Schneider et al., 2011) by mid of October 2018. The study, presented in this paper, complements this survey by investigating the multiplicity of the exoplanet hosts (stars but also brown dwarfs), whose planets were indirectly detected either via RV measurements or transit observations in the range of time between mid of October 2018 until end of September 2020, as well as all exoplanet hosts, known so far, with planets, which were directly detected by imaging observations. At the end of September 2020 the EPE lists about 4,350 exoplanets, and about 400 of them were detected around the hosts studied in this work.

(Sub)stellar Companions are expected to be located at the same distance to the Sun as the exoplanet hosts and form common proper motion pairs with them, in particular wide companions with projected separations of hundreds and thousands of au, i.e. the typical targets of this study. Hence, in order to clearly detect such companions and to prove the equidistance of these objects and the exoplanet hosts, in this study we have taken into account only Gaia DR2 sources with an accurate five parameter astrometric solution, i.e. which exhibit precise measurements of their parallax ($\pi/\sigma(\pi) > 3$) and proper motion ($\mu/\sigma(\mu) > 3$). Thereby, sources with negative parallaxes are neglected. As in the Gaia DR2 a parallax uncertainty of 0.7 mas is reached for faint sources down to $G = 20$ mag, the survey is furthermore constrained to exoplanet hosts, which are located within a distance of 500 pc around the Sun (i.e. $\pi > 2$ mas), to assure $\pi/\sigma(\pi) > 3$ even for the faintest companions, detectable in this survey. This distance constraint is slightly relaxed to $\pi + 3\sigma(\pi) \gtrapprox 2$ mas, i.e. taking into account also the parallax uncertainty of the hosts. By the end of September 2020, in total 289 exoplanet hosts are listed in the EPE, which fulfill this distance constraint, and hence are selected as targets for this study. The properties of all targets are summarized in **Table 1** and their histograms are illustrated in **Figure 1**. On average, the targets are solar like stars most frequently found within 150 pc around the Sun, which exhibit proper motions in the range between about 2 and 10,400 mas/yr, and G-band magnitudes from about 3.7 to 20.8 mag. In particular, the sub-sample of direct imaging exoplanet hosts emerges as a peak in the age distribution at young ages, as all these targets are typically younger than 0.1 Gyr, in contrast to hosts of RV and transiting exoplanets, which are older than 1 Gyr in general.

TABLE 1 | The properties of all targets of this study. The corresponding histograms are shown in **Figure 1**.

	Distance (pc)	μ (mas/yr)	G (mag)	Age (Gyr)	Mass ($M_\odot$)
Min	1.8	1.7	3.7	0.001	0.016
Max	586	10,394	20.8	14.9	20
Ave	137	270	10.8	3.5	1.1
Med	94	65	10.7	2.1	1.0

The companion search radius, applied in this project around the selected targets, is limited to a maximal projected separation of 10,000 au, which guarantees that the majority of wide companions of the exoplanet hosts are detectable in this study, as described by Mugrauer (2019). This upper separation limit results in an angular search radius around the targets of $r[arc\,\mathrm{sec}] = 10\pi[\mathrm{mas}]$. Within this radius around the targets the companionship of all sources, listed in the Gaia DR2 with an accurate five parameter astrometric solution was investigated. For the verification of the equidistance of all detected sources with the associated exoplanet hosts, the difference $\Delta\pi$ between their parallaxes was calculated, taking into account also the excess noise of their astrometric solutions. Common proper motion of the detected sources and the targets was checked with the precise Gaia DR2 proper motions of the exoplanet hosts μ_{PH} and the sources μ_{Comp}. In addition, we have also derived for all sources the differential proper motion: $\mu_{\mathrm{rel}} = \left|\mu_{\mathrm{PH}} - \mu_{\mathrm{comp}}\right|$, which yields the common proper motion index (cpm − index = $\left|\mu_{\mathrm{PH}} + \mu_{\mathrm{comp}}\right|/\mu_{\mathrm{rel}}$), which characterizes the degree of common proper motion of the detected sources and the exoplanet hosts.

Following the companion identification procedure ($sig\text{-}\Delta\pi \leq 3$ and cpm − index ≥ 3), as defined by Mugrauer (2019) the majority of all sources (> 99.88%), detected within the applied search radius around the targets, can clearly be excluded as companions, as they are either not located at the same distances as the exoplanet hosts and/or do not share a common proper motion with them. In contrast, for 61 detected objects their companionship with the targets could clearly be proven with their precise Gaia DR2 astrometry. For all these companions we have determined their relative astrometry to the exoplanet hosts (angular separation ρ, and position angle PA), as well as their projected separation *sep*, derived with their angular separation and the parallax of the targets.

The absolute G-band magnitude of all companions was derived from their apparent G-band photometry, the parallax of the associated exoplanet hosts, as well as their Apsis-Priam G-band extinction estimate, all listed in the Gaia DR2. If there was no extinction estimate given for a companion, the extinction estimate of the exoplanet host was used instead or if not available, its extinction estimate, listed in the StarHorse catalog (Anders et al., 2019). In the case that no G-band extinction is available at all it was derived from V-band extinction measurements of the exoplanet hosts, listed either in the VizieR data base[2] (Ochsenbein et al.,

[1]Online available at: http://exoplanet.eu/

[2]Online available at: https://vizier.u-strasbg.fr/

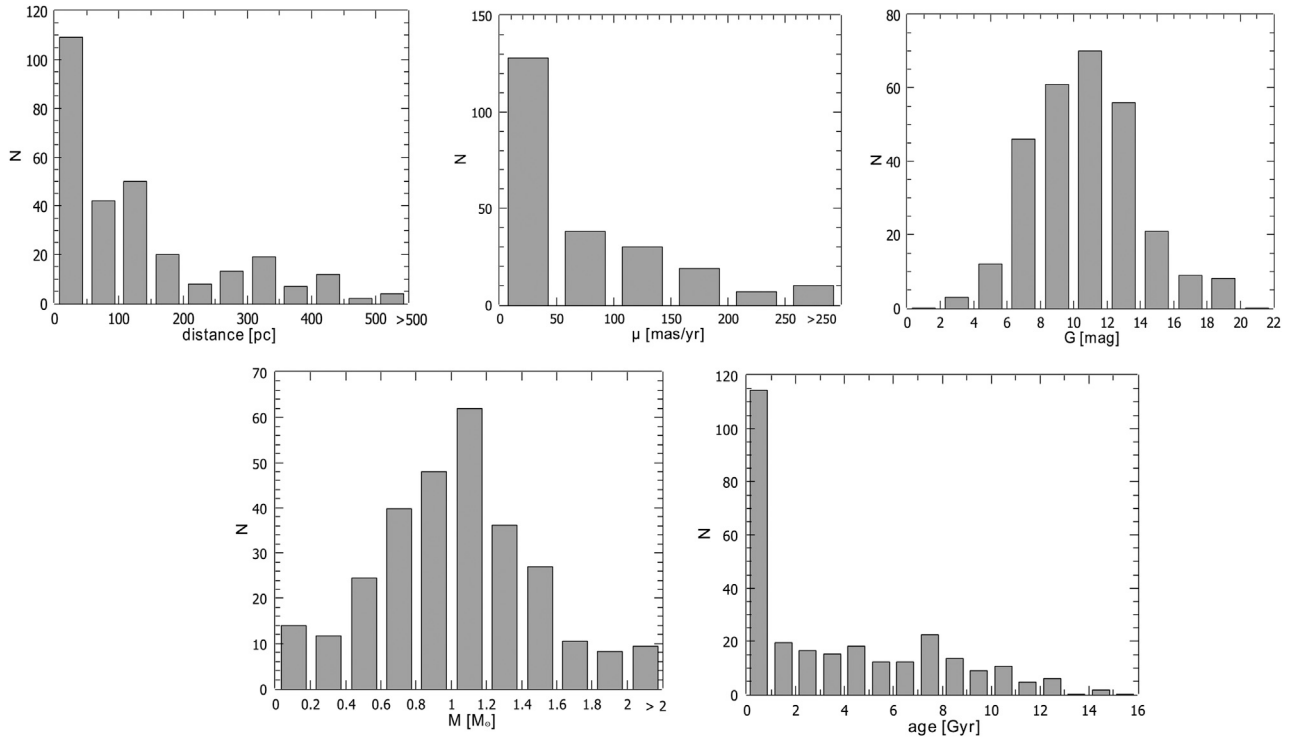

FIGURE 1 | The histograms of the individual properties of all targets of this study.

2000) or in the literature, adopting $A_G/A_V = 0.77$, as described by Mugrauer (2019).

The masses and effective temperatures of all detected companions were determined from their derived absolute G-band magnitudes using the evolutionary models of (sub)stellar objects from Baraffe et al. (2015), as well as the ages of the exoplanet hosts, as listed in the EPE. Thereby, we adopt the same age for the planet hosts and their companions. We determined the masses and effective temperatures of the companions via interpolation of the model grid with the age closest to that of the exoplanet hosts. For verification of the obtained results the properties of the companions derived from their G-band magnitudes were compared with those, determined from the near-infrared photometry, taken from the 2MASS Point Source catalog (Skrutskie et al., 2006), if available. For the near-infrared extinction we have used the relations: $A_{Ks}/A_V = 0.12$, $A_H/A_V = 0.17$, and $A_J/A_V = 0.26$, as described in Mugrauer (2019). A graphical comparison of the masses obtained from the G-band and the 2MASS photometry are shown in **Figure 2**. The identity is illustrated as gray dashed line in this figure. For all companions the derived masses agree well with each other, with deviations that remain below the 3σ level (the same holds also for the temperature estimates not shown here). Objects, whose masses were determined by extrapolation from the used model grids as such as those with bad quality (quality flags all but A) or contaminated 2MASS photometry were excluded in this comparison.

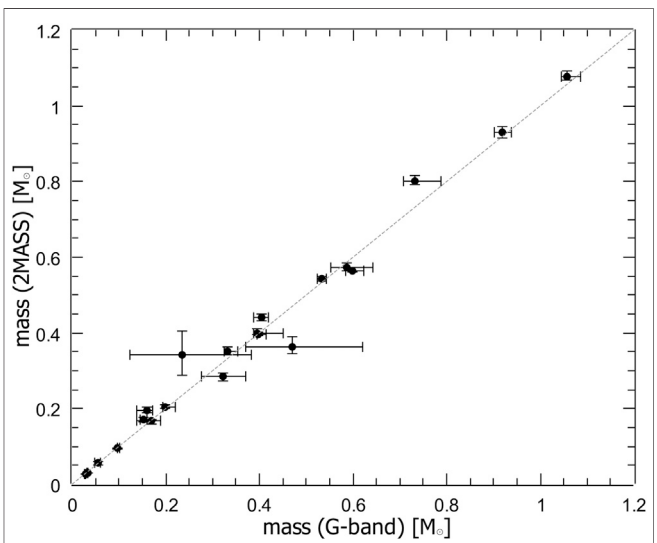

FIGURE 2 | Comparison of the mass of the detected companions, derived from their G-band and infrared 2MASS photometry.

Eventually for all companions, which were detected in this study, we have estimated their escape velocity $\mu_{\rm esc}\,[{\rm mas\,yr^{-1}}] = 2\pi\sqrt{2M\pi_{\rm PH}^3/\rho}$ with their angular separation ρ and the parallax of the associated exoplanet hosts both in the unit of milli-arcsec (mas), as well as the total mass M of the system (in the unit $M_\odot$),

TABLE 2 | Gaia astro- and photometry of all exoplanet hosts and their companions, detected in this study.

Name	π (mas)	$\mu_\alpha \cos(\delta)$ (mas/yr)	μ_δ (mas/yr)	epsi (mas)	sig-epsi	G (mag)	A_G (mag)	
HD 1160 A*	7.9417 ± 0.0764	20.089 ± 0.138	−14.575 ± 0.099	0.121	6.0	7.1074 ± 0.0003	$0.1347^{+0.1300}_{-0.0968}$	
HD 1160 C	6.9946 ± 0.2739	20.605 ± 0.333	−16.215 ± 0.311	0.739	37	15.3505 ± 0.0207		
Gliese 49 A*	101.4650 ± 0.0335	731.135 ± 0.041	90.690 ± 0.048	—	—	8.6628 ± 0.0007	$0.6030^{+0.2220}_{-0.4095}$	
Gliese 49 B	101.6371 ± 0.0806	730.740 ± 0.163	86.352 ± 0.225	0.190	13	11.9238 ± 0.0033		
HD 8326 A*	32.5591 ± 0.0466	−58.470 ± 0.120	−224.887 ± 0.064	—	—	8.4749 ± 0.0004		
HD 8326 B	32.4362 ± 0.0589	−57.577 ± 0.156	−224.122 ± 0.088	0.347	27	14.2066 ± 0.0006	$0.2940^{+0.2446}_{-0.0438}$	
HD 13167 A*	6.6859 ± 0.0485	43.770 ± 0.077	−38.126 ± 0.079	—	—	8.1600 ± 0.0003		
HD 13167 B	6.7931 ± 0.1254	44.134 ± 0.215	−39.358 ± 0.212	0.444	3.3	17.4513 ± 0.0022	$0.2431^{+0.0597}_{-0.0648}$	SHC
HR 858 A*	31.2565 ± 0.0700	123.229 ± 0.070	105.788 ± 0.151	0.086	3.9	6.2480 ± 0.0003	$0.1320^{+0.1061}_{-0.0911}$	
HR 858 B	32.3014 ± 0.1670	137.125 ± 0.213	105.865 ± 0.302	0.835	63	16.0464 ± 0.0031		
HD 18015 A*	8.0490 ± 0.0517	63.053 ± 0.089	− 4.359 ± 0.082	—	—	7.7219 ± 0.0005		
HD 18015 B	7.9413 ± 0.0415	64.638 ± 0.071	− 4.668 ± 0.066	—	—	12.2361 ± 0.0008	$0.1440^{+0.0361}_{-0.0325}$	
K2-288 B*	15.2166 ± 0.2007	185.476 ± 0.708	−74.070 ± 0.618	0.766	70	14.5451 ± 0.0017		
K2-288 A	14.2879 ± 0.0807	187.057 ± 0.151	−69.591 ± 0.116	0.418	41	13.3090 ± 0.0009	$0.5668^{+0.0884}_{-0.0824}$	SHC
HD 23472 A*	25.5897 ± 0.0261	−102.571 ± 0.050	−43.917 ± 0.059	—	—	9.3848 ± 0.0002	$0.0783^{+0.1742}_{-0.0703}$	
HD 23472 B	25.5060 ± 0.0732	−103.019 ± 0.154	−42.771 ± 0.169	0.490	16.1	15.8312 ± 0.0014		
HD 24085 B*	18.1859 ± 0.0245	− 9.249 ± 0.048	−97.358 ± 0.050	—	—	7.4250 ± 0.0002		
HD 24085 A	18.1430 ± 0.0226	−10.234 ± 0.043	−97.151 ± 0.049	—	—	7.2719 ± 0.0002	$0.6682^{+0.5911}_{-0.3903}$	
HII 1348 A* (SB)	6.9890 ± 0.0490	21.401 ± 0.120	−45.705 ± 0.060	—	—	12.2439 ± 0.0012		
HII 1348 C	6.6456 ± 0.1763	20.250 ± 0.337	−45.292 ± 0.235	0.429	4.1	17.0303 ± 0.0017	$1.1810^{+0.3091}_{-0.3321}$	
HII 1348 D	7.8946 ± 1.7831	23.361 ± 4.630	−42.219 ± 2.330	2.369	0.9	20.7790 ± 0.0151	$0.6550^{+0.3718}_{-0.4581}$	
HATS-57 A*	3.5495 ± 0.0392	−12.664 ± 0.046	−14.115 ± 0.040	—	—	12.1816 ± 0.0007	$0.0548^{+0.1726}_{-0.0423}$	
HATS-57 B	3.4904 ± 0.1265	−12.064 ± 0.174	−14.764 ± 0.142	—	—	17.5558 ± 0.0012		
FU Tau A*	7.5981 ± 0.1497	6.895 ± 0.376	−21.026 ± 0.202	0.732	83	15.2412 ± 0.0024	$2.2620^{+0.2597}_{-0.4841}$	
FU Tau B	7.4909 ± 1.2887	12.450 ± 4.056	−21.761 ± 1.903	3.516	4.6	20.4799 ± 0.0074		
DH Tau A*	7.3880 ± 0.0693	7.065 ± 0.117	−20.699 ± 0.079	—	—	12.4961 ± 0.0090		
DH Tau C	7.4011 ± 0.0520	6.899 ± 0.113	−21.207 ± 0.074	—	—	11.9692 ± 0.0013	$2.6683^{+0.3698}_{-0.1714}$	
51 Eri A*	33.5770 ± 0.1354	44.352 ± 0.227	−63.833 ± 0.178	0.562	190	5.1224 ± 0.0017	$0.1740^{+0.2663}_{-0.1123}$	
51 Eri B (SB)	37.9633 ± 0.3662	59.587 ± 0.717	−52.419 ± 0.618	1.958	2030	9.7247 ± 0.0011		
2M 0441+23 C*	8.3040 ± 0.3778	8.955 ± 0.931	−21.431 ± 0.456	1.350	5.7	18.9668 ± 0.0068		
2M 0441+23 AB	8.0161 ± 0.0832	8.300 ± 0.189	−21.553 ± 0.103	0.529	79	13.8267 ± 0.0011	$1.0577^{+0.9503}_{-0.4138}$	
NGTS-6 A*	3.2151 ± 0.0148	− 9.339 ± 0.025	−21.9950 ± 0.026	—	—	13.8175 ± 0.0006		
NGTS-6 B	3.2231 ± 0.0653	− 9.301 ± 0.107	−22.1300 ± 0.114	0.203	1.3	17.0603 ± 0.0009	$0.3627^{+0.1024}_{-0.1403}$	
AB Dor AC*	65.3199 ± 0.1440	29.150 ± 0.251	164.4210 ± 0.299	0.850	317	6.6738 ± 0.0018		
AB Dor BD	67.0283 ± 0.0901	66.366 ± 0.155	125.8990 ± 0.189	0.522	111	11.3560 ± 0.0012	$1.3528^{+0.5192}_{-0.4435}$	
HD 39855 A*	42.9636 ± 0.0346	92.854 ± 0.046	−24.4660 ± 0.063	—	—	7.3211 ± 0.0002		
HD 39855 B	42.9612 ± 0.0369	96.166 ± 0.055	−11.8960 ± 0.065	—	—	10.0503 ± 0.0006	$0.1920^{+0.2268}_{-0.1257}$	
NGTS-10 A*	3.0798 ± 0.2610	− 2.323 ± 0.343	10.5270 ± 0.395	2.152	1,100	14.2604 ± 0.0034		
NGTS-10 B	0.2965 ± 0.0802	− 1.120 ± 0.219	9.6710 ± 0.161	0.064	0.3	15.5926 ± 0.0014	$0.7679^{+1.1986}_{-0.5770}$	SHC
L2 Pup A*	15.61 ± 0.99	106.31 ± 0.96	324.99 ± 1.08	—	—	9.8208 ± 0.2812		HIP
L2 Pup B	16.4131 ± 0.0574	105.895 ± 0.097	327.272 ± 0.099	0.368	12	15.7099 ± 0.0009	$0.2940^{+0.3029}_{-0.0934}$	
HIP 38594 A*	56.1868 ± 0.0297	−300.905 ± 0.044	200.923 ± 0.045	—	—	9.0853 ± 0.0003		
HIP 38594 B	56.1234 ± 0.0799	−297.867 ± 0.126	206.598 ± 0.257	—	—	16.0444 ± 0.0005	$0.3670^{+0.7758}_{-0.2630}$	
WASP-180 A*	3.9093 ± 0.0517	−14.052 ± 0.091	− 3.169 ± 0.055	—	—	10.9134 ± 0.0007		
WASP-180 B	3.8618 ± 0.0734	−12.705 ± 0.172	− 2.710 ± 0.103	—	—	11.7712 ± 0.0008	$0.0930^{+0.1560}_{-0.0534}$	
HD 79211 B*	157.8851 ± 0.0414	−1573.120 ± 0.061	−660.121 ± 0.058	—	—	7.0477 ± 0.0004		
HD 79211 A	157.8796 ± 0.0366	−1546.100 ± 0.059	−569.127 ± 0.060	—	—	6.9689 ± 0.0005	$0.3757^{+0.3264}_{-0.2078}$	
HD 85628 A*	5.8297 ± 0.0318	6.051 ± 0.055	−15.398 ± 0.051	—	—	8.1740 ± 0.0004	$0.5012^{+0.1438}_{-0.2262}$	
HD 85628 B	5.9508 ± 0.0366	5.856 ± 0.066	−13.252 ± 0.060	0.296	18	14.0490 ± 0.0047		
TOI 717 A*	28.7709 ± 0.0783	−26.092 ± 0.176	62.064 ± 0.260	0.045	0.5	12.6410 ± 0.0005	$0.3110^{+0.1274}_{-0.0211}$	
TOI 717 B	28.7588 ± 0.0824	−23.995 ± 0.177	62.081 ± 0.273	0.060	1.0	12.7386 ± 0.0008		
G 196-3 A*	45.8611 ± 0.0388	−141.177 ± 0.055	−202.394 ± 0.053	0.000	0.5	10.6123 ± 0.0005	$1.0645^{+0.4919}_{-0.4836}$	
G 196-3 B	44.3549 ± 0.8128	−137.820 ± 0.928	−208.523 ± 1.671	2.210	3.3	20.1697 ± 0.0085		
LTT 3780 A*	45.4644 ± 0.0827	−341.409 ± 0.114	−247.870 ± 0.105	0.137	6.6	11.8465 ± 0.0005	$0.5015^{+0.2595}_{-0.3436}$	
LTT 3780 B	45.2879 ± 0.1081	−341.379 ± 0.149	−248.419 ± 0.135	0.414	23	14.4855 ± 0.0008		
MASCARA-3 A*	10.3320 ± 0.0333	−56.184 ± 0.053	−34.808 ± 0.064	—	—	8.2375 ± 0.0004	$0.2400^{+0.2740}_{-0.1150}$	
MASCARA-3 B	11.0260 ± 0.1268	−50.757 ± 0.325	−37.811 ± 0.200	0.799	160	13.0002 ± 0.0109		
2M J1101-7732 A*	5.4081 ± 0.1877	−22.653 ± 0.435	2.062 ± 0.397	1.271	12	18.3299 ± 0.0023		
2M J1101-7732 B	5.4333 ± 0.3368	−23.668 ± 0.748	1.931 ± 0.723	1.836	6.1	19.4040 ± 0.0047	$0.5900^{+0.1200}_{-0.1200}$	✠
WASP-175 A*	1.8260 ± 0.0399	−24.306 ± 0.057	6.033 ± 0.057	—	—	12.7065 ± 0.0002		
WASP-175 B	1.7947 ± 0.0308	−24.064 ± 0.045	6.185 ± 0.045	—	—	14.2462 ± 0.0003	$0.0965^{+0.0966}_{-0.0876}$	
CHXR 73 A*	5.2343 ± 0.1759	−22.193 ± 0.233	0.215 ± 0.206	0.815	12	17.2934 ± 0.0014	$3.4650^{+1.0250}_{-1.0250}$	✠
CHXR 73 C	5.2502 ± 0.2218	−22.937 ± 0.433	− 1.261 ± 0.347	1.241	14	17.9098 ± 0.0021		

(Continued on following page)

TABLE 2 | (*Continued*) Gaia astro- and photometry of all exoplanet hosts and their companions, detected in this study.

Name	π (mas)	$\mu_\alpha \cos(\delta)$ (mas/yr)	μ_δ (mas/yr)	epsi (mas)	sig-epsi	G (mag)	A_G (mag)	
GJ 414 A*	84.0803 ± 0.0471	591.622 ± 0.081	−197.247 ± 0.091	—	—	7.7281 ± 0.0007		
GJ 414 B	84.1971 ± 0.0579	604.831 ± 0.081	−206.442 ± 0.075	—	—	9.0471 ± 0.0011	$0.6100^{+0.5656}_{-0.3221}$	
HD 97334 A*	44.1428 ± 0.0383	−249.387 ± 0.090	−151.590 ± 0.071	—	—	6.2410 ± 0.0006	$0.0555^{+0.1848}_{-0.0415}$	
HD 97334 BC	42.8724 ± 1.1025	−236.349 ± 2.133	−152.068 ± 2.109	5.342	15	19.9859 ± 0.0135		
HD 233832 A*	16.9952 ± 0.0752	−473.960 ± 0.075	124.167 ± 0.087	—	—	9.9456 ± 0.0005		
HD 233832 B	17.0667 ± 0.0532	−478.645 ± 0.048	119.122 ± 0.088	—	—	12.7187 ± 0.0004	$0.2288^{+0.2054}_{-0.1079}$	
2M J1155-7919 A*	9.8862 ± 0.0585	−41.179 ± 0.127	− 4.336 ± 0.086	0.490	35	14.8180 ± 0.0017	$0.4158^{+0.0616}_{-0.0052}$	✠
2M J1155-7919 B	9.8211 ± 0.5264	−39.738 ± 1.216	− 4.656 ± 0.687	1.387	1.4	19.9246 ± 0.0079		
NGTS-5 A*	3.2310 ± 0.0272	13.650 ± 0.041	− 4.688 ± 0.042	—	—	13.5260 ± 0.0004	$0.1970^{+0.1050}_{-0.1174}$	
NGTS-5 B	2.9428 ± 0.1254	13.938 ± 0.209	− 4.331 ± 0.180	0.422	3.0	17.3160 ± 0.0016		
2M J1450-7841 A*	10.9480 ± 0.5046	−37.597 ± 0.881	−23.654 ± 0.895	2.345	5.0	19.6858 ± 0.0060	$0.5000^{+0.5000}_{-0.5000}$	✠
2M J1450-7841 B	8.6592 ± 0.9023	−34.984 ± 2.047	−22.162 ± 1.764	2.067	1.1	20.6501 ± 0.0097		
WASP-189 A*	9.9990 ± 0.0747	−50.564 ± 0.109	−23.788 ± 0.115	0.082	2.2	6.5537 ± 0.0004	$0.2652^{+0.1599}_{-0.2306}$	SHC
WASP-189 B	10.7202 ± 0.1648	−50.594 ± 0.165	−24.037 ± 0.178	0.475	25	14.3874 ± 0.0024		
HIP 73990 A*	9.0326 ± 0.0648	−27.432 ± 0.106	−29.028 ± 0.089	—	—	8.0678 ± 0.0009		
HIP 73990 D	8.9507 ± 0.0899	−27.728 ± 0.159	−29.245 ± 0.135	0.457	28	14.6580 ± 0.0007	$1.1073^{+0.6427}_{-0.4489}$	
TOI 905 A*	6.2745 ± 0.0285	−25.839 ± 0.033	−41.150 ± 0.051	—	—	11.0813 ± 0.0004	$0.2703^{+0.1330}_{-0.1606}$	SHC
TOI 905 B	7.8542 ± 0.5489	−18.290 ± 0.763	−39.819 ± 0.788	1.423	25	17.2149 ± 0.0375		
2M 1510 A*	27.2203 ± 0.2665	−118.747 ± 0.492	−46.865 ± 0.420	1.112	18	17.4870 ± 0.0018	$0.9266^{+0.1360}_{-0.0121}$	SHC
2M 1510 B	27.6869 ± 0.4939	−117.448 ± 0.893	−45.713 ± 0.746	1.710	7.8	18.8855 ± 0.0035		
β Cir A*	35.1736 ± 0.4253	−96.742 ± 0.491	−136.541 ± 0.621	1.852	1770	3.9732 ± 0.0026	$0.2560^{+0.2260}_{-0.1598}$	
β Cir B	34.7836 ± 0.6840	−92.763 ± 0.829	−138.156 ± 1.469	2.701	15	19.4335 ± 0.0051		
KELT-23 A*	7.8912 ± 0.0219	0.434 ± 0.039	−12.217 ± 0.041	—	—	10.1820 ± 0.0004	$0.0680^{+0.0996}_{-0.0505}$	
KELT-23 B	7.8949 ± 0.0529	1.567 ± 0.093	−11.903 ± 0.107	0.284	6.8	15.5209 ± 0.0014		
K2-290 A*B	3.6365 ± 0.0503	27.225 ± 0.099	−16.893 ± 0.066	—	—	10.8204 ± 0.0004	$0.8900^{+0.2570}_{-0.2655}$	
K2-290 C	4.0531 ± 0.2711	27.465 ± 0.593	−16.484 ± 0.370	0.556	1.2	18.5920 ± 0.0027		
GQ Lup A*	6.5868 ± 0.0473	−14.257 ± 0.097	−23.596 ± 0.066	0.110	5.7	11.2608 ± 0.0089	$2.7645^{+0.3426}_{-0.4140}$	
GQ Lup C	5.4925 ± 0.4597	−14.807 ± 0.972	−21.947 ± 0.653	2.960	59	18.3740 ± 0.0037		
HIP 77900 A*	6.6037 ± 0.1196	−13.357 ± 0.187	−25.272 ± 0.110	0.212	21	6.1129 ± 0.0006	$0.1852^{+0.1535}_{-0.0360}$	
HIP 77900 B	5.2279 ± 0.9696	−13.908 ± 1.517	−23.265 ± 1.097	2.007	4.3	19.5660 ± 0.0057		
USco 1602-2401 A*	6.9484 ± 0.0661	−11.850 ± 0.119	−24.032 ± 0.051	—	—	11.8656 ± 0.0026	$1.8885^{+0.1123}_{-0.1186}$	SHC
USco 1602-2401 B	6.3381 ± 0.2030	−12.699 ± 0.325	−23.872 ± 0.187	0.829	40	16.3640 ± 0.0010		
HIP 79098 A (SB)*	6.8337 ± 0.1176	− 9.823 ± 0.210	−28.119 ± 0.163	0.289	35	5.8264 ± 0.0006	$0.4640^{+0.1440}_{-0.2381}$	
HIP 79098 C	7.1870 ± 0.1476	−10.979 ± 0.271	−26.128 ± 0.189	0.666	27	16.1091 ± 0.0012		
USco 1610-1913 A*	7.4960 ± 0.0718	− 9.342 ± 0.206	−23.591 ± 0.111	0.168	12	12.6962 ± 0.0049	$0.3850^{+0.3850}_{-0.3850}$	✠
USco 1610-1913 B	6.9600 ± 0.3719	− 7.043 ± 1.112	−24.982 ± 0.576	1.301	7.0	18.7225 ± 0.0029		
USco 1612-1800 A*	6.3156 ± 0.0747	− 7.418 ± 0.161	−21.148 ± 0.112	0.427	31	14.5532 ± 0.0007	$0.3850^{+0.3850}_{-0.3850}$	✠
USco 1612-1800 B	6.0413 ± 0.3224	− 7.002 ± 0.698	−19.738 ± 0.512	1.112	4.0	18.8810 ± 0.0032		
ROXs 12 A*	7.2894 ± 0.0417	− 7.185 ± 0.090	−24.851 ± 0.059	0.158	6.9	13.2655 ± 0.0013	$1.8000^{+1.0000}_{-1.0000}$	✠
ROXs 12 C	7.2328 ± 0.0738	− 6.577 ± 0.151	−25.106 − 0:099	0.354	20	14.7659 ± 0.0113		
HATS-48 A*	3.7648 ± 0.0237	3.125 ± 0.031	6.146 ± 0.029	—	—	13.8951 ± 0.0002	$0.5090^{+0.1876}_{-0.3705}$	
HATS-48 B	3.6354 ± 0.4432	2.951 ± 0.469	5.201 ± 0.446	0.576	0.6	19.3368 ± 0.0037		
GJ 752 A*	169.1590 ± 0.0520	−579.043 ± 0.088	−1332.740 ± 0.081	—	—	8.0976 ± 0.0011		
GJ 752 B	168.9620 ± 0.1299	−598.177 ± 0.245	−1365.270 ± 0.227	0.855	98	14.3212 ± 0.0007	$1.4208^{+0.2795}_{-0.1719}$	
HD 181234 A*	20.9155 ± 0.0564	−122.751 ± 0.098	−318.277 ± 0.098	—	—	8.3693 ± 0.0004	$0.3670^{+0.1987}_{-0.0723}$	
HD 181234 B	20.8683 ± 0.1458	−117.558 ± 0.192	−323.292 ± 0.211	0.520	27	14.2207 ± 0.0012		
Wendelstein-1 A*	3.2470 ± 0.0317	4.131 ± 0.041	− 1.832 ± 0.039	—	—	15.0324 ± 0.0005	$0.5240^{+0.4730}_{-0.4315}$	
Wendelstein-1 B	3.5833 ± 0.4053	3.862 ± 0.508	− 2.194 ± 0.536	1.038	1.9	19.3979 ± 0.0031		
2M J2126-81 A*	29.2836 ± 0.0690	59.843 ± 0.111	−107.723 ± 0.114	0.303	48	10.8133 ± 0.0021	$0.2157^{+0.4319}_{-0.0470}$	SHC
2M J2126-81 B	29.2463 ± 0.9205	56.511 ± 1.656	−115.369 ± 2.441	4.299	4.4	20.7247 ± 0.0094		
TOI 132 A*	6.0809 ± 0.0366	35.553 ± 0.043	−53.055 ± 0.054	0.090	3.6	11.3208 ± 0.0007	$0.1535^{+0.1606}_{-0.1430}$	
TOI 132 B	5.9683 ± 0.2251	35.417 ± 0.280	−52.488 ± 0.361	0.955	7.4	18.4470 ± 0.0015		
NGTS-7 A*	7.2497 ± 0.1203	−27.003 ± 0.114	−16.225 ± 0.178	0.610	72	14.9154 ± 0.0020	$0.5000^{+0.5000}_{-0.5000}$	✠
NGTS-7 B	6.5232 ± 0.0787	−28.601 ± 0.112	−14.776 ± 0.364	0.203	4.4	15.5134 ± 0.0012		
DS Tuc A*	22.6663 ± 0.0354	79.464 ± 0.074	−67.440 ± 0.045	—	—	8.3193 ± 0.0010		
DS Tuc B	22.6504 ± 0.0297	78.022 ± 0.064	−65.746 ± 0.037	—	—	9.3993 ± 0.0014	$0.3210^{+0.2350}_{-0.1034}$	
1RXS J2351+3127 A*	23.2183 ± 0.0524	106.584 ± 0.064	−87.761 ± 0.038	0.083	3.9	12.5145 ± 0.0005		
1RXS J2351+3127 C	23.1794 ± 0.0592	105.757 ± 0.070	−87.787 ± 0.041	0.285	32	13.2004 ± 0.0006	$0.4190^{+0.4250}_{-0.0410}$	

Comments on individual objects:

HD 1160 A hosts a brown dwarf companion (HD 1160 B, detected by Nielsen et al., 2012), which is listed as exoplanet in the EPE.

The exoplanet host star HD 24085 B is the secondary component of a binary system, whose primary star HD 24085 A is also known as HD 24062.

HII 1348 A is a spectroscopic binary with a brown dwarf companion (HII 1348 B, discovered by Geißler et al., 2012), which is listed as exoplanet in the EPE.

DH Tau A hosts a brown dwarf companion (DH Tau B), which was detected by Itoh et al. (2005) and is listed as exoplanet in the EPE. DH Tau C (alias DI Tau) is the wide primary component of this system.

2M 0441+23 C is an exoplanet host brown dwarf (Bowler and Hillenbrand, 2015), which is listed in the EPE.
The bright AGB star L2 Pup A is listed in the Gaia DR2 but with a parallax (π = 7.3644 ± 0.6149 mas) that significantly differs from its HIPPARCOS-value (π = 15.61 ± 0.99 mas, van Leeuwen, 2007). Furthermore, it should be noted that the G-band brightness of this star, as listed in the Gaia DR2, is several magnitudes fainter than expected (e.g. G = 3.97 ± 0.54 mag, as estimated by Smart and Nicastro, 2014). Therefore, we only use here the Gaia DR2 equatorial coordinates of this star, while we adopt the HIPPARCOS-values of its parallax and proper motion, which is indicated with the flag HIP in this table.
HIP 73990 A is the host star of two brown dwarfs (HIP 73990 B and C, revealed by Hinkley et al., 2015), which are both listed as exoplanets in the EPE.
GQ Lup A is listed as exoplanet host star in the EPE, whose substellar companion was detected by Neuhäuser et al. (2005). The star exhibits a wide stellar companion, whose WDS designation (GQ Lup C) is used here.
HIP 79098 A is a spectroscopic binary and hosts the brown dwarf HIP 79098 B (Janson et al., 2019), which is listed as exoplanet in the EPE.
ROXs 12 A is the host star of the brown dwarf ROXs 12 B, detected by Kraus et al. (2014), which is listed as exoplanet in the EPE.
1RXS J2351+3127 A hosts a brown dwarf companion (1RXS J2351+3127 B, discovered by Bowler et al., 2012), which is listed as exoplanet in the EPE.
HII 1348 A, FU Tau A, G 196-3 A, 2M J1155-7919 A, HD 97334 A, β Cir A, HIP 77900 A, USco 1602-2401 A, USco 1610-1913 A, USco 1612-1800 A, and 2M J2126-81 A, are all listed as exoplanet host stars in the EPE, whose substellar companions were detected and characterized in this study, using data from the Gaia DR2.
2M J1101-7732 A, 2M J1450-7841 A, 2M 1510 A are all brown dwarfs, which are listed as exoplanet hosts in the EPE, whose substellar companions were detected and characterized in this study with Gaia DR2 data.

i.e. the sum of the mass of the companions, derived as described above, and the mass of the associated exoplanet hosts, taken from the EPE. This estimation can be considered as an upper limit of the escape velocity as the projected separation is smaller than the physical separation of the objects.

3 DETECTED COMPANIONS OF EXOPLANET HOSTS

The Gaia astro- and photometry of all exoplanet hosts and their companions, detected in this study, are listed in **Table 2**. The derived properties of the companions are summarized in **Table 3**–**5**. In all tables the exoplanet host systems or the companions are sorted by their right ascension. The used identifier of the targets corresponds either to the one used in the EPE or is a slightly abbreviated version of it. In contrast to the planet definition used by the EPE, in which substellar objects below 60 $M_{\rm Jup}$ are defined as exoplanets, we follow here the planet definition based on the deuterium burning limit (as described e.g. by Basri, 2000), i.e. all substellar objects below 13 $M_{\rm Jup}$ are classified as exoplanets, while more massive objects below the substellar/stellar mass limit (at about 0.072 $M_\odot$ for solar metallicity) as brown dwarfs, respectively. Thereby the given masses of the exoplanets, detected by radial velocity measurements, correspond to minimum-masses ($M \sin(i)$) due to the unknown orbital inclination, while masses of direct imaging planets are usually derived from their spectrophotometry with evolutionary models.

In **Table 2** for each exoplanet host and its detected co-moving companion(s) their Gaia DR2 parallax π, proper motion in right ascension and declination ($\mu_\alpha \cos(\delta)$ and μ_δ), astrometric excess noise (epsi) with its significance (sig-epsi), apparent G-band magnitude, as well as the used Apsis-Priam G-band extinction estimate A_G are listed. In the case that the G-band extinction was taken from the StarHorse catalog this is indicated with the SHC flag, or with the ✠ flag if the G-band extinction was derived from V-band extinction measurements, either listed in the VizieR database or from the literature. In this table the exoplanet hosts are indicated with *, and known spectroscopic binary stars among them with (SB).

Table 3 lists for each detected companion its angular separation (ρ) and position angle (PA) to the associated exoplanet host, which were determined with the Gaia DR2 astrometry of the objects for the (Gaia reference) epoch 2015.5. The relative astrometry of the companions exhibits an uncertainty on average of 0.3 mas in angular separation, and 0.002° in position angle, respectively. In the following columns of **Table 3** we list the parallax difference ($\Delta\pi$) with its significance (in brackets calculated by taking into account also the Gaia astrometric excess noise[3]) between the exoplanet hosts and their detected companions, their differential proper motion $\mu_{\rm rel}$ with its significance, and the cpm-index of all systems. The precise Gaia DR2 astrometry proves the equidistance (sig-$\Delta\pi < 2.3\sigma$, average value of 0.5σ) and common proper motion (cpm − index > 6, average cpm − index = 118) of the exoplanet hosts and their companions. If these companions are not listed yet as companion (-candidates) in the Washington Double Star Catalog (WDS from hereon, Mason et al., 2001) this is indicated with the ★ flag in last column of **Table 3**. In the case that the companion is not listed in the WDS but was reported in literature before, additional information is given in the notes of this table.

In **Table 4** beside the equatorial coordinates (α, δ both for epoch 2015.5) of all detected companions, their derived absolute G-band magnitude M_G, projected separation *sep* to the associated exoplanet host (relative uncertainty about 1%, on average), mass, and effective temperature $T_{\rm eff}$ are summarized. The flags listed in the last column of this table are defined as follows:

- PRI: An Apsis-Priam temperature estimate is available for the detected companion, which could be compared with the effective temperature of the companion, derived from its absolute G-band photometry using the Baraffe et al. (2015) models.
- 2MA: The companion is listed in the 2MASS Point Source catalog.
- BPRP: The $G_{\rm BP} - G_{\rm RP}$ color of the exoplanet host and of the detected companion is listed in the Gaia DR2, hence a color comparison was feasible.
- EXT: Because of its brightness the companion exceeds the magnitude range of the Baraffe et al. (2015) evolutionary

[3]The astrometric excess noise is conservatively considered here as additional parallax uncertainty of the source.

TABLE 3 | The relative astrometry and WDS status of all detected companions.

Companion	ρ (arcsec)	PA (°)	$\Delta\pi$ (mas)	sig-$\Delta\pi$	μ_{rel} (mas/yr)	sig-μ_{rel}	cpm-index	Not in WDS
HD 1160 C	5.14549 ± 0.00018	349.53223 ± 0.00259	0.95 ± 0.28	3.3 (1.2)	1.72 ± 0.33	5.2	30	
Gliese 49 B	294.45989 ± 0.00011	75.52728 ± 0.00002	0.17 ± 0.09	2.0 (0.8)	4.36 ± 0.23	19	338	
HD 8326 B	56.88131 ± 0.00005	147.16909 ± 0.00006	0.12 ± 0.08	1.6 (0.3)	1.18 ± 0.17	7.1	394	
HD 13167 B	20.06421 ± 0.00010	24.77589 ± 0.00028	0.11 ± 0.13	0.8 (0.2)	1.28 ± 0.23	5.7	91	★
HR 858 B	8.35742 ± 0.00013	15.79337 ± 0.00060	1.04 ± 0.18	5.8 (1.2)	13.90 ± 0.22	62	24	★
HD 18015 B	7.08916 ± 0.00006	316.16832 ± 0.00045	0.11 ± 0.07	1.6 (1.6)	1.61 ± 0.11	14	79	
K2-288 A	0.78692 ± 0.00018	340.38240 ± 0.01437	0.93 ± 0.22	4.3 (1.0)	4.75 ± 0.64	7.4	84	★[b]
HD 23472 B	9.56924 ± 0.00008	45.28294 ± 0.00046	0.08 ± 0.08	1.1 (0.2)	1.23 ± 0.18	7.0	181	★
HD 24085 A	75.91260 ± 0.00003	263.05666 ± 0.00002	0.04 ± 0.03	1.3 (1.3)	1.01 ± 0.06	16	194	★
HII 1348 C	36.02849 ± 0.00016	276.87735 ± 0.00017	0.34 ± 0.18	1.9 (0.7)	1.22 ± 0.35	3.5	82	★
HII 1348 D	55.01726 ± 0.00090	182.06892 ± 0.00182	0.91 ± 1.78	0.5 (0.3)	4.00 ± 3.05	1.3	25	★
HATS-57 B	14.44086 ± 0.00010	282.25351 ± 0.00032	0.06 ± 0.13	0.4 (0.4)	0.88 ± 0.16	5.4	43	★
FU Tau B	5.68952 ± 0.00112	123.57637 ± 0.00858	0.11 ± 1.30	0.1 (0.0)	5.60 ± 4.05	1.4	8	
DH Tau C	15.29981 ± 0.00007	126.08805 ± 0.00023	0.01 ± 0.09	0.2 (0.2)	0.53 ± 0.11	4.7	83	
51 Eri B (SB)	66.96749 ± 0.00027	162.62918 ± 0.00028	4.39 ± 0.39	11.2 (2.1)	19.04 ± 0.71	27	8	
2M 0441+23 AB	12.31449 ± 0.00036	57.55273 ± 0.00133	0.29 ± 0.39	0.7 (0.2)	0.67 ± 0.94	0.7	70	
NGTS-6 B	5.36108 ± 0.00005	116.68846 ± 0.00060	0.01 ± 0.07	0.1 (0.0)	0.14 ± 0.12	1.2	342	★
AB Dor BD	8.87930 ± 0.00018	347.19358 ± 0.00097	1.71 ± 0.17	10.1 (1.7)	53.56 ± 0.33	164	6	
HD 39855 B	10.72622 ± 0.00004	19.55064 ± 0.00017	0.00 ± 0.05	0.0 (0.0)	13.00 ± 0.09	145	15	
NGTS-10 B	1.12234 ± 0.00023	334.73644 ± 0.01107	2.78 ± 0.27	10.2 (1.3)	1.48 ± 0.41	3.6	14	★[c]
L2 Pup B	32.80132 ± 0.00052	63.66528 ± 0.00099	0.80 ± 0.99	0.8 (–)	2.32 ± 1.08	2.2	296	★
HIP 38594 B	399.81589 ± 0.00012	208.91546 ± 0.00001	0.06 ± 0.09	0.7 (0.7)	6.44 ± 0.24	27	113	
WASP-180 B	4.86185 ± 0.00006	138.92126 ± 0.00081	0.05 ± 0.09	0.5 (0.5)	1.42 ± 0.19	7.6	19	
HD 79211 A	17.08255 ± 0.00004	277.72812 ± 0.00014	0.01 ± 0.06	0.1 (0.1)	94.92 ± 0.08	1,136	35	
HD 85628 B	4.33622 ± 0.00004	224.93946 ± 0.00056	0.12 ± 0.05	2.5 (0.4)	2.15 ± 0.08	27	14	★[d]
TOI 717 B	65.46692 ± 0.00016	88.63021 ± 0.00020	0.01 ± 0.11	0.1 (0.1)	2.10 ± 0.25	8.4	64	
G 196-3 B	16.06941 ± 0.00055	209.15563 ± 0.00166	1.51 ± 0.81	1.9 (0.6)	6.99 ± 1.53	4.6	71	
LTT 3780 B	15.78849 ± 0.00011	97.14133 ± 0.00038	0.18 ± 0.14	1.3 (0.4)	0.55 ± 0.17	3.2	1,535	
MASCARA-3 B	2.06449 ± 0.00010	173.15273 ± 0.00345	0.69 ± 0.13	5.3 (0.9)	6.20 ± 0.31	20	21	★[e]
2M J1101-7732 B	1.42656 ± 0.00041	30.00553 ± 0.01621	0.03 ± 0.39	0.1 (0.0)	1.02 ± 0.86	1.2	45	
WASP-175 B	7.25020 ± 0.00003	4.95541 ± 0.00027	0.03 ± 0.05	0.6 (0.6)	0.29 ± 0.07	3.9	175	★[f]
CHXR 73 C	46.10344 ± 0.00027	248.30821 ± 0.00031	0.02 ± 0.28	0.1 (0.0)	1.65 ± 0.42	3.9	27	★
GJ 414 B	34.15873 ± 0.00007	262.44625 ± 0.00011	0.12 ± 0.07	1.6 (1.6)	16.09 ± 0.12	139	78	
HD 97334 BC	89.88421 ± 0.00098	245.04583 ± 0.00060	1.27 ± 1.10	1.2 (0.2)	13.05 ± 2.13	6.1	44	
HD 233832 B	4.93691 ± 0.00004	266.38672 ± 0.00079	0.07 ± 0.09	0.8 (0.8)	6.88 ± 0.11	63	143	
2M J1155-7919 B	5.75435 ± 0.00047	227.86140 ± 0.00458	0.07 ± 0.53	0.1 (0.0)	1.48 ± 1.20	1.2	55	★[g]
NGTS-5 B	26.89147 ± 0.00011	116.31597 ± 0.00021	0.29 ± 0.13	2.2 (0.7)	0.46 ± 0.20	2.3	63	★
2M J1450-7841 B	4.23901 ± 0.00099	313.26065 ± 0.01318	2.29 ± 1.03	2.2 (0.7)	3.01 ± 2.17	1.4	29	★[h]
WASP-189 B	9.41610 ± 0.00010	70.78901 ± 0.00095	0.72 ± 0.18	4.0 (1.4)	0.25 ± 0.21	1.2	446	★
HIP 73990 D	47.27427 ± 0.00009	56.65125 ± 0.00010	0.08 ± 0.11	0.7 (0.2)	0.37 ± 0.18	2.0	219	★
TOI 905 B	2.24803 ± 0.00050	100.34253 ± 0.01658	1.58 ± 0.55	2.9 (1.0)	7.67 ± 0.76	10	12	
2M 1510 B	6.77139 ± 0.00046	209.28499 ± 0.00431	0.47 ± 0.56	0.8 (0.2)	1.74 ± 0.95	1.8	146	★[i]
β Cir B	217.62247 ± 0.00055	199.25875 ± 0.00013	0.39 ± 0.81	0.5 (0.1)	4.29 ± 1.08	4.0	78	
KELT-23 B	4.54135 ± 0.00006	127.68919 ± 0.00069	0.00 ± 0.06	0.1 (0.0)	1.18 ± 0.10	12	21	★[j]
K2-290 C	11.25119 ± 0.00017	179.97609 ± 0.00151	0.42 ± 0.28	1.5 (0.7)	0.47 ± 0.44	1.1	135	★[k]
GQ Lup C	16.11286 ± 0.00039	114.61327 ± 0.00099	1.09 ± 0.46	2.4 (0.4)	1.74 ± 0.70	2.5	31	
HIP 77900 B	22.27990 ± 0.00044	12.74996 ± 0.00267	1.38 ± 0.98	1.4 (0.6)	2.08 ± 1.14	1.8	27	★[l]
USco 1602-2401 B	7.21512 ± 0.00008	353.20771 ± 0.00157	0.61 ± 0.21	2.9 (0.7)	0.86 ± 0.34	2.5	62	
HIP 79098 C	65.29721 ± 0.00018	101.86730 ± 0.00008	0.35 ± 0.19	1.9 (0.5)	2.30 ± 0.28	8.3	25	★[m]
USco 1610-1913 B	5.82725 ± 0.00040	113.57990 ± 0.00238	0.54 ± 0.38	1.4 (0.4)	2.69 ± 1.01	2.7	19	
USco 1612-1800 B	3.18438 ± 0.00019	10.65437 ± 0.00561	0.27 ± 0.33	0.8 (0.2)	1.47 ± 0.54	2.7	29	★[n]
ROXs 12 C	37.14026 ± 0.00004	185.99483 ± 0.00012	0.06 ± 0.08	0.7 (0.1)	0.66 ± 0.17	3.9	79	★[o]
HATS-48 B	5.43813 ± 0.00025	267.59024 ± 0.00322	0.13 ± 0.44	0.3 (0.2)	0.96 ± 0.45	2.2	13	★[p]
GJ 752 B	75.48951 ± 0.00011	152.49075 ± 0.00009	0.20 ± 0.14	1.4 (0.2)	37.74 ± 0.25	153	78	
HD 181234 B	5.17023 ± 0.00011	56.61253 ± 0.00118	0.05 ± 0.16	0.3 (0.1)	7.22 ± 0.22	32	95	
Wendelstein-1 B	11.79208 ± 0.00024	232.62838 ± 0.00116	0.34 ± 0.41	0.8 (0.3)	0.45 ± 0.53	0.9	20	★
2M J2126-81 B	217.49441 ± 0.00082	123.98914 ± 0.00024	0.04 ± 0.92	0.0 (0.0)	8.34 ± 2.34	3.6	30	
TOI 132 B	19.64887 ± 0.00018	151.44437 ± 0.00044	0.11 ± 0.23	0.5 (0.1)	0.58 ± 0.36	1.6	218	★
NGTS-7 B	1.13095 ± 0.00014	117.57142 ± 0.01072	0.73 ± 0.14	5.1 (1.1)	2.16 ± 0.30	7.3	30	★[q]
DS Tuc B	5.36461 ± 0.00003	347.65815 ± 0.00047	0.02 ± 0.05	0.3 (0.3)	2.22 ± 0.08	29	93	
1RXS J2351+3127 C	126.01641 ± 0.00005	98.50769 ± 0.00002	0.04 ± 0.08	0.5 (0.1)	0.83 ± 0.09	8.7	333	

Comments on individual companions:

[a]*This companion was first reported by Vanderburg et al. (2019), who have already verified its equidistance and common proper motion with the exoplanet host star HR 858 A using Gaia DR2 data, consistent with the results, obtained in this study.*

[b]This companion was detected by Feinstein et al. (2019) and its companionship with the exoplanet host star K2-288 B was proven with Gaia DR2 astrometry, confirmed by the astrometric analysis, carried out in the study, presented here.
[c]This star was already noticed in the Gaia DR2 by McCormac et al. (2020) as common proper motion companion of the exoplanet host star NGTS-10 A, consistent with the results, derived in this study.
[d]This companion of the exoplanet host star HD 85628 A was discovered by Dorval et al. (2020) in the Gaia DR2, who found its parallax and proper motion consistent with that of the exoplanet host star, confirmed by the astrometric analysis, presented here.
[e]This companion was detected with AO imaging by Rodriguez et al. (2019) using Keck/NIRC 2, but is also listed in the Gaia DR2, whose astrometry was used by this team to verify the equidistance and common proper motion of this companion with the exoplanet host star MASCARA-3 A, as done in this study.
[f]This companion was already reported by Nielsen et al. (2019), who proved its companionship with the exoplanet host star WASP-175 A with Gaia DR2 astrometry, consistent with the results derived here.
[g]The equidistance and common proper motion of this substellar object with the exoplanet host star 2M J1155-7919 A was verified by Dickson-Vandervelde et al. (2020) using Gaia DR2 data, as done in this work.
[h]This companion was detected by Burgasser et al. (2017) and its common proper motion with the brown dwarf 2M J1450-7841 A, listed in the EPE, was verified with ground based astrometry, confirmed in this study with Gaia DR2 data, which furthermore proves the equidistance of both objects.
[i]This companion was noticed by Triaud et al. (2020) in the Gaia DR2 as equidistant and co-moving companion of the brown dwarf 2M 1510 A, which is listed in the EPE, consistent with our results.
[j]KELT-23 B was first discovered by (Johns et al., 2019) with Keck/NIRC2 AO imaging, who used Gaia DR2 astrometry to prove the equidistance and common proper motion of the companion with the exoplanet host star KELT-23 A, as done in this study.
[k]This companion was already described by Hjorth et al. (2019), who have verified it to be equidistant and co-moving with the exoplanet host star K2-290 A, using Gaia DR2 data, a conclusion, which is confirmed by the analysis, presented here. Furthermore, this team identified an additional but closer stellar companion-candidate of the exoplanet host star (K2-290 B) with Subrau/IRCS AO imaging, which however still needs astrometric confirmation of its companionship. Due to its close angular separation to K2-290 A we adopt here this object as companion of the exoplanet host star.
[l]This companion was revealed spectro-photometrically by Aller et al. (2013). With Gaia DR2 astrometry we prove here its companionship with the exoplanet host star HIP 77900 A.
[m]HIP 79098 C was reported by (Janson et al., 2019) as equidistant and co-moving companion of the exoplanet host star HIP 79098 A, based on its Gaia DR2 astrometry, confirmed by the analysis of the companion, which is presented here.
[n]This companion was revealed spectro-photometrically by Aller et al. (2013). The equidistance and common proper motion of this companion with the exoplanet host star USco 1612-1800 A was proven in this study, with Gaia DR2 astrometry.
[o]This star was identified by (Bowler et al., 2017) as companion of ROXs 12 A, based on its radial velocity and proper motion. We prove the equidistance of both stars with their Gaia DR2 astrometry, which also confirms their common proper motion.
[p]This companion was reported by (Hartman et al., 2020), who used the Gaia DR2 astrometry to confirm its companionship with the exoplanet host star HATS-48 A, as done in this work.
[q]NGTS-7 B was revealed by (Jackman et al., 2019) as companion of the exoplanet host star NGTS-7 A using Gaia DR2 astrometry, as done in this study.

models. Therefore, the properties of the companion were estimated via extrapolation from the two brightest sources of the used model isochrone.
- WD: The detected companion is a white dwarf.
- BD: The detected companion is a brown dwarf.

Finally, in **Table 5** we summarize all those detected companions, whose differential proper motion $\mu_{\rm rel}$ significantly exceeds their expected escape velocity $\mu_{\rm rel}$. Companions, which are already known to be members of hierarchical triple star systems, are indicated with the flag *** in the last column of this table.

Among all 289 targets, whose multiplicity was investigated in the study, whose results are presented in this paper, 41 binary and five hierarchical triple star systems with exoplanets were identified. This yields a multiplicity rate of the targets of 16 ± 2%, very well consistent with the multiplicity rate of exoplanet host stars of 15 ± 1%, reported before by Mugrauer (2019). This is as expected, as the sensitivities of the two surveys should agree well with each other, as the brightness and mass of their targets match, and the distance of the targets from this survey is on average about 40% smaller than that of the targets from Mugrauer (2019), resulting in a reduction in the distance modulus of only about 1 mag. In total, 61 companions (48 stars and 13 brown dwarfs) could be detected in the Gaia DR2 around the targets. The detected substellar companions are all listed as exoplanets in the EPE. The cumulative distribution functions of the derived properties (projected separation, mass and effective temperature) of theses companions, are illustrated in **Figures 3–5**. The separation-mass diagram of the companions is shown in **Figure 6**. As described above, the accurate Gaia DR2 astrometry proves the equidistance and common proper motion of all detected companions with the associated exoplanet hosts, and for the majority of these companions their differential proper motion to the exoplanet hosts is slower than their estimated escape velocity, facts that are expected for gravitationally bound systems. In contrast, the differential proper motion of the companions, which are listed in **Table 5**, exceeds their estimated escape velocity, possibly indicating a higher degree of multiplicity[4]. Indeed, one of these companions (51 Eri BC) is already known to be a close binary itself. The remaining two companions and their primaries are promising targets for follow-up observations to check their multiplicity status e.g. with high contrast AO imaging observations.

All detected companions exhibit projected separations to the associated exoplanet hosts in the range between 52 and 9,555 au (average separation of about 2,310 au). The highest companion frequency is found at projected separations between about 240 and 400 au and half of all companions are located at projected separations below about 1,240 au. The closest detected companion is K2-288 A, which is separated from the exoplanet host star K2-288 B by 52 au, and it is the only companion identified in this study within a projected separation of 100 au. The masses of the companions range between 0.016 and 1.66 $M_\odot$ (average mass of 0.36 $M_\odot$) and companions are found most frequently in the substellar mass

[4]Additional close companions either of the exoplanet hosts or of the companions force these objects on close orbits with high orbital velocities around a common barycenter that could induce the observed high differential velocities.

TABLE 4 | The equatorial coordinates and derived physical properties of all detected companions.

Companion	α (°)	δ (°)	M_G (mag)	sep (au)	mass ($M_\odot$)	T_{eff} (K)	Flags
HD 1160 C	3.98858470355	4.25245524714	$9.72^{+0.10}_{-0.13}$	648	$0.378^{+0.021}_{-0.016}$	3503^{+25}_{-19}	BPRP PRI
Gliese 49 B	15.83942593995	62.36588062663	$11.35^{+0.41}_{-0.22}$	2,902	$0.169^{+0.020}_{-0.030}$	3211^{+40}_{-74}	2MA BPRP PRI
HD 8326 B	20.54104760211	−26.90734439784	$11.48^{+0.04}_{-0.25}$	1747	$0.198^{+0.023}_{-0.003}$	3257^{+37}_{-7}	2MA BPRP PRI
HD 13167 B	32.06020575541	−24.69051459458	$11.33^{+0.07}_{-0.06}$	3,001	$0.211^{+0.006}_{-0.007}$	3279^{+9}_{-10}	2MA BPRP
HR 858 B	42.98571355919	−30.81182706733	$13.39^{+0.09}_{-0.11}$	267	$0.112^{+0.003}_{-0.002}$	2926^{+20}_{-19}	BPRP PRI
HD 18015 B	43.36225373946	− 8.84661863284	$6.62^{+0.04}_{-0.04}$	881	$0.747^{+0.004}_{-0.004}$	4650^{+20}_{-18}	2MA BPRP PRI
K2-288 A	55.44420842474	18.26869720107	$8.65^{+0.09}_{-0.09}$	52	$0.534^{+0.010}_{-0.010}$	3777^{+30}_{-28}	2MA
HD 23472 B	55.46315889099	−62.76539647729	$12.79^{+0.07}_{-0.18}$	374	$0.129^{+0.006}_{-0.002}$	3038^{+30}_{-13}	2MA BPRP PRI
HD 24085 A	56.19506729271	−70.02706843481	$2.90^{+0.39}_{-0.59}$	4,174	$1.254^{+0.088}_{-0.058}$	6339^{+211}_{-139}	2MA BPRP PRI EXT
HII 1348 C	56.81444339267	24.39176993016	$10.07^{+0.33}_{-0.31}$	5,155	$0.322^{+0.048}_{-0.046}$	3436^{+58}_{-60}	2MA BPRP PRI ***
HII 1348 D	56.82474725542	24.37529892928	$14.35^{+0.46}_{-0.37}$	7,872	$0.055^{+0.005}_{-0.006}$	2602^{+78}_{-96}	BD 2MA BPRP ***
HATS-57 B	60.94413061754	−19.05596683949	$10.25^{+0.05}_{-0.18}$	4,068	$0.331^{+0.023}_{-0.007}$	3448^{+24}_{-7}	2MA BPRP
FU Tau B	65.89894960541	25.04979704793	$12.62^{+0.49}_{-0.26}$	749	$0.018^{+0.002}_{-0.003}$	2553^{+38}_{-71}	BD 2MA BPRP
DH Tau C	67.42700661202	26.54688636442	$3.64^{+0.17}_{-0.37}$	2071	$1.655^{+0.228}_{-0.106}$	4837^{+164}_{-77}	2MA BPRP PRI EXT
51 Eri B (SB)	69.40630139702	− 2.49157819607	$7.18^{+0.11}_{-0.27}$	1994	$0.733^{+0.056}_{-0.024}$	3962^{+116}_{-49}	2MA BPRP PRI ***
2M 0441+23 AB[a]	70.44024465438	23.03268965375	$7.37^{+0.43}_{-0.96}$	1,483	$0.241^{+0.147}_{-0.061}$	3308^{+300}_{-138}	2MA BPRP
NGTS-6 B	75.79692465277	−30.40013000839	$9.23^{+0.14}_{-0.10}$	1,667	$0.457^{+0.013}_{-0.018}$	3618^{+21}_{-29}	2MA BPRP PRI
AB Dor BD	82.18603484814	−65.44557858318	$9.08^{+0.44}_{-0.52}$	136	$0.466^{+0.061}_{-0.059}$	3645^{+167}_{-104}	2MA BPRP PRI ***
HD 39855 B	88.62713212305	−19.70163948841	$8.02^{+0.13}_{-0.23}$	250	$0.598^{+0.024}_{-0.014}$	3978^{+103}_{-41}	2MA BPRP PRI
NGTS-10 B	91.87213254706	−25.59461438962	$7.27^{+0.61}_{-1.21}$	364	$0.665^{+0.121}_{-0.059}$	4327^{+606}_{-284}	
L2 Pup B	108.39678197580	−44.63427669967	$11.39^{+0.17}_{-0.33}$	2,101	$0.203^{+0.032}_{-0.012}$	3270^{+49}_{-26}	
HIP 38594 B	118.48449010900	−25.39952189079	$14.43^{+0.26}_{-0.78}$	7,116	~ 0.6		WD 2MA BPRP PRI
WASP-180 B	123.39313443835	− 1.98380547425	$4.64^{+0.06}_{-0.16}$	1,244	$1.057^{+0.029}_{-0.011}$	5778^{+93}_{-36}	2MA BPRP PRI
HD 79211 A	138.58391575741	52.68415915741	$7.59^{+0.21}_{-0.33}$	108	$0.644^{+0.034}_{-0.022}$	4180^{+153}_{-97}	2MA BPRP PRI
HD 85628 B	147.57796550484	−66.11477795490	$7.38^{+0.23}_{-0.15}$	744	$0.675^{+0.016}_{-0.025}$	4282^{+66}_{-104}	BPRP PRI
TOI 717 B	147.98872815946	2.11708155887	$9.72^{+0.02}_{-0.13}$	2,275	$0.398^{+0.017}_{-0.003}$	3519^{+25}_{-3}	2MA BPRP PRI
G 196-3 B	151.08506490419	50.38228242112	$17.41^{+0.48}_{-0.49}$	350	$0.032^{+0.002}_{-0.002}$	1987^{+94}_{-93}	BD 2MA BPRP
LTT 3780 B	154.64934761666	−11.71834621199	$12.27^{+0.34}_{-0.26}$	347	$0.149^{+0.014}_{-0.014}$	3127^{+43}_{-58}	2MA BPR PPRI
MASCARA-3 B	161.90924448675	71.65515762432	$7.83^{+0.12}_{-0.28}$	200	$0.625^{+0.030}_{-0.013}$	4074^{+126}_{-53}	
2M J1101-7732 B	165.33045751133	−77.54374799758	$12.48^{+0.14}_{-0.14}$	264	$0.019^{+0.001}_{-0.001}$	2574^{+21}_{-21}	BD
WASP-175 B	166.31900970217	−34.12073886500	$5.46^{+0.10}_{-0.11}$	3,971	$0.919^{+0.018}_{-0.016}$	5290^{+65}_{-60}	2MA BPR PPRI
CHXR 73 C	166.56385863699	−77.63060598303	$8.04^{+1.03}_{-1.03}$	8,808	$0.235^{+0.148}_{-0.112}$	3280^{+295}_{-260}	2MA BPRP
GJ 414 B	167.76359381364	30.44392150823	$8.06^{+0.32}_{-0.57}$	406	$0.587^{+0.056}_{-0.034}$	3971^{+249}_{-110}	2MABPRP PRI
HD 97334 BC[b]	168.10555672848	35.80289455668	$18.16^{+0.04}_{-0.19}$	2036	$0.028^{+0.001}_{-0.001}$	1845^{+36}_{-8}	BD 2MA BPRP
HD 233832 B	171.51750545565	50.37622350226	$8.64^{+0.11}_{-0.21}$	290	$0.531^{+0.022}_{-0.012}$	3775^{+68}_{-36}	2MA BPRP PRI
2M J1155-7919 B	178.76276748600	−79.32082818366	$14.48^{+0.02}_{-0.06}$	582	$0.016^{+0.001}_{-0.001}$	2366^{+10}_{-2}	BD 2MA BPRP
NGTS-5 B	221.06499706987	5.60206193982	$9.67^{+0.12}_{-0.11}$	8,323	$0.405^{+0.014}_{-0.016}$	3530^{+22}_{-20}	2MA BPRP
2M J1450-7841 B	222.67064914833	−78.69407266366	$15.35^{+0.51}_{-0.51}$	387	$0.031^{+0.005}_{-0.003}$	2328^{+114}_{-100}	BD 2MA BPRP
WASP-189 B	225.68920534342	− 3.03062676806	$9.12^{+0.23}_{-0.16}$	942	$0.479^{+0.021}_{-0.030}$	3646^{+33}_{-48}	2MA BPRP PRI
HIP 73990 D	226.82470360183	−29.49738818566	$8.33^{+0.45}_{-0.64}$	5,234	$0.470^{+0.151}_{-0.098}$	3576^{+191}_{-107}	2MA BPRP PRI
TOI 905 B	227.66059753260	−71.36174373792	$10.93^{+0.17}_{-0.14}$	358	$0.251^{+0.014}_{-0.016}$	3340^{+21}_{-25}	
2M 1510 B	227.69777941730	−28.30671294175	$15.13^{+0.03}_{-0.14}$	249	$0.033^{+0.001}_{-0.001}$	2376^{+31}_{-6}	BD 2MA BPRP
β Cir B	229.33920903332	−58.85886078926	$16.91^{+0.16}_{-0.23}$	6,187	$0.063^{+0.002}_{-0.002}$	2159^{+47}_{-48}	BD 2MA BPRP
KELT-23 B	232.14912993468	66.35793842725	$9.94^{+0.05}_{-0.10}$	575	$0.368^{+0.014}_{-0.007}$	3487^{+15}_{-7}	2MA BPRP PRI
K2-290 C	234.85788601749	−20.20202286624	$10.51^{+0.27}_{-0.26}$	3,094	$0.292^{+0.033}_{-0.026}$	3404^{+38}_{-41}	2MA BPRP***
GQ Lup C	237.30537201266	−35.65336961027	$9.70^{+0.42}_{-0.34}$	2,446	$0.075^{+0.016}_{-0.015}$	2897^{+14}_{-33}	2MA BPRP
HIP 77900 B	238.62692763313	−27.33270712891	$13.48^{+0.05}_{-0.16}$	3,374	$0.020^{+0.001}_{-0.001}$	2519^{+22}_{-8}	BD BPRP
USco 1602-2401 B[c]	240.71312906858	−24.03074240242	$8.69^{+0.12}_{-0.12}$	1,038	$0.238^{+0.016}_{-0.017}$	3280^{+25}_{-27}	2MA BPRP PRI
HIP 79098 C	242.20150369275	−23.68925441843	$9.82^{+0.24}_{-0.15}$	9,555	$0.159^{+0.013}_{-0.020}$	3176^{+24}_{-40}	2MA BPRP PRI ***
USco 1610-1913 B	242.63466253957	−19.21910506083	$12.71^{+0.39}_{-0.39}$	777	$0.025^{+0.003}_{-0.003}$	2615^{+47}_{-47}	BD 2MA BPRP
USco 1612-1800 B	243.20402838620	−18.01380384763	$12.50^{+0.39}_{-0.39}$	504	$0.026^{+0.003}_{-0.003}$	2642^{+48}_{-48}	BD BPRP
ROXs 12 C	246.61560598363	−25.45695531769	$7.28^{+1.00}_{-1.00}$	5,095	$0.474^{+0.259}_{-0.181}$	3657^{+343}_{-289}	2MA BPR PPRI
HATS-48 B	288.66902407326	−59.57941400923	$11.71^{+0.37}_{-0.19}$	1,444	$0.181^{+0.013}_{-0.022}$	3219^{+30}_{-60}	2MA BPRP
GJ 752 B	289.23745710752	5.14456304678	$14.04^{+0.17}_{-0.28}$	446	$0.098^{+0.005}_{-0.002}$	2785^{+60}_{-36}	2MA BPRP PRI
HD 181234 B	290.00108472870	−9.32417966740	$10.46^{+0.07}_{-0.20}$	247	$0.297^{+0.026}_{-0.007}$	3412^{+29}_{-11}	2MA BPRP PRI
Wendelstein-1 B	299.04791069915	17.56797448132	$11.43^{+0.43}_{-0.47}$	3,632	$0.202^{+0.047}_{-0.030}$	3264^{+72}_{-70}	2MA BPRP
2M J2126-81 B	321.71158783493	−81.67526360458	$17.84^{+0.05}_{-0.43}$	7,427	$0.020^{+0.001}_{-0.004}$	1851^{+41}_{-77}	BD 2MA BPRP
TOI 132 B	338.40325545731	−43.44166603901	$12.21^{+0.14}_{-0.16}$	3,231	$0.152^{+0.009}_{-0.006}$	3137^{+27}_{-24}	2MA BPRP
NGTS-7 B	352.52202473338	−38.97006605140	$9.32^{+0.50}_{-0.50}$	156	$0.384^{+0.097}_{-0.091}$	3495^{+102}_{-97}	
DS Tuc B	354.91457052896	−69.19458723114	$5.86^{+0.10}_{-0.24}$	237	$0.834^{+0.060}_{-0.027}$	5040^{+180}_{-79}	2MA BPRP PRI
1RXS J2351+3127 C	357.93142859121	31.45083817280	$9.61^{+0.04}_{-0.43}$	5,427	$0.394^{+0.057}_{-0.007}$	3522^{+98}_{-8}	2MA BPRP PRI

[a]*2M 0441+23 B is a close brown dwarf companion of 2M 0441+23 A.*

[b]*HD 97334 BC is a binary brown dwarf system.*

[c]*The brown dwarf USco 1602-2401 B was detected by Aller et al. (2013) and its possible companionship to USco 1602-2401 A, was revealed with photometry and follow-up spectroscopy, which was finally proven in this study with the Gaia DR2 astrometry of the companion, i.e. confirmation of equidistance, and common proper motion, as well as test for gravitational stability. USco 1602-2401 B is one of 14 reported substellar companions, detected by Gaia, which were also characterized in this study using their Gaia DR2 astro- and photometry. In general, the derived mass of these substellar companions agrees well with the mass given in the literature, with a deviation of only a few M_{Jup}, on average. In contrast, for USco 1602-2401 B Aller et al. (2013) derived a mass of $41^{+20}_{-13} M_{Jup}$ at an age of 5 Myr ($47^{+20}_{-18} M_{Jup}$ at 10 Myr) adopting a distance of about 145 pc and no extinction. With the Gaia DR2 parallax and the Starhorse extinction estimate of the primary star and the G-band photometry of the companion we obtained a significantly higher mass of $0.238^{+0.016}_{-0.017} M_{\odot}$ at 5 Myr ($0.309^{+0.020}_{-0.019} M_{\odot}$ at 10 Myr). Adopting A_G = 0 mag yields a mass of the companion of $0.071^{+0.001}_{-0.001} M_{\odot}$ for 5 Myr, and $0.104^{+0.001}_{-0.001} M_{\odot}$ for 10 Myr, respectively. Therefore, we classify this companion here as low-mass star.*

TABLE 5 | List of all detected companions, whose differential proper motion μ_{rel} exceeds their estimated escape velocity μ_{esc}.

Companion	μ_{rel} (mas/yr)	μ_{esc} (mas/yr)	
51 Eri B (SB)	19.04 ± 0.71	11.298 ± 0.144	***
HIP 38594 B	6.44 ± 0.24	4.965 ± 0.082	
TOI 905 B	7.67 ± 0.76	3.090 ± 0.144	

regime between 0.016 up to 0.033 $M_{\odot}$, while more massive companions are detected at a lower but constant frequency up to about 0.7 $M_{\odot}$, and only about 10% of all the detected companions exhibit masses larger than 0.7 $M_{\odot}$. The companions exhibit effective temperatures in the range between about 1850 and 6350 K (average temperature of about 3400 K), which corresponds to spectral types of L3 to F6 (M3, on average), according to the $T_{\rm eff} - SpT$ relation[5] from (Pecaut and Mamajek, 2013).

In general the effective temperature of the detected companions, determined with their derived absolute G-band magnitude, using the evolutionary Baraffe et al. (2015) models, agree well with their Gaia DR2 Apsis-Priam temperature estimate (if available) with a characteristic deviation of about ±350 K, consistent with the typical uncertainty of the different temperature estimates, which is in the order of about 330 K. Only in the case of HIP 38594 B the temperature estimate, based on the absolute G-band photometry of the companion significantly deviates by more than 2300 K from its Apsis-Priam temperature estimate, which is also about 900 K higher than the one of the associated exoplanet host star HIP 38594 A. Furthermore, the companion appears bluer ($\Delta(G_{\rm BP} - G_{\rm RP}) = -0.669 \pm 0.004$ mag) than its primary although it is about 7 mag fainter in the G-band than the exoplanet host star. The intrinsic faintness and high temperature of HIP 38594 B clearly indicates that this companion is a white dwarf. This conclusion is consistent with the results of Subasavage et al. (2008), who have already classified the companion spectroscopically as a white dwarf, and have denote it as WD 0751-252. For this degenerated companion we adopt here a mass of about 0.6 $M_{\odot}$.

In **Figure 7** the G-band magnitude difference of all detected companions to the associated exoplanet hosts is plotted vs. their angular separation. For comparison we show as dashed line in this figure the estimate of the Gaia detection limit, reported by Mugrauer (2019) which was further constrained by Mugrauer and Michel (2020). Companions of exoplanet hosts brighter than 12.8 mag are plotted as open circles those of hosts, which are fainter than that magnitude limit, as filled black circles, respectively. A magnitude difference of about 5 mag is reached at an angular separation of about two arcsec, consistent with the estimate of the Gaia detection limit, determined by Mugrauer (2019). Only two companions significantly exceed the limit estimate, namely K2-288 A at an angular separation of about 0.8 arcsec with $\Delta G \sim 1.2$ mag and HIP 77900 B, at 22.3 arcsec with $\Delta G \sim 13.5$ mag. While K2-288 A is a companion of a target fainter than $G = 12.8$ mag for which Gaia reaches a higher sensitivity at angular separations slightly below one arcsec (up to 3 mag, as described by Mugrauer and Michel, 2020) the detection of HIP 77900 B indicates that the given limit estimate might be too conservative at angular separations beyond about 20 arcsec.

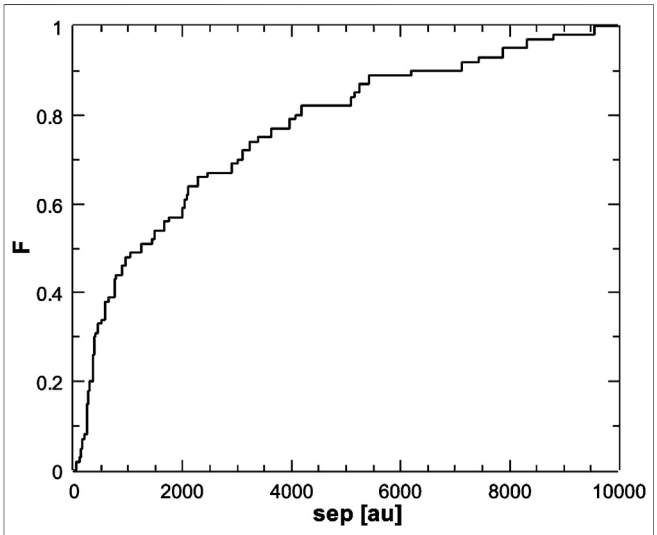

FIGURE 3 | The cumulative distribution function of the projected separation (sep) of all detected companions to the associated exoplanet hosts.

4 SUMMARY AND OUTLOOK

The study, presented here, is a continuation of a survey, which was initiated at the Astrophysical Institute and University Observatory Jena, to investigate the multiplicity status of exoplanet hosts and to characterize the properties of their detected (sub)stellar companions, using accurate Gaia astro-

[5]Online available at: http://www.pas.rochester.edu/~emamajek/EEM_dwarf_UBVIJHK_colors_Teff.txt

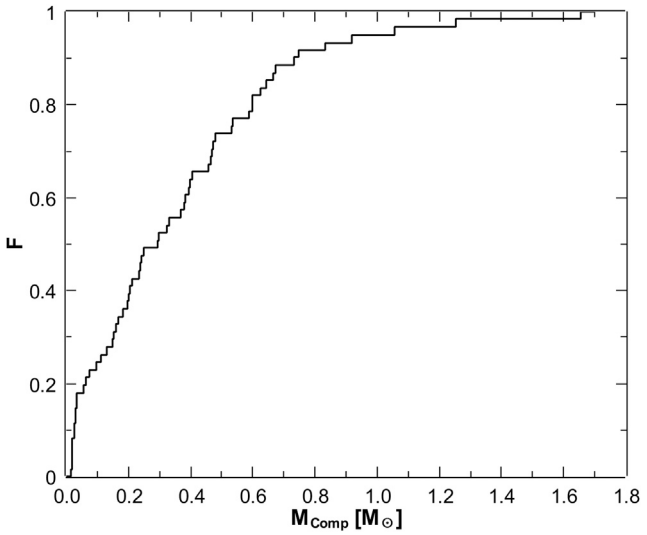

FIGURE 4 | The cumulative distribution function of the mass of all companions, detected in this study.

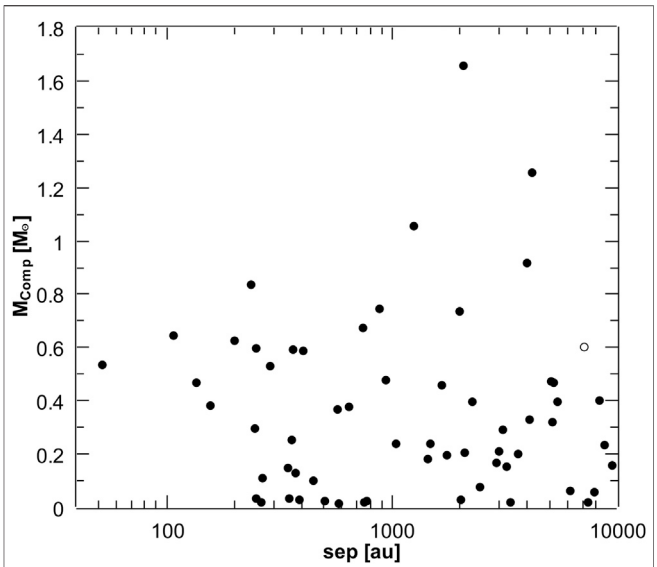

FIGURE 6 | The mass of all companions, detected in this study, plotted over their projected separation (sep) to the associated exoplanet hosts. The white dwarf companion HIP 38594 B, is illustrated as open circle.

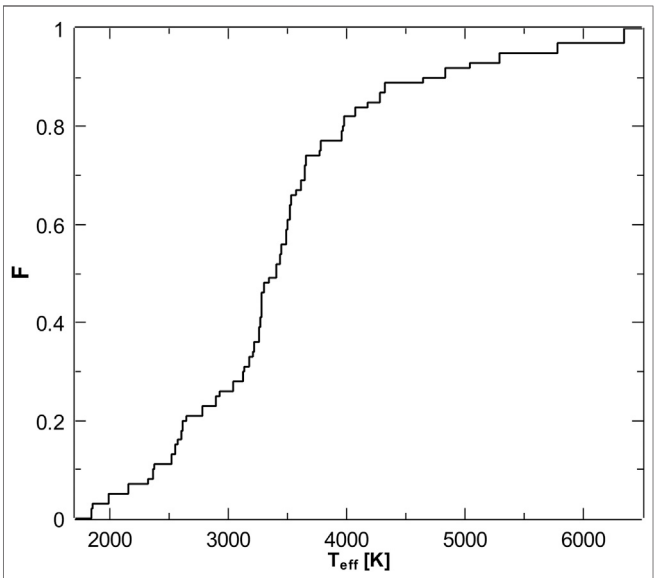

FIGURE 5 | The cumulative distribution function of the effective temperature of all detected companions.

and photometry. In this paper the multiplicity of 289 exoplanet hosts was explored and (sub)stellar companions were detected around 60 targets. The companionship of these objects with the exoplanet hosts could be proven with their accurate Gaia DR2 astrometry (equidistance, common proper motion, and differential proper motion smaller than the expected escape velocity). The mass and effective temperature of all companions were determined with their derived absolute G-band photometry and the Baraffe et al. (2015) evolutionary models of (sub)stellar objects. In total, 61 companions (beside 48 stellar companions, among them the white dwarf HIP 38594 B, also 13 brown dwarfs) were detected in this project, and 14 of these objects are neither listed in the WDS as companion (-candidate)s of the targets nor were described in the literature before. A total of 41 binary and five triple star systems with exoplanets, were identified in this study, yielding a multiplicity rate of the targets of about 16%, which is very well consistent with the multiplicity rate of exoplanet host stars, reported by Mugrauer (2019). Following the standard procedure of our survey, all detected companions and their derived properties will be made available online in the VizieR database. The survey, whose latest results are presented here, is an ongoing project as more and more exoplanet hosts are detected by different planet detection methods, whose multiplicity status needs to be investigated. Furthermore, there are sources, listed in the Gaia DR2, within the applied search radius around the targets, which still lack a five parameter astrometric solution. Hence, further companions of the exoplanet hosts, investigated here, should exist, whose companionship can be proven with accurate astrometric measurements, provided by future data releases of the ESA-Gaia mission, e.g. the Gaia EDR3, planed to be published end of 2020.

The results of this survey, which is mainly sensitive for wide companions of exoplanet hosts, combined with those of our currently ongoing large high contrast imaging surveys (sensitive for close companions), carried out with SPHERE/VLT and AstraLux/CAHA (first results are already published e.g. by Ginski et al., 2020) will yield a complete characterization of the multiplicity status of the observed targets. This will eventually allow to draw conclutions on the impact of the stellar multiplicity on the formation process of planets and the evolution of their orbits.

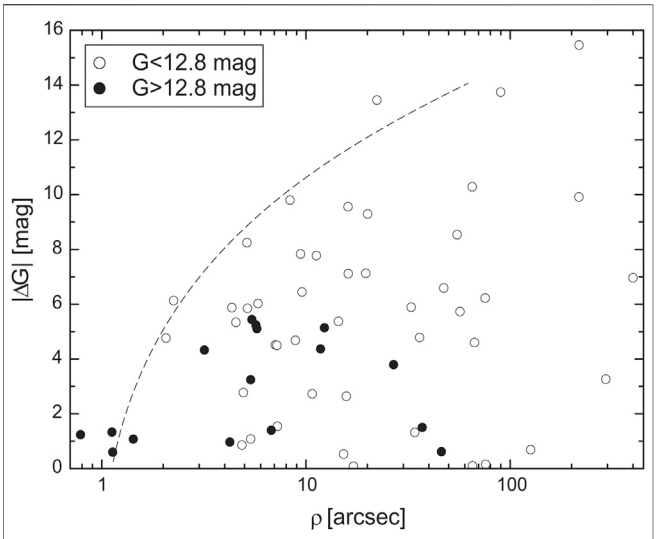

FIGURE 7 | The G-band magnitude difference of all detected companions, plotted over their angular separation to the associated exoplanet hosts.

DATA AVAILABILITY STATEMENT

Publicly available datasets were analyzed in this study. This data can be found here: https://vizier.u-strasbg.fr/viz-bin/VizieR-3?-source=I/345/gaia2&-out.max=50&-out.form=HTML%20Table&-out.add=_r&-out.add=_RAJ,_DEJ&-sort=_r&-oc.form=sexa.

AUTHOR CONTRIBUTIONS

K-UM and MM have worked together on the data analysis and its publication.

ACKNOWLEDGMENTS

We thank the two anonymous referees for their helpful and constructive comments on the manuscript. We made use of data from: (1) the Simbad and VizieR databases, both operated at CDS in Strasbourg, France. (2) the European Space Agency (ESA) mission Gaia (https://www.cosmos.esa.int/gaia), processed by the Gaia Data Processing and Analysis Consortium (DPAC, https://www.cosmos.esa.int/web/gaia/dpac/consortium). Funding for the DPAC has been provided by national institutions, in particular the institutions participating in the Gaia Multilateral Agreement. (3) the Two Micron All Sky Survey, which is a joint project of the University of Massachusetts and the Infrared Processing and Analysis Center/California Institute of Technology, funded by the National Aeronautics and Space Administration and the National Science Foundation.

REFERENCES

Aller, K. M., Kraus, A. L., Liu, M. C., Burgett, W. S., Chambers, K. C., Hodapp, K. W., et al. (2013). A pan-STARRS + UKIDSS search for young, wide planetary-mass companions in upper scorpius. *ApJ* 773, 63. doi:10.1088/0004-637X/773/1/63

Anders, F., Khalatyan, A., Chiappini, C., Queiroz, A. B., Santiago, B. X., Jordi, C., et al. (2019). Photo-astrometric distances, extinctions, and astrophysical parameters for Gaia DR2 stars brighter than G = 18. *A&A* 628, A94. doi:10.1051/0004-6361/201935765

Bailer-Jones, C. A. L., Andrae, R., Arcay, B., Astraatmadja, T., Bellas-Velidis, I., Berihuete, A., et al. (2013). TheGaiaastrophysical parameters inference system (Apsis). *A&A* 559, A74. doi:10.1051/0004-6361/201322344

Baraffe, I., Homeier, D., Allard, F., and Chabrier, G. (2015). New evolutionary models for pre-main sequence and main sequence low-mass stars down to the hydrogen-burning limit. *A&A* 577, A42. doi:10.1051/0004-6361/201425481

Basri, G. (2000). Observations of Brown dwarfs. *Annu. Rev. Astron. Astrophys.* 38, 485–519. doi:10.1146/annurev.astro.38.1.485

Bowler, B. P., and Hillenbrand, L. A. (2015). Near-infrared spectroscopy of 2M0441+2301 AabBab: a quadruple system spanning the stellar to planetary mass regimes. *ApJ* 811, L30. doi:10.1088/2041-8205/811/2/L30

Bowler, B. P., Kraus, A. L., Bryan, M. L., Knutson, H. A., Brogi, M., Rizzuto, A. C., et al. (2017). The young substellar companion ROXs 12 B: near-infrared spectrum, system Architecture, and spin-orbit misalignment. *AJ* 154, 165. doi:10.3847/1538-3881/aa88bd

Bowler, B. P., Liu, M. C., Shkolnik, E. L., Dupuy, T. J., Cieza, L. A., Kraus, A. L., et al. (2012). Planets around low-mass stars (PALMS). I. A substellar companion to the young M dwarf 1RXS J235133.3+312720. *ApJ* 753, 142. doi:10.1088/0004-637X/753/2/142

Burgasser, A. J., Looper, D. L., and Kirkpatrick, J. D. (2017). A candidate wide Brown dwarf binary in the argus association: 2MASS J14504216-7841413 and 2MASS J14504113-7841383. *Res. Notes AAS* 1, 42. doi:10.3847/2515-5172/aa9ff0

Dickson-Vandervelde, D. A., Wilson, E. C., and Kastner, J. H. (2020). Identification of the youngest known substellar object within ~100 pc. *Res. Notes AAS* 4, 25. doi:10.3847/2515-5172/ab7344

Dorval, P., Talens, G. J. J., Otten, G. P. P. L., Brahm, R., Jordán, A., Torres, P., et al. (2020). MASCARA-4 b/bRing-1 b: A retrograde hot Jupiter around a bright A-type star. *A&A* 635, A60. doi:10.1051/0004-6361/201935611

Duchêne, G., and Kraus, A. (2013). Stellar multiplicity. *Annu. Rev. Astron. Astrophys.* 51, 269–310. doi:10.1146/annurev-astro-081710-102602

Feinstein, A. D., Schlieder, J. E., Livingston, J. H., Ciardi, D. R., Howard, A. W., Arnold, L., et al. (2019). K2-288Bb: a small temperate planet in a low-mass binary system discovered by citizen scientists. *AJ* 157, 40. doi:10.3847/1538-3881/aafa70

Gaia CollaborationBrown, A. G. A., Vallenari, A., Prusti, T., de Bruijne, J. H. J., Babusiaux, C., et al. (2018). Gaia Data Release 2. Summary of the contents and survey properties. *A&A* 616, A1. doi:10.1051/0004-6361/201833051

Geißler, K., Metchev, S. A., Pham, A., Larkin, J. E., McElwain, M., and Hillenbrand, L. A. (2012). A substellar common proper-motion companion to the pleiad H II 1348. *ApJ* 746, 44. doi:10.1088/0004-637X/746/1/44

Ginski, C., Mugrauer, M., Adam, C., Vogt, N., and van Holstein, R. (2020). How many suns are in the sky? A sphere multiplicity survey of exoplanet host stars I – Four new close stellar companions including a white dwarf. Available at: http://arxiv.org/abs/2009.10363.

Hartman, J. D., Jordán, A., Bayliss, D., Bakos, G. Á., Bento, J., Bhatti, W., et al. (2020). HATS-47b, HATS-48Ab, HATS-49b, and HATS-72b: four warm giant planets transiting K dwarfs. *AJ* 159, 173. doi:10.3847/1538-3881/ab7821

Hinkley, S., Kraus, A. L., Ireland, M. J., Cheetham, A., Carpenter, J. M., Tuthill, P., et al. (2015). Discovery of seven companions to intermediate-mass stars with extreme mass ratios in the scorpius-centaurus association. *ApJ* 806, L9. doi:10.1088/2041-8205/806/1/L9

Hjorth, M., Justesen, A. B., Hirano, T., Albrecht, S., Gandolfi, D., Dai, F., et al. (2019). K2-290: a warm Jupiter and a mini-Neptune in a triple-star system. *MNRAS* 484, 3522–3536. doi:10.1093/mnras/stz139

Itoh, Y., Hayashi, M., Tamura, M., Tsuji, T., Oasa, Y., Fukagawa, M., et al. (2005). A young Brown dwarf companion to DH tauri. *ApJ* 620, 984–993. doi:10.1086/427086

Jackman, J. A. G., Wheatley, P. J., Bayliss, D., Gill, S., Hodgkin, S. T., Burleigh, M. R., et al. (2019). NGTS-7Ab: an ultrashort-period brown dwarf transiting a tidally locked and active M dwarf. *MNRAS* 489, 5146–5164. doi:10.1093/mnras/stz2496

Janson, M., Asensio-Torres, R., André, D., Bonnefoy, M., Delorme, P., Reffert, S., et al. (2019). The B-Star Exoplanet Abundance Study: a co-moving 16-25 MJup companion to the young binary system HIP 79098. *A&A* 626, A99. doi:10.1051/0004-6361/201935687

Johns, D., Reed, P. A., Rodriguez, J. E., Pepper, J., Stassun, K. G., Penev, K., et al. (2019). KELT-23Ab: a hot Jupiter transiting a near-solar twin close to the TESS and JWST continuous viewing zones. *AJ* 158, 78. doi:10.3847/1538-3881/ab24c7

Kraus, A. L., Ireland, M. J., Cieza, L. A., Hinkley, S., Dupuy, T. J., Bowler, B. P., et al. (2014). Three wide planetary-mass companions to FW Tau, ROXs 12, and ROXs 42B. *ApJ* 781, 20. doi:10.1088/0004-637X/781/1/20

Mason, B. D., Wycoff, G. L., Hartkopf, W. I., Douglass, G. G., and Worley, C. E. (2001). The 2001 US naval observatory Double star CD-ROM. I. The Washington Double star catalog. *AJ* 122, 3466. doi:10.1086/323920

McCormac, J., Gillen, E., Jackman, J. A. G., Brown, D. J. A., Bayliss, D., Wheatley, P. J., et al. (2020). NGTS-10b: the shortest period hot Jupiter yet discovered. *MNRAS* 493, 126–140. doi:10.1093/mnras/staa115

Mugrauer, M., and Ginski, C. (2015). High-contrast imaging search for stellar and substellar companions of exoplanet host stars. *MNRAS* 450, 3127–3136. doi:10.1093/mnras/stv771

Mugrauer, M., Ginski, C., and Seeliger, M. (2014). New wide stellar companions of exoplanet host stars. *MNRAS* 439, 1063–1070. doi:10.1093/mnras/stu044

Mugrauer, M., and Michel, K. U. (2020). Gaia search for stellar companions of TESS objects of interest. Available at: http://arxiv.org/abs/2009.12234.

Mugrauer, M. (2019). Search for stellar companions of exoplanet host stars by exploring the second ESA-Gaia data release. *MNRAS* 490, 5088–5102. doi:10.1093/mnras/stz2673

Neuhäuser, R., Guenther, E. W., Wuchterl, G., Mugrauer, M., Bedalov, A., and Hauschildt, P. H. (2005). Evidence for a co-moving sub-stellar companion of GQ Lup. *A&A* 435, L13–L16. doi:10.1051/0004-6361:200500104

Nielsen, E. L., Liu, M. C., Wahhaj, Z., Biller, B. A., Hayward, T. L., Boss, A., et al. (2012). The gemini NICI planet-finding campaign: discovery of a multiple system orbiting the young A star HD 1160. *ApJ* 750, 53. doi:10.1088/0004-637X/750/1/53

Nielsen, L. D., Bouchy, F., Turner, O. D., Anderson, D. R., Barkaoui, K., Benkhaldoun, Z., et al. (2019). WASP-169, WASP-171, WASP-175, and WASP-182: three hot Jupiters and one bloated sub-Saturn mass planet discovered by WASP-South. *MNRAS* 489, 2478–2487. doi:10.1093/mnras/stz2351

Ochsenbein, F., Bauer, P., and Marcout, J. (2000). The VizieR database of astronomical catalogues. *Astron. Astrophys. Suppl. Ser.* 143, 23–32. doi:10.1051/aas:2000169

Pecaut, M. J., and Mamajek, E. E. (2013). Intrinsic colors, temperatures, and bolometric corrections of pre-main-sequence stars. *ApJS* 208, 9. doi:10.1088/0067-0049/208/1/9

Ricker, G. R., Winn, J. N., Vanderspek, R., Latham, D. W., Bakos, G. Á., Bean, J. L., et al. (2015). Transiting exoplanet survey satellite (TESS). *JATIS* 1, 014003. doi:10.1117/1.JATIS.1.1.014003

Rodriguez, J. E., Eastman, J. D., Zhou, G., Quinn, S. N., Beatty, T. G., Penev, K., et al. (2019). KELT-24b: a 5M J planet on a 5.6 day well-aligned orbit around the young V = 8.3 F-star HD 93148. *AJ* 158, 197. doi:10.3847/1538-3881/ab4136

Schneider, J., Dedieu, C., Le Sidaner, P., Savalle, R., and Zolotukhin, I. (2011). Defining and cataloging exoplanets: the exoplanet.eu database. *A&A* 532, A79. doi:10.1051/0004-6361/201116713

Skrutskie, M. F., Cutri, R. M., Stiening, R., Weinberg, M. D., Schneider, S., Carpenter, J. M., et al. (2006). The two Micron all sky survey (2MASS). *Astron. J.* 131, 1163–1183. doi:10.1086/498708

Smart, R. L., and Nicastro, L. (2014). The initialGaiasource list. *A&A* 570, A87. doi:10.1051/0004-6361/201424241

Subasavage, J. P., Henry, T. J., Bergeron, P., Dufour, P., and Hambly, N. C. (2008). The solar neighborhood. Xx. Discovery and characterization of 21 new nearby white dwarf systems. *Astronomical J.* 136, 899–908. doi:10.1088/0004-6256/136/3/899

Triaud, A. H. M. J., Burgasser, A. J., Burdanov, A., Kunovac Hodžić, V., Alonso, R., Bardalez Gagliuffi, D., et al. (2020). An eclipsing substellar binary in a young triple system discovered by speculoos. *Nat. Astron.* 4, 650–657. doi:10.1038/s41550-020-1018-2

van Leeuwen, F. (2007). Validation of the new Hipparcos reduction. *A&A* 474, 653–664. doi:10.1051/0004-6361:20078357

Vanderburg, A., Huang, C. X., Rodriguez, J. E., Becker, J. C., Ricker, G. R., Vanderspek, R. K., et al. (2019). Tess spots a compact system of super-earths around the naked-eye star HR 858. *ApJ* 881, L19. doi:10.3847/2041-8213/ab322d

Conflict of Interest: The authors declare that the research was conducted in the absence of any commercial or financial relationships that could be construed as a potential conflict of interest.

frontiers in Astronomy and Space Sciences

BRIEF RESEARCH REPORT
published: 29 March 2021
doi: 10.3389/fspas.2021.625230

Robo-AO and SOAR High-Resolution Surveys of Exoplanet Hosting Stars

Carl Ziegler[1]*, *Nicholas Law*[2], *Christoph Baranec*[3], *Reed Riddle*[4] and *Andrei Tokovinin*[5]

[1]Department of Physics, Engineering and Astronomy, Stephen F. Austin State University, Nacogdoches, TX, United States, [2]Department of Physics and Astronomy, University of North Carolina at Chapel Hill, Chapel Hill, NC, United States, [3]Institute for Astronomy, University of Hawai'i at Mānoa, Hilo, HI, United States, [4]Division of Physics, Mathematics, and Astronomy, California Institute of Technology, Pasadena, CA, United States, [5]Cerro Tololo Inter-American Observatory, La Serena, Chile

In the past decade, space-based transit surveys have delivered thousands of potential planet-hosting systems. Each of these needs to be vetted and characterized using follow-up high-resolution imaging. We perform comprehensive imaging surveys of the candidate exoplanets detected by the Kepler and TESS missions using the fully autonomous Robo-AO system and the largely autonomous SOAR speckle imaging system. The surveys yielded hundreds of previously unknown close binary systems hosting exoplanets and resulted in verification of hundreds of exoplanet systems. Evidence of the interaction between binary stars and planetary systems was also detected, including a deep deficit of planets in close binary systems.

Keywords: exoplanets, adaptive optics, speckle interferometry, binary stars, high-resolution imaging

OPEN ACCESS

Edited by:
Steve B. Howell,
National Aeronautics and Space Administration (NASA), United States

Reviewed by:
Luca Fossati,
Austrian Academy of Sciences, Austria
John Livingston,
The University of Tokyo, Japan

***Correspondence:**
Carl Ziegler
carl.ziegler@sfasu.edu

Specialty section:
This article was submitted to Exoplanets, a section of the journal Frontiers in Astronomy and Space Sciences

Received: *02 November 2020*
Accepted: *08 January 2021*
Published: *29 March 2021*

Citation:
Ziegler C, Law N, Baranec C, Riddle R and Tokovinin A (2021) Robo-AO and SOAR High-Resolution Surveys of Exoplanet Hosting Stars. Front. Astron. Space Sci. 8:625230. doi: 10.3389/fspas.2021.625230

1 INTRODUCTION

Over the past decade, the Kepler telescope (Borucki et al., 2010) and its follow-up mission, the Transiting Exoplanet Survey Satellite (TESS, Ricker et al., 2014), have detected the majority of known exoplanets. Each satellite consists of high-precision photometers, able to measure the brightness of thousands of stars simultaneously. A planet passing in front of one of these stars as seen from Earth, a transit, will result in a slight dip in brightness (the size of the dip being related to relative sizes of the planet and star). Periodic dimming of a star is therefore potential evidence of an orbiting exoplanet.

The addition of a second star in the system, so that the light from both is blended together, results in a shallower brightness dip during transit. The size of the planet, which is estimated based on the depth of the brightness dip, is biased small when the light from a second object is included. The nearby star may actually be an eclipsing binary system. When blended with the brighter target star, the large dips from the eclipsing stars may result in a planet-like signal. Both the Kepler and TESS missions were blind to wide binary stars, which were not removed from either Kepler (Brown et al., 2011) or TESS (Stassun et al., 2019) input catalogs. The majority of close binary stars (those within an arcsecond of separation) are not known in advance due to the typically low-resolution of seeing-limited observations and the resolution limit of Gaia DR2 (Ziegler et al., 2018b).

Resolving close binary systems requires high-resolution imaging from the ground. Conventional systems, such as laser GuideStar adaptive optics (LGS-AO) instruments, require long overheads before observations can begin, typically on the order of 15–20 min [e.g., Keck-AO (Wizinowich et al., 2006)], and are generally only available on large telescopes (apertures greater than 8 m). With thousands of targets requiring such observations, approximately a hundred dedicated nights would be required to complete a comprehensive survey. Practically, this is outside the allocated time that will be provided for this purpose. In the first few years of the Kepler mission, the follow-up campaign proceeded with a patchwork of smaller surveys performed on different telescopes observing in both

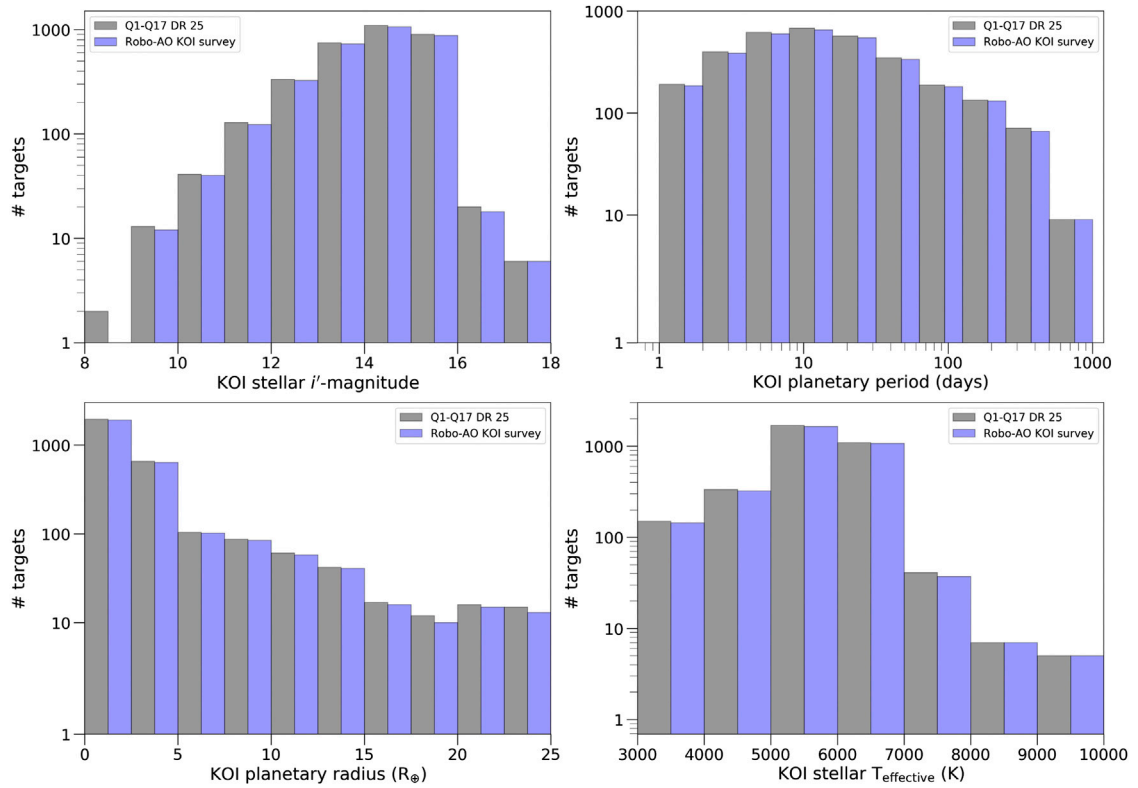

FIGURE 1 | The properties of KOIs observed in the Robo-AO survey are compared to the full set of KOIs from Q1–Q17 (Borucki et al., 2010; Borucki et al., 2011a; Borucki et al., 2011b; Batalha et al., 2013; Burke et al., 2014; Rowe et al., 2014; Coughlin et al., 2016; Mathur et al., 2017).

visible and infrared bands (Howell et al., 2011; Adams et al., 2012; Adams et al., 2013; Horch et al., 2012; Lillo-Box et al., 2012; Dressing et al., 2014; Horch et al., 2014; Lillo-Box et al., 2014; Marcy et al., 2014). These disparate sources of data limited the broad statistical studies that could be performed to understand how planets form and evolve in tight binary systems.

A high-resolution instrument which also has high observing efficiency is therefore required to perform such a large survey. Through full automation, Robo-AO achieves observing time efficiencies that are an order-of-magnitude greater than those of conventional high-resolution instruments. Between 2012 and 2016, Robo-AO was used by our team to observe every Kepler Object of Interest (KOI) system (Law et al., 2014; Baranec et al., 2016; Ziegler et al., 2017; Ziegler et al., 2018a; Ziegler et al., 2018c). These observations were typically sensitive to nearby stars as close as the diffraction limit of the telescope (approximately 0.15″) and to stars up to six magnitudes fainter than the target star. Within this survey, nearly 95% of Kepler planetary candidates host stars (3,857 KOIs in total) were observed, and 620 stars with separations less than a few arcseconds were detected.

Beginning in late 2018 and continuing to present, the Southern Astrophysical Research telescope (SOAR) has performed speckle observations of TESS planet candidates. Speckle imaging on SOAR typically reaches the diffraction limit on bright targets ($V < \sim 12$), including most TESS targets (TESS Objects of Interest, or TOIs), and the observation sequence is optimized to be capable of up to 300 observations a night (Tokovinin, 2018). The first results from this survey, covering 542 TESS targets with 117 detected companions, was recently published in Ziegler et al., (2020). Additional 357 TESS targets observed by SOAR will be presented in an upcoming work.

This article provides a summary of the surveys and their results. We describe in detail the observations from each instrument in **Section 2** and summarize the results of the surveys in **Section 3**. We conclude in **Section 4**.

2 OBSERVATIONS

2.1 Robo-AO

The objective of the Robo-AO Kepler survey was to take image in high-resolution of every candidate planet host star detected by the Kepler telescope. We therefore targeted every KOI from the available data releases (culminating with the Kepler DR25 catalog based on Q1-Q17 data) (Borucki et al., 2010; Borucki et al., 2011a; Borucki et al., 2011b; Batalha et al., 2013; Burke et al., 2014; Rowe et al., 2014; Coughlin et al., 2016; Mathur et al., 2017). We removed KOIs that were flagged as false positives using Kepler data at the time of the observation runs.

The properties of targeted KOIs in the Robo-AO survey are presented in **Figure 1**. The distributions in magnitude, planetary radius, planetary orbital period, and stellar temperature of the

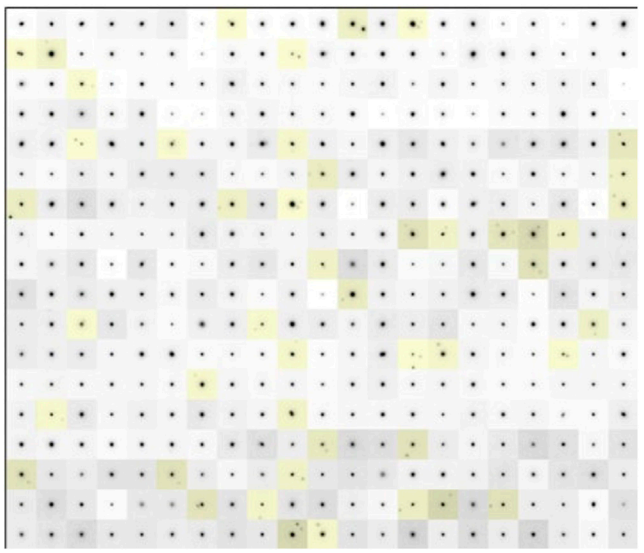

FIGURE 2 | Robo-AO centered cutout images of Kepler planetary candidate host stars. Systems with discovered nearby stars are highlighted. Shown are ~10% of the targets from the Robo-AO survey of KOIs, the largest adaptive optics survey of exoplanet hosts yet performed. Results from this survey have been used to validate over a thousand planets.

observed stars are similar to the full set of KOIs from Q1 to Q17 that have CANDIDATE dispositions based on only Kepler data. This is a result of the comprehensive nature of this survey. An example of the Robo-AO images within this survey is presented in **Figure 2**.

The Robo-AO instrument was mounted on telescopes at Palomar and Kitt Peak during the course of this survey (Baranec et al., 2014b; Baranec et al., 2017; Jensen-Clem et al., 2018). To correct high-order wavefront aberrations introduced by atmospheric turbulence, the adaptive optics system of Robo-AO runs at a loop rate of 1.2 kHz. The delivered performance of the system (median Strehl ratios of 9% and 4% in the *i*′-band at Palomar and Kitt Peak) allowed identification of companion stars down to the diffraction limit of the telescope. A long-pass filter that cuts on at 600 nm (LP600) was used for observations of the KOI targets. This filter is a good approximation of the Kepler bandpass at redder wavelengths, while also reducing the blue wavelengths that reduce the performance of the adaptive optics correction. A comparison of the LP600 passband to the Kepler passband is presented in **Figure 1** of Law et al., (2014). The majority of the survey (3,313 KOIs) was performed with Robo-AO mounted on the Palomar 1.5 m telescope between 2012, July 16 and 2015, June 12 (UT). An additional 532 KOIs were observed with Robo-AO mounted on the Kitt Peak 2.1 m telescope between 2016, June 8 and 2016, July 15 (UT).

The Robo-AO system achieves a typical FWHM resolution of 0.15″ (at the diffraction limit). An electron-multiplying CCD (EMCCD) is used to record the images. This camera allows short frame rates, useful for software corrections for tip and tilt using a faint ($m_V < 16$) natural guide star in the field of view. In **Table 1** we summarize the specifications for the Robo-AO KOI survey.

TABLE 1 | The specifications of the Robo-AO KOI survey.

KOI targets	3,857
FWHM resolution	~0.15" (@600–750 nm)
Observation wavelengths	600–950 nm
Detector format	$1{,}024^2$ pixels
Pixel scale	43 mas/pix (palomar)
	35 mas/px (kitt peak)
Exposure time	90 s
Targets observed/hour	20
Observation dates	2012 July 16 –
At palomar 1.5 m	2015 June 12
Observation dates	2016 June 8 –
At Kitt peak 2.1 m	2016 July 15

A currently in-development Robo-AO 2 system (Baranec et al., 2014a) mounted on the UH-88 in telescope on Maunakea will be used in the future to take image in high-resolution of Northern TESS planet candidate hosts.

2.2 SOAR Speckle Imaging

We are observing TESS planet candidate hosts with the high-resolution camera (HRCam) imager on the 4.1 m SOAR telescope. TESS targets have been observed during 13 separate runs in 2018–2020. Over the course of these observations, 95% (707) of the 742 bright (T < 13) candidate planet host stars from the two-year primary TESS mission that are observable from the South (dec < + 20°) have been observed in high-resolution in the SOAR TESS survey. Observations of planet candidates from the extended TESS mission are ongoing. The properties of the targeted stars are plotted in **Figure 3** and the survey specifications are listed in **Table 2**.

The observation procedure and data reduction are described in detail in Tokovinin (2018) and in Ziegler et al. (2020). In summary, an 11 s burst of 400 images is taken with an Andor iXon-888 camera. Each image consists of 200 × 200 binned pixels that are centered on the target star. The images subtend an angular region on the sky that is 6.3″ on a side, giving a plate scale of 0.01575″/pixel. A custom IDL script reduces the resulting datacube. A power spectrum is computed, and, if the target star is a binary, characteristic fringes are apparent. Modeling the power spectrum provides the separation, magnitude difference, and position angle of the companion. The Fourier transform of the power spectrum is the speckle autocorrelation function (ACF). Secondary stars will appear as mirrored peaks in the ACF, appearing at the separation and position angle of the companion. The frames in the datacube are shift-and-added, centering each on the brightest pixel, to determine the true position of the companion and remove the 180-degree ambiguity. Examples of typical speckle data are available in **Figure 4** in Tokovinin (2018). The observations in the SOAR TESS survey were taken in *I*-band. This bandpass (λ_{cen} = 824 nm, $\Delta\lambda$ = 170 nm) is similar to the bandpass used by TESS.

3 IMPACT OF BINARY STARS ON PLANETARY SYSTEMS

3.1 Binary Fractions

Within the Robo-AO Kepler survey, we found 610 stars within 4″ of 559 planetary candidate hosts (out of an observed total of 3,857

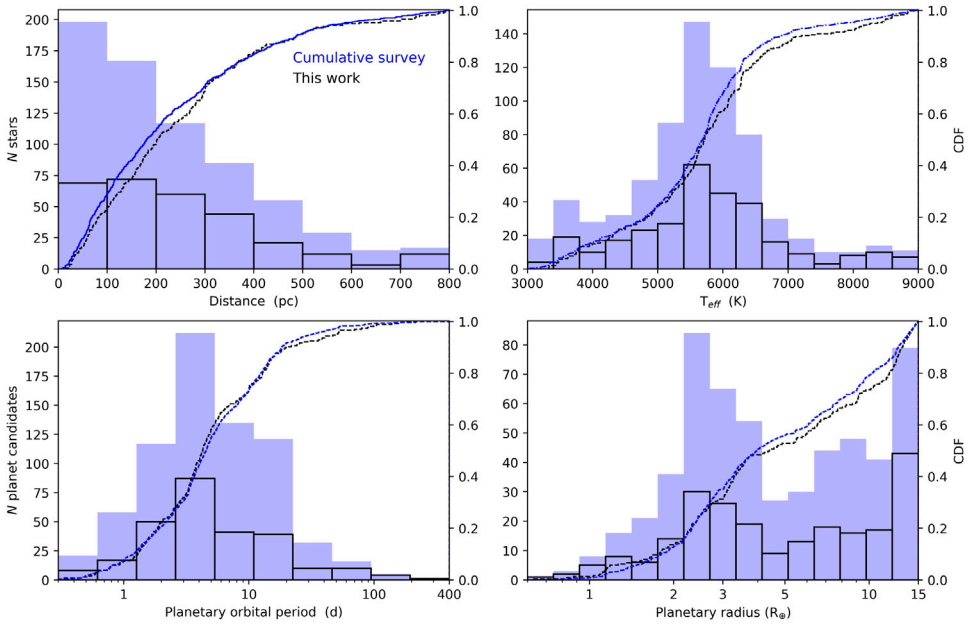

FIGURE 3 | The properties of the 653 TESS planet candidate hosts observed in the SOAR TESS survey from Ziegler et al., (2020) and in preparation (this work). A cumulative density function for each property is overplotted in black. Targets identified as known or likely false positives, 196 in total, have been removed.

TABLE 2 | The specifications of the SOAR speckle TESS survey.

TOI targets	875
FWHM resolution	~0.06″ (@700–900 nm)
Observation wavelengths	λ_c = 824 nm, $\Delta\lambda$ = 170 nm
Detector format	200^2 pixels
Pixel scale	15.7 mas/pix
Exposure time	11 s
Targets observed/hour	~30
Observation dates	2018 Oct 21—on-going

KOIs). This implies a nearby star fraction rate with the detection sensitivity of Robo-AO (separations between ~0.15″ and 4.0″ and typically $\Delta m \leq 6$) of 14.5 ± 0.6%. A triple star fraction (two additional stars within 4.0" of the target) of 1.2 ± 0.2% and a quadruple star fraction of $0.08^{+0.06}_{-0.03}$% were also detected.

Simulations using simulated galactic star fields and observational evidence suggest that most nearby stars at separations $< 1''$ are likely bound (Horch et al., 2014; Ziegler et al., 2018c). We find that 5.3 ± 0.3% of KOIs have another star within 1.5″ and 10.7 ± 0.5% within 3″.

The SOAR TESS survey finds companion rates to transiting exoplanet candidate hosts within 1.5″ and 3″ of 16.2 ± 1.7% and 23.2 ± 2.0% within 1.5″ and 3″, respectively.

The TESS nearby star rates are significantly higher than the Kepler rates. If we assume a physical separation distribution for binaries around exoplanet hosts as we find for field stars (Raghavan et al., 2010) which peaks at 50 AU, many more real binaries would be resolvable around TESS planet hosts (average distance of ~200 pc) compared to Kepler planet hosts (average distance of ~500 pc). The TESS system is also generally brighter (by ~3 mags on average), making fainter companions more readily detectable.

3.2 Radius Corrections

The additional flux from a stellar companion will reduce the transit depth in a photometric light curves. This dilution will result in an underestimated planetary radius. In general, it is not known which of the two stars hosts the planet in an S-type configuration (i.e., a planet in a binary system that orbits only one of the stars) (Horch et al., 2014). Gaidos et al., (2016) provide some evidence, however, that typically the primary (brightest) star is more likely to be the planet host. We therefore estimated correction factors for radius estimates for either host scenario. The detailed description of how the radii of planet candidates are corrected for the presence of a previously unknown stellar companion is provided in Ziegler et al., (2018c).

We find, for the Kepler planets, that, if we assume that all the planets orbit around the primary stars, the planetary radii increase by a factor of 1.08 on average. This factor is relatively small, as generally the companions are much fainter than the primary stars and thus the dilution of the transit is small. We found a similar correction factor for TESS planets of 1.11. Instead, if we assume all planets orbit around the secondary stars (and assuming these are not line-of-sight asterisms, but gravitationally bound to the primary), the radii of the TESS planets will increase, on average, by a factor of 2.55, slightly less than 3.29 found for Kepler planets. If we instead assume that the planet candidates are equally likely to be hosted by the primary or secondary star, we find average radius correction factors for Kepler planets of 2.18 and for TESS planets of 1.82.

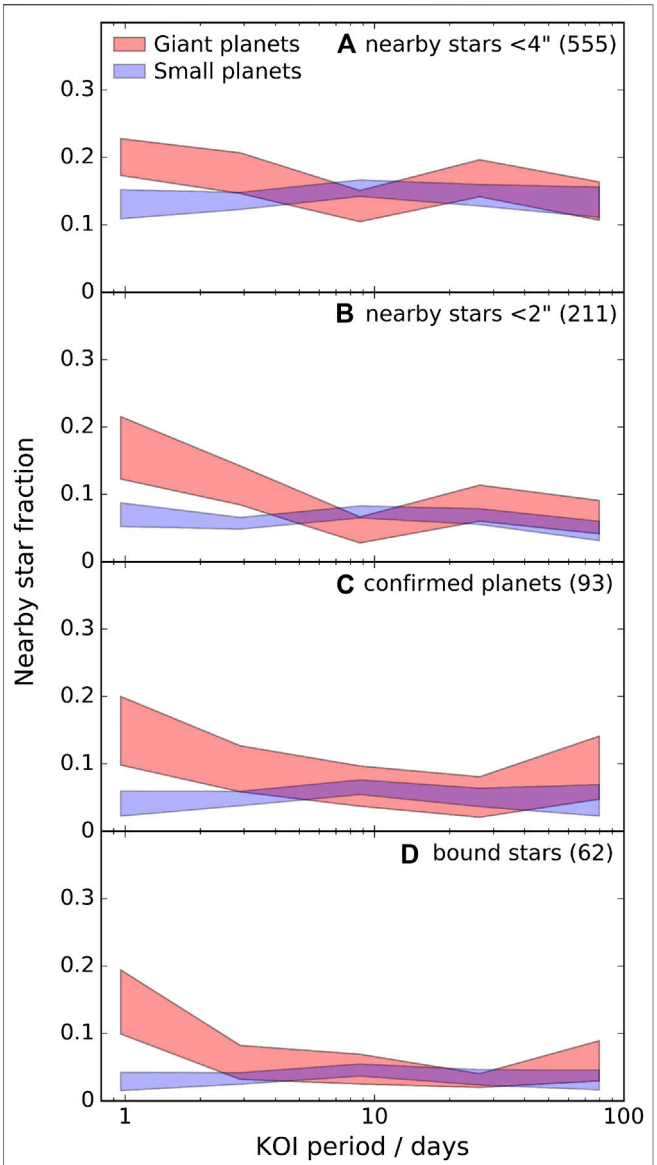

FIGURE 4 | The binary fraction for two planetary populations (giant and small) is shown as a function of orbital period, with 1σ uncertainty regions shaded. The top panel is the original sample, with each subsequent panel removing systems, as described in the text, to clean the sample. In each panel, the number of systems used is shown in parentheses.

Unassociated background or foreground stars are typically found at larger separations from the primary star. If we limit our sample to just TESS systems with separations less than 1″ (to increase the fraction of gravitationally bound companions), we find, using the assumptions of all primary star hosts, all secondary star hosts, and equal mix of primary and secondary star hosts, correction factors of 1.14, 1.90, and 1.55, respectively. The final figure agrees with the correction factor from the Robo-AO survey of Kepler planets of 1.54, as well as from two independent studies of 1.6 (Ciardi et al., 2015) and 1.64 (Hirsch et al., 2017).

In summary, it is clear that the presence of a previously unknown stellar companion has a significant effect on our understanding of any possible planets within the system (increasing their radii by ~60% on average). The composition of smaller planets, in particular, is highly dependent on their estimated radius, particularly if they fall below or above the radius gap at approximately 1.6–1.9 Earth radii (Rogers, 2015; Fulton et al., 2017; Van Eylen et al., 2018) between rocky planets (super-Earths) and those with large gaseous envelopes (sub-Neptunes).

3.3 Giant Planet Migration

It is expected from theoretical planet formation models that the gravitational influence of a stellar companion may drive planets that form at large separations inward, into short-period orbits (Fabrycky and Tremaine, 2007; Katz et al., 2011; Naoz et al., 2012). Smaller planets may be ejected by migrating larger planets in this scenario, resulting in a high fraction of short period giant planets in systems with stellar companions (Xie et al., 2014).

We searched for evidence of these effects using a cleaned sample of binary targets from the Robo-AO Kepler survey, removing known or suspected false positives (Morton and Johnson, 2011; Fressin et al., 2013) and only using likely bound systems as determined by photometric distance estimates Ziegler et al. (2018a).

We find that, after successive cuts to improve the sample (see **Figure 4**), short-period (1–3 days) giant and small planets have a binarity rate of $12.8\%^{+5.6\%}_{-2.8\%}$ and $2.4\%^{+1.8\%}_{-0.9\%}$, respectively. This is a 2.6σ discrepancy between giant and small planets.[1] A significant difference in the binarity rate of the two populations is not found at any other orbital period range.

Ngo et al., (2015) found a similar result in an NIR survey of hot Jupiter hosts, which were twice as likely to have stellar companions as compared to field stars at a 2.8σ significance. The binary fraction found in their survey was significantly higher (51%), likely a result of differences in observational methods and sensitivity (e.g., increased sensitivity in the infrared to M-dwarf companions). The binary fraction for hot Jupiter hosts in the Robo-AO survey is in agreement with the 12% rate found by Roell et al., (2012), who used seeing-limited observations to detect close companions.

3.4 Close Binary Suppression of Planets

A close stellar companion can significantly reduce the probability that planets can form and survive around a star. Yet, we still find planets in close binary systems. We use the data from the SOAR TESS survey to understand how binary stars interact with planetary systems.

Kraus et al., (2016) found that few Kepler host stars are in solar system scale binary systems (separations within 50 AU), implying that planets are significantly less likely to form in these systems. The TESS planets take generally larger and shorter periods than the Kepler planets, due to the reduced photometric precision of TESS and survey strategy. Unlike Kepler, however, the TESS planets are spread across the sky, not in a limited region, and

[1]Errors for both populations are based on Poissonian statistics (Burgasser et al., 2003).

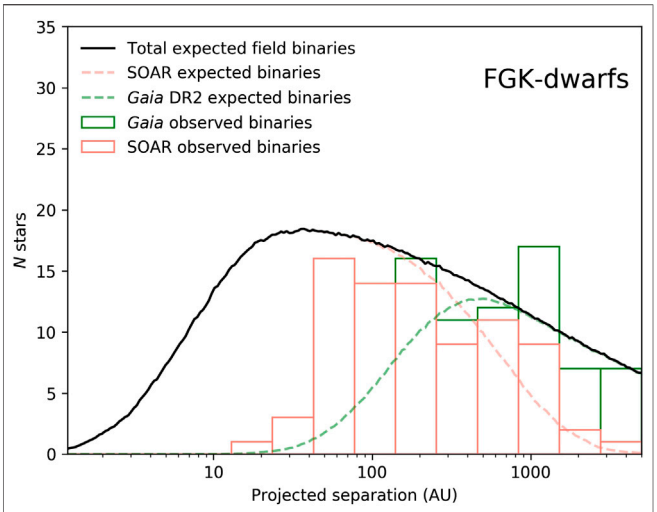

FIGURE 5 | In red and green, the number of observed companions from SOAR and in Gaia DR2 for solar-type TESS planet candidate hosts in logarithmic bins of projected separation of 0.25 dex width. Companions found by both SOAR and Gaia are included in the SOAR sample. In black is the expected distribution from a multiplicity study of field stars (Raghavan et al., 2010), combining both field binaries that would be detected by SOAR and Gaia. The expected binaries from SOAR and Gaia, individually, are also plotted. These distributions take into account the detection sensitivity of both SOAR and Gaia. The observed distribution shows a clear paucity of TESS planet candidate host binaries at projected separations less than ~40 AU compared to the field stars and are consistent with field expectations at wider separations.

allow us to sample a more diverse set of the Galactic stellar population.

Similar to Kraus et al., (2016), we use the field binary statistics of Raghavan et al., (2010) to compare the planet candidate hosting planets. Any differences between the two samples may be a result of planet formation suppression. For this analysis, we first cull the sample of 875 observed TOIs using several parameters (non-Solar type stars, false positives, and high contrast systems) to a final sample consisting of 484 stars. We supplement the SOAR observations with common proper motion pairs found in Gaia DR2 (Gaia Collaboration et al., 2018).

A histogram of the observed distribution of binaries based on projected separation compared to the simulated survey of field stars is shown in **Figure 5**. A deep deficit of observed exoplanet candidate systems with close binaries is apparent, indicating that these systems are treacherous for planet formation and evolution. A simple two-parameter suppression model, a step function reduction in binaries by 90^{+2}_{-3}% at 34^{+9}_{-6} AU physical separation, fits the observed distribution.

The exact mechanism that suppresses the survival of planets in these systems is unclear, but several theories have been put forth. Quintana et al., (2007) suggest that stellar companions may stir planetesimals, increasing their velocity and reducing their density in the protoplanetary disc. Naoz et al., (2012) suggest that binary stars perturb planetary orbits, resulting in tidal migration that can lead to planetary ejection. Jang-Condell et al., (2008) and Kraus et al., (2012) find evidence that stellar companions reduce the material in, and lifetime of, protoplanetary discs. Lastly, Alexander (2012) suggests that the additional radiation from the companion increases photoevaporation in the disc, stripping gaseous planets of their atmospheres. Why can some systems survive while others are destroyed? More observations of these systems (to determine association between the two stars, identify the planet host, and map out physical rather than the snapshot projected separation) and the detection of more systems, particularly close binary systems that do host planets, will likely bring more insight. These systems are relatively rare and serve as the most stringent tests for theoretical formation models.

4 CONCLUSION

The Kepler and TESS missions provided the community the significant challenge of needing thousands of high-resolution images to confirm and characterize exoplanet systems. Robo-AO and SOAR speckle imaging are uniquely suited to perform those observations in a comprehensive and uniform manner. Over four years, Robo-AO imaged nearly all of the Kepler planet candidates. This corrected the planetary radius estimates for over 600 systems and led to the verification of over a thousand planets (Morton et al., 2016). The TESS survey is observing every TESS planet candidate visible from the South. Currently over 800 targets have been observed, with over 200 having nearby companions, and the speckle observations have contributed to the confirmation of over 40 planets [e.g.,Espinoza et al., (2019); Jones et al. (2019); Quinn et al., (2019); Rodriguez et al., (2019); Vanderburg et al., (2019)]. This has resulted in the best evidence yet that close, Solar System scale binary systems suppress planet formation. The TESS survey is ongoing with targets from the extended mission being observed.

Data from the Robo-AO survey of Kepler planet candidate host stars are available at the survey website[2]. Data from the SOAR telescope observations of TESS planet candidate host stars are available on the Exoplanet Follow-up Observation Program website[3].

DATA AVAILABLITY STATEMENT

Publicly available datasets were analyzed in this study. This data can be found here: Kepler ExoFOP.

AUTHOR CONTRIBUTIONS

CZ performed the data reduction for the Robo-AO survey. NL, CB, and RR built and maintained the Robo-AO instrument and ran the observations of the exoplanet hosts. AT performed the speckle observations on the SOAR telescope.

[2]http://roboaokepler.com/.
[3]https://exofop.ipac.caltech.edu/tess/index.php.

FUNDING

This research was supported by the NASA Exoplanets Research Program, grant No. NNX 15AC91G. CZ and WH acknowledge support from the North Carolina Space Grant consortium. TM was supported by NASA, grant No. NNX 14AE11G under the Kepler Participating Scientist Program.

ACKNOWLEDGMENTS

We thank the observatory staff at Kitt Peak for their efforts to assist Robo-AO KP operations and are grateful to the Palomar Observatory staff for their support of Robo-AO on the 1.5 m telescope. The Robo-AO instrument was developed with support from the National Science Foundation under grants AST-0906060, AST-0960343, and AST-1207891, IUCAA, the Mt. Cuba Astronomical Foundation, and by a gift from Samuel Oschin. The Robo-AO team thanks NSF and NOAO for making the Kitt Peak 2.1 m telescope available. Robo-AO KP is a partnership between the California Institute of Technology, the University of Hawai'i, the University of North Carolina at Chapel Hill, the Inter-University Centre for Astronomy and Astrophysics (IUCAA) at Pune, India, and the National Central University, Taiwan. The Murty family feels very happy to have added a small value to this important project. Robo-AO KP is also supported by grants from the John Templeton Foundation and the Mt. Cuba Astronomical Foundation. Some data are based on observations at Kitt Peak National Observatory, National Optical Astronomy Observatory (NOAO Prop. ID: 15B-3001), which is operated by the Association of Universities for Research in Astronomy (AURA) under cooperative agreement with the National Science Foundation. This research used observations obtained at the Southern Astrophysical Research (SOAR) telescope, which is a joint project of the Ministério da Ciência, Tecnologia, Inovações e Comunicações (MCTIC) do Brasil, the U.S. National Optical Astronomy Observatory (NOAO), the University of North Carolina at Chapel Hill (UNC), and Michigan State University (MSU). This article includes data collected by the TESS mission. Funding for the TESS mission is provided by the NASA Explorer Program. This work has made use of data from the European Space Agency (ESA) mission Gaia (https://www.cosmos.esa.int/gaia), processed by the Gaia Data Processing and Analysis Consortium (DPAC, https://www.cosmos.esa.int/web/gaia/dpac/consortium). This research has made use of the Exoplanet Follow-up Observation Program website, which is operated by the California Institute of Technology, under contract with the National Aeronautics and Space Administration under the Exoplanet Exploration Program. This research has made use of the NASA Exoplanet Archive, which is operated by the California Institute of Technology, under contract with the National Aeronautics and Space Administration under the Exoplanet Exploration Program. Facilities: PO:1.5 m (Robo-AO), KPNO:2.1 m (Robo-AO), SOAR (HRCam).

REFERENCES

Adams, E. R., Ciardi, D. R., Dupree, A. K., Gautier, T. N., III, Kulesa, C., and McCarthy, D. (2012). Adaptive optics images of kepler objects of interest. *AJ* 144, 42. doi:10.1088/0004-6256/144/2/42

Adams, E. R., Dupree, A. K., Kulesa, C., and McCarthy, D. (2013). Adaptive optics images. II. 12 kepler objects of interest and 15 confirmed transiting planets. *AJ* 146, 9. doi:10.1088/0004-6256/146/1/9

Alexander, R. (2012). The dispersal of protoplanetary disks around binary stars. *ApJ* 757, L29. doi:10.1088/2041-8205/757/2/L29

Baranec, C., Riddle, R., and Law, N. M. (2017). Automated adaptive optics. ArXiv e-prints. Available at: https://arxiv.org/abs/1709.07103

Baranec, C., Riddle, R., Law, N. M., Chun, M. R., Lu, J. R., Connelley, M. S., et al. (2014a). "Second generation Robo-AO instruments and systems," In *Adaptive optics systems IV* (Bellingham, WA: SPIE), Vol. 9148, 914812. doi:10.1117/12.2055552

Baranec, C., Riddle, R., Law, N. M., Ramaprakash, A. N., Tendulkar, S., Hogstrom, K., et al. (2014b). High-efficiency autonomous laser adaptive optics. *ApJ* 790, L8. doi:10.1088/2041-8205/790/1/L8

Baranec, C., Ziegler, C., Law, N. M., Morton, T., Riddle, R., Atkinson, D., et al. (2016). Robo-AO kepler planetary candidate survey. II. Adaptive optics imaging of 969 kepler exoplanet candidate host stars. *AJ* 152, 18. doi:10.3847/0004-6256/152/1/18

Batalha, N. M., Rowe, J. F., Bryson, S. T., Barclay, T., Burke, C. J., Caldwell, D. A., et al. (2013). Planetary candidates observed by kepler. III. Analysis of the first 16 months of data. *ApJs* 204, 24. doi:10.1088/0067-0049/204/2/24

Borucki, W. J., Koch, D., Basri, G., Batalha, N., Brown, T., Caldwell, D., et al. (2010). Kepler planet-detection mission: introduction and first results. *Science* 327, 977. doi:10.1126/science.1185402

Borucki, W. J., Koch, D. G., Basri, G., Batalha, N., Boss, A., Brown, T. M., et al. (2011a). Characteristics of kepler planetary candidates based on the first data set. *ApJ* 728, 117. doi:10.1088/0004-637X/728/2/117

Borucki, W. J., Koch, D. G., Basri, G., Batalha, N., Brown, T. M., Bryson, S. T., et al. (2011b). Characteristics of planetary candidates observed by kepler. II. Analysis of the first four months of data. *ApJ* 736, 19. doi:10.1088/0004-637X/736/1/19

Gaia CollaborationBrown, A. G. A., Vallenari, A., Prusti, T., de Bruijne, J. H. J., Babusiaux, C., et al. (2018). Gaia data release 2. Summary of the contents and survey properties. *Astron. Astrophys.* 616, A1. doi:10.1051/0004-6361/201833051

Brown, T. M., Latham, D. W., Everett, M. E., and Esquerdo, G. A. (2011). Kepler input catalog: photometric calibration and stellar classification. *AJ* 142, 112. doi:10.1088/0004-6256/142/4/112

Burgasser, A. J., Kirkpatrick, J. D., Reid, I. N., Brown, M. E., Miskey, C. L., and Gizis, J. E. (2003). Binarity in Brown dwarfs: T dwarf binaries discovered with the hubble space telescope wide field planetary camera 2. *ApJ* 586, 512–526. doi:10.1086/346263

Burke, C. J., Bryson, S. T., Mullally, F., Rowe, J. F., Christiansen, J. L., Thompson, S. E., et al. (2014). Planetary candidates observed by kepler IV: planet sample from Q1-Q8 (22 Months). *ApJs* 210, 19. doi:10.1088/0067-0049/210/2/19

Ciardi, D. R., Beichman, C. A., Horch, E. P., and Howell, S. B. (2015). Understanding the effects of stellar multiplicity on the derived planet radii from transit surveys: implications for kepler, K2, and TESS. *ApJ* 805, 16. doi:10.1088/0004-637X/805/1/16

Coughlin, J. L., Mullally, F., Thompson, S. E., Rowe, J. F., Burke, C. J., Latham, D. W., et al. (2016). Planetary candidates observed by kepler. VII. The first fully uniform catalog based on the entire 48-month data set (Q1-Q17 DR24). *ApJs* 224, 12. doi:10.3847/0067-0049/224/1/12

Dressing, C. D., Adams, E. R., Dupree, A. K., Kulesa, C., and McCarthy, D. (2014). Adaptive optics images. III. 87 kepler objects of interest. *AJ* 148, 78. doi:10.1088/0004-6256/148/5/78

Espinoza, N., Brahm, R., Henning, T., Jordán, A., Dorn, C., Rojas, F., et al. (2019). HD 213885b: a transiting 1-day-period super-Earth with an Earth-like composition around a bright (V = 7.9) star unveiled by TESS. *Mon. Not. R. Astron. Soc.* 491 (2), 2982–2999. doi:10.1093/mnras/stz3150

Fabrycky, D., and Tremaine, S. (2007). Shrinking binary and planetary orbits by kozai cycles with tidal friction. *ApJ* 669, 1298–1315. doi:10.1086/521702

Fressin, F., Torres, G., Charbonneau, D., Bryson, S. T., Christiansen, J., Dressing, C. D., et al. (2013). The false positive rate of kepler and the occurrence of planets. *ApJ* 766, 81. doi:10.1088/0004-637X/766/2/81

Fulton, B. J., Petigura, E. A., Howard, A. W., Isaacson, H., Marcy, G. W., Cargile, P. A., et al. (2017). The California-kepler survey. III. a gap in the radius distribution of small planets. *AJ* 154, 109. doi:10.3847/1538-3881/aa80eb

Gaidos, E., Mann, A. W., Kraus, A. L., and Ireland, M. (2016). They are small worlds after all: revised properties of kepler M dwarf stars and their planets. *Mon. Not. Roy. Astron. Soc.* 457, 2877–2899. doi:10.1093/mnras/stw097

Hirsch, L. A., Ciardi, D. R., Howard, A. W., Everett, M. E., Furlan, E., Saylors, M., et al. (2017). Assessing the effect of stellar companions from high-resolution imaging of kepler objects of interest. *AJ* 153, 117. doi:10.3847/1538-3881/153/3/117

Horch, E. P., Howell, S. B., Everett, M. E., and Ciardi, D. R. (2014). Most sub-arcsecond companions of kepler exoplanet candidate host stars are gravitationally bound. *ApJ* 795, 60. doi:10.1088/0004-637X/795/1/60

Horch, E. P., Howell, S. B., Everett, M. E., and Ciardi, D. R. (2012). Observations of binary stars with the differential speckle survey instrument. IV. Observations of kepler, CoRoT, and hipparcos stars from the gemini north telescope. *AJ* 144, 165. doi:10.1088/0004-6256/144/6/165

Howell, S. B., Everett, M. E., Sherry, W., Horch, E., and Ciardi, D. R. (2011). Speckle camera observations for the NASA kepler mission follow-up Program. *AJ* 142, 19. doi:10.1088/0004-6256/142/1/19

Jang-Condell, H., Mugrauer, M., and Schmidt, T. (2008). Disk truncation and planet formation in γ cephei. *ApJ* 683, L191. doi:10.1086/591791

Jensen-Clem, R., Duev, D. A., Riddle, R., Salama, M., Baranec, C., Law, N. M., et al. (2018). The performance of the robo-AO laser guide star adaptive optics system at the Kitt peak 2.1 m telescope. *AJ* 155, 32. doi:10.3847/1538-3881/aa9be6

Jones, M. I., Brahm, R., Espinoza, N., Wang, S., Shporer, A., Henning, T., et al. (2019). HD 2685 b: a hot Jupiter orbiting an early F-type star detected by TESS. *Astron. Astrophys.* 625, A16. doi:10.1051/0004-6361/201834640

Katz, B., Dong, S., and Malhotra, R. (2011). Long-term cycling of kozai-lidov cycles: extreme eccentricities and inclinations excited by a distant eccentric perturber. *Phys. Rev. Lett.* 107, 181101. doi:10.1103/PhysRevLett.107.181101

Kraus, A. L., Ireland, M. J., Hillenbrand, L. A., and Martinache, F. (2012). The role of multiplicity in disk evolution and planet formation. *ApJ* 745, 19. doi:10.1088/0004-637X/745/1/19

Kraus, A. L., Ireland, M. J., Huber, D., Mann, A. W., and Dupuy, T. J. (2016). The impact of stellar multiplicity on planetary systems. I. The ruinous influence of close binary companions. *AJ* 152, 8. doi:10.3847/0004-6256/152/1/8

Law, N. M., Morton, T., Baranec, C., Riddle, R., Ravichandran, G., Ziegler, C., et al. (2014). Robotic laser adaptive optics imaging of 715 kepler exoplanet candidates using robo-AO. *ApJ* 791, 35. doi:10.1088/0004-637X/791/1/35

Lillo-Box, J., Barrado, D., and Bouy, H. (2014). High-resolution imaging of Kepler planet host candidates. a comprehensive comparison of different techniques. *Astron. Astrophys.* 566, A103. doi:10.1051/0004-6361/201423497

Lillo-Box, J., Barrado, D., and Bouy, H. (2012). Multiplicity in transiting planet-host stars. a lucky imaging study of kepler candidates. *Astron. Astrophys.* 546, A10. doi:10.1051/0004-6361/201219631

Marcy, G. W., Isaacson, H., Howard, A. W., Rowe, J. F., Jenkins, J. M., Bryson, S. T., et al. (2014). Masses, radii, and orbits of small kepler planets: the transition from gaseous to rocky planets. *ApJs* 210, 20. doi:10.1088/0067-0049/210/2/20

Mathur, S., Huber, D., Batalha, N. M., Ciardi, D. R., Bastien, F. A., Bieryla, A., et al. (2017). Revised stellar properties of kepler targets for the Q1-17 (DR25) transit detection run. *ApJs* 229, 30. doi:10.3847/1538-4365/229/2/30

Morton, T. D., Bryson, S. T., Coughlin, J. L., Rowe, J. F., Ravichandran, G., Petigura, E. A., et al. (2016). False positive probabilities for all kepler objects of interest: 1284 newly validated planets and 428 likely false positives. *ApJ* 822, 86. doi:10.3847/0004-637X/822/2/86

Morton, T. D., and Johnson, J. A. (2011). On the low false positive probabilities of kepler planet candidates. *ApJ* 738, 170. doi:10.1088/0004-637X/738/2/170

Naoz, S., Farr, W. M., and Rasio, F. A. (2012). On the formation of hot jupiters in stellar binaries. *ApJ* 754, L36. doi:10.1088/2041-8205/754/2/L36

Ngo, H., Knutson, H. A., Hinkley, S., Crepp, J. R., Bechter, E. B., Batygin, K., et al. (2015). Friends of hot jupiters. II. no correspondence between hot-jupiter spin-orbit misalignment and the incidence of directly imaged stellar companions. *ApJ* 800, 138. doi:10.1088/0004-637X/800/2/138

Quinn, S. N., Becker, J. C., Rodriguez, J. E., Hadden, S., Huang, C. X., Morton, T. D., et al. (2019). Near-resonance in a system of sub-Neptunes from TESS. *AJ* 158 (5), 177. doi:10.3847/1538-3881/ab3f2b

Quintana, E. V., Adams, F. C., Lissauer, J. J., and Chambers, J. E. (2007). Terrestrial planet formation around individual stars within binary star systems. *ApJ* 660, 807–822. doi:10.1086/512542

Raghavan, D., McAlister, H. A., Henry, T. J., Latham, D. W., Marcy, G. W., Mason, B. D., et al. (2010). A survey of stellar families: multiplicity of solar-type stars. *ApJs* 190, 1–42. doi:10.1088/0067-0049/190/1/1

Ricker, G. R., Winn, J. N., Vanderspek, R., Latham, D. W., Bakos, G. Á., Bean, J. L., et al. (2014). "Transiting exoplanet survey satellite (TESS)," In Space telescopes and instrumentation 2014: optical, infrared, and millimeter wave, Bellingham, WA, August 28, 2014 (Bellingham, WA: Society of Photo-Optical Instrumentation Engineers (SPIE)), Vol. 9143, 914320. doi:10.1117/12.2063489

Rodriguez, J. E., Quinn, S. N., Huang, C. X., Vanderburg, A., Penev, K., Brahm, R., et al. (2019). An eccentric massive jupiter orbiting a subgiant on a 9.5-day period discovered in the transiting exoplanet survey satellite full frame images. *AJ* 157, 191. doi:10.3847/1538-3881/ab11d9

Roell, T., Neuhäuser, R., Seifahrt, A., and Mugrauer, M. (2012). Extrasolar planets in stellar multiple systems. *A&A* 542, A92. doi:10.1051/0004-6361/201118051

Rogers, L. A. (2015). Most 1.6 earth-radius planets are not rocky. *ApJ* 801, 41. doi:10.1088/0004-637X/801/1/41

Rowe, J. F., Bryson, S. T., Marcy, G. W., Lissauer, J. J., Jontof-Hutter, D., Mullally, F., et al. (2014). Validation of kepler's multiple planet candidates. III. light curve analysis and announcement of hundreds of new multi-planet systems. *ApJ* 784, 45. doi:10.1088/0004-637X/784/1/45

Stassun, K. G., Oelkers, R. J., Paegert, M., Torres, G., Pepper, J., De Lee, N., et al. (2019). The revised TESS input catalog and candidate target list. *AJ* 158 (4), 138. doi:10.3847/1538-3881/aade86

Tokovinin, A. (2018). Ten years of speckle interferometry at SOAR. *PASP* 130, 035002. doi:10.1088/1538-3873/aaa7d9

Van Eylen, V., Agentoft, C., Lundkvist, M. S., Kjeldsen, H., Owen, J. E., Fulton, B. J., et al. (2018). An asteroseismic view of the radius valley: stripped cores, not born rocky. *MNRAS* 479, 4786–4795. doi:10.1093/mnras/sty1783

Vanderburg, A., Huang, C. X., Rodriguez, J. E., Becker, J. C., Ricker, G. R., Vanderspek, R. K., et al. (2019). TESS spots a compact system of super-earths around the naked-eye star HR 858. *Astrophys. J. Lett.* 881 (1), L19. doi:10.3847/2041-8213/ab322d

Wizinowich, P. L., Le Mignant, D., Bouchez, A. H., Campbell, R. D., Chin, J. C. Y., Contos, A. R., et al. (2006). The W. M. Keck observatory laser guide star adaptive optics system: overview. *Publ. Astron. Soc. Pac.* 118, 297–309. doi:10.1086/499290

Xie, J.-W., Wu, Y., and Lithwick, Y. (2014). Frequency of close companions among kepler planets—a transit time variation study. *ApJ* 789, 165. doi:10.1088/0004-637X/789/2/165

Ziegler, C., Law, N. M., Baranec, C., Howard, W., Morton, T., Riddle, R., et al. (2018a). Robo-AO kepler survey. V. the effect of physically associated stellar companions on planetary systems. *AJ* 156, 83. doi:10.3847/1538-3881/aace59

Ziegler, C., Law, N. M., Baranec, C., Morton, T., Riddle, R., De Lee, N., et al. (2018b). Measuring the recoverability of close binaries in Gaia DR2 with the robo-AO kepler survey. *AJ* 156, 259. doi:10.3847/1538-3881/aad80a

Ziegler, C., Law, N. M., Baranec, C., Riddle, R., Duev, D. A., Howard, W., et al. (2018c). Robo-AO kepler survey. IV. the effect of nearby stars on 3857 planetary candidate systems. *AJ* 155 (4), 161. doi:10.3847/1538-3881/aab042

Ziegler, C., Law, N. M., Morton, T., Baranec, C., Riddle, R., Atkinson, D., et al. (2017). Robo-AO kepler planetary candidate survey. III. adaptive optics imaging of 1629 kepler exoplanet candidate host stars. *AJ* 153, 66. doi:10.3847/1538-3881/153/2/66

Ziegler, C., Tokovinin, A., Briceño, C., Mang, J., Law, N., and Mann, A. W. (2020). SOAR TESS survey. I. sculpting of TESS planetary systems by stellar companions. *AJ* 159, 19. doi:10.3847/1538-3881/ab55e9

Conflict of Interest: The authors declare that the research was conducted in the absence of any commercial or financial relationships that could be construed as a potential conflict of interest.

frontiers in Astronomy and Space Sciences

ORIGINAL RESEARCH
published: 15 April 2021
doi: 10.3389/fspas.2021.640830

Circumbinary Habitable Zones in the Presence of a Giant Planet

Nikolaos Georgakarakos[1,2*], *Siegfried Eggl*[3,4,5,6] *and Ian Dobbs-Dixon*[1,2,7]

[1] Division of Science, New York University Abu Dhabi, Abu Dhabi, United Arab Emirates, [2] Center for Astro, Particle and Planetary Physics (CAP[3]), New York University Abu Dhabi, Abu Dhabi, United Arab Emirates, [3] Department of Astronomy, University of Washington, Seattle, WA, United States, [4] Vera C. Rubin Observatory, Tucson, AZ, United States, [5] Department of Aerospace Engineering, University of Chicago at Urbana-Champaign, Urbana, IL, United States, [6] IMCCE, Observatoire de Paris, Paris, France, [7] Center for Space Sciences, New York University Abu Dhabi, Abu Dhabi, United Arab Emirates

Determining habitable zones in binary star systems can be a challenging task due to the combination of perturbed planetary orbits and varying stellar irradiation conditions. The concept of "dynamically informed habitable zones" allows us, nevertheless, to make predictions on where to look for habitable worlds in such complex environments. Dynamically informed habitable zones have been used in the past to investigate the habitability of circumstellar planets in binary systems and Earth-like analogs in systems with giant planets. Here, we extend the concept to potentially habitable worlds on circumbinary orbits. We show that habitable zone borders can be found analytically even when another giant planet is present in the system. By applying this methodology to Kepler-16, Kepler-34, Kepler-35, Kepler-38, Kepler-64, Kepler-413, Kepler-453, Kepler-1647, and Kepler-1661 we demonstrate that the presence of the known giant planets in the majority of those systems does not preclude the existence of potentially habitable worlds. Among the investigated systems Kepler-35, Kepler-38, and Kepler-64 currently seem to offer the most benign environment. In contrast, Kepler-16 and Kepler-1647 are unlikely to host habitable worlds.

Keywords: planet-star interactions, celestial mechanics, astrobiology, circumbinary planets, habitable planets, methods: analytical

OPEN ACCESS

Edited by:
Francesco Marzari, University of Padua, Italy

Reviewed by:
Silvano Desidera, Osservatorio Astronomico di Padova (INAF), Italy
Diego Turrini, National Institute of Astrophysics (INAF), Italy

***Correspondence:**
Nikolaos Georgakarakos
ng53@nyu.edu

Specialty section:
This article was submitted to Exoplanets, a section of the journal Frontiers in Astronomy and Space Sciences

Received: *12 December 2020*
Accepted: *12 March 2021*
Published: *15 April 2021*

Citation:
Georgakarakos N, Eggl S and Dobbs-Dixon I (2021) Circumbinary Habitable Zones in the Presence of a Giant Planet. Front. Astron. Space Sci. 8:640830. doi: 10.3389/fspas.2021.640830

1. INTRODUCTION

Over the past three decades exoplanet researchers have discovered more than four thousands planets outside our Solar System[1]. Improvements in detection techniques have now reached a point where finding planets of similar size to our Earth has become a reality. Four of the planets in the Trappist-1 system (Gillon et al., 2016) or TOI-700d (Gilbert et al., 2020; Rodriguez et al., 2020) are prime examples. Several planets in those systems orbit their host star inside the habitable zone. The habitable zone is the region where a terrestrial planet on a circular orbit about its host star can support liquid water on its surface (Kasting et al., 1993). A number of planets have been found to reside in binary stars systems, some of which even orbit both stars (e.g., Doyle et al., 2011; Welsh et al., 2012; Kostov et al., 2014). We refer to the latter as circumbinary planets. Unresolved questions regarding the formation and dynamical evolution of such systems (Marzari and Thebault, 2019) have motivated a number of studies in recent years, particularly on whether or not such systems

[1] https://exoplanetarchive.ipac.caltech.edu/

could host potentially habitable worlds (Haghighipour and Kaltenegger, 2013; Kane and Hinkel, 2013; Cuntz, 2014, 2015; Forgan, 2014; Jaime et al., 2014; Cukier et al., 2019; Shevchenko et al., 2019; Yadavalli et al., 2020). Some of the challenges in assessing habitability in binary star systems arises from the fact that one has to account for two sources of radiation, possibly of different spectral type. Moreover, the distance of the planet to each star keep changing over time in a non-trivial manner due to gravitational interactions between the planet and the two stars.

The introduction of "dynamically informed habitable zones" allowed Eggl et al. (2012) to study the prospects for habitability of planets orbiting a single star in a binary star system. Dynamically informed habitable zones for systems with a potentially habitable world on a circumbinary orbit were developed in Eggl (2018) and Eggl et al. (2020). In this work, we improve on previous analytic estimates for circumbinary dynamically informed habitable zones and extend the concept to systems that are known to host an additional giant planet. Here we refer to giant planets as bodies with masses ranging from Neptune mass up to a few Jupiter masses.

The structure of this paper is as follows: in the next section we explain the general principles behind dynamically informed habitable zones and construct the required tools to extend the concept to include a giant planet in the system. In section 3 we investigate the potential of binary star systems with known circumbinary planets observed during the Kepler mission (e.g., Doyle et al., 2011; Welsh et al., 2012; Kostov et al., 2014) to host additional potentially habitable worlds. Finally, in section 4 we summarize and discuss the work presented here.

2. DYNAMICALLY INFORMED HABITABLE ZONES

The nearly circular orbit of the Earth around the Sun ensures that the planet receives an almost constant amount of radiation on a permanent basis. That assumption falters for a circumbinary planet, however. The second star provides an additional source of radiation, and more importantly, it is also a source of gravitational perturbations for the planetary orbit. Even if a planet is on an initially circular orbit around the binary, the orbit will become elliptic over time (see e.g., Georgakarakos, 2009; Georgakarakos and Eggl, 2015). As a consequence, the planet experiences time dependent irradiation. Depending on how effectively the climate on the planet can buffer changes in incoming radiation its response to radiative forcing can differ widely (see e.g., Popp and Eggl, 2017; Way and Georgakarakos, 2017; Haqq-Misra et al., 2019; Wolf et al., 2020). In order to capture the various responses defined by a planet's climate inertia, we make use of so-called "dynamically informed habitable zones" (DIHZs) (see e.g., Georgakarakos et al., 2018). DIHZs not only take the orbital evolution of the planet around the binary into account, but they can even trace habitable zone limits for different climate inertia values a planet may have. Climate inertia is defined as the time it takes climate parameters, such as the mean surface temperature, to react to radiative forcing. The faster the mean surface temperature changes, the lower the climate inertia of a planet is.

In order to account for the effect of climate inertia, we follow the general methodology as outlined in (Eggl et al., 2012) and (Georgakarakos et al., 2018) and introduce three different DIHZs: the permanently habitable zone (PHZ), the averaged habitable zone (AHZ), and the extended habitable zone (EHZ). The PHZ is the most conservative region. For a planet to reside in the PHZ means that it stays continuously within habitable insolation limits in spite of orbit-induced variability. In other words, the PHZ is the region where a planet with essentially zero climate inertia could remain habitable on stellar evolution timescales. On the other end of the spectrum is the averaged habitable zone, where a planet is assumed to buffer all variations in irradiation and remains habitable as long as the insolation average stays within habitable limits. This scenario corresponds to a planet with a very high climate inertia.

The extended habitable zone lies between the above extremes by assuming that the planetary climate has limited buffering capabilities. The EHZ is defined as the region where the planet stays on average plus minus one standard deviation within habitable insolation limits. In order to calculate DIHZ borders for circumbinary systems, we need to understand (a) whether or not a configuration is dynamical stable, (b) how the orbital evolution of the system affects the amount of radiation the planet receives, and (c) how the combined quantity and spectral distribution of the star light influences the climate of a potentially habitable world.

2.1. Dynamical Stability

Dynamical stability is a necessary condition for habitability of a circumbinary planet. If a planet is ejected from a system, water that may be present on its surface will ultimately freeze. There are a number of ways to predict whether or not a potentially habitable world is on a stable orbit (e.g., see Georgakarakos, 2008). In this work, we make use of the empirical condition developed in Holman and Wiegert (1999) which provides critical semi-major axis values below which planetary orbits around binary stars become unstable. The critical semi-major axis in a circumbinary system depends on the eccentricity, semi-major axis, and mass ratio of the binary as can be seen from the following equation:

$$\begin{aligned} a_c \;=\; & [(1.60 \pm 0.04) + (5.10 \pm 0.05)e_b + (-2.22 \pm 0.11)e_b^2 \\ & + (4.12 \pm 0.09)\mu + (-4.27 \pm 0.17)e_b\mu + (-5.09 \pm 0.11)\mu^2 \\ & + (4.61 \pm 0.36)e_b^2\mu^2]a_b, \end{aligned} \tag{1}$$

where a_b is the semi-major axis of the binary, e_b is the eccentricity of the binary and $\mu = m_2/(m_1 + m_2)$; m_1 and m_2 are the masses of the two stars ($m_1 > m_2$ without loss of generality). A value of planetary semi-major axis below a_c indicates that the planet will escape from the system or collide with one of the stars.

Once we confirm that a potentially habitable planet is on a stable orbit, we can proceed to investigate how much radiation it receives from the two stars. The latter depends on the orbit of the planet which evolves over time. By modeling the evolution of the stellar and planetary orbits we can estimate the actual amount and spectral composition of the radiation the planet receives. To

this end we make use of an analytic orbit propagation technique for circumbinary planets developed in Georgakarakos and Eggl (2015).

2.2. The Classical Habitable Zone

For systems consisting of a star and a terrestrial planet on a fixed circular orbit, the limits of the classical habitable zone (CHZ) read

$$r_I = \left(\frac{L}{S_I}\right)^{\frac{1}{2}} \quad \text{and} \quad r_O = \left(\frac{L}{S_O}\right)^{\frac{1}{2}}, \tag{2}$$

where r is the distance of the planet to its host star in astronomical units, L is the host star's luminosity in solar luminosities, and S_I and S_O are effective insolation values or "spectral weights" (Kasting et al., 1993). The latter correspond to the number of solar constants that trigger a runaway greenhouse process (subscript I) evaporating surface oceans, or a snowball state (subscript O) freezing oceans on a global scale. Spectral weights are functions of the effective temperature of the host star and, therefore, they take the specific wavelength distribution of a star's light into account. They can be calculated by the expressions below which can be found in Kopparapu et al. (2014):

$$\begin{aligned} S_I &= 1.107 + 1.332 \cdot 10^{-4} T_c + 1.580 \cdot 10^{-8} T_c^2 \\ &- 8.308 \cdot 10^{-12} T_c^3 - 1.931 \cdot 10^{-15} T_c^4 \end{aligned} \tag{3}$$

$$\begin{aligned} S_O &= 0.356 + 6.171 \cdot 10^{-5} T_c + 1.698 \cdot 10^{-9} T_c^2 \\ &- 3.198 \cdot 10^{-12} T_c^3 - 5.575 \cdot 10^{-16} T_c^4. \end{aligned} \tag{4}$$

$T_c = T_{eff}/1\ K - 5780$, with T_{eff} being the effective temperature of the star, while the value of 5780 used in the above fit formulae corresponds to the effective temperature $T_\odot$ of the Sun. The coefficients in Equations (3) and (4) refer to a planet of one Earth mass but similar functions are available for different terrestrial planet masses. In case stellar luminosities have not been observed directly, one can use stellar radii R_* and effective temperatures T_{eff} instead:

$$\frac{L}{L_\odot} = \left(\frac{R_*}{R_\odot}\right)^2 \left(\frac{T_{eff}}{T_\odot}\right)^4,$$

where $R_\odot$ is the radius of the Sun.

2.3. The Permanently Habitable Zone

We will now use the above concepts to determine the permanently habitable zone. In order to find the borders of the region wherein the planet stays always within habitable insolation limits, i.e., the PHZ, we need to find the effective insolation extrema a circumbinary planet is likely to encounter. In hierarchical systems of two stars and a circumbinary planet, the planetary semi-major axis remains practically constant over time. In addition, if a system is coplanar, the time evolution of the eccentricity vectors determines the geometric configuration at any given moment. Assuming furthermore that the gravitational effect of the planet on the stellar binary is negligible, maximum and minimum insolation configurations are determined through the maximum planetary eccentricity e_p^{max}. We use the expressions derived in Georgakarakos and Eggl (2015) that allow us to calculate e_p^{max} as a function of initial conditions and system parameters. The apocenter and pericenter distance between the planet and the barycenter of the binary star can in turn be expressed through the maximum eccentricity as well as the semi-major axis of the planetary orbit a_p, i.e., $Q_p = a_p(1 + e_p^{max})$ and $q_p = a_p(1 - e_p^{max})$. **Figure 1** is a schematic representation of our system, meant to help the reader visualize configurations that lead to insolation extrema. The planet receives maximum insolation when it is at pericenter with respect to the binary barycenter and closer to the brighter star, i.e., when the angle ϕ between the line that connects the stars and the line that connects the planet to the binary barycenter is $\phi = 0^\circ$. Thus, the three bodies are aligned and the mathematical expression that determines the inner edge of the PHZ is

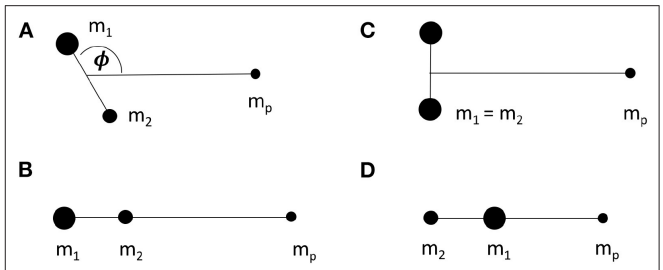

FIGURE 1 | A schematic representation of possible binary star - planet geometries representing irradiation minima: **(A–C)** and maxima **(D)** for various mass ratios of the binary star (m_2/m_1). A standard mass-luminosity relation for main sequence stars is assumed. The more massive star is m_1, the less massive star is m_2, and the planet is represented by m_p.

$$PHZ_I : \frac{L_1}{S_{1,I}(q_p - \mu Q_b)^2} + \frac{L_2}{S_{2,I}[q_p + (1-\mu)Q_b]^2} \leq 1, \tag{5}$$

where $Q_b = a_b(1+e_b)$. Note that we have normalized the stellar luminosities with their respective spectral weights in order to account for the effect of each star's individual spectral energy distribution on the planetary climate. The minimum insolation configuration is not as straight forward to determine. If one star is substantially more massive and luminous than the other a minimum can be reached when the brighter star is farthest from the planet and the planet is at apocenter with respect to the barycenter of the binary star. This is the case when $\phi = 180^\circ$ which corresponds to the following condition for the outer edge of the PHZ

$$PHZ_O : \frac{L_1}{S_{1,O}(Q_p + \mu Q_b)^2} + \frac{L_2}{S_{2,O}[Q_p - (1-\mu)Q_b]^2} \geq 1, \tag{6}$$

If we have two stars of equal mass, then the minimum radiation configuration is reached when $\phi = 90^\circ$. Hence, the minimum insolation condition in this case is

$$PHZ_O : \frac{1}{Q_p^2 + 0.5Q_b^2}\left(\frac{L_1}{S_{1,O}} + \frac{L_2}{S_{2,O}}\right) \geq 1. \tag{7}$$

When the mass ratio of the binary is close to–but not exactly–equal to one (with $m_1 > m_2$) and the planet is located at

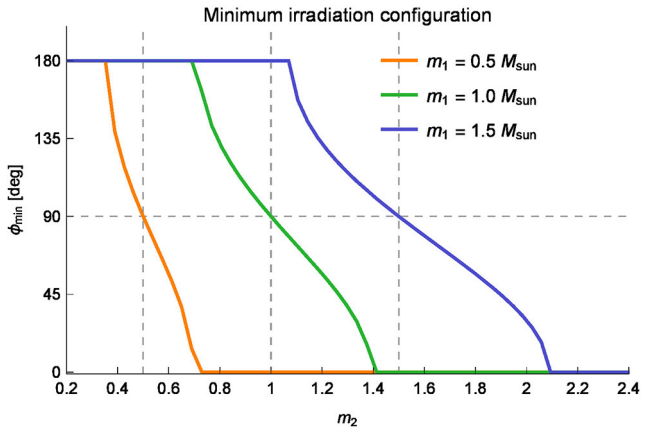

FIGURE 2 | Angle ϕ_{min} for the minimum planetary insolation configuration against the mass of the secondary star m_2 for various masses of the primary star m_1. We assume a planet on a circular orbit at a distance of 2.37 au from the binary barycenter, while the binary stars are evolved on a circular orbit with a semi-major axis of 1 au.

a suitable distance, the minimum insolation geometry occurs between $\phi = 90^\circ$ and $\phi = 180^\circ$. **Figure 2** illustrates this behavior for a variety of binary mass ratios. We note, however that the difference in insolation received by the planet between said configurations is small (∼10%). We limit our approach to comparing the perpendicular and straight line configurations and use the one that provides the smallest value. Consequently the minimum insolation condition for the outer border of the PHZ reads

$$PHZ_O: \quad min\left\{\frac{L_1}{S_{1,O}(Q_p+\mu Q_b)^2}+\frac{L_2}{S_{2,O}[Q_p-(1-\mu)Q_b]^2}, \right. \\ \left. \frac{L_1}{S_{1,O}(Q_p^2+\mu^2 Q_b^2)}+\frac{L_2}{S_{2,O}[Q_p^2+(1-\mu)^2 Q_b^2]}\right\} \geq 1. \quad (8)$$

One can find the numeric values for the borders of the PHZ by solving Equations (5) through (8) for a_p.

We would like to point out here that for all the above insolation extrema configurations we have assumed that the stars are point masses. In reality, however, the stars have finite sizes. Depending on the distance between the two stars and on the distance between the planet and the binary, it is possible that when the three bodies are aligned the planet may receive reduced insolation due to the eclipsed star. In such a scenario, the minimum insolation configuration (**Figure 1C**) will still be valid. On the other hand, the maximum insolation configuration (**Figure 1D**) would provide a smaller insolation value. Wolf et al. (2020) have shown, however, that eclipses have little effect on the overall stability of the climate. But even if the insolation change is considerable, as soon as the three bodies get out of alignment, the planet will then receive near maximum insolation. Hence, Equation (5) constitutes a reasonable approximation for our purposes.

2.4. The Averaged Habitable Zone

The averaged habitable zone is the region around a binary star where a planet remains habitable inspite of variations in irradiation. That is, as long as the insolation average is compatible with habitable limits a planet with a high climate inertia can remain potentially habitable. The averaged over time radiation that a planet receives when orbiting a single star is

$$\langle S\rangle = \frac{1}{P}\int_0^P \frac{L}{r_p^2(t)}dt = \frac{n_p}{2\pi}\int_0^{2\pi}\frac{L\,df_p}{n_p a_p^2\sqrt{1-e_p^2}} = \frac{L}{a_p^2\sqrt{1-e_p^2}}, \quad (9)$$

where L is the stellar luminosity, P the period of the planetary motion, n_p is the mean motion of the planet, f_p is its true anomaly, and r_p the distance between the source of radiation and the planet; we made use of the well-known relation $r_p^2 df_p/dt = n_p a_p^2\sqrt{1-e_p^2}$. We can now extend this simple relation to circumbinary orbits. Assuming that the distance between the two stars is small compared to the distance between the planet and the binary star barycenter, i.e., the orbital period of the binary pair is much smaller than that of the planet, we can approximate the average over time insolation around the binary by placing the two stars at their barycenter and make use of Equation (9). In other words we approximate the three body system as a two-body problem with a central "hybrid star" that has the combined mass, luminosity, and spectral energy distribution of the stellar binary. This leads to

$$\langle S\rangle = \frac{L_1+L_2}{a_p^2\sqrt{1-\langle e_p^2\rangle}}, \quad (10)$$

where $\langle e_p^2\rangle$ is the averaged square planetary eccentricity over time and initial angles as given in Georgakarakos and Eggl (2015). Under those assumptions the borders of the AHZ are defined through the following inequalities

$$AHZ_I: \frac{L_1/S_{1,I}+L_2/S_{2,I}}{a_p^2\sqrt{1-\langle e_p^2\rangle}} \leq 1 \quad (11)$$

and

$$AHZ_O: \frac{L_1/S_{1,O}+L_2/S_{2,O}}{a_p^2\sqrt{1-\langle e_p^2\rangle}} \geq 1. \quad (12)$$

Note that $\langle e_p^2\rangle$ generally depends on a_p in a non-trivial way. The full expression for $\langle e_p^2\rangle$ along with the expression for e_p^{max} is provided in the **Appendix**. Once more, solving Equations (11) and (12) for a_p yields the numeric values for the borders of the AHZ.

2.5. The Extended Habitable Zone

The definition of the extended habitable zone in section 2 translates into the following equations:

$$\langle S\rangle + \sigma = S_I \quad \text{and} \quad \langle S\rangle - \sigma = S_O. \quad (13)$$

TABLE 1 | Mean physical parameters and orbital elements for the Kepler-16(AB), Kepler-34(AB), Kepler-35(AB), Kepler-38(AB), Kepler-64(AB), Kepler-413(AB), Kepler-453(AB), Kepler-1647(AB), and Kepler-1661(AB) stellar binaries.

System	$M_1(M_\odot)$	$M_2(M_\odot)$	$R_1(R_\odot)$	$R_2(R_\odot)$	$T_{eff1}(K)$	$T_{eff2}(K)$	$a_b(au)$	e_b
Kepler-16	0.6897	0.20255	0.6489	0.22623	4450.0	3311.0	0.22431	0.15944
Kepler-34	1.0479	1.0208	1.1618	1.0927	5913.0	5867.0	0.22882	0.52087
Kepler-35	0.8876	0.8094	1.0284	0.7861	5606.0	5202.0	0.17617	0.1421
Kepler-38	0.949	0.249	1.757	0.2724	5640.0	3325.0	0.1469	0.1032
Kepler-64	1.528	0.378	1.734	0.408	6407.0	3561.0	0.1744	0.2117
Kepler-413	0.820	0.5423	0.7761	0.484	4700.0	3463.0	0.10148	0.0365
Kepler-453	0.944	0.1951	0.833	0.2150	5527.0	3226.0	0.18539	0.0524
Kepler-1647	1.210	0.975	1.7903	0.9663	6210.0	5770.0	0.1276	0.1593
Kepler-1661	0.841	0.262	0.762	0.276	5100.0	3585.0	0.187	0.112

The uncertainties can be found in the corresponding references in section 3.

The standard deviation σ can be found via the insolation variance

$$\sigma^2 = \langle S^2 \rangle - \langle S \rangle^2. \tag{14}$$

We already have an expression for $\langle S \rangle$ from Equation (10), but we are yet to find $\langle S^2 \rangle$. For a planet around a single star, $\langle S^2 \rangle$ is

$$\langle S^2 \rangle = \frac{1}{P}\int_0^P \frac{L^2}{r_p^4(t)}dt = \frac{n_p}{2\pi}\int_0^{2\pi} \frac{(1+e_p\cos f_p)^2}{a_p^2(1-e_p^2)^2} \frac{L^2 df_p}{n_p a_p^2\sqrt{1-e_p^2}} = \frac{L^2(1+e_p^2/2)}{a_p^4(1-e_p^2)^{5/2}}. \tag{15}$$

Using the same approach that lead to Equation (10), namely combining the stellar binary into a "hybrid star" we can construct a closed analytic expression for $\langle S^2 \rangle$ of a circumbinary planet, namely

$$\langle S^2 \rangle = \frac{(L_1+L_2)^2(1+\langle e_p^2\rangle/2)}{a_p^4(1-\langle e_p^2\rangle)^{5/2}}. \tag{16}$$

Combining Equations (10) and (16) and normalizing the individual stellar contributions with the respective spectral weights $X_i \in \{S_{i,I}, S_{i,O}\}$, where i is the index of the respective star, yields:

$$\sigma_X^2 = \left(\frac{L_1}{X_1}+\frac{L_2}{X_2}\right)^2 \frac{1}{a_p^4(1-\langle e_p^2\rangle)}\left[\frac{1+\langle e_p^2\rangle/2}{(1-\langle e_p^2\rangle)^{3/2}}-1\right]. \tag{17}$$

The inner border of the EHZ is then defined through

$$EHZ_I : \left(\frac{L_1}{S_{1,I}}+\frac{L_2}{S_{2,I}}\right)\frac{1}{a_p^2\sqrt{1-\langle e_p^2\rangle}} \left\{1+\sqrt{\left[\frac{1+\langle e_p^2\rangle/2}{(1-\langle e_p^2\rangle)^{3/2}}-1\right]}\right\} \leq 1, \tag{18}$$

while the outer border is defined via

$$EHZ_O : \left(\frac{L_1}{S_{1,O}}+\frac{L_2}{S_{2,O}}\right)\frac{1}{a_p^2\sqrt{1-\langle e_p^2\rangle}} \left\{1-\sqrt{\left[\frac{1+\langle e_p^2\rangle/2}{(1-\langle e_p^2\rangle)^{3/2}}-1\right]}\right\} \geq 1 \tag{19}$$

Numerical values for the inner and outer EHZ borders can be found via solving the above equations for a_p.

3. APPLICATION TO KEPLER SYSTEMS WITH KNOWN CIRCUMBINARY PLANETS

In order to demonstrate the merit of dynamically informed habitable zones, we apply our method to the Kepler circumbinary planets. For that purpose we select Kepler-16 (Doyle et al., 2011), Kepler-34 and Kepler-35 (Welsh et al., 2012), Kepler-38 (Orosz et al., 2012), Kepler-64 (Schwamb et al., 2013), Kepler-413 (Kostov et al., 2014), Kepler-453 (Welsh et al., 2015), Kepler-1647 (Kostov et al., 2016), and Kepler-1661 (Socia et al., 2020). Kepler-47 (Orosz et al., 2019) has three planets and is, therefore, beyond the limits of our model. The masses of Kepler-38b, Kepler-64b, Kepler-453b are not well-defined. For those cases, we have decided to use the upper limit provided in the relevant publications. The necessary for our calculations parameters of the selected systems can be found in **Table 1** (binary star) and **Table 2** (planet).

First, we calculate all dynamically informed habitable zones assuming no giant planets are present in the systems. That provides us with a first idea of the location of the habitable zones and how the presence of the second star affects the location and extent of the various habitable zones. Then we include the existing giant planet in our model and examine its effect on the habitability of an additional hypothetical terrestrial planet. In both stages, we allowed the eccentricities of the binary and the existing planet to vary. That way we get a better picture of the effect of orbital eccentricity, an important quantity that regulates distances between bodies, on the extent of habitable zones in the system. In order to simplify the complex dynamics

in the presence of the giant planet, we acknowledge the double hierarchical structure of the problem that allows us to consider the binary as one massive body located at the barycenter. The two stars at their barycenter are considered as one body of mass $m_b = m_1 + m_2$, therefore reducing the four-body problem to a three-body one. To describe the dynamical evolution of such a system we made use of the relevant equations in Georgakarakos and Eggl (2015) when $a_{gp} < a_p$ and Eggl et al. (2012) and Georgakarakos (2003, 2005) when $a_{gp} > a_p$, where a_{gp} is the semi-major axis of the orbit of the giant planet. The stability of that particular kind of triple system was assessed using the criterion developed in Petrovich (2015). The corresponding empirical formula is based on numerical simulations of a star and two planets. The planet-star mass ratios investigated in Petrovich (2015) ranged from 10^{-4} to 10^{-2}, the ratio of the planetary semi-major axes was in the interval $[3, 10]$, while the planetary eccentricities took values in the interval $[0, 0.9]$.

A terrestrial planet on an initially circular orbit in a star-planet-planet system is stable against either ejections or collisions with the central object when

$$\frac{a_p}{a_{gp}(1+e_{gp})} > 2.4\left(\frac{m_{gp}}{m_1+m_2}\right)^{1/3}\left(\frac{a_p}{a_{gp}}\right)^{1/2}. \quad (20)$$

Here, m_{gp} is the mass of the giant planet and e_{gp} its orbital eccentricity. The above expression is valid when the giant planet is closer to the binary than the terrestrial planet. If the giant planet orbits externally to the terrestrial planet, then the criterion becomes

$$\frac{a_{gp}(1-e_{gp})}{a_p} > 2.4\left(\frac{m_{gp}}{m_1+m_2}\right)^{1/3}\left(\frac{a_{gp}}{a_p}\right)^{1/2}. \quad (21)$$

Strictly speaking, the planetary systems investigated here do not fall in the planet-star mass ratios investigated in Petrovich (2015). The planet to planet mass ratio, however, remains within those limits which is ultimately more important for the validity of the stability criterion at hand. This hypothesis can be supported by the reasonable agreement between the stability estimates given by Equations (20) and (21) and those in Georgakarakos (2013), where hierarchical triple systems with a wide range of masses and on initially circular orbits where integrated numerically and their stability limit was determined.

We now proceed to calculating habitable zones for the aforementioned Kepler systems. In a first step, we ignore the presence of residing giant planets in the respective systems. Considering a potential terrestrial planet orbiting the stellar binary, we can determine the borders of the classical and dynamically informed habitable zones for all the Kepler systems under investigation. As we can see from the left column plots of **Figures 3–5**, all systems but one have well-defined habitable zones and would be capable of hosting a broad range of potentially habitable worlds. The only exception to that is Kepler-16, where more than half of the habitable zone is truncated due to dynamical instability arising from the gravitational perturbations of the stellar binary. A terrestrial planet could only survive near the outer border of the habitable zone with the additional

TABLE 2 | Mean mass, semi-major axis, and eccentricity for Kepler-16b, Kepler-34b, Kepler-35b, Kepler-38b, Kepler-64b, Kepler-413b, Kepler-453b, Kepler-1647b, and Kepler-1661b. The uncertainties can be found in the corresponding references in section 3.

System	$m_p(M_J)$	a_p (au)	e_p
Kepler-16	0.333	0.7048	0.00685
Kepler-34	0.22	1.0896	0.182
Kepler-35	0.127	0.60345	0.042
Kepler-38	< 0.384(95% conf.)	0.4644	< 0.032(95% conf.)
Kepler-64	< 0.531(99.7% conf.)	0.634	0.0539
Kepler-413	0.21	0.3553	0.1181
Kepler-453	< 0.050	0.7903	0.0359
Kepler-1647	1.52	2.7205	0.0581
Kepler-1661	0.053	0.633	0.057

TABLE 3 | Habitable zone limits for Kepler-16, Kepler-34, Kepler-35, Kepler-38, Kepler-64, Kepler-413, Kepler-453, Kepler-1647, and Kepler-1661.

System	CHZ (au)	PHZ (au)	EHZ (au)	AHZ (au)	RHZ (au)	H&K (au)	CHZ-K13 (au)
Kepler-16	0.40–0.74	–	–	–	0.46–0.70	0.40–0.76	0.41-0.74
Kepler-34	1.56–2.75	2.10–2.25	1.79–2.47	1.60–2.76	1.60–2.74	1.51–2.85	1.62–2.77
Kepler-35	1.12–1.99	1.23–1.90	1.15–1.96	1.12–1.99	1.16–1.97	1.09–2.10	1.16–2.01
Kepler-38	1.61–2.84	1.68–2.77	1.62–2.82	1.61–2.84	1.64–2.81	1.63–2.82	1.66–2.86
Kepler-64	1.96–3.41	2.08–3.28	2.00–3.36	1.96–3.41	2.00–3.37	2. 00–3.40	2.02–3.44
Kepler-413	0.55–1.01	0.69–0.87	0.60–0.95	0.55–1.01	0.58–0.98	-	-
Kepler-453	0.74–1.31	1.00–1.20	1.21–1.27	1.27–1.31	0.77 -1.28	-	-
Kepler-1647	2.12–3.71	-	-	-	2.16– 3.67	-	-
Kepler-1661	0.60–1.08	0.82–0.64	0.94–1.03	1.03–1.08	0.64–1.04	-	-

RHZ is the radiative habitable zone described in Cuntz (2014, 2015) and Wang and Cuntz (2019), while the H&K column presents the results of Haghighipour and Kaltenegger (2013). Finally, the column CHZ-K13 provides values for our classical zone using Kopparapu et al. (2013) as that specific version of the climate model is also used by Haghighipour and Kaltenegger (2013).

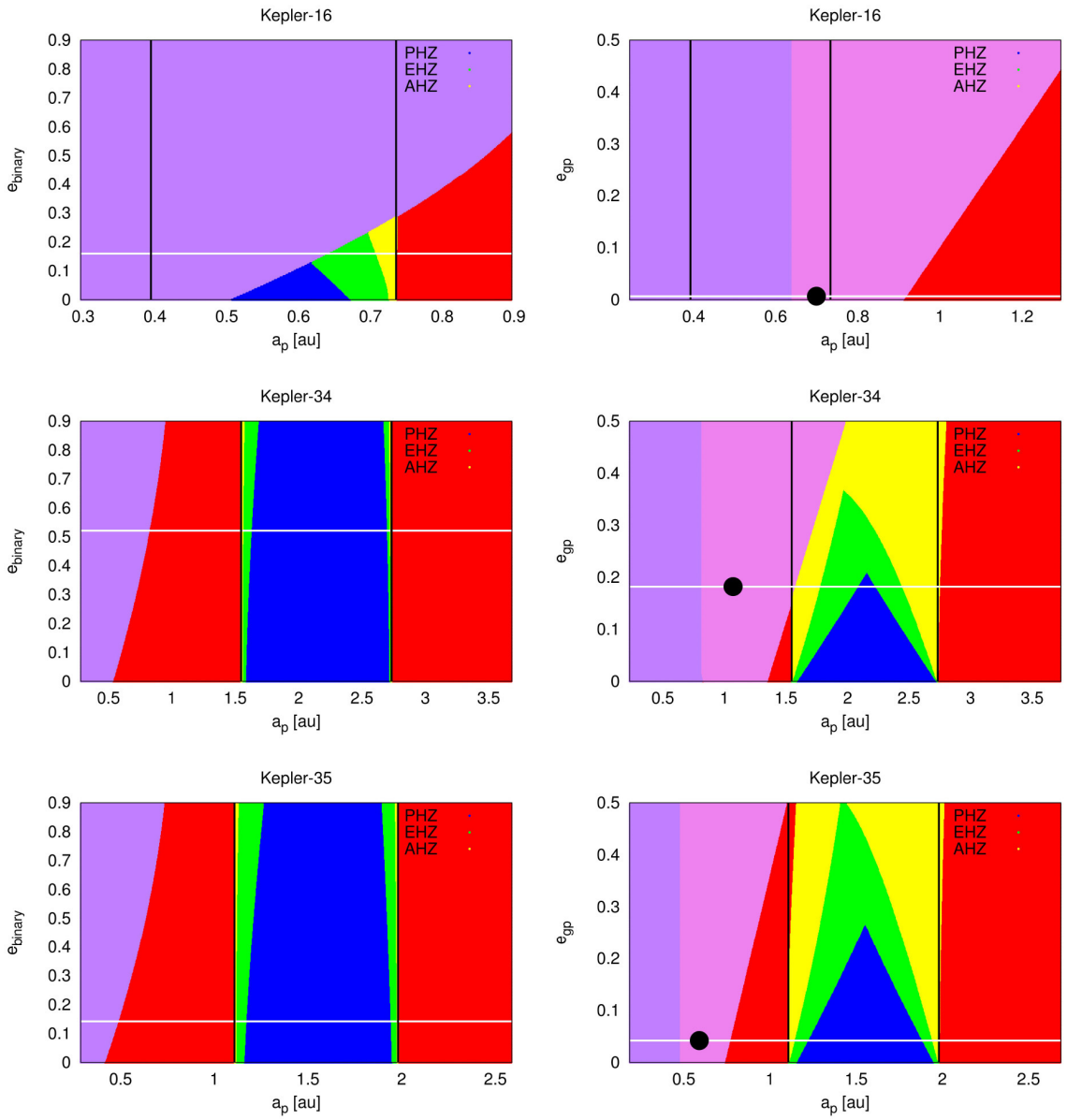

FIGURE 3 | Dynamically informed habitable zones for the Kepler-16, Kepler-34, and Kepler-35 systems. Plots in the left column show the different types of habitable zones without the presence of the known giant planets. The right column includes the influence of the known giant planets. Red colored regions correspond to uninhabitable areas, blue, green, yellow, and purple colors denote the PHZ, the EHZ, the AHZ, and unstable areas according to Holman and Wiegert (1999) stability criterion, respectively. Violet colored areas mark regions of dynamical instability caused by the giant planet in the system (Petrovich, 2015 dynamical stability criterion). The vertical black lines denote the classical habitable zone limits, while the horizontal white line in the left column plots marks the current eccentricity of the binary star orbit. In the right column graphs, the white line marks the current eccentricity of the giant planet orbit. Finally, the black dot in the right column plots shows the position of the giant planet in the presented parameter space.

requirement that it does not have a low climate inertia since the PHZ has been completely eliminated.

When we add the giant planet in our model (right column plots of **Figures 3–5**), we notice that in Kepler-16 and Kepler-1647 the added gravitational effect of the giant planet renders the entire habitable zone dynamically unstable. Regarding Kepler-16, this is in agreement with other studies such as Quarles et al. (2012), Liu et al. (2013). Note that these results do not exclude the presence of potentially habitable moons around Kepler-16b. In the Kepler-1647 system, the giant planet is located near the middle of the habitable zone. Although Kepler-453b and Kepler-1661b are located inside the classical habitable zones like the other two giant planets mentioned above, they allow a terrestrial planet to exist near the outer border of the habitable zone and they may even allow that planet to have a partial PHZ. This is because of the relatively small

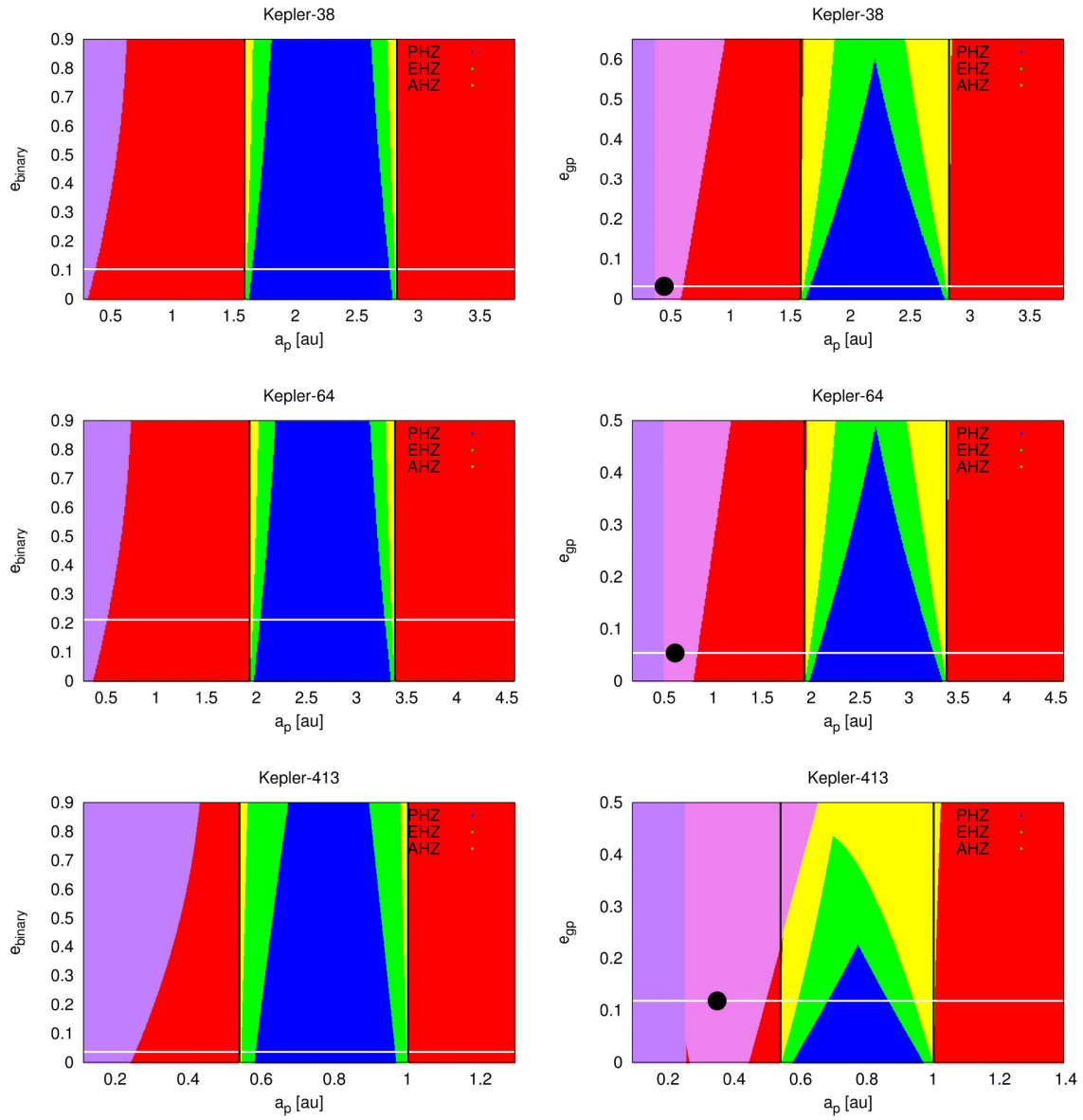

FIGURE 4 | Same as **Figure 3** for Kepler-38, Kepler-64, and Kepler-413.

masses (Neptune mass) and eccentricities of those planets. In contrast, Kepler-1647b is $1.5M_J$ and resides near the center of the habitable zone.

Regarding the remaining systems, the entire classical habitable zone is essentially dynamically stable. The difference between dynamically informed habitable zones with and without the giant planet perturbers shows, however, that the influence of giant planets goes beyond dynamical instability. In Kepler-34, potentially habitable worlds with low climate inertia could only remain habitable in a tiny region centered around 2.17 au. This can be seen from a comparison between the extent of the PHZ and the black vertical lines in the middle row right panel of **Figure 3**. Relatively dry planets with a low concentration of greenhouse gases would fall into this category. On the other hand, Kepler-35, Kepler-38, and Kepler-64 could host potentially habitable worlds with low climate inertia over a significant fraction (more than 75%) of their classical habitable zone (**Figures 4**, **5**). Finally, the extent of the PHZ of Kepler-413 is around 40% of its classical habitable zone. While not prohibitive, the presence of giant planets in Kepler-34, Kepler-413, Kepler-453, and Kepler-1661 requires additional terrestrial worlds to buffer significant variations in irradiation in order to remain habitable.

For comparison, some results from Haghighipour and Kaltenegger (2013), Cuntz (2014), Cuntz (2015), and Wang and

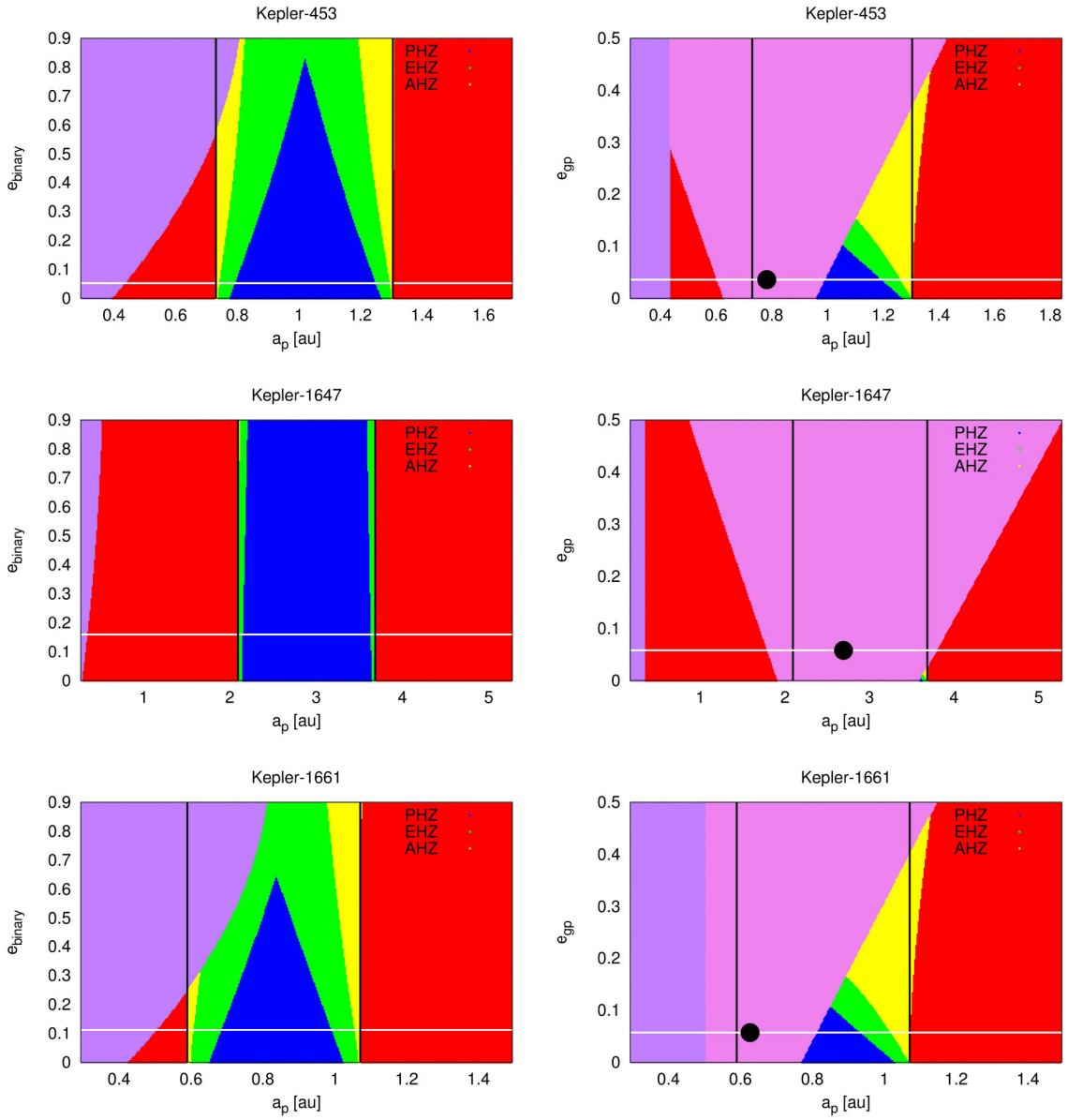

FIGURE 5 | Same as **Figure 3** for Kepler-453, Kepler-1647, and Kepler-1661.

Cuntz (2019) are also provided. Our results seem to be in good agreement with those of Cuntz (2014, 2015) and Wang and Cuntz (2019), with our classical habitable zone being a bit wider. In order to compare with Haghighipour and Kaltenegger (2013), we use Kopparapu et al. (2013) to calculate our classical habitable zone as that specific climate model was used by Haghighipour and Kaltenegger (2013) for their habitable zone calculations. In this case, however, it is more difficult to make a direct comparison as Haghighipour and Kaltenegger (2013) used time variable habitable zones centered at the primary star. Habitable zones borders for the Kepler systems under investigation are presented in **Table 3**.

4. DISCUSSION AND SUMMARY

We present an analytical approach to determine dynamically informed habitable zones in binary star systems with a circumbinary giant planet. The method takes into consideration the orbital evolution of the giant and terrestrial planet as well as different responses of planetary climates to variations in the quantity and spectral energy distribution of incoming radiation. It does not apply, however, during the planet formation stage, when we can have planets migrating due to interactions with the protoplanetary disk or planet-planet scattering events during late stage formation. In addition, we do not consider systems where

there is significant tidal interaction between the two stars which may lead to changes in the orbit and rotation rates of the stars, as well as to changes in the emission of XUV radiation that can affect the atmosphere of a planet within the habitable zone (e.g., Sanz-Forcada et al., 2014; Johnstone et al., 2019).

As the method mainly relies on analytical equations, it can provide a quick assessment of the capability of terrestrial circumbinary planets in complex dynamical environments to retain liquid water on their surface. The construction and comparison of dynamically informed habitable zones, i.e., the PHZ, the EHZ and the AHZ allows us to better understand where potentially habitable worlds with different climate characteristics can exist in binary star systems. The method presented here is very versatile as it has been constructed in such a way that it does not depend on the dynamical model and the insolation limits.

In this work, we investigated the effects of stellar binarity and circumbinary giant planets on the habitable zones of nine systems observed by the Kepler mission. We confirm earlier studies that suggest Kepler-16 is not suitable for hosting a terrestrial planet within its classical habitable zone. The situation is similar for Kepler-1647. In contrast, Kepler-34, Kepler-35, Kepler-38, Kepler-64, and Kepler-413 seemed more promising with Kepler-38 being the best candidate in this respect. Kepler-453 and Kepler-1661 stand between the previous two categories of systems. We find that nearly equal binary mass ratios and small eccentricities of the perturbing bodies provide favorable, from the orbital evolution point of view, conditions for an Earth-like planet to exist in the habitable zone. We show, furthermore, that the presence of a giant planet can have a significant effect on the potential habitability of terrestrial worlds in the same system. We, thus, recommend gravitational perturbations of known giant planets to be taken into account in future studies regarding habitability in binary star systems.

DATA AVAILABILITY STATEMENT

The original contributions presented in the study are included in the article/supplementary material, further inquiries can be directed to the corresponding author/s.

AUTHOR CONTRIBUTIONS

NG and SE: conceptualization, methodology, investigation, resources, and writing–original draft preparation-revised version. NG: software and data curation. NG, SE, and ID-D: validation. All authors have read and agreed to the published version of the manuscript.

ACKNOWLEDGMENTS

SE acknowledges support from the DIRAC Institute in the Department of Astronomy at the University of Washington. The DIRAC Institute is supported through generous gifts from the Charles and Lisa Simonyi Fund for Arts and Sciences, and the Washington Research Foundation. The results reported herein benefited from collaborations and/or information exchange within NASA's Nexus for Exoplanet System Science (NExSS) research coordination network sponsored by NASA's Science Mission Directorate. This research has made use of the NASA Exoplanet Archive, which is operated by the California Institute of Technology, under contract with the National Aeronautics and Space Administration under the Exoplanet Exploration Program.

REFERENCES

Cukier, W., Kopparapu, R. K., Kane, S. R., Welsh, W., Wolf, E., Kostov, V., et al. (2019). Habitable zone boundaries for circumbinary planets. *Publ. Astron. Soc. Pac.* 131:124402. doi: 10.1088/1538-3873/ab50cb

Cuntz, M. (2014). S-type and P-type habitability in stellar binary systems: a comprehensive approach. I. Method and applications. *Astrophys. J.* 780:14. doi: 10.1088/0004-637X/780/1/14

Cuntz, M. (2015). S-type and P-type habitability in stellar binary systems: a comprehensive approach. II. Elliptical orbits. *Astrophys. J.* 798:101. doi: 10.1088/0004-637X/798/2/101

Doyle, L. R., Carter, J. A., Fabrycky, D. C., Slawson, R. W., Howell, S. B., Winn, J. N., et al. (2011). Kepler-16: a transiting circumbinary planet. *Science* 333:1602. doi: 10.1126/science.1210923

Eggl, S. (2018). "Habitability of Planets in Binary Star Systems," in *Handbook of Exoplanets*, eds H. J. Deeg and J. A. Belmonte (Springer International Publishing), 61.

Eggl, S., Georgakarakos, N., and Pilat-Lohinger, E. (2020). Habitable zones in binary star systems: a zoology. *Galaxies* 8:65. doi: 10.3390/galaxies8030065

Eggl, S., Pilat-Lohinger, E., Georgakarakos, N., Gyergyovits, M., and Funk, B. (2012). An analytic method to determine habitable zones for S-type planetary orbits in binary star systems. *Astrophys. J.* 752:74. doi: 10.1088/0004-637X/752/1/74

Forgan, D. (2014). Assessing circumbinary habitable zones using latitudinal energy balance modelling. *Mon. Not. R. Astron. Soc.* 437, 1352–1361. doi: 10.1093/mnras/stt1964

Georgakarakos, N. (2003). Eccentricity evolution in hierarchical triple systems with eccentric outer binaries. *Mon. Not. R. Astron. Soc.* 345, 340–348. doi: 10.1046/j.1365-8711.2003.06942.x

Georgakarakos, N. (2005). Erratum: eccentricity evolution in hierarchical triple systems with eccentric outer binaries. *Mon. Not. R. Astron. Soc.* 362:748. doi: 10.1111/j.1365-2966.2005.09441.x

Georgakarakos, N. (2008). Stability criteria for hierarchical triple systems. *Celest. Mech. Dynam. Astron.* 100, 151–168. doi: 10.1007/s10569-007-9109-2

Georgakarakos, N. (2009). Improved equations for eccentricity generation in hierarchical triple systems. *Mon. Not. R. Astron. Soc.* 392, 1253–1263. doi: 10.1111/j.1365-2966.2008.14143.x

Georgakarakos, N. (2013). The dependence of the stability of hierarchical triple systems on the orbital inclination. *New Astron.* 23, 41–48. doi: 10.1016/j.newast.2013.02.004

Georgakarakos, N., and Eggl, S. (2015). Analytic orbit propagation for transiting circumbinary planets. *Astrophys. J.* 802:94. doi: 10.1088/0004-637X/802/2/94

Georgakarakos, N., Eggl, S., and Dobbs-Dixon, I. (2018). Giant planets: good neighbors for habitable worlds? *Astrophys. J.* 856:155. doi: 10.3847/1538-4357/aaaf72

Gilbert, E. A., Barclay, T., Schlieder, J. E., Quintana, E. V., Hord, B. J., Kostov, V. B., et al. (2020). The First Habitable-zone Earth-sized Planet from TESS. I. Validation of the TOI-700 System. *Astron. J.* 160:116. doi: 10.3847/1538-3881/aba4b2

Gillon, M., Jehin, E., Lederer, S. M., Delrez, L., de Wit, J., Burdanov, A., et al. (2016). Temperate Earth-sized planets transiting a nearby ultracool dwarf star. *Nature* 533, 221–224. doi: 10.1038/nature17448

Haghighipour, N., and Kaltenegger, L. (2013). Calculating the habitable zone of binary star systems. II. P-type binaries. *Astrophys. J.* 777:166. doi: 10.1088/0004-637X/777/2/166

Haqq-Misra, J., Wolf, E. T., Welsh, W. F., Kopparapu, R. K., Kostov, V., and Kane, S. R. (2019). Constraining the magnitude of climate extremes from time-varying instellation on a circumbinary terrestrial planet. *J. Geophys. Res.* 124, 3231–3243. doi: 10.1029/2019JE006222

Holman, M. J., and Wiegert, P. A. (1999). Long-term stability of planets in binary systems. *Astron. J.* 117, 621–628. doi: 10.1086/300695

Jaime, L. G., Aguilar, L., and Pichardo, B. (2014). Habitable zones with stable orbits for planets around binary systems. *Mon. Not. R. Astron. Soc.* 443, 260–274. doi: 10.1093/mnras/stu1052

Johnstone, C. P., Pilat-Lohinger, E., Lüftinger, T., Güdel, M., and Stökl, A. (2019). Stellar activity and planetary atmosphere evolution in tight binary star systems. *Astron. Astrophys.* 626:A22. doi: 10.1051/0004-6361/201832805

Kane, S. R., and Hinkel, N. R. (2013). On the habitable zones of circumbinary planetary systems. *Astrophys. J.* 762:7. doi: 10.1088/0004-637X/762/1/7

Kasting, J. F., Whitmire, D. P., and Reynolds, R. T. (1993). Habitable zones around main sequence stars. *Icarus* 101, 108–128. doi: 10.1006/icar.1993.1010

Kopparapu, R. K., Ramirez, R., Kasting, J. F., Eymet, V., Robinson, T. D., Mahadevan, S., et al. (2013). Erratum: "habitable zones around main-sequence stars: new estimates" (2013, ApJ, 765, 131)</A>. *Astrophys. J.* 770:82. doi: 10.1088/0004-637X/770/1/82

Kopparapu, R. K., Ramirez, R. M., SchottelKotte, J., Kasting, J. F., Domagal-Goldman, S., and Eymet, V. (2014). Habitable zones around main-sequence stars: dependence on planetary mass. *Astrophys. J. Lett.* 787:L29. doi: 10.1088/2041-8205/787/2/L29

Kostov, V. B., McCullough, P. R., Carter, J. A., Deleuil, M., Díaz, R. F., Fabrycky, D. C., et al. (2014). Kepler-413b: a slightly misaligned, neptune-size transiting circumbinary planet. *Astrophys. J.* 784:14. doi: 10.1088/0004-637X/784/1/14

Kostov, V. B., Orosz, J. A., Welsh, W. F., Doyle, L. R., Fabrycky, D. C., Haghighipour, N., et al. (2016). Kepler-1647b: the largest and longest-period kepler transiting circumbinary planet. *Astrophys. J.* 827:86. doi: 10.3847/0004-637X/827/1/86

Liu, H.-G., Zhang, H., and Zhou, J.-L. (2013). Where to find habitable "Earths" in circumbinary systems. *Astrophys. J. Lett.* 767:L38. doi: 10.1088/2041-8205/767/2/L38

Marzari, F., and Thebault, P. (2019). Planets in binaries: formation and dynamical evolution. *Galaxies* 7:84. doi: 10.3390/galaxies7040084

Orosz, J. A., Welsh, W. F., Carter, J. A., Brugamyer, E., Buchhave, L. A., Cochran, W. D., et al. (2012). The neptune-sized circumbinary planet Kepler-38b. *Astrophys. J.* 758:87. doi: 10.1088/0004-637X/758/2/87

Orosz, J. A., Welsh, W. F., Haghighipour, N., Quarles, B., Short, D. R., Mills, S. M., et al. (2019). Discovery of a third transiting planet in the Kepler-47 circumbinary system. *Astron. J.* 157:174. doi: 10.3847/1538-3881/ab0ca0

Petrovich, C. (2015). The stability and fates of hierarchical two-planet systems. *Astrophys. J.* 808:120. doi: 10.1088/0004-637X/808/2/120

Popp, M., and Eggl, S. (2017). Climate variations on Earth-like circumbinary planets. *Nat. Commun.* 8:14957. doi: 10.1038/ncomms14957

Quarles, B., Musielak, Z. E., and Cuntz, M. (2012). Habitability of Earth-mass planets and moons in the Kepler-16 system. *Astrophys. J.* 750:14. doi: 10.1088/0004-637X/750/1/14

Rodriguez, J. E., Vanderburg, A., Zieba, S., Kreidberg, L., Morley, C. V., Eastman, J. D., et al. (2020). The first habitable-zone Earth-sized planet from TESS. II. Spitzer confirms TOI-700 d. *Astron. J.* 160:117. doi: 10.3847/1538-3881/aba4b3

Sanz-Forcada, J., Desidera, S., and Micela, G. (2014). Effects of X-ray and extreme UV radiation on circumbinary planets. *Astron. Astrophys.* 570:A50. doi: 10.1051/0004-6361/201323231

Schwamb, M. E., Orosz, J. A., Carter, J. A., Welsh, W. F., Fischer, D. A., Torres, G., et al. (2013). Planet hunters: a transiting circumbinary planet in a quadruple star system. *Astrophys. J.* 768:127. doi: 10.1088/0004-637X/768/2/127

Shevchenko, I. I., Melnikov, A. V., Popova, E. A., Bobylev, V. V., and Karelin, G. M. (2019). Circumbinary planetary systems in the solar neighborhood: stability and habitability. *Astron. Lett.* 45, 620–626. doi: 10.1134/S1063773719080097

Socia, Q. J., Welsh, W. F., Orosz, J. A., Cochran, W. D., Endl, M., Quarles, B., et al. (2020). Kepler-1661 b: a neptune-sized kepler transiting circumbinary planet around a grazing eclipsing binary. *Astron. J.* 159:94. doi: 10.3847/1538-3881/ab665b

Wang, Z., and Cuntz, M. (2019). S-type and P-type habitability in stellar binary systems: a comprehensive approach. III. Results for Mars, Earth, and Super-Earth Planets. *Astrophys. J.* 873:113. doi: 10.3847/1538-4357/ab0377

Way, M. J., and Georgakarakos, N. (2017). Effects of variable eccentricity on the climate of an Earth-like world. *Astrophys. J. Lett.* 835:L1. doi: 10.3847/2041-8213/835/1/L1

Welsh, W. F., Orosz, J. A., Carter, J. A., Fabrycky, D. C., Ford, E. B., Lissauer, J. J., et al. (2012). Transiting circumbinary planets Kepler-34 b and Kepler-35 b. *Nature* 481, 475–479. doi: 10.1038/nature10768

Welsh, W. F., Orosz, J. A., Short, D. R., Cochran, W. D., Endl, M., Brugamyer, E., et al. (2015). Kepler 453 b - The 10th kepler transiting circumbinary planet. *Astrophys. J.* 809:26. doi: 10.1088/0004-637X/809/1/26

Wolf, E. T., Haqq-Misra, J., Kopparapu, R., Fauchez, T. J., Welsh, W. F., Kane, S. R., et al. (2020). The resilience of habitable climates around circumbinary stars. *J. Geophys. Res.* 125:e06576. doi: 10.1029/2020JE006576

Yadavalli, S. K., Quarles, B., Li, G., and Haghighipour, N. (2020). Effects of flux variation on the surface temperatures of Earth-analog circumbinary planets. *Mon. Not. R. Astron. Soc.* 499, 1506–1521. doi: 10.1093/mnras/staa2980

Conflict of Interest: The authors declare that the research was conducted in the absence of any commercial or financial relationships that could be construed as a potential conflict of interest.

APPENDIX

Planetary Eccentricity Equations

We follow Georgakarakos and Eggl (2015) to calculate the maximum orbital eccentricity e_p^{max} and average squared eccentricity $\langle e_p^2 \rangle$ for a circumbinary planet:

$$e_p^{max} = \frac{m_1 m_2}{(m_1+m_2)^{\frac{4}{3}} M^{\frac{2}{3}}} \frac{1}{X^{\frac{4}{3}}} \left[\frac{3}{2} + \frac{17}{2}e_b^2 + \frac{1}{X}\left(3 + 19e_b + \frac{21}{8}e_b^2 - \frac{3}{2}e_b^3\right)\right] + 2\left|\frac{K_2}{K_1 - K_3}\right| \tag{22}$$

and

$$\langle e_p^2 \rangle = \frac{m_1^2 m_2^2}{(m_1+m_2)^{\frac{8}{3}} M^{\frac{4}{3}}} \frac{1}{X^{\frac{8}{3}}} \left[\frac{9}{8} + \frac{27}{8}e_b^2 + \frac{887}{64}e_b^4 - \frac{975}{64}\frac{1}{X}e_b^4\sqrt{1-e_b^2} + + \frac{1}{X^2}\left(\frac{225}{64} + \frac{6619}{64}e_b^2 - \frac{26309}{512}e_b^4 - \frac{393}{64}e_b^6\right)\right] + 2\left(\frac{K_2}{K_1 - K_3}\right)^2, \tag{23}$$

where

$$M = m_1 + m_2 + m_p \tag{24}$$

$$X = \sqrt{\frac{m_1+m_2}{M}}\left(\frac{a_p}{a_b}\right)^{\frac{3}{2}} \tag{25}$$

$$K_1 = \frac{3}{8}\frac{\sqrt{\mathcal{G}M}m_1 m_2 a_b^2}{(m_1+m_2)^2 a_p^{\frac{7}{2}}}(2 + 3e_b^2) \tag{26}$$

$$K_2 = \frac{15}{64}\frac{\sqrt{\mathcal{G}M}m_1 m_2 (m_1 - m_2) a_b^3}{(m_1+m_2)^3 a_p^{\frac{9}{2}}} e_b (4 + 3e_b^2) \tag{27}$$

$$K_3 = \frac{3}{4}\frac{\sqrt{\mathcal{G}}m_p a_b^{\frac{3}{2}}\sqrt{1-e_b^2}}{(m_1+m_2)^{\frac{1}{2}} a_p^3}, \tag{28}$$

and $\mathcal{G}$ is the gravitational constant.

Equations (22) and (23) were also used when we added the giant planet to our model and the orbit of the giant planet was interior to that of the terrestrial planet. In order to use the above equations in that respect, we replace m_1 with $m_b = m_1 + m_2$, m_2 with m_{gp}, a_b with a_{gp}, e_b with e_{gp} and $M = m_b + m_{gp} + m_p$.

When the orbit of the giant planet was exterior to that of the terrestrial planet, we used the below equations from Eggl et al. (2012) and Georgakarakos (2003, 2005) (with the notation of this work):

$$e_p^{max} = \frac{m_{gp}}{MX^{5/3}}\left[\frac{15}{64}\frac{m_1 - m_p}{(m_1+m_p)^{2/3}M^{1/3}}\frac{(4 + 11e_{gp}^2)}{(1-e_{gp}^2)^{5/2}} + \frac{3}{4} + \frac{11}{4}\frac{1}{X^{1/3}}\frac{(1+e_{gp})^3}{(1-e_{gp}^2)^3}\frac{1}{X^{4/3}}\frac{(1+e_{gp})^4(6+11e_{gp})}{(1-e_{gp}^2)^{9/2}}\right] + 2\frac{C}{B-A}, \tag{29}$$

and

$$\langle e_p^2 \rangle = \frac{m_{gp}^2}{M^2}\frac{1}{X^4(1-e_{gp}^2)^{\frac{9}{2}}}\left\{\frac{43}{8} + \frac{129}{8}e_{gp}^2 + \frac{129}{64}e_{gp}^4 + \frac{1}{(1-e_{gp}^2)^{\frac{3}{2}}}\left(\frac{43}{8} + \frac{645}{16}e_{gp}^2 + \frac{1935}{64}e_{gp}^4 + + \frac{215}{128}e_{gp}^6\right) + \frac{1}{X^2(1-e_{gp}^2)^3}\left[\frac{365}{18} + \frac{44327}{144}e_{gp}^2 + \frac{119435}{192}e_{gp}^4 + \frac{256105}{1152}e_{gp}^6 + \frac{68335}{9216}e_{gp}^8 + + \frac{1}{(1-e_{gp}^2)^{\frac{3}{2}}}\left(\frac{365}{18} + \frac{7683}{16}e_{gp}^2 + \frac{28231}{16}e_{gp}^4 + \frac{295715}{192}e_{gp}^6 + \frac{2415}{8}e_{gp}^8 + \frac{12901}{2048}e_{gp}^{10}\right)\right] + + \frac{1}{X(1-e_{gp}^2)^{\frac{3}{2}}}\left[\frac{61}{3} + \frac{305}{2}e_{gp}^2 + \frac{915}{8}e_{gp}^4 + \frac{305}{48}e_{gp}^6 + \frac{1}{(1-e_{gp}^2)^{\frac{3}{2}}}\left(\frac{61}{3} + \frac{854}{3}e_{gp}^2 + + \frac{2135}{4}e_{gp}^4 + \frac{2135}{12}e_{gp}^6 + \frac{2135}{384}e_{gp}^8\right)\right] + m_*^2 X^{\frac{2}{3}}(1-e_{gp}^2)\left[\frac{225}{256} + \frac{3375}{1024}e_{gp}^2 + \frac{7625}{2048}e_{gp}^4 + + \frac{29225}{8192}e_{gp}^6 + \frac{48425}{16384}e_{gp}^8 + \frac{825}{2048}e_{gp}^{10} + \frac{1}{(1-e_{gp}^2)^{\frac{3}{2}}}\left(\frac{225}{256} + \frac{2925}{1024}e_{gp}^2 + \frac{775}{256}e_{gp}^4 + + \frac{2225}{8192}e_{gp}^6 + \frac{25}{512}e_{gp}^8\right)\right] + m_*^2\frac{1}{X^{\frac{4}{3}}(1-e_{gp}^2)^2}\left[\frac{8361}{4096} + \frac{125415}{8192}e_{gp}^2 + \frac{376245}{32768}e_{gp}^4 + + \frac{41805}{65536}e_{gp}^6 + \frac{1}{(1-e_{gp}^2)^{\frac{3}{2}}}\left(\frac{8361}{4096} + \frac{58527}{2048}e_{gp}^2 + \frac{877905}{16384}e_{gp}^4 + \frac{292635}{16384}e_{gp}^6 + \frac{292635}{524288}e_{gp}^8\right)\right]\right\} + 2\left(\frac{C}{B-A}\right)^2, \tag{30}$$

where

$$M = m_b + m_p + m_{gp} \tag{31}$$

$$m_* = \frac{m_p - m_b}{(m_b+m_p)^{2/3}M^{1/3}} \tag{32}$$

$$X = \sqrt{\frac{m_b+m_p}{M}}\left(\frac{a_{gp}}{a_p}\right)^{\frac{3}{2}} \tag{33}$$

$$C = \frac{5}{4}\frac{(m_b - m_p)e_{gp}a_p}{(m_b+m_p)(1-e_{gp}^2)^{5/2}a_{gp}} \tag{34}$$

$$B = \frac{1}{(1-e_{gp}^2)^{3/2}} \tag{35}$$

$$A = \frac{m_b m_p M^{1/2}}{m_{gp}(m_b+m_p)^{3/2}}\frac{1}{(1-e_{gp})^2}\left(\frac{a_p}{a_{gp}}\right)^{1/2}. \tag{36}$$

The above equations can be used for nearly coplanar systems and systems that are not close to mean motion resonances. Also, the equations become less reliable as the maximum planetary eccentricity gets larger than 0.2–0.25.

frontiers in Astronomy and Space Sciences

REVIEW
published: 20 April 2021
doi: 10.3389/fspas.2021.625552

Binary Gravitational Perturbations and Their Influence on the Habitability of Circumstellar Planets

Elke Pilat-Lohinger and Ákos Bazsó*

Department of Astrophysics, University of Vienna, Vienna, Austria

In order to assess the habitability of planets in binary star systems, not only astrophysical considerations regarding stellar and atmospheric conditions are needed, but orbital dynamics and the architecture of the system also play an important role. Due to the strong gravitational perturbations caused by the presence of the second star, the study of planetary orbits in double star systems requires special attention. In this context, we show the important role of the main gravitational perturbations (resonances) and review our recently developed methods which allow a quick determination of locations of secular resonances (SRs) in binary stars for circumstellar planetary motion where a giant planet has to move exterior to the habitable zone (HZ). These methods provide the basis for our online-tool ShaDoS which allows a quick check of circumstellar HZs regarding secular perturbations. It is important to know the locations of SRs since they can push a dynamically quiet HZ into a high-eccentricity state which will change the conditions for habitability significantly. Applications of SHaDoS to the wide binary star HD106515 AB and the tight system HD41004 AB reveal a quiet HZ for both systems. However, the study of these systems indicates only for the tight binary star a possible change of the HZ's dynamical state if the orbital parameters change due to new observational data.

Keywords: circumstellar motion, perturbations, resonances, semi-analytical method, online-tool, habitability, combined analytical method

OPEN ACCESS

Edited by:
Francesco Marzari,
University of Padua, Italy

Reviewed by:
Philippe Thebault,
Université de Sciences Lettres de Paris, France
Luca Malavolta,
University of Padua, Italy

****Correspondence:***
Elke Pilat-Lohinger
elke.pilat-lohinger@univie.ac.at

Specialty section:
This article was submitted to Exoplanets, a section of the journal Frontiers in Astronomy and Space Sciences

Received: *03 November 2020*
Accepted: *15 March 2021*
Published: *20 April 2021*

Citation:
Pilat-Lohinger E and Bazsó Á (2021) Binary Gravitational Perturbations and Their Influence on the Habitability of Circumstellar Planets. Front. Astron. Space Sci. 8:625552. doi: 10.3389/fspas.2021.625552

1. INTRODUCTION

Since the discovery of 51 Peg b (Mayor and Queloz, 1995) thousands of exoplanets have been detected so far [see the *Extrasolar Planet Encyclopedia*[1] Schneider et al. (2011) or the *NASA Exoplanet archive*[2]]. However, of the nearly 3,500 planetary systems none harbors a habitable world similar to planet Earth. This fact raises the question if Earth-like habitability requires a certain planetary system architecture where e.g., giant planets are orbiting the host-star exterior to the habitable zone (HZ). It can be expected that such a configuration has a less violent terrestrial planet formation process than a planetary system where the giant planet is closer to the host-star than the HZ. The giant planet formed probably at a larger distance to the star and migrated inwards by crossing the HZ which could cause problems for the terrestrial planet formation in the HZ.

Thus, in this study we considered only systems where the giant planet is exterior to the HZ and investigate the occurrence of strong perturbations in the HZ. Studies of planetary motion in binary stars are of special interest as a high fraction of stars in the solar neighborhood are members of binary and multiple star systems. Observational surveys by

[1]http://exoplanet.eu
[2]http://exoplanetarchive.ipac.caltech.edu

Duquennoy et al. (1991) and Raghavan et al. (2010) established that in the solar neighborhood (up to 25 parsec) about 40–45 % of all Sun-like stars (spectral types F6-K3) are members of binary and multiple star systems. Tokovinin (2014) derived a fraction of 33 % of binary stars from a sample of about 4800 F-/G-type main-sequence stars within 67 parsec of the Sun. For more details see Duchêne and Kraus (2013).

The *Catalog of Exoplanets in Binary Star Systems*[3] lists about 100 planetary systems which indicates that exoplanets are not restricted to single-stars. But it is doubtful whether these environments are more hostile for the existence of planets or not (see e.g., Boss, 2006; Bromley and Kenyon, 2015; Jang-Condell, 2015). In a study based on *Kepler* data (Armstrong et al., 2014) the occurrence rate of co-planar circumbinary planets has been found to be similar to that for single stars. Circumbinary motion is also known as P-type motion (Dvorak, 1984, 1986) where a planet orbits both stars. However, the Catalog of Exoplanets in Binary Star Systems indicate that most of the exoplanets in binary star systems orbit only one star which is known as circumstellar or S-type motion (Dvorak, 1984, 1986).

Theoretical stability studies of S- and P-type motion have been carried out decades before the detection of exoplanets (see e.g., Harrington, 1977). Studies by Rabl and Dvorak (1988) and Dvorak et al. (1989) published the stability boundaries of S- and P-type motion in equal-mass binary stars as a function of the binary's eccentricity. This study has been repeated and extended to a wider range of binary star configurations by Holman and Wiegert (1999). In their study they provide expressions for the stability boundaries which depend on the mass-ratio and the binary's eccentricity for both, circumstellar and circumbinary configurations. In connection to this study, Pilat-Lohinger and Dvorak (2002) analyzed the stability of S-type motion using the Fast Lyapunov indicator (FLI)[4]. In addition, Pilat-Lohinger et al. (2003) investigated the stability of inclined P-type planetary orbits.

The detections of exoplanets in tight binary stars like γ Cephei b (Hatzes et al., 2003), Gliese 86 b (Santos et al., 2000), and HD 41004 Ab (Zucker et al., 2004) have led to a growing interest in understanding planetary formation in such stellar systems. There are binary specific problems for planet formation due to the gravitational interaction of the secondary star resulting in e.g., a truncated protoplanetary disk (see e.g., Artymowicz and Lubow, 1994; Savonije et al., 1994) which influences the formation and evolution of planets throughout several stages of the planet-forming process. For more details about the problems of planet formation in binary stars we refer the reader to Marzari and Thebault (2019) and references therein.

In case of circumstellar motion mainly the outer edge of the disk is influenced (Kley and Nelson, 2010; Müller and Kley, 2012) while for circumbinary disks mainly the inner edge is affected (Rafikov, 2013).

During the planet-formation stage where planetesimals (km-sized bodies) collide and merge to Moon-sized embryos dynamical perturbations play an important role, as planetesimal accretion requires low encounter velocities. Thébault et al. (2006) showed that planetesimal accretion cannot occur at distances beyond 1 au from the host-star in tight binaries with separation of 20 au. This result raises questions about the formation of detected planets in tight binary stars (Thébault et al., 2004, 2008, 2009; Thebault, 2011). Moreover, Fragner et al. (2011) have found an increase of impact velocities when studying the dynamical behavior of planetesimals taking into the self gravity of the gas disk. Some years later, Gyergyovits et al. (2014) studied the full interaction of more than 2,000 embryos with a gas disk in a γ Cephei-like configuration. They concluded that the growth from embryos to planets within a dynamically evolving gas disk is strongly altered by the dynamical evolution of the disk, which leads to a decreased probability for planet formation at least in the inner parts of the gas disk.

Apart from these problems of planetary embryo formation, the late planet-formation stage where embryo-sized bodies grow to planets can be easily simulated by N-body calculations (Haghighipour and Raymond, 2007; Quintana et al., 2007; Pilat-Lohinger et al., 2018). A detailed discussion on planet formation in binary star systems can be found in Thebault and Haghighipour (2015).

A weak point in all these numerical studies is certainly the treatment of collisions where usually the so-called *perfect merging* of two bodies is assumed without taking into account any fragmentation or mass-loss of the bodies due to the collision. However, Bancelin et al. (2017) studied the collision parameters (impact angle and velocity) in tight binary stars and showed that the perfect merging approach can significantly overestimate the water content and mass of the formed planets. Thus, this simplified approach has to be replaced by a more realistic one that includes results of detailed collision simulations.

The habitability of planets in binary stars is certainly an interesting issue, especially due to the fact that most of the stars in the solar neighborhood build such stellar systems. Considering the different spectral types, especially F to M type stars are of interest for habitability studies, since the life-times of these stars on the main sequence are sufficiently long (see Kasting et al., 1993) to permit the evolution of life on a terrestrial-like planet in the HZ. For a summary of astrophysical conditions for planetary habitability we refer the reader to Güdel et al. (2014).

In a binary star system, an important requirement for habitability is certainly the dynamical stability of the HZ. Moreover, the influence of the secondary star will increase the planet's eccentricity which also affect the insolation on a planet in the HZ where the perturbations depend on the distance and the eccentricity of the secondary star. Eggl et al. (2012) has found a correlation of both, eccentricity and insolation and introduced various classes of HZs in binary star systems: (i) permanent, (ii) extended, and (iii) averaged HZ. An application of this HZ classification to binary star systems in the solar neighborhood is shown in Eggl et al. (2013).

In recent years, different approaches for the determination of HZs in binary stars have been published e.g., (Haghighipour and

[3]http://www.univie.ac.at/adg/schwarz/multiple.html

[4]The FLI is a well-known chaos indicator introduced by Froeschlé et al. (1997) that determines the orbital behavior via the growth of the largest tangent vector of a trajectory. A linear growth of this vector denotes regular planetary motion while an exponential growth indicates chaos for the orbit.

Kaltenegger, 2013; Kaltenegger and Haghighipour, 2013; Cuntz, 2014). For a detailed review on this topic we refer the reader to Eggl et al. (2020).

In this study, we focus on the gravitational influence of the secondary star on planetary motion in the HZ. We consider binary star systems with a gas giant in an orbit exterior to the HZ and a terrestrial planet in the HZ. The interplay of these bodies causes perturbations like mean motion resonances (MMRs) and secular resonances (SRs) whose locations strongly depend on the architecture of the system. Such resonances can also influence the habitability of planets in the HZ. Thus, it is important to determine the locations of resonances, which is easy for MMRs but not for SRs. However, for the SRs new methods have been developed that allow a quick determination of the SR location (Pilat-Lohinger et al., 2016; Bazsó et al., 2017; Bazsó and Pilat-Lohinger, 2020).

In this paper, we will briefly discuss these methods and show some applications to real binary systems that host a giant planet. The structure of this paper is the following: First we define the dynamical model and describe the gravitational perturbation. Then we introduce the semi analytical method (SAM) to determine the location of an SR. Subsequently, we describe the basics of the recently published combined analytical method (CAM) and its application for the online tool named *SHaDoS*. Finally, we apply SHaDoS to some real binary-star–planet systems and discuss the results.

2. BASIC INFORMATION

2.1. Dynamical Model

In our study, we focus on circumstellar planetary motion where (i) a terrestrial planet is located in the primary stars' HZ, (ii) a gas giant is moving in an orbit exterior to the HZ, and (iii) the secondary star is a far away perturber. First of all, the planets have to move on stable circumstellar orbits around the primary star. The stability of the planetary motion depends strongly on the distance of the two stars, their eccentricity and their masses. To ensure that the outer planet i.e., the giant planet moves inside the stable region of the primary star, it is advisable to apply the investigations by Pilat-Lohinger and Dvorak (2002) and Holman and Wiegert (1999). However, the situation for two planets is more complex due to arising resonances among the planets which may overlap with those of the secondary star. Therefore, Marzari and Gallina (2016) investigated such systems using a Frequency Map Analysis method to study the influence of the secondary star on the two planets orbiting the primary star. In their study, they obtained a semi-empirical equation that defines the minimum semi-major axis of the secondary star for which the two-planet system is stable.

Nevertheless, the presence of a distant secondary star will perturb the giant planet, which might pass the perturbations to the terrestrial planet in the HZ. In our study, we are primarily interested in the orbital behavior of the terrestrial planet in the HZ and how perturbations of the giant planet and the secondary star may affect its motion. In case these perturbations cause high eccentricity motion in the HZ then the planet's habitability would be affected, especially when it leaves the HZ periodically.

2.2. Gravitational Perturbations

It is well-known that in N-body systems consisting of more than two massive bodies variations of the orbital parameters occur due to gravitational interactions between these bodies. Thus, in binary star systems that host a planet such variations occur. These mutual gravitational interaction between celestial bodies can lead to resonances which appear when the ratio of two frequencies f_1 and f_2 can be expressed as a rational number: $|f_1/f_2| = p/q, \quad p, q \in \mathbb{N}$. Depending on the frequencies that are involved, a typical time-scale can be associated to any resonance. As resonances may lead to significant changes in the orbital motion with large variations in eccentricity, the planet's habitability could be affected. Usually, the HZ is a quite narrow region thus, the planet might leave the HZ periodically due to its eccentricity motion. Therefore, it is important to determine the locations of resonances, where mean motion and secular resonances are considered in our study.

Mean Motion Resonances (MMRs) occur when $n'/n \sim j_1/j_2$ where n and n' are the mean motions[5] of e.g., the two planets and j_1, j_2 are integers. The location of an MMR can be easily derived from the third Kepler law:

$$a_{\mathrm{res}} = a' \left(\frac{n'}{n}\right)^{2/3} \left(\frac{M+m}{M+m'}\right)^{1/3} \tag{1}$$

where a_{res} is the resonant semi-major axis and M, m and m' are the masses of the host-star and the two planets, respectively. MMRs can be the source of both stability and chaos, which depends sensitively upon the orbital parameters.

Secular Resonances (SRs) arise when one of the precession frequencies of a test-planet (either of the argument of perihelion ω or of the node Ω) is equal (or a linear combination) of the proper modes of the giant planet. The strongest secular perturbations occur at locations when

$$q g_{TP} - p g_{GP} \sim 0 \tag{2}$$

where q, p are integers, g_{TP} and g_{GP} are the proper frequencies of the test-planet and the giant planet, respectively. For $p = q = 1$, the proper frequencies of the test-planet and the giant planet are equal which causes the strongest effects. The location of an SR with the giant planet can thus be determined by applying Equation (2) to test-planets of a certain area. Therefore, the proper frequencies of the orbits of all test-planets and the giant planet have to be determined which usually requires long-term computations of the dynamical system where the integration time depends on the distance of the two stars. For a tight binary star like γ Cephei or HD41004 AB with a stellar separation of 20 au, calculations over some 10^6 years are needed. However, the computation time increases with the stellar distance a_B (as discussed in Bazsó et al., 2017). Thus, for wide binaries such a study can be quite time-consuming. In addition, the time series of the orbital computations must be analyzed using e.g., a Fast Fourier Transformation to determine the main frequency in the Fourier spectrum of an orbit which represents

[5] mean motion=*Orbital Period*/2π.

the proper frequency. Fourier spectra of strongly perturbed orbits are littered with frequencies which makes it is impossible to determine their proper frequencies and is also an indication for a perturbation due to a resonance.

To overcome the time-consuming procedure of identifying the proper frequency via Fourier analysis of each orbit, a new semi-analytical approach has been introduced by Pilat-Lohinger et al. (2016) and Bazsó et al. (2017).

3. QUICK METHODS TO DETERMINE LOCATIONS OF AN SR

For the development of our semi-analytical method, the tight binary star HD41004 AB has been used. In this binary star system a giant planet (of $2.5 M_{Jup}$) has been discovered (Zucker et al., 2004) orbiting the primary star HD41004 A (a K2V star of 0.7 M_{Sun}) at about 1.64 au. The secondary star (a M dwarf of 0.42 M_{Sun}) is at a distance of about 23 au. The eccentricities of the binary and of the giant planet are not well-known. Thus, we used an eccentricity of 0.2 for both. This binary-star–planet configuration shows strong perturbations around 0.4 au that indicate an SR which has been studied in detail by Pilat-Lohinger et al. (2016).

3.1. Semi-Analytical Approach

In the study by Pilat-Lohinger et al. (2016) the numerical effort for the determination of the proper frequencies could be reduced by applying the Laplace-Lagrange secular perturbation theory (see e.g., Murray and Dermott, 1999) to obtain an analytical solution for test-planets (with negligible mass) in the area between 0.2 and 0.6 au in the HD41004 AB system. The secular frequency of test-planets (g_{TP}) was deduced using the following secular linear approximation (see e.g., Murray and Dermott, 1999):

$$g_{TP} = \frac{n}{4} \sum_{i=1}^{2} \frac{m_i}{m_0} \alpha_i^2 b_{3/2}^{(1)}(\alpha_i) \tag{3}$$

where $\alpha_i = a/a_i$ for $i = 1, 2$ and a_1, a_2, a are the semi-major axes of the giant planet, the secondary and the test-planet, respectively. m_1 and m_2 are the masses of the giant planet and the secondary and m_0 is the mass of the primary star. $b_{3/2}^{(1)}$ is a Laplace coefficient. Considering a planar system, the secular frequency s which is related to the node Ω, has not been taken into account. Moreover, this theory is restricted to low inclination and low eccentricity motion.

Pilat-Lohinger et al. (2016) showed that the analytical values of proper frequencies for the test-planets were in good agreement with the numerical solution and save computation time for the determination of the location of SR.

Thus, to satisfy Equation (2) only the numerical integration of the giant planet's orbit in the binary star has to be carried out for a computation time which covers the secular period of the binary star. From this numerical simulation, the proper frequency of the giant planet has to be determined via Fourier analysis. Therefore, this semi-analytical method (SAM) represents a quick approach to define the position of SRs for circumstellar planetary motion in binary stars.

3.2. The Location of the SR

The location of the SR is defined by the semi-major axis of the test-planet which proper frequency equals the one of the giant planet. **Figure 1** illustrates the application of SAM to different binary-star–planet configurations to figure out the influence of the secondary star on the location of the SR. For these plots the HD41004 AB configuration has been used, where the distance between the two stars was varied between 20, 30, and 40 au (in the left panel) and the mass of the secondary star was changed from an M-star (of 0.42 solar mass) to either a K-(of 0.7 solar mass) or G-type star (of 1 solar mass). The eccentricities of the binary and of the giant planet were set to 0.2.

The left panel of **Figure 1** shows the influence of the distance of the two stars on the location of the SR. The diagonal curve represents the analytically derived proper periods of test-planets orbiting the host-star in the region between 0.1 and 1.5 au. Whereas, this curve does not vary significantly for the different stellar separations, strong changes are visible for the proper period of the giant plant which is represented by the horizontal line in the corresponding color of the stellar distance. The intersection of an horizontal line with the same colored curve defines the location of the SR in the system. Different intersection points show clearly that the SR is shifted to smaller semi-major axes—thus toward the host-star—with increasing the distance of the two stars.

In the same way, the right panel of **Figure 1** indicates the influence of the mass of the secondary on the location of the SR. For low-mass M-type stars (0.4 M_{Sun}, red line/curve) it can be seen that the SR is closer to the host-star than for a more massive secondary, like a K-type (0.7 M_{Sun}, green line/curve) or a G-type star (1 M_{Sun}, blue line/curve).

Furthermore, the study by Pilat-Lohinger et al. (2016) showed that a change in the binary's eccentricity has stronger effects on the location of the SR than a change in the giant planet's eccentricity. Note that eccentricity motion widens the area which is affected by the SR. To determine the width of the SR, Pilat-Lohinger et al. (2016) calculated the SR location by using the peri- and apo-center positions instead of a_{GP} and found good results for the binary star HD41004 AB.

An application of SAM to binary star systems with stellar separations up to 100 au and a discovered exoplanet in a circumstellar orbit has been published by Bazsó et al. (2017). The aim of this study was to check the HZ of the host-stars regarding secular perturbations that could alter the conditions for habitability. In this context, SAM has been used also for systems where the giant planet orbits the host-star interior to the HZ (= interior case) and not only for systems where the giant planet is exterior to the HZ (= exterior case) like in the test-system HD41004 AB. In a first approach SAM did not work for the numerous interior cases because no crossing of the giant planet's proper frequency with one of the test-planet's proper frequency was found. Only by adding the effect of general relativity for the interior cases, the method worked well for these systems Bazsó et al. (see 2017).

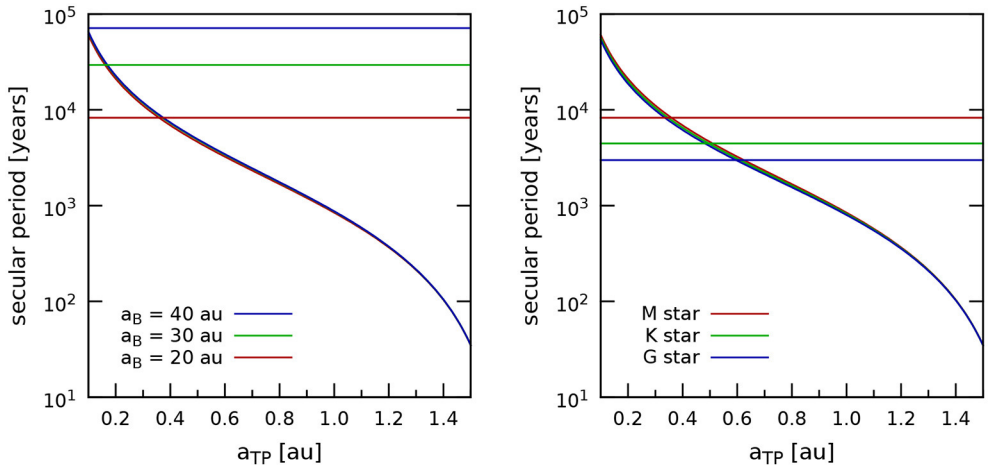

FIGURE 1 | Shows on the y-axis the proper periods either for test-planets orbiting the host-star between 0.1 and 1.5 au (x-axis) or for the giant planet (horizontal lines). These plots are the result from a study of the HD41004 AB system, where the giant planet orbits the primary star at 1.64 au and the eccentricities of the binary and the giant planet were set to 0.2 in a planar configuration. Curves represent the proper periods of the test-planets in the considered area (x-axis), where the different colors belong to the binary separations of 20 au (red), 30 au (green), and 40 au (blue) in the left panel or various stellar types of the secondary star: M-type (red, 0.4 solar mass), K-type (green, 0.7 solar mass), and G-type (blue 1 solar mass) in the right panel. In both panels, the proper periods of the giant planet are given by the horizontal lines. Intersections of a curve with a horizontal line of the same color define the location of an SRs for a certain configuration. The left panel indicates the dependency of the SR location on the distance of the two stars where the SR location moves toward the host-star when the distance between the two stars increases. The right panel shows the changes due to the secondary star's mass where the SR location moves toward the host-star if the mass of the secondary decreases. These panels are reproduced from Pilat-Lohinger et al. (2019).

Even if the application of SAM saves a lot of computation time when studying numerous binary-star–planet configurations regarding dynamical conditions for habitability. However, the method cannot be used for an internet-tool.

Therefore, further improvements are needed to speed up the procedure which is only feasible with an analytical approach for the giant planet's proper frequency.

3.3. Analytical Model for Giant Planet's Proper Frequency

Assuming that the dynamical evolution of the giant planet's orbit is dominated by the secular interaction with the perturber (the secondary star), a simple approach to obtain analytical values for the giant planet's proper frequency has been provided by Heppenheimer (1978):

$$g_H = \frac{3}{4} n_{GP} \left(\frac{m_B}{m_A}\right) \left(\frac{a_{GP}}{a_B}\right)^3 (1 - e_B^2)^{-3/2}, \tag{4}$$

where g_H is a first order approximation (in masses) for the proper frequency of the giant planet, n_{GP} is its mean motion, m_A and m_B are the masses of the primary and the secondary star, a_{GP} and a_B are the semi-major axes of the giant planet and the secondary star and e_B is the eccentricity of the binary.

The Heppenheimer model has been developed for the restricted three body problem, where the planet's mass is negligible compared to the stellar masses. A suitable improvement[6] of the Heppenheimer model is provided in the study by Andrade-Ines and Eggl (2017) who established a simple and more accurate secular model where the giant planet acts like a mass-less body relative to the two stars. This model can be used also for tight binary stars with stellar separations of only two to three times the distance of the giant planet to the host-star.

The new approach by Andrade-Ines and Eggl (2017) is defined as:

$$g_{GP} = g_H(1 - \delta_g) \tag{5}$$

where δ_g is an empirical correction term. The model expresses the secular precession frequency g_{GP} as a polynomial function of (i) the mass-ratio of the binary star, (ii) the semi-major axis ratio a_{GP}/a_B, and (iii) the perturber's eccentricity e_B. The expression of δ_g has usually less than 20 terms. For the exact values we refer to Equation (24) in Andrade-Ines and Eggl (2017).

Equation (5) is applicable to a wide range of binary stars. Regarding the semi-major axes ratio, it covers the range of currently observed exoplanets in binary systems. Only the range of binary's eccentricities does not cover all systems where an exoplanet has been discovered.

Applying Equation (5) for the solution of g_{GP} in Equation (2) we obtain a fully analytical approach which is called *Combined Analytical Method (CAM)* in Bazsó and Pilat-Lohinger (2020). The CAM is a promising method that allows a very quick determination of the location of secular perturbations for circumstellar planetary motion in binary star systems.

Our main interest is to define the dynamical state of circumstellar HZs and to classify *perturbed (pHZ)* and *quiet HZs*

[6]Such a correction to the secular precession frequency can be found in previous attempts, e.g., Giuppone et al. (2011).

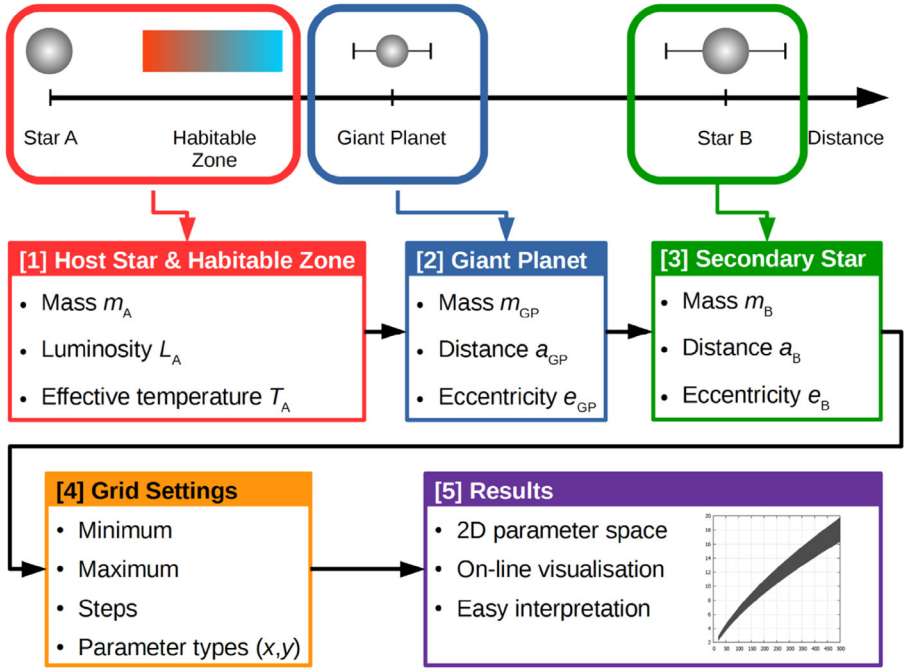

FIGURE 2 | Flow chart of the online tool *SHaDoS*.

(qHz). In this regard, CAM might help to exclude binary-star–planet systems (with pHZs) from the observational search of habitable planets. Moreover, CAM is fast enough to be applied for an internet-tool.

4. ONLINE-TOOL: SHADOS

SHaDoS is an acronym for **S**ecular perturbations in **Ha**bitable zones of **Do**uble **S**tars and is accessible at https://www.univie.ac.at/adg/shados/index.html. It implements the CAM model and solves Equation (2) for any given set of orbital parameters. **Figure 2** presents the flow chart of this online-tool which shows an object-oriented approach where a four-step input process yields the desired results in 2D diagrams. In each step the tool needs input from the user about the parameters of (i) the host-star, (ii) the giant planet, (iii) the secondary star, and (iv) the parameter space of the resulting plot.

Step 1: The required input parameters of the host star are the *luminosity, effective temperature*, and *mass*. According to these parameters, the tool will determine the borders of the host-star's HZ[7] using the approach by Kopparapu et al. (2014) where the effective temperatures are limited to the range $2600 \leq T_{\text{eff}} \leq 7200$ K. For some stellar types, namely F, G, K, and M-type main-sequence stars the standard input data is provided by the tool which can be modified via the *user defined* input. Based on this input the HZ will be calculated.

Step 2: The required parameters of the giant planet are the *mass* (in Jupiter-masses), *distance to the host star* (semi-major axis in au) which must be exterior to the HZ, and *orbital eccentricity* which is restricted to elliptic orbits.

Step 3: The required parameters of the secondary star are the *mass* (in solar mass), *distance to the host-star* (in au), and the *eccentricity* which is restricted to values $0 \leq e_B \leq 0.6$ due to limitations in the analytical model.

Step 4: Following parameters for the 2D-plots can be chosen by the user: there are five options for the x-axis, which are *planet mass, secondary star mass, planet distance, secondary star distance*, and *secondary star eccentricity* for which the user has to specify the minimum and maximum values and the steps in-between (for the grid). And for the y-axis there are three options which are *planet distance, secondary star distance*, and *secondary star eccentricity*.

With the input of all parameters the online-tool performs the calculations and provides a 2D plot depending on the selection in Step 4 which can be saved if desired. This plot usually shows a gray-shaded area which defines the parameters that might perturb the host-star's HZ.

Due to the constraints of the methods used in SHaDoS and the requirement that the giant planet has to be exterior to the HZ, the application to real systems is still very limited. In addition, for most binary star systems the eccentricity is not known which also has strong influence on dynamical studies. Even if nowadays the number of suitable circumstellar systems is rare, we expect an increase of such systems in the near future, especially when the PLATO 2.0 mission starts the observations.

[7]Note that the single star HZ corresponds to the averaged HZ in binary stars.

5. APPLICATION OF SHADOS

To demonstrate the functionality of *SHaDoS*, we have selected two binary system from the *Binary Catalog of Exoplanets* which fulfill the requirements for an application of the online-tool. These are the wide binary star HD106515 AB and the tight binary HD41004 AB. The latter has also been used for the development of SAM. For the first system, we show all possible combinations provided in Step 4 while for the other for HD41004 AB we present only the most interesting plots.

5.1. The Wide Binary Star HD106515 AB

HD106515 AB consists of two G-type stars, with masses of 0.91 and 0.88 solar-masses for the primary and the secondary star, respectively. The distance of the two stars is 345 au and the binary's eccentricity is 0.42. Desidera et al. (2012) detected a quite massive planet (9.61 Jupiter-masses) orbiting the primary star at a distance of 4.59 au in an eccentric orbit ($e = 0.572$). Since the HZ of a G-type star is between 0.95 and 1.7 au, the giant planet is exterior to the HZ as required for the application of *SHaDoS*.

The first 2D-plot of *SHaDoS* (**Figure 3**) shows the secondary's semi-major axis vs. the giant planet's semi-major axis, where the gray-shaded area indicates all combinations of semi-major axes in the chosen range of the x- and y-axes which would cause a secular perturbation in the HZ of the primary star. Considering the observational data of the HD106515 AbB system, **Figure 3** shows clearly, that one of the two celestial bodies must be moved quite a lot, either closer to the primary (i.e., the secondary to 50 au) or farther away (i.e., the planet to $18 - 22$ au) to find an SR in the primary's HZ. Since the orbital parameters of exoplanets show large uncertainties and some of them might change when new observational data is available, the plots from the application of SHaDoS indicate also to what extend such changes of the orbital parameters might influence the dynamical state of the HZ (e.g., if a qHZ turns into a pHZ or vice versa). For the HD106515 AbB system such changes must be significantly large which seems unlikely to happen thus HD106515 A has a quiet HZ.

More possible parameter combinations—according to the input in Step 4—are shown in **Figures 4–6**. Each panel of these figures shows a gray-shaded area from which we get the information whether the host-star's HZ is perturbed or not. For the observed configuration of HD106515 AbB the resulting 2D-plots of *SHaDoS* clearly indicate a qHZ of HD106515 A. Secular perturbations in the HZ would occur only if at least one of the parameters shown in the various panels is changed to values in gray area.

5.2. The Tight Binary Star HD41004 AB

HD41004 AB consists of a K- and an M-type main-sequence star as primary and secondary, respectively. The masses are 0.7 solar mass for the K star and 0.4 solar mass for the M star. Actually, both stars have a sub-stellar companion, but in our study, the close-in brown dwarf orbiting the M-type star has been ignored.

In the vicinity of the primary (between 1.3 and 1.64 au) a gas giant (of about 2.5 Jupiter-mass) has been detected (Zucker et al., 2004). It orbits the K star exterior to the HZ. Thus, the system allows an application of *SHaDoS*. Different values for the eccentricities of the binary and the giant planet have

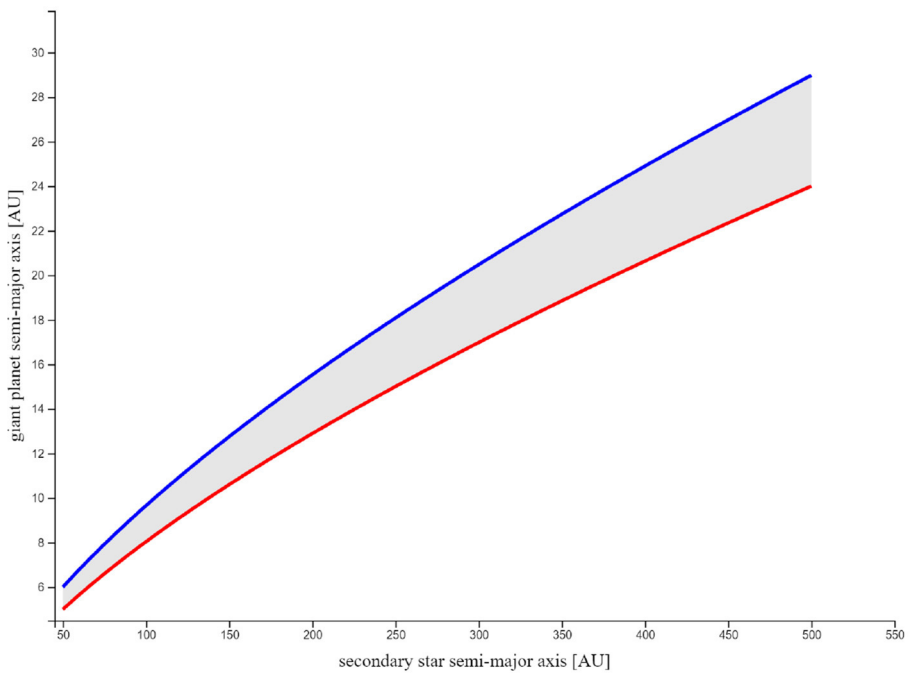

FIGURE 3 | Result of the online-tool *SHaDoS* for the binary system HD106515 AB. The gray stripe shows which combinations may lead to an SR in the primary star's HZ for the defined semi-major axis range of the secondary star (x-axis) and the giant planet (y-axis).

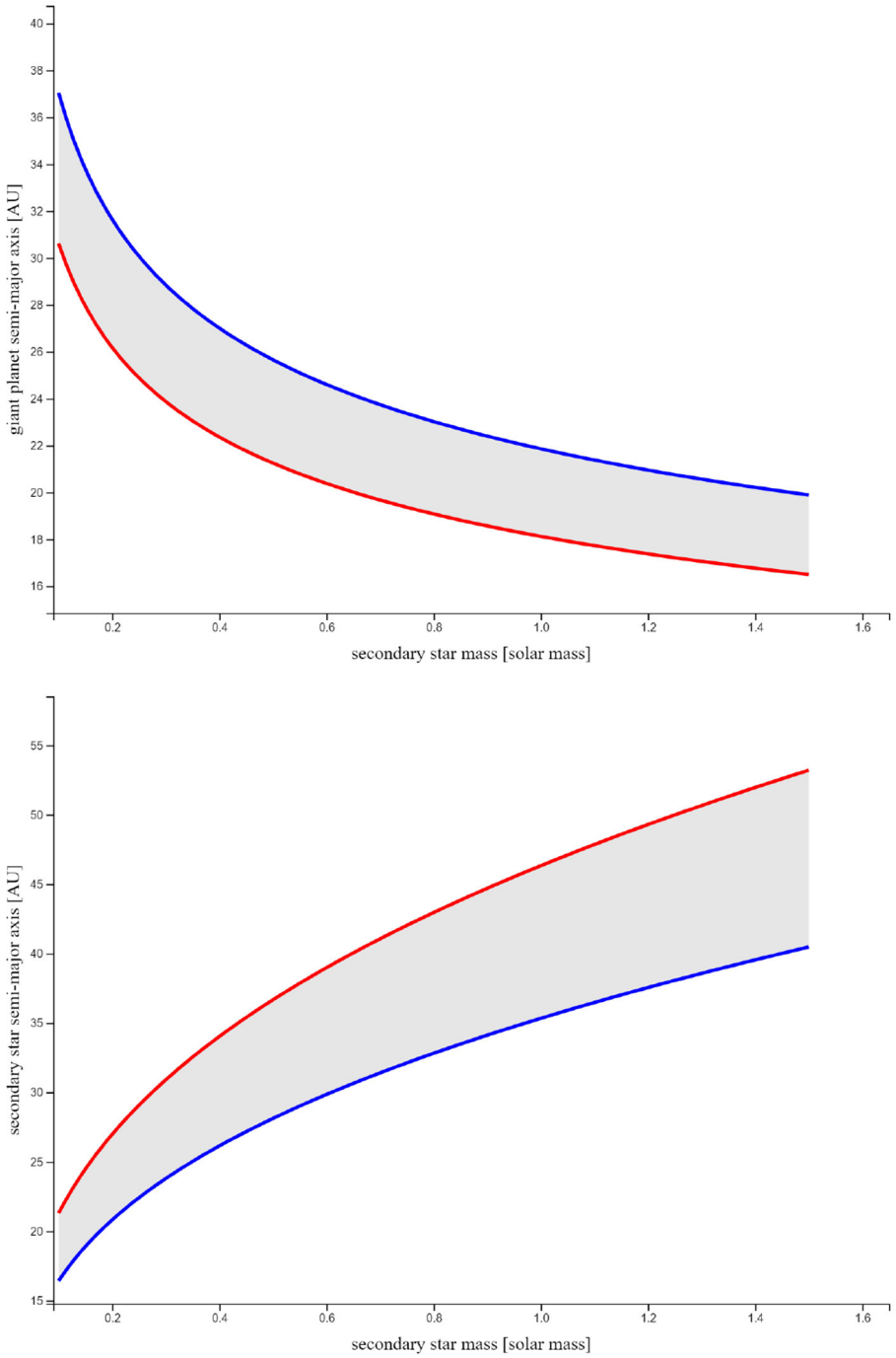

FIGURE 4 | Same as **Figure 3** but for the variation of the stellar mass (x-axis) vs. the variation of the semi-major axis either of the giant planet **(Upper)** or of the secondary star **(Lower)** in the y-axes.

been published but these are quite uncertain. Thus, in the application of *SHaDoS*, the eccentricities were set to 0.2 for both bodies.

Figure 7 shows three 2D-plots of the online-tool *SHaDoS*, where the top panel displays the semi-major axis of the secondary star on the x-axis and that of the giant planet on the y-axis. This plot indicates that for the published values of the semi-major axes ($a_{GP} = 1.64$ au and $a_B = 23$ au) there are secular perturbations in the vicinity of the HZ of HD41004 A but the HZ itself is not perturbed. The middle panel displays the secondary star's semi-major axis vs. binary eccentricity which indicates that in case of high eccentricity motion of the binary ($0.4 < e_B < 0.9$) there

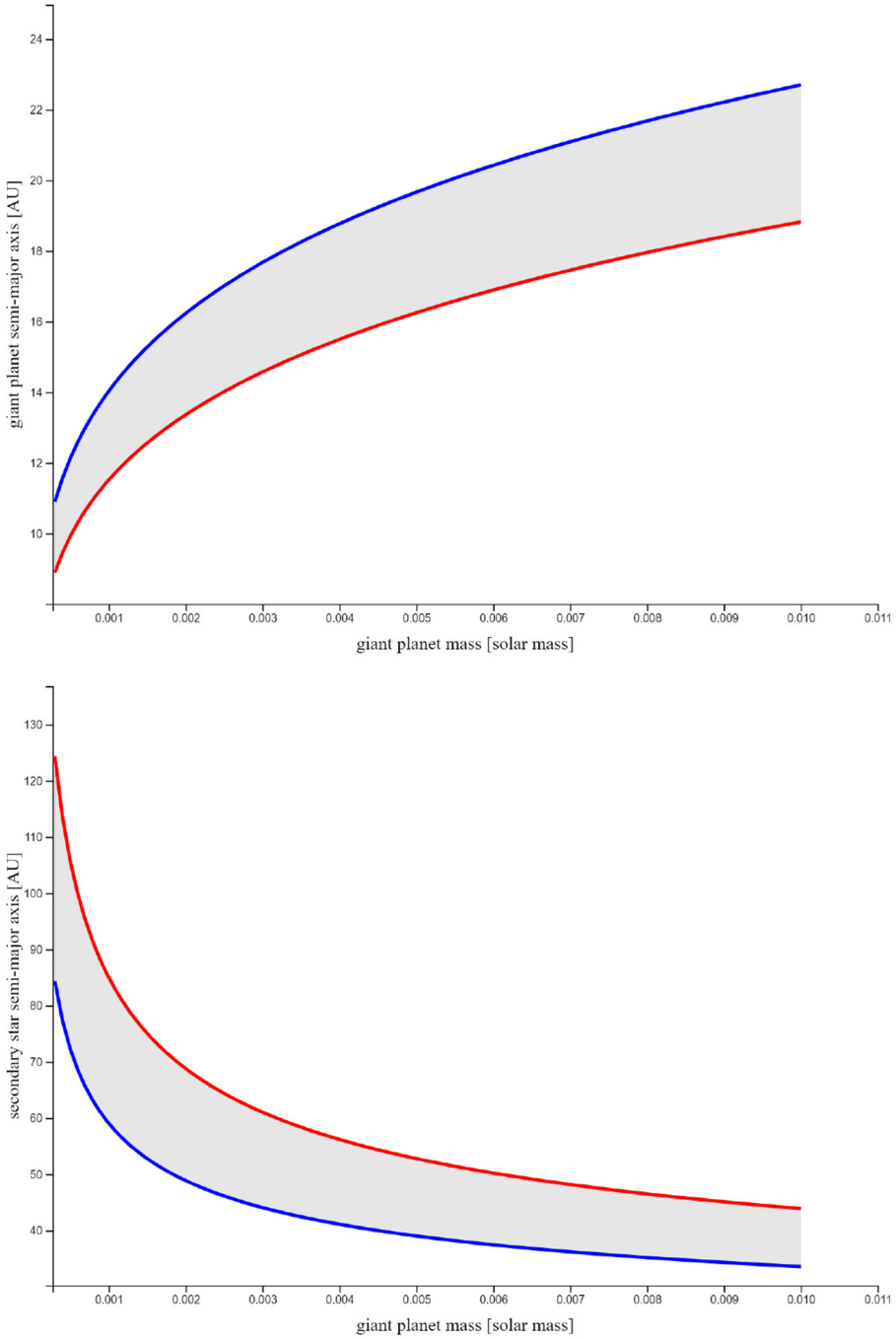

FIGURE 5 | Same as **Figure 3** but for the variation of the giant planet's mass (x-axis) vs. the variation of the semi-major axis either of the giant planet **(Upper)** or of the secondary star **(Lower)** in the y-axes.

would be a high probability that the HZ of the K-type star would be perturbed by an SR. The bottom panel indicates the same but for different masses of the giant planet on the x-axis.

Since the eccentricities of the HD41004 AbB system are not well-determined, it is quite probable that the HZ of the K-type star might change into a pHZ if the orbital parameters vary due to new observational data.

6. DISCUSSION AND CONCLUSION

In this study, we presented recently developed methods to determine the location of secular perturbations for circumstellar (or S-type) planetary motion in binary stars with a special emphasis to planets in the cirumstellar HZ in such systems. We did not take into account circumbinary (or P-type) planetary

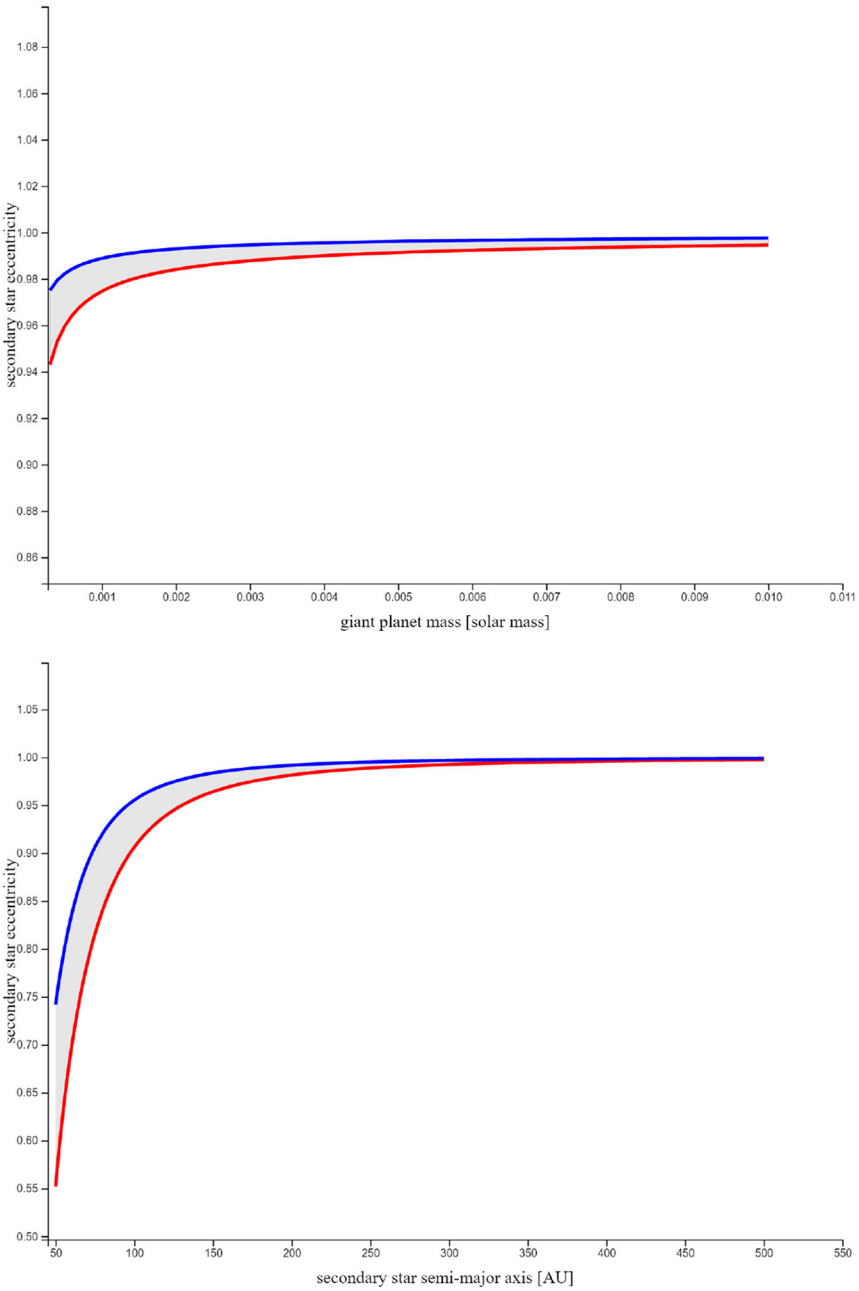

FIGURE 6 | Same as **Figure 3** but for the variation of the giant planet's mass (x-axis) vs. a variation of the binary's eccentricity on the y-axis **(Upper)**. The **(Lower)** shows a variation of the secondary star's semi-major axis (x-axis) vs. the binary's eccentricity (y-axis).

motion as we assume stronger stellar perturbations for a planet in the HZ due to interactions of the stars (e.g., colliding stellar winds; Johnstone et al., 2015) especially in the early phase of a system which could severely affect the conditions for planetary habitability.

The appearance of secular resonances (SR) in circumstellar HZs was investigated for certain binary-star–planet configurations where the giant planet orbits the host-star exterior to the HZ. Considering planar systems, SRs are caused by the precession of the giant planet's perihelion which results from gravitational interaction with the secondary star. Moreover, limitations of the adopted methods have restricted our study to eccentricities ≤ 0.6 for the planet and the binary star.

In a first step we replaced the fully numerical approach by a *semi-analytical method (SAM)*, which uses the Laplace-Lagrange theory (Murray and Dermott, 1999) to define the proper frequencies/periods of all test-planets moving in a certain area of the host-star. Pilat-Lohinger et al. (2016) showed that

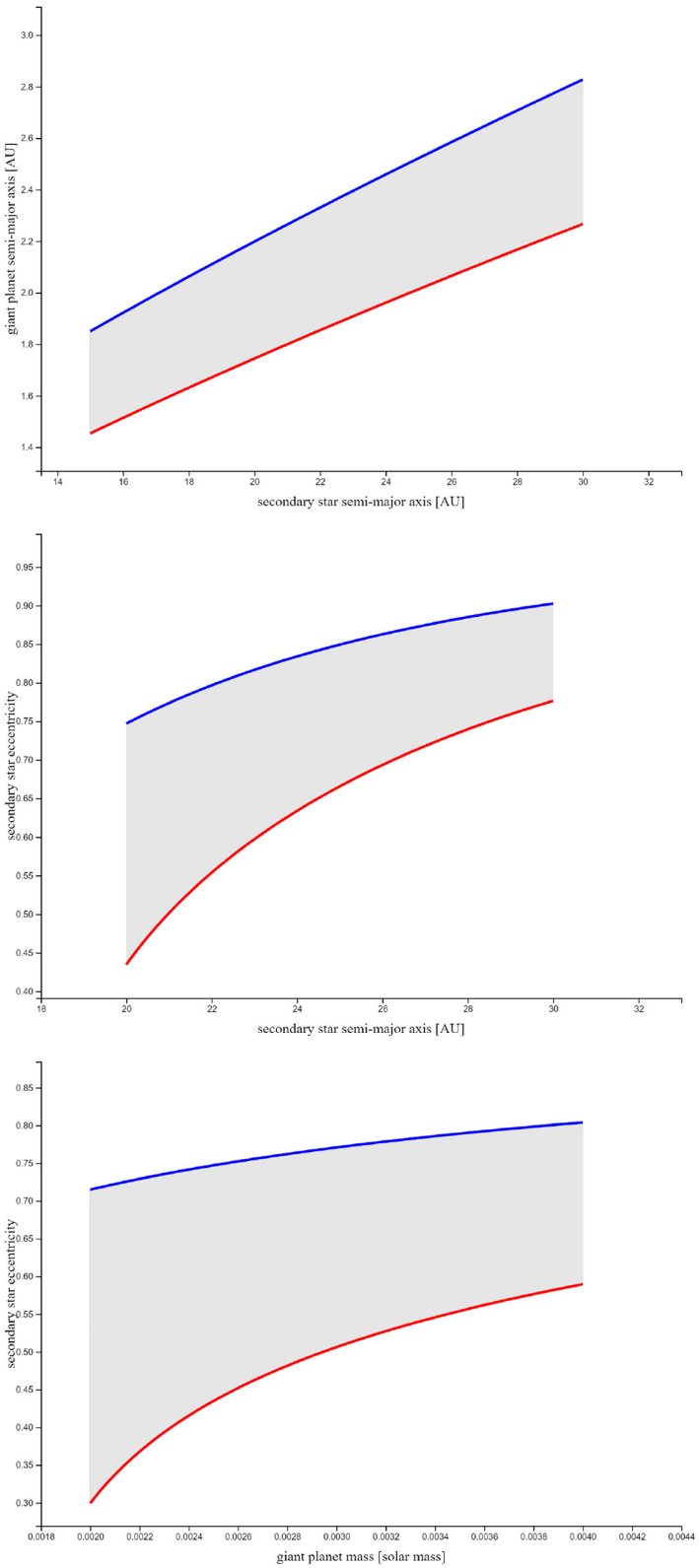

FIGURE 7 | Results for HD41004 AbB. The gray stripe in each panel indicates conditions that cause perturbations in the primary's HZ due to an SR. The top panel shows the result for the semi-major axis of the secondary star (x-axis) and the giant planet (y-axis). In the middle panel the y-axis shows the binary's eccentricity. In the bottom panel, the x-axis shows the giant planet's mass.

these analytically determined values of proper frequencies are in good agreement with the numerical results. Thus, the application of SAM removed a huge amount of time-consuming numerical computations. Only one computation for the determination of the giant planet's proper frequency remains.

However, a general parameter study to distinguish between systems with either qHZ or pHZ needs a parameter space of at least five variables (i.e., mass-ratio of the binary star, mass of the giant planet, semi-major axes of the secondary star and the giant planet, and the eccentricity of the binary) where a change of each parameter will modify the location of a resonance makes therefore, the application of SAM is still too costly in terms of time. Only a fully analytical approach could realize such a study in a reasonable time.

We strove to replace the numerical part for the determination of the giant planet's proper frequency by an analytical method. In this context, the approach by Andrade-Ines and Eggl (2017) has been found to be appropriate for our studies. By joining the Laplace-Lagrange method and the Andrade-Ines–Eggl approach we obtained a *combined analytical method (CAM)* which can easily perform all computations of the 5-dimension parameter space very quickly.

Instead of doing a huge amount of calculations in order to compile a catalog which states the dynamical behavior of the circumstellar HZ in various binary-star–planet configurations, we decided to develop an online-tool which applies CAM. The online-tool is named *SHaDoS* (=**S**ecular perturbations in **Ha**bitable zones of **Do**uble **S**tars)[8] and is easy to use. After a 4-Step input procedure the user gets a 2D-plot which indicates the parameters which would cause a secular resonance in the circumstellar HZ of the host-star by a gray-shaded area. To demonstrate *SHaDoS* we showed applications to a wide binary star (HD106515 AB) and a tight binary star (HD41004 AB) and analyzed the primaries' HZ regarding secular perturbations. Using the observational data, we have found a qHZ for both systems.

[8]https://www.univie.ac.at/adg/shados/index.html

Moreover, the plots of the wide binary star indicate that the probability of a change in the dynamical behavior of the HZ is extremely low—only if new observations should yield significantly different orbital parameters. While in case of the tight binary star changes of the orbital parameters could lead to a pHZ.

Thus, the presented methods can be considered as an important contribution to the habitability research of exoplanets as an SR could affect the motion of a planet in the HZ by increasing the eccentricity. Such variations of eccentricity due to SRs usually happen on a long time-scale and could lead to a misestimation of planetary habitability in such systems. Detected planets in the HZ on nearly circular orbits could move onto highly eccentric orbits after some thousands to millions of years. This would certainly influence the conditions of habitability of these planets.

Even if the number of real systems for which SHaDoS can be applied is still very low, we expect that the number of such systems will increase significantly in the near future when large telescopes like ELT or the Rubin Observatory start observing and especially, when the space mission PLATO 2.0 is launched and starts to explore the sky.

AUTHOR CONTRIBUTIONS

All authors listed have made a substantial, direct and intellectual contribution to the work, and approved it for publication.

ACKNOWLEDGMENTS

The authors acknowledge the support from the Austrian Science Fund (FWF), project S11608-N16, part of the NFN Pathways to Habitability. EP-L wants to thank F. Marzari for the invitation to this Special Edition on The Effect of Stellar Multiplicity on Exoplanetary Systems. And we want to thank the referees who helped to improve the paper.

REFERENCES

Andrade-Ines, E., and Eggl, S. (2017). Secular orbit evolution in systems with a strong external perturber - A simple and accurate model. *Astron. J.* 153:148. doi: 10.3847/1538-3881/153/4/148

Armstrong, D. J., Osborn, H. P., Brown, D. J. A., Faedi, F., Gómez Maqueo Chew, Y., Martin, D. V., et al. (2014). On the abundance of circumbinary planets. *Mon. Not. R. Astron. Soc.* 444, 1873–1883. doi: 10.1093/mnras/stu1570

Artymowicz, P., and Lubow, S. H. (1994). Dynamics of binary-disk interaction. 1: resonances and disk gap sizes. *Astrophys. J.* 421, 651–667. doi: 10.1086/173679

Bancelin, D., Pilat-Lohinger, E., Maindl, T. I., Ragossnig, F., and Schäfer, C. (2017). The Influence of orbital resonances on the water transport to objects in the circumprimary habitable zone of binary star systems. *Astron. J.* 153:269. doi: 10.3847/1538-3881/aa7202

Bazsó, Á., and Pilat-Lohinger, E. (2020). Fear the shadows of the giants: on secular perturbations in circumstellar habitable zones of double stars. *Astron. J.* 160:2. doi: 10.3847/1538-3881/ab9104

Bazsó, Á., Pilat-Lohinger, E., Eggl, S., Funk, B., Bancelin, D., and Rau, G. (2017). Dynamics and habitability in circumstellar planetary systems of known binary stars. *Mon. Not. R. Astron. Soc.* 466, 1555–1566. doi: 10.1093/mnras/stw3095

Boss, A. P. (2006). Gas giant protoplanets formed by disk instability in binary star systems. *Astrophys. J.* 641, 1148–1161. doi: 10.1086/500530

Bromley, B. C., and Kenyon, S. J. (2015). Planet formation around binary stars: tatooine made easy. *Astrophys. J.* 806:98. doi: 10.1088/0004-637X/806/1/98

Cuntz, M. (2014). S-type and P-type habitability in stellar binary systems: a comprehensive approach. I. Method and applications. *Astrophys. J.* 780:14. doi: 10.1088/0004-637X/780/1/14

Desidera, S., Gratton, R., Carolo, E., Martinez Fiorenzano, A. F., Endl, M., Mesa, D., et al. (2012). A long-period massive planet around HD 106515A. *Astron. Astrophys.* 546:A108. doi: 10.1051/0004-6361/201220038

Duchêne, G., and Kraus, A. (2013). Stellar multiplicity. *Annu. Rev. Astron. Astrophys.* 51, 269–310. doi: 10.1146/annurev-astro-081710-102602

Duquennoy, A., Mayor, M., and Halbwachs, J.-L. (1991). Multiplicity among solar type stars in the solar neighbourhood. I - CORAVEL radial velocity observations of 291 stars. *Astron. Astrophys. Suppl.* 88, 281–324.

Dvorak, R. (1984). Numerical experiments on planetary orbits in double stars. *Celest. Mech.* 34, 369–378. doi: 10.1007/978-94-009-5331-4_31

Dvorak, R. (1986). Critical orbits in the elliptic restricted three-body problem. *Astron. Astrophys.* 167, 379–386.

Dvorak, R., Froeschle, C., and Froeschle, C. (1989). Stability of outer planetary orbits (P-types) in binaries. *Astron. Astrophys.* 226, 335–342.

Eggl, S., Georgakarakos, N., and Pilat-Lohinger, E. (2020). Habitable zones in binary star systems: a zoology. *Galaxies* 8:65. doi: 10.3390/galaxies8030065

Eggl, S., Pilat-Lohinger, E., Funk, B., Georgakarakos, N., and Haghighipour, N. (2013). Circumstellar habitable zones of binary-star systems in the solar neighbourhood. *Mon. Not. R. Astron. Soc.* 428, 3104–3113. doi: 10.1093/mnras/sts257

Eggl, S., Pilat-Lohinger, E., Georgakarakos, N., Gyergyovits, M., and Funk, B. (2012). An analytic method to determine habitable zones for S-type planetary orbits in binary star systems. *Astrophys. J.* 752:74. doi: 10.1088/0004-637X/752/1/74

Fragner, M. M., Nelson, R. P., and Kley, W. (2011). On the dynamics and collisional growth of planetesimals in misaligned binary systems. *Astron. Astrophys.* 528:A40. doi: 10.1051/0004-6361/201015378

Froeschlé, C., Lega, E., and Gonczi, R. (1997). Fast lyapunov indicators. Application to asteroidal motion. *Celest. Mech. Dynam. Astron.* 67, 41–62. doi: 10.1023/A:1008276418601

Giuppone, C. A., Leiva, A. M., Correa-Otto, J., and Beaugé, C. (2011). Secular dynamics of planetesimals in tight binary systems: application to γ-Cephei. *Astron. Astrophys.* 530:A103. doi: 10.1051/0004-6361/201016375

Güdel, M., Dvorak, R., Erkaev, N., Kasting, J., Khodachenko, M., Lammer, H., et al. (2014). "Astrophysical conditions for planetary habitability," in *Protostars and Planets VI*, eds H. Beuther, R. S. Klessen, C. P. Dullemond, and T. Henning (Tucson, AZ: University of Arizona Press), 883.

Gyergyovits, M., Eggl, S., Pilat-Lohinger, E., and Theis, C. (2014). Disc-protoplanet interaction. Influence of circumprimary radiative discs on self-gravitating protoplanetary bodies in binary star systems. *Astron. Astrophys.* 566:A114. doi: 10.1051/0004-6361/201321854

Haghighipour, N., and Kaltenegger, L. (2013). Calculating the habitable zone of binary star systems. II. P-type binaries. *Astrophys. J.* 777:166. doi: 10.1088/0004-637X/777/2/166

Haghighipour, N., and Raymond, S. N. (2007). Habitable planet formation in binary planetary systems. *Astrophys. J.* 666, 436–446. doi: 10.1086/520501

Harrington, R. S. (1977). Planetary orbits in binary stars. *Astron. J.* 82, 753–756. doi: 10.1086/112121

Hatzes, A. P., Cochran, W. D., Endl, M., McArthur, B., Paulson, D. B., Walker, G. A. H., et al. (2003). A planetary companion to γ Cephei A. *Astrophys. J.* 599, 1383–1394. doi: 10.1086/379281

Heppenheimer, T. A. (1978). On the formation of planets in binary star systems. *Astron. Astrophys.* 65, 421–426.

Holman, M. J., and Wiegert, P. A. (1999). Long-term stability of planets in binary systems. *Astron. J.* 117, 621–628. doi: 10.1086/300695

Jang-Condell, H. (2015). On the likelihood of planet formation in close binaries. *Astrophys. J.* 799:147. doi: 10.1088/0004-637X/799/2/147

Johnstone, C. P., Zhilkin, A., Pilat-Lohinger, E., Bisikalo, D., Güdel, M., and Eggl, S. (2015). Colliding winds in low-mass binary star systems: wind interactions and implications for habitable planets. *Astron. Astrophys.* 577:A122. doi: 10.1051/0004-6361/201425134

Kaltenegger, L., and Haghighipour, N. (2013). Calculating the habitable zone of binary star systems. I. S-type binaries. *Astrophys. J.* 777:165. doi: 10.1088/0004-637X/777/2/165

Kasting, J. F., Whitmire, D. P., and Reynolds, R. T. (1993). Habitable zones around main sequence stars. *Icarus* 101, 108–128. doi: 10.1006/icar.1993.1010

Kley, W., and Nelson, R. P. (2010). "Early evolution of planets in binaries: planet–disk interaction," in *Planets in Binary Star Systems*, eds N. Haghighipour (Dordrecht: Springer), 135–164.

Kopparapu, R. K., Ramirez, R. M., Schottelkotte, J., Kasting, J. F., Domagal-Goldman, S., and Eymet, V. (2014). Habitable zones around main-sequence stars: dependence on planetary mass. *Astrophys. J. Lett.* 787:L29. doi: 10.1088/2041-8205/787/2/L29

Marzari, F., and Gallina, G. (2016). Stability of multiplanet systems in binaries. *Astron. Astrophys.* 594:A89. doi: 10.1051/0004-6361/201628342

Marzari, F., and Thebault, P. (2019). Planets in binaries: formation and dynamical evolution. *Galaxies* 7:84. doi: 10.3390/galaxies7040084

Mayor, M., and Queloz, D. (1995). A Jupiter-mass companion to a solar-type star. *Nature* 378, 355–359. doi: 10.1038/378355a0

Müller, T. W. A., and Kley, W. (2012). Circumstellar disks in binary star systems. Models for γ Cephei and α Centauri. *Astron. Astrophys.* 539:A18. doi: 10.1051/0004-6361/201118202

Murray, C. D., and Dermott, S. F. (1999). *Solar System Dynamics*. Cambridge, UK: Cambridge University Press.

Pilat-Lohinger, E., Bazsó, Á., and Funk, B. (2016). A quick method to identify secular resonances in multi-planet systems with a binary companion. *Astron. J.* 152:139. doi: 10.3847/0004-6256/152/5/139

Pilat-Lohinger, E., and Dvorak, R. (2002). Stability of S-type orbits in binaries. *Celest. Mech. Dynam. Astron.* 82, 143–153. doi: 10.1023/A:1014586308539

Pilat-Lohinger, E., Eggl, S., and Bazsó, Á. (2019). "Planetary habitability in binary systems," in *Advances in Planetary Science: Volume 4*, ed F. I. Ordway (World Scientific Publishing Co. Pte. Ltd.)

Pilat-Lohinger, E., Funk, B., and Dvorak, R. (2003). Stability limits in double stars. A study of inclined planetary orbits. *Astron. Astrophys.* 400, 1085–1094. doi: 10.1051/0004-6361:20021811

Pilat-Lohinger, E., Sándor, Z., Gyergyovits, M., and Bazsó, Á. (2018). "Planets in binary stars," in *Accretion Processes in Cosmic Sources - II*, eds F. Giovannelli, and L. Sabau-Graziati (Trieste: Sissa Medialab srl Partita), 10.

Quintana, E. V., Adams, F. C., Lissauer, J. J., and Chambers, J. E. (2007). Terrestrial planet formation around individual stars within binary star systems. *Astrophys. J.* 660, 807–822. doi: 10.1086/512542

Rabl, G., and Dvorak, R. (1988). Satellite-type planetary orbits in double stars - A numerical approach. *Astron. Astrophys.* 191, 385–391.

Rafikov, R. R. (2013). Building tatooine: suppression of the direct secular excitation in Kepler circumbinary planet formation. *Astrophys. J. Lett.* 764:L16. doi: 10.1088/2041-8205/764/1/L16

Raghavan, D., McAlister, H. A., Henry, T. J., Latham, D. W., Marcy, G. W., Mason, B. D., et al. (2010). A Survey of stellar families: multiplicity of solar-type stars. *Astrophys. J. Suppl.* 190, 1–42. doi: 10.1088/0067-0049/190/1/1

Santos, N. C., Mayor, M., Naef, D., Pepe, F., Queloz, D., Udry, S., et al. (2000). The CORALIE survey for Southern extra-solar planets. IV. Intrinsic stellar limitations to planet searches with radial-velocity techniques. *Astron. Astrophys.* 361, 265–272.

Savonije, G. J., Papaloizou, J. C. B., and Lin, D. N. C. (1994). On tidally induced shocks in accretion discs in close binary systems. *Mon. Not. R. Astron. Soc.* 268:13. doi: 10.1093/mnras/268.1.13

Schneider, J., Dedieu, C., Le Sidaner, P., Savalle, R., and Zolotukhin, I. (2011). Defining and cataloging exoplanets: the exoplanet.eu database. *Astron. Astrophys.* 532:A79. doi: 10.1051/0004-6361/201116713

Thebault, P. (2011). Against all odds? Forming the planet of the HD 196885 binary. *Celest. Mech. Dynam. Astron.* 111, 29–49. doi: 10.1007/s10569-011-9346-2

Thebault, P., and Haghighipour, N. (2015). "Planet Formation in Binaries," in *Planetary Exploration and Science: Recent Advances and Applications*, eds. S. Jin, N. Haghighipour, W.-H. Ip (Heidelberg: Springer Geophysics), 309–340. doi: 10.1007/978-3-662-45052-9_13

Thébault, P., Marzari, F., and Scholl, H. (2006). Relative velocities among accreting planetesimals in binary systems: the circumprimary case. *Icarus* 183, 193–206. doi: 10.1016/j.icarus.2006.01.022

Thébault, P., Marzari, F., and Scholl, H. (2008). Planet formation in α Centauri A revisited: not so accretion friendly after all. *Mon. Not. R. Astron. Soc.* 388, 1528–1536. doi: 10.1111/j.1365-2966.2008.13536.x

Thébault, P., Marzari, F., and Scholl, H. (2009). Planet formation in the habitable zone of α Centauri B. *Mon. Not. R. Astron. Soc.* 393, L21–L25. doi: 10.1111/j.1745-3933.2008.00590.x

Thébault, P., Marzari, F., Scholl, H., Turrini, D., and Barbieri, M. (2004). Planetary formation in the γ Cephei system. *Astron. Astrophys.* 427, 1097–1104. doi: 10.1051/0004-6361:20040514

Tokovinin, A. (2014). From binaries to multiples. II. Hierarchical multiplicity of F and G dwarfs. *Astron. J.* 147:87. doi: 10.1088/0004-6256/147/4/87

Zucker, S., Mazeh, T., Santos, N. C., Udry, S., and Mayor, M. (2004). Multi-order TODCOR: application to observations taken with the CORALIE echelle spectrograph. II. A planet in the system HD 41004. *Astron. Astrophys.* 426, 695–698. doi: 10.1051/0004-6361:20040384

Conflict of Interest: The authors declare that the research was conducted in the absence of any commercial or financial relationships that could be construed as a potential conflict of interest.

frontiers in Astronomy and Space Sciences

ORIGINAL RESEARCH
published: 23 June 2021
doi: 10.3389/fspas.2021.628396

Follow-Up and Validation of K2 and TESS Planetary Systems With Keck NIRC2 Adaptive Optics Imaging

Joshua E. Schlieder[1], Erica J. Gonzales[2], David R. Ciardi[3], Rahul I. Patel[3], Ian J. M. Crossfield[4], Justin R. Crepp[5], Courtney D. Dressing[6], Thomas Barclay[1,7] and Andrew W. Howard[8]*

[1] Exoplanets and Stellar Astrophysics Laboratory, NASA Goddard Space Flight Center, Greenbelt, MD, United States, [2] Department of Astronomy and Astrophysics, University of California, Santa Cruz, Santa Cruz, CA, United States, [3] Caltech/IPAC-NASA Exoplanet Science Institute, Pasadena, CA, United States, [4] Department of Physics and Astronomy, University of Kansas, Lawrence, KS, United States, [5] Department of Physics, University of Notre Dame, Notre Dame, IN, United States, [6] Astronomy Department, University of California, Berkeley, Berkeley, CA, United States, [7] University of Maryland, Baltimore County, Baltimore, MD, United States, [8] Department of Astronomy, California Institute of Technology, Pasadena, CA, United States

OPEN ACCESS

Edited by:
Francesco Marzari, University of Padua, Italy

Reviewed by:
Ilaria Carleo, Wesleyan University, United States
Riccardo Claudi, Osservatorio Astronomico di Padova (INAF), Italy

***Correspondence:**
Joshua E. Schlieder
joshua.e.schlieder@nasa.gov

Specialty section:
This article was submitted to Exoplanets, a section of the journal Frontiers in Astronomy and Space Sciences

Received: *11 November 2020*
Accepted: *30 March 2021*
Published: *23 June 2021*

Citation:
Schlieder JE, Gonzales EJ, Ciardi DR, Patel RI, Crossfield IJM, Crepp JR, Dressing CD, Barclay T and Howard AW (2021) Follow-Up and Validation of K2 and TESS Planetary Systems With Keck NIRC2 Adaptive Optics Imaging. Front. Astron. Space Sci. 8:628396. doi: 10.3389/fspas.2021.628396

High resolution imaging (HRI) is a critical part of the transiting exoplanet follow-up and validation process. HRI allows previously unresolved stellar companions and background blends to be resolved, vetting false positive signals and improving the radii measurements of true planets. Through a multi-semester Keck NIRC2 adaptive optics imaging program, we have pursued HRI of K2 and TESS candidate planet host systems to provide the transiting exoplanet community with necessary data for system validation and characterization. Here we present a summary of our ongoing program that includes an up to date list of targets observed, a description of the observations and data reduction, and a discussion of planetary systems validated by the community using these data. This observing program has been key in NASA's K2 and TESS missions reaching their goals of identifying new exoplanets ideal for continued follow-up observations to measure their masses and investigate their atmospheres. Once processed, all observations presented here are available as calibrated images and resulting contrast curves through the Exoplanet Follow-up Observing Program (ExoFOP) website. We encourage members of the exoplanet community to use these data products in their ongoing planetary system validation and characterization efforts.

Keywords: adaptive optics—stars, binary stars, multiple stars, exoplanets, exoplanet candidates, exoplanet characterization

1. INTRODUCTION

The era of high-precision, space-based photometry to discover transiting exoplanets has led to a revolution in our understanding of planets beyond our solar system. NASA's *Kepler* mission (Borucki et al., 2010), which launched in 2009 and observed targets in a ∼115 sq. deg. part of the sky for nearly 4 years, identified ∼4,000 candidate transiting planets (Thompson et al., 2018). This sample allowed for ground breaking constraints on the statistical distribution and frequency of exoplanets (e.g., Dressing and Charbonneau, 2015; Fulton et al., 2017) and the discovery of many interesting individual systems (Lissauer et al., 2011; Quintana et al., 2014).

After hardware failures, the *Kepler* mission ended and the observatory was re-purposed as the K2 mission (Howell et al., 2014), a community driven, time domain photometry survey of 19 fields around the ecliptic plane. Compared to *Kepler*, K2 surveyed an order of magnitude more sky, accessed more diverse stellar populations, and observed a larger numberof bright targets amenable to follow-up observations. The exoplanet community has so far identified more than 1,300 candidate planets in K2 data (e.g., Kruse et al., 2019, and references therein). In this haul, K2 revealed small candidates transiting bright host stars suitable for detailed characterization (Crossfield et al., 2015; Montet et al., 2015) and allowed for additional statistical studies of the exoplanet population (Hardegree-Ullman et al., 2020). After the space craft expended its fuel in the Fall of 2018, it was no longer able to point precisely enough to perform science observations and the observatory was decommissioned.

The Transiting Exoplanet Survey Satellite (TESS, Ricker et al., 2015) launched in April 2018 and continues the *Kepler*/K2 transiting planet discovery legacy with a nearly all-sky survey. TESS observes in ∼27 day Sectors and has so far obtained high precision photometric time-series over ≈80% of the sky to search for transiting planets. The mission aims to discover small planets around the closest brightest stars, leading to systems that are ideal for mass measurements and atmospheric characterization. So far, TESS has identified more than 3,000 candidate planets when those identified by the project (Guerrero and TESS Science Office, 2021) and the community[1] are taken into account. The mission is providing some of the most promising small planets for atmosphere characterization with the upcoming James Webb Space Telescope (JWST, e.g., Kostov et al., 2019).

An essential part of the process to confirm and characterize the ever increasing number of transiting exoplanet candidates is large scale, coordinated follow-up observations. Traditional confirmation of planet-like signals relies on precision radial velocity (PRV) spectroscopy to directly measure stellar reflex motion due to planets and derive planet masses. However, RV confirmation requires resource intensive long-term monitoring programs and may not be possible for faint targets and small planets due to signal-to-noise and expected RV amplitudes. In the majority of cases, a more tractable path to convert a candidate to a reliable planet requires follow-up to rule out sources of false positive signals (e.g., bound and background eclipsing binaries) with high statistical significance. Typical follow-up includes spectroscopy to determine the host star properties, lower precision RV screening for massive, short period companions, and imaging to identify bound companions and background sources. Statistical validation and dedicated follow-up has been used to rule out false-positives at high confidence for a large number of the *Kepler*, K2, and TESS candidates described previously. So far, approximately 2,400 *Kepler* candidates, more than 400 K2 candidates, and more than 100 TESS candidates have been validated or confirmed.

High spatial resolution imaging (HRI) has been critical to candidate exoplanet validation efforts. HRI has become the standard technique for detecting companion stars and background eclipsing binaries closer than 1″ and is a vital input for the statistical validation of small planets beyond the reach of RV observations. In addition to validation, HRI is crucial for measuring the true planetary radii and planet sizes by measuring the photometric blending of their hosts with bound and background stars (Ciardi et al., 2015). Here we describe a key program in a large HRI follow-up campaign to characterize K2 and TESS planetary systems. The program uses Keck NIRC2 adaptive optics (AO) imaging to discover and characterize close-in bound and background sources and provide the necessary data to validate high priority K2 and TESS targets, study exoplanet host star multiplicity, correct planetary radii for dilution from newly discovered companions, and place constraints on exoplanet demographics and occurrence rates. In subsequent sections we provide details on the construction of the program, our observations and analyses, and the results. We also discuss future plans with these data and, once processed, make available reduced data products for each observed target through the NASA Exoplanet Archive Exoplanet Follow-up Observing Program (ExoFOP) services for K2 and TESS. We encourage the exoplanet community to use these data in their ongoing analyses.

2. MATERIALS AND METHODS

2.1. Overview of the Observing Program

Following the need for HRI observations demonstrated with *Kepler* candidates and the transition to the community driven K2 mission, our team and collaborators undertook a large-scale effort to identify, follow-up, and validate K2 planet candidates (Crossfield et al., 2016, 2018; Dressing et al., 2017a,b, 2019; Livingston et al., 2018; Mayo et al., 2018; Petigura et al., 2018; Yu et al., 2018). As a key part of the follow-up campaign, we organized a multi-facility HRI program to observe and characterize K2 candidate exoplanet systems. As the K2 mission ended in 2018, the TESS mission began routine science operations and began delivering new exoplanet candidates. With this transition, we expanded our HRI follow-up program to pursue TESS targets through the TESS Follow-up Observers Program (TFOP).

Here we describe a portion of the K2 and TESS HRI program that was competitively pursued through the public NASA Keck time allocation[2]. We provide details on the NASA Keck observing programs allocated for these observations in **Table 1**. In the following sub-sections we describe our approaches to target selection, observations, data reduction, and analysis.

2.2. Target Selection

For the K2 aspect of the HRI program, we selected targets from the list of candidate exoplanet systems identified by this team and collaborators. The majority of these systems were identified in publicly available K2 data by our team using a multi-step process. K2 time-series were corrected for systematic errors introduced by the degraded pointing performance of the observatory using the `k2phot` software package[3]. Planet candidates were then

[1]https://exofop.ipac.caltech.edu/tess/view_ctoi.php

[2]https://nexsci.caltech.edu/missions/KeckSolicitation/

[3]https://github.com/petigura/k2phot

TABLE 1 | NASA Keck observing programs and nights.

Semester	ID #	UT Date	Weather	Notes
		2017-09-10	Clear skies	1/2 night
2017B	N213	2017-09-11	Clear skies	Full night
		2017-12-29	Clear skies	Full night
2018A	N119	2018-02-08	Fog, clouds	1/2 night
		2018-04-25	Clear skies	Full night
2018B	N214	2018-08-14	Clear skies	1/2 night
		2018-12-17	Clear skies	1/2 night
		2019-03-25	Clouds	1/2 night
2019A	N115	2019-04-07	Clear skies	1/2 night
		2019-06-09	Clear skies	1/2 night
2020A	N93	2020-05-28	Clouds	Full night

TABLE 2 | K2 targets and observation details[a].

EPIC ID	Semester	Date UT	Filter	T_{int} (s)	Coadds
201498078	2017B	2017-12-29	Br-γ	5	1
202071645	2017B	2017-12-29	*J*cont	12	1
202071645	2017B	2017-12-29	Br-γ	10	1
202126852	2017B	2017-12-29	*J*cont	4	1
202126852	2017B	2017-12-29	Br-γ	10	1
205916793	2017B	2017-09-11	Br-γ	20	1
206026136	2017B	2017-09-11	Br-γ	28	1
206155547	2017B	2017-09-11	K_p	11	1
206192335	2017B	2017-09-11	*J*	0.5	1
206192335	2017B	2017-09-11	Br-γ	6	1
210484192	2017B	2017-12-29	*J*cont	10	1
210484192	2017B	2017-12-29	*J*cont	5	1
210484192	2017B	2017-12-29	Br-γ	3	1
210484192	2018A	2018-02-08	Br-γ	1	1
210484192	2018A	2018-02-08	*J*	1	1
210508766	2017B	2017-12-29	K_p	45	1
210693462	2017B	2017-12-29	*J*	40	1
210693462	2018B	2018-12-17	*J*cont	10	1
210693462	2017B	2017-12-29	K_p	20	1
210693462	2018B	2018-12-17	Br-γ	20	1

[a] *This is a portion of the full table provided as an example of the format and content. The full table is available in electronic formation as* ***Supplementary Data Table 1****.*

identified using the TERRA algorithm, adapted for use on K2 light curves from *Kepler* (Petigura et al., 2013). Diagnostic plots describing threshold crossing events (TCEs) were then visually vetted by a team of human volunteers to remove the most obvious false positives in the form of eclipsing binaries, stellar variability, and instrumental noise and produce lists of exoplanet candidates for each K2 campaign. Additional, community candidates identified using other systematics correction algorithms and planet search approaches were also considered. These included candidates resulting from the light curve detrending approaches described in Vanderburg and Johnson (2014), Aigrain et al. (2016), and Luger et al. (2016) and the planet searches described in Pope et al. (2016), Vanderburg et al. (2016), and Kruse et al. (2019). The combined potential targets were prioritized for Keck AO imaging follow-up on the basis of planet radius (planets $\leq$4 $R_\oplus$ were preferred), host star properties ($R_* < 1.5\ R_\odot$, $V \lesssim$ 14 mag), and the planet's prospects as a future target for PRV mass measurements and transmission spectroscopy. This led to a total of 174 candidate K2 exoplanet systems being targeted in this program. The observed K2 targets and their observing parameters are provided in **Table 2**. This table is a portion of the full K2 target table and is provided as an example of the format and content. The full table is available in electronic formation as **Supplementary Data Table 1**.

The TESS aspect of the HRI program was organized through the TESS Follow-up Observing Program (TFOP)[4] and drew targets from the lists of exoplanet candidates publicly released by the TESS project. Building on the community driven, *ad-hoc* approach to follow-up from K2, TFOP was designed to prioritize and perform observations to go from a large sample of planet candidates (thousands) to a small sample of targets for PRV mass measurements ($\sim$100). Once transit-like events are identified in TESS 2-min cadence data by the Science Processing Operations Center (SPOC) mission pipeline (Jenkins et al., 2016) and in 30-min cadence data by the MIT Science Operations Center (SOC) Quick Look Pipeline (QLP), manual vetting of both SPOC and QLP transit events is performed by a dedicated SOC team to provide a list of the most likely planet candidates. These candidates are then disseminated to the TFOP community for follow-up. The TESS observations presented here are part of TFOP Sub-Group 3 (SG3), which targets candidates with HRI to detect nearby sources unresolved by seeing limited observations ($\lesssim 1''$). The TESS mission began public releases of exoplanet candidates, called TESS Objects of Interest (TOIs), that fed into TFOP in September of 2018[5]. To select TESS targets for Keck AO imaging, we primarily considered TOI systems with small planets that would be most suitable for PRV follow-up to measure planet masses. This included selection on both the host star properties ($R_* < 1.5\ R_\odot$, $V \lesssim 14$ mag) and the candidate planets ($R_p \leq 4\ R_\oplus$). We also requested additional interesting TESS targets from the broader exoplanet community. This led to a total of 72 candidate TESS systems being targeted so far in this program. The observed TESS targets are detailed in **Table 3**. This table is a portion of the full TESS target table and is provided as an example of the format and content. The full table is available in electronic formation as **Supplementary Data Table 2**.

2.3. Observations

The observations described here cover nights in Keck semesters 2017B, 2018A, 2018B, 2019A, and 2020A; spanning the dates UT September 09 2017 to UT May 28 2020. The details of each observing run are provided in **Table 1**. In each of the observing runs, we used the NIRC2 instrument behind the

[4]https://tess.mit.edu/followup/

[5]https://tev.mit.edu/data/collection/193/

TABLE 3 | TESS targets and observation details[a].

TIC ID	Semester	Date UT	Filter	T_{int} (s)	Coadds
13684720	2020A	2020-05-28	*K*	0.75	1
19025965	2019A	2019-03-25	Br-γ	15	1
19451711	2019A	2019-03-25	*J*cont	0.4	50
19451711	2019A	2019-03-25	Br-γ	5	2
19451711	2019A	2019-03-25	Br-γ	1	2
19519368	2019A	2019-03-25	Br-γ	1	5
27649847	2019A	2019-04-07	Br-γ	15	1
31374837	2019A	2019-03-25	*K*	10	1
31374837	2019A	2019-03-25	*K*	1	20
33692729	2019A	2019-03-25	Br-γ	30	1
37770169	2019A	2019-03-25	*K*	1	30
71512186	2019A	2019-04-07	Br-γ	0.18	10
71512186	2019A	2019-04-07	Br-γ	0.18	50
73540072	2020A	2020-05-28	Br-γ	15	1
73540072	2020A	2020-05-28	Br-γ	20	1

[a]*This is a portion of the full table provided as an example of the format and content. The full table is available in electronic formation as* ***Supplementary Data Table 2****.*

TABLE 4 | NIRC2 filters used.

Filter	λ_c μm	Bandpass μm
Narrow band		
*K*cont	2.2706	0.0296
Br-γ	2.1686	0.0326
*J*cont	1.2132	0.0198
Broad band		
K	2.196	0.336
K_s	2.146	0.311
K_p	2.124	0.351
H	1.633	0.296
J	1.248	0.163

Natural Guide Star (NGS) AO system (Wizinowich et al., 2000) on the 10 m Keck-II telescope. The observations were obtained in a number of narrow and broad-band filters with central wavelengths near $\sim$2.2 μm to maximize the sensitivity to faint, low-mass companions. The exact choice of filter was dictated by the target NIR magnitude and the observing conditions (broader filters were used for fainter targets and in degraded conditions). If a potential companion was detected in quick look analyses, the target was also observed with shorter wavelength NIR filters, typically *J*-band, to facilitate companion color analyses. A full list of the NIRC2 filters used in this program is provided in **Table 4**. We used the narrow-angle mode of the camera to provide a pixel scale of 9.942 mas pixel^{-1} and a full field-of-view of 10″.

All of the observations in this program followed the standard dither set-up for NIRC2 observations that avoids the noisier lower-left quadrant of the detector. The observing sequences used a dither pattern with a step-size of 3″ that was repeated three times, with each dither offset 0.5″ from the previous, resulting in 9 frames. Integration times varied from <1 to 60 s per dither, depending on target NIR magnitudes, and typically used 1 coadd. Detailed information on the observations of each target are included in **Tables 2**, **3**.

2.4. Data Reduction and Analysis

All of the data in this program was reduced and analyzed using standard imaging approaches. The dithered science frames were dark corrected using calibration observations obtained each night. Sky frames were produced from the median average of the dithered science frames. Flats were produced from the median average of dark subtracted flat-field observations obtained each night. The science frames were then sky-subtracted and flat-fielded. The reduced frames where then combined into a single image via an intrapixel interpolation scheme that co-aligns and median-coadds the frames while conserving flux. The final images are oriented with North up and East to left. Typical NIRC2 AO images obtained in good conditions have a resolution of $\sim$0.05″ (FWHM).

We estimated the sensitivity to these companions in each final, combined image by injecting simulated sources in 45° azimuthal increments at discrete separations that were integer multiples of the central source's FWHM (following Furlan et al., 2017). To estimate the contrast sensitivity, the flux of each simulated source was increased until aperture photometry yielded a 5σ detection. The final contrast sensitivity as a function of separation was calculated by averaging all of the limits at that separation. Beginning approximately with the first TESS target observations in this program, we introduced contrast sensitivity uncertainties into our standard analyses. Uncertainties were estimated by measuring the RMS dispersion of the 5σ limits in each azimuthal annulus at each discrete separation. This process leads to contrast curves (in Δmag) for each target observation that represent the 5σ sensitivity limits of the imaging data as a function of separation from the central source. The NIRC2 observations typically yields NIR contrasts $\gtrsim$7 mag at 0.5″ separations, and $\gtrsim$4 mag at 0.1″ separations, providing access to faint, close-in companions (see e.g., Crossfield et al., 2016, their Figure 5).

3. RESULTS

After processing, the results of this observing program are made publicly available for community use on the NASA Exoplanet Archive's ExoFOP-K2[6] and ExoFOP-TESS[7] websites. For each observation we include: the reduced, combined images as FITS files, contrast curves as ASCII tables, and publication ready figures showing the contrast curve and final image as an inset.

[6]https://exofop.ipac.caltech.edu/k2/
[7]https://exofop.ipac.caltech.edu/tess/

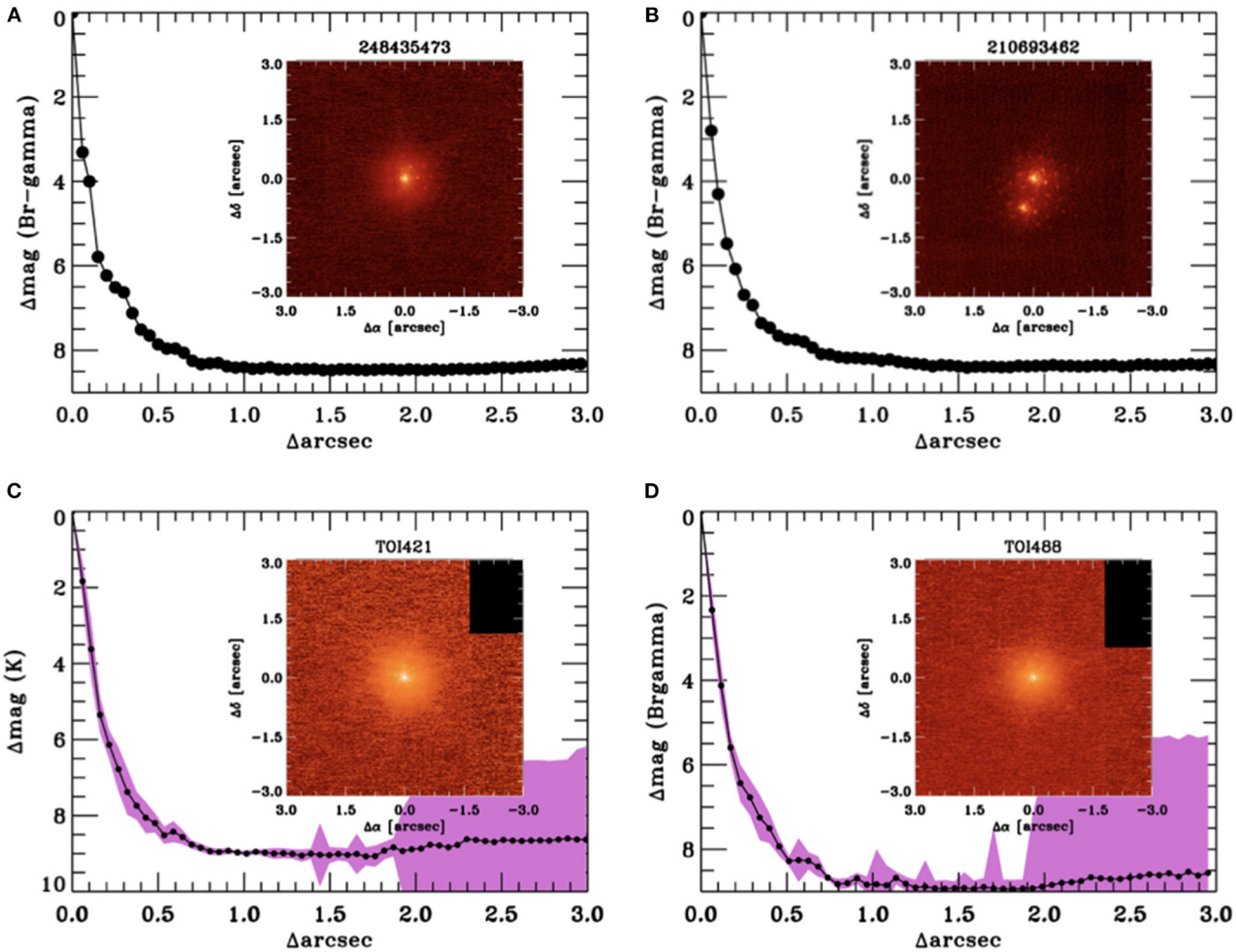

FIGURE 1 | High-resolution images and 5σ contrast curves of stars hosting validated transiting exoplanets obtained in this Keck AO imaging program. **(A)** Br-γ observations of K2-266 (EPIC 248435473, Rodriguez et al., 2018). **(B)** Br-γ observations of K2-288 (EPIC 210693462, Feinstein et al., 2019). The observations revealed a faint companion to the southeast, K2-288B, that likely hosts the exoplanet. **(C)** K-band observations of TOI-421 (Carleo et al., 2020). **(D)** Br-γ observations of GJ 3473 (TOI-488). In **(C,D)**, the shaded regions represent the uncertainties in the contrast sensitivity estimates described in the text. Once processed, these contrast curves with reduced image insets are available for all targets observed in this program via the ExoFOP website. **(A–C)** are reproduced with permission of the AAS.

Figure 1 includes example reduced images and contrast curves from a selection of K2 and TESS targets in this program.

3.1. HRI in Planet Validation

The HRI data resulting from this observing program are key inputs to efforts to statistically validate transiting exoplanet candidates. HRI places deep constraints on the presence of bound and background sources in the vicinity of the presumed host stars that are blended in the much lower resolution images from *Kepler*/K2 and TESS used to produced light curves. These blended sources along the line of sight can host eclipsing binaries (EBs), that when diluted by the brighter primary source, mimic planet transits in the light curve. HRI is an observationally inexpensive and effective approach to mitigate contamination from blends.

The process of exoplanet validation systematically explores the large parameter space that could contain planet mimicking configurations and statistically constrain the probability. In practice, validation software combines light curve data, stellar properties, and observing constraints (i.e., contrast curves from HRI) with statistical priors on the likelihood of false positives. The aforementioned priors include simulations of the stellar population near the target and common false positive configurations (e.g., bound, background, and hierarchical EBs). The result of the validation analysis is the probability that a given transit signal is caused by one of the false positive scenarios explored or a true planet, the false positive probability (FPP). Validation is a powerful technique to confirm small planets beyond the reach of PRV measurements (like those in the habitable zone) and planets that orbit fainter stars. Several validation software packages have been developed and

used by the *Kepler*, K2, and TESS communities. These include `BLENDER` (Torres et al., 2011), `PASTIS` (Díaz et al., 2014), `vespa` (Morton, 2012, 2015), and `TRICERATOPS` (Giacalone and Dressing, 2020).

The HRI observations presented here, along with other complementary HRI observations from other Keck programs and other imaging facilities, have contributed to the validation of many hundreds of transiting exoplanet systems. For example, these data were key in the validation of many systems from the K2 mission. Some systems of note include K2-233, a young early-K dwarf hosting three small planets (David et al., 2018); K2-266, a K dwarf in a wide binary hosting at least four planets with one significantly misaligned (Rodriguez et al., 2018); and K2-288B, an M dwarf in a binary system hosting a small habitable-zone planet discovered by citizen scientists (Feinstein et al., 2019). The HRI observations of TESS targets are also beginning to validate and characterize systems around brighter, closer stars. This includes the TOI-421 system, three planets orbiting a bright G dwarf (Carleo et al., 2020); GJ 3473 (TOI-488), a nearby M dwarf hosting a hot, transiting, Earth-size planet (Kemmer et al., 2020), and TOI-503, a short period brown dwarf transiting an A type star (Šubjak et al., 2020).

4. DISCUSSION

The Keck HRI program described here and complementary observations with other facilities are ongoing and continue to secure time through the NASA Keck and other TACs. Future observations of high-priority TESS candidate planet hosts through TFOP SG3 will provide further characterizing data and progress the TESS mission toward its scientific goals via continued system validation. The data in hand will be included in forthcoming publications to present the full list of newly discovered companions and their properties, the multiplicity statistics of K2 and TESS planet host stars (e.g., Matson et al., 2018) and the effects of multiplicity on planetary systems (e.g., Kraus et al., 2016; Ziegler et al., 2018, 2020).

The observations will also be critical in future analyses of K2 and TESS exoplanet demographics and occurrence rates (e.g., Hardegree-Ullman et al., 2020; Zink et al., 2020). The HRI observations allow true planet radii to be included in these analysis. In the absence of HRI observations, planet radii could be underestimated due to dilution from unresolved, nearby sources that cause photometric blending of the transit (Ciardi et al., 2015; Furlan et al., 2017). Planet demographic and occurrence rates studies that do not account for these blends may overestimate the frequency of small planets. The inclusion of HRI data will improve our understanding of the true distributions and frequencies of planets across the Galaxy.

In addition to studies enabled directly by the HRI data, planetary systems validated and characterized in the context of HRI feed into further characterization efforts. This includes Doppler mass measurements and transmission and emission spectroscopy to detect planet atmospheres. These observations place direct constraints on the bulk compositions and chemical constituents of exoplanets. This is particularly true for the bright targets discovered by K2 and TESS that are most amenable to these measurements as we enter the era of extreme PRV observations and the JWST.

5. CONCLUSIONS

Here we summarized our multi-year campaign to observe K2 and TESS candidate exoplanet host stars using Keck NIRC2 AO imaging through the NASA Keck time allocation. The hundreds of targets we have observed continue to contribute to the validation of key new exoplanet systems and will be the focus of future studies delving into host star multiplicity and exoplanet occurrence rates. The TESS aspect of our program is ongoing through the TFOP consortium and will continue to provide HRI observations of high-priority candidate TESS systems. This includes ideal targets for further characterization to measure planet masses and study exoplanet atmospheres with current and future facilities. We encourage the exoplanet community to explore the calibrated and reduced data products we make available through ExoFOP and use these results in their validation and characterization efforts.

DATA AVAILABILITY STATEMENT

The Keck HRI datasets obtained through the described programs are publicly available from the Keck Observatory Archive (KOA) on a rolling basis following a proprietary period [https://www2.keck.hawaii.edu/koa/public/koa.php]. Once they are processed, the calibrated and reduced data products resulting from the described programs are publicly available from the ExoFOP websites for the K2 and TESS missions [https://exofop.ipac.caltech.edu/k2/ and https://exofop.ipac.caltech.edu/tess/].

AUTHOR CONTRIBUTIONS

JS led the manuscript, produced the tables and figure, performed the observations, and wrote the NASA Keck proposals. EG contributed to the text and tables, performed the observations, and wrote the NASA Keck proposals. DC contributed to the text, tables, and figure, performed the data reduction, produced the publicly available data products, and performed the observations. RP and IC contributed to the text and performed the observations. JC, CD, TB, and AH contributed to the text. All authors contributed to the NASA Keck proposals that led to the described data.

FUNDING

This work was supported by multiple NASA Keck PI Data Awards, administered by the NASA Exoplanet Science Institute.

ACKNOWLEDGMENTS

We thank the Keck observatory support and staff astronomers for aiding in our acquisition of Keck data. Data presented herein were obtained at the W. M. Keck Observatory from

telescope time allocated to the National Aeronautics and Space Administration through the agency's scientific partnership with the California Institute of Technology and the University of California. The Observatory was made possible by the generous financial support of the W. M. Keck Foundation. The authors recognize and acknowledge the significant cultural role and reverence that the summit of Maunakea has always had within the indigenous Hawaiian community. We were most fortunate to conduct observations from this mountain.

SUPPLEMENTARY MATERIAL

The Supplementary Material for this article can be found online at: https://www.frontiersin.org/articles/10.3389/fspas.2021.628396/full#supplementary-material

REFERENCES

Aigrain, S., Parviainen, H., and Pope, B. J. S. (2016). K2SC: flexible systematics correction and detrending of K2 light curves using Gaussian process regression. *Mon. Not. RAS* 459, 2408–2419. doi: 10.1093/mnras/stw706

Borucki, W. J., Koch, D., Basri, G., Batalha, N., Brown, T., Caldwell, D., et al. (2010). Kepler planet-detection mission: introduction and first results. *Science* 327:977. doi: 10.1126/science.1185402

Carleo, I., Gandolfi, D., Barragán, O., Livingston, J. H., Persson, C. M., Lam, K. W. F., et al. (2020). The multiplanet system TOI-421. *Astron. J.* 160:114. doi: 10.3847/1538-3881/aba124

Ciardi, D. R., Beichman, C. A., Horch, E. P., and Howell, S. B. (2015). Understanding the effects of stellar multiplicity on the derived planet radii from transit surveys: implications for Kepler, K2, and TESS. *Astrophys. J.* 805:16. doi: 10.1088/0004-637X/805/1/16

Crossfield, I. J. M., Ciardi, D. R., Petigura, E. A., Sinukoff, E., Schlieder, J. E., Howard, A. W., et al. (2016). 197 Candidates and 104 validated planets in K2's first five fields. *Astrophys. J. Suppl.* 226:7. doi: 10.3847/0067-0049/226/1/7

Crossfield, I. J. M., Guerrero, N., David, T., Quinn, S. N., Feinstein, A. D., Huang, C., et al. (2018). A TESS dress rehearsal: planetary candidates and variables from K2 campaign 17. *Astrophys. J. Suppl.* 239:5. doi: 10.3847/1538-4365/aae155

Crossfield, I. J. M., Petigura, E., Schlieder, J. E., Howard, A. W., Fulton, B. J., Aller, K. M., et al. (2015). A nearby M star with three transiting super-earths discovered by K2. *Astrophys. J.* 804:10. doi: 10.1088/0004-637X/804/1/10

David, T. J., Crossfield, I. J. M., Benneke, B., Petigura, E. A., Gonzales, E. J., Schlieder, J. E., et al. (2018). Three small planets transiting the bright young field star K2–233. *Astron. J.* 155:222. doi: 10.3847/1538-3881/aabde8

Díaz, R. F., Almenara, J. M., Santerne, A., Moutou, C., Lethuillier, A., and Deleuil, M. (2014). PASTIS: Bayesian extrasolar planet validation–I. General framework, models, and performance. *Mon. Not. RAS* 441, 983–1004. doi: 10.1093/mnras/stu601

Dressing, C. D., and Charbonneau, D. (2015). The occurrence of potentially habitable planets orbiting M dwarfs estimated from the full Kepler dataset and an empirical measurement of the detection sensitivity. *Astrophys. J.* 807:45. doi: 10.1088/0004-637X/807/1/45

Dressing, C. D., Hardegree-Ullman, K., Schlieder, J. E., Newton, E. R., Vand erburg, A., Feinstein, A. D., et al. (2019). Characterizing K2 candidate planetary systems orbiting low-mass stars. IV. Updated properties for 86 cool dwarfs observed during campaigns 1–17. *Astron. J.* 158:87. doi: 10.3847/1538-3881/ab2895

Dressing, C. D., Newton, E. R., Schlieder, J. E., Charbonneau, D., Knutson, H. A., Vanderburg, A., et al. (2017a). Characterizing K2 candidate planetary systems orbiting low-mass stars. I. Classifying low-mass host stars observed during campaigns 1–7. *Astrophys. J.* 836:167. doi: 10.3847/1538-4357/836/2/167

Dressing, C. D., Vanderburg, A., Schlieder, J. E., Crossfield, I. J. M., Knutson, H. A., Newton, E. R., et al. (2017b). Characterizing K2 candidate planetary systems orbiting low-mass stars. II. Planetary systems observed during campaigns 1–7. *Astron. J.* 154:207. doi: 10.3847/1538-3881/aa89f2

Feinstein, A. D., Schlieder, J. E., Livingston, J. H., Ciardi, D. R., Howard, A. W., Arnold, L., et al. (2019). K2–288Bb: a small temperate planet in a low-mass binary system discovered by citizen scientists. *Astron. J.* 157:40. doi: 10.3847/1538-3881/aafa70

Fulton, B. J., Petigura, E. A., Howard, A. W., Isaacson, H., Marcy, G. W., Cargile, P. A., et al. (2017). The California-Kepler survey. III. A gap in the radius distribution of small planets. *Astron. J.* 154:109. doi: 10.3847/1538-3881/aa80eb

Furlan, E., Ciardi, D. R., Everett, M. E., Saylors, M., Teske, J. K., Horch, E. P., et al. (2017). The Kepler follow-up observation program. I. A catalog of companions to Kepler stars from high-resolution imaging. *Astron. J.* 153:71. doi: 10.3847/1538-3881/153/2/71

Giacalone, S., and Dressing, C. D. (2020). `triceratops`: A tool for rapid validation of *TESS* objects of interest and application to 424 planet candidates. *arXiv* 2002.00691.

Guerrero, N., and TESS Science Office (2021). "TESS objects of interest catalog in the TESS prime mission and beyond," in *American Astronomical Society Meeting Abstracts, Volume 53 of American Astronomical Society Meeting Abstracts*, 117.01.

Hardegree-Ullman, K. K., Zink, J. K., Christiansen, J. L., Dressing, C. D., Ciardi, D. R., and Schlieder, J. E. (2020). Scaling K2. I. Revised parameters for 222,088 K2 stars and a K2 planet radius valley at 1.9 $R_{\oplus}$. *Astrophys. J. Suppl.* 247:28. doi: 10.3847/1538-4365/ab7230

Howell, S. B., Sobeck, C., Haas, M., Still, M., Barclay, T., Mullally, F., et al. (2014). The K2 mission: characterization and early results. *Publ. ASP* 126:398. doi: 10.1086/676406

Jenkins, J. M., Twicken, J. D., McCauliff, S., Campbell, J., Sanderfer, D., Lung, D., et al. (2016). *The TESS Science Processing Operations Center, Volume 9913 of Society of Photo-Optical Instrumentation Engineers (SPIE) Conference Series*, 99133E. doi: 10.1117/12.2233418

Kemmer, J., Stock, S., Kossakowski, D., Kaminski, A., Molaverdikhani, K., Schlecker, M., et al. (2020). Discovery of a hot, transiting, earth-sized planet and a second temperate, non-transiting planet around the M4 dwarf GJ 3473 (TOI-488). *arXiv* 2009.10432. doi: 10.1051/0004-6361/202038967

Kostov, V. B., Schlieder, J. E., Barclay, T., Quintana, E. V., Colón, K. D., Brand e, J., et al. (2019). The L 98–59 system: three transiting, terrestrial-size planets orbiting a nearby M dwarf. *Astron. J.* 158:32. doi: 10.3847/1538-3881/ab2459

Kraus, A. L., Ireland, M. J., Huber, D., Mann, A. W., and Dupuy, T. J. (2016). The impact of stellar multiplicity on planetary systems. I. The ruinous influence of close binary companions. *Astron. J.* 152:8. doi: 10.3847/0004-6256/152/1/8

Kruse, E., Agol, E., Luger, R., and Foreman-Mackey, D. (2019). Detection of hundreds of new planet candidates and eclipsing binaries in K2 campaigns 0–8. *Astrophys. J. Suppl.* 244:11. doi: 10.3847/1538-4365/ab346b

Lissauer, J. J., Fabrycky, D. C., Ford, E. B., Borucki, W. J., Fressin, F., Marcy, G. W., et al. (2011). A closely packed system of low-mass, low-density planets transiting Kepler-11. *Nature* 470, 53–58. doi: 10.1038/nature09760

Livingston, J. H., Crossfield, I. J. M., Petigura, E. A., Gonzales, E. J., Ciardi, D. R., Beichman, C. A., et al. (2018). Sixty validated planets from K2 campaigns 5–8. *Astron. J.* 156:277. doi: 10.3847/1538-3881/aae778

Luger, R., Agol, E., Kruse, E., Barnes, R., Becker, A., Foreman-Mackey, D., et al. (2016). EVEREST: pixel level decorrelation of K2 light curves. *Astron. J.* 152:100. doi: 10.3847/0004-6256/152/4/100

Matson, R. A., Howell, S. B., Horch, E. P., and Everett, M. E. (2018). Stellar companions of exoplanet host stars in K2. *Astron. J.* 156:31. doi: 10.3847/1538-3881/aac778

Mayo, A. W., Vanderburg, A., Latham, D. W., Bieryla, A., Morton, T. D., Buchhave, L. A., et al. (2018). 275 Candidates and 149 validated planets orbiting bright stars in K2 campaigns 0–10. *Astron. J.* 155:136. doi: 10.3847/1538-3881/aaadff

Montet, B. T., Morton, T. D., Foreman-Mackey, D., Johnson, J. A., Hogg, D. W., Bowler, B. P., et al. (2015). Stellar and planetary properties of K2 campaign 1 candidates and validation of 17 planets, including a planet receiving earth-like insolation. *Astrophys. J.* 809:25. doi: 10.1088/0004-637X/809/1/25

Morton, T. D. (2012). An efficient automated validation procedure for exoplanet transit candidates. *Astrophys. J.* 761:6. doi: 10.1088/0004-637X/761/1/6

Morton, T. D. (2015). *VESPA: False Positive Probabilities Calculator*. Astrophysics Source Code Library, record ascl:1503.011.

Petigura, E. A., Crossfield, I. J. M., Isaacson, H., Beichman, C. A., Christiansen, J. L., Dressing, C. D., et al. (2018). Planet candidates from K2 campaigns 5–8 and follow-up optical spectroscopy. *Astron. J.* 155:21. doi: 10.3847/1538-3881/aa9b83

Petigura, E. A., Marcy, G. W., and Howard, A. W. (2013). A plateau in the planet population below twice the size of earth. *Astrophys. J.* 770:69. doi: 10.1088/0004-637X/770/1/69

Pope, B. J. S., Parviainen, H., and Aigrain, S. (2016). Transiting exoplanet candidates from K2 campaigns 5 and 6. *Mon. Not. RAS* 461, 3399–3409. doi: 10.1093/mnras/stw1373

Quintana, E. V., Barclay, T., Raymond, S. N., Rowe, J. F., Bolmont, E., Caldwell, D. A., et al. (2014). An earth-sized planet in the habitable zone of a cool star. *Science* 344, 277–280. doi: 10.1126/science.1249403

Ricker, G. R., Winn, J. N., Vanderspek, R., Latham, D. W., Bakos, G. Á., Bean, J. L., et al. (2015). Transiting exoplanet survey satellite (TESS). *J. Astron. Telesc. Instr. Syst.* 1:014003. doi: 10.1117/1.JATIS.1.1.014003

Rodriguez, J. E., Becker, J. C., Eastman, J. D., Hadden, S., Vanderburg, A., Khain, T., et al. (2018). A compact multi-planet system with a significantly misaligned ultra short period planet. *Astron. J.* 156:245. doi: 10.3847/1538-3881/aae530

Šubjak, J., Sharma, R., Carmichael, T. W., Johnson, M. C., Gonzales, E. J., Matthews, E., et al. (2020). TOI-503: the first known brown-dwarf Am-star binary from the TESS mission. *Astron. J.* 159:151. doi: 10.3847/1538-3881/ab7245

Thompson, S. E., Coughlin, J. L., Hoffman, K., Mullally, F., Christiansen, J. L., Burke, C. J., et al. (2018). Planetary candidates observed by Kepler. VIII. A fully automated catalog with measured completeness and reliability based on data release 25. *Astrophys. J. Suppl.* 235:38. doi: 10.3847/1538-4365/aab4f9

Torres, G., Fressin, F., Batalha, N. M., Borucki, W. J., Brown, T. M., Bryson, S. T., et al. (2011). Modeling Kepler transit light curves as false positives: rejection of blend scenarios for Kepler-9, and validation of Kepler-9 d, a super-earth-size planet in a multiple system. *Astrophys. J.* 727:24. doi: 10.1088/0004-637X/727/1/24

Vanderburg, A., and Johnson, J. A. (2014). A technique for extracting highly precise photometry for the two-wheeled Kepler mission. *Publ. ASP* 126:948. doi: 10.1086/678764

Vanderburg, A., Latham, D. W., Buchhave, L. A., Bieryla, A., Berlind, P., Calkins, M. L., et al. (2016). Planetary candidates from the first year of the K2 mission. *Astrophys. J. Suppl.* 222:14. doi: 10.3847/0067-0049/222/1/14

Wizinowich, P., Acton, D. S., Shelton, C., Stomski, P., Gathright, J., Ho, K., et al. (2000). First light adaptive optics images from the Keck II telescope: a new era of high angular resolution imagery. *Publ. ASP* 112, 315–319. doi: 10.1086/316543

Yu, L., Crossfield, I. J. M., Schlieder, J. E., Kosiarek, M. R., Feinstein, A. D., Livingston, J. H., et al. (2018). Planetary candidates from K2 campaign 16. *Astron. J.* 156:22. doi: 10.3847/1538-3881/aac6e6

Ziegler, C., Law, N. M., Baranec, C., Howard, W., Morton, T., Riddle, R., et al. (2018). Robo-AO Kepler survey. V. The effect of physically associated stellar companions on planetary systems. *Astron. J.* 156:83. doi: 10.3847/1538-3881/aace59

Ziegler, C., Tokovinin, A., Briceño, C., Mang, J., Law, N., and Mann, A. W. (2020). SOAR TESS survey. I. Sculpting of TESS planetary systems by stellar companions. *Astron. J.* 159:19. doi: 10.3847/1538-3881/ab55e9

Zink, J. K., Hardegree-Ullman, K. K., Christiansen, J. L., Petigura, E. A., Dressing, C. D., Schlieder, J. E., et al. (2020). Scaling K2. III. Comparable planet occurrence in the FGK samples of campaign 5 and Kepler. *Astron. J.* 160:94. doi: 10.3847/1538-3881/aba123

Conflict of Interest: The authors declare that the research was conducted in the absence of any commercial or financial relationships that could be construed as a potential conflict of interest.

Advantages of publishing in Frontiers

OPEN ACCESS
Articles are free to read for greatest visibility and readership

FAST PUBLICATION
Around 90 days from submission to decision

HIGH QUALITY PEER-REVIEW
Rigorous, collaborative, and constructive peer-review

TRANSPARENT PEER-REVIEW
Editors and reviewers acknowledged by name on published articles

Frontiers
Avenue du Tribunal-Fédéral 34
1005 Lausanne | Switzerland

Visit us: www.frontiersin.org
Contact us: frontiersin.org/about/contact

REPRODUCIBILITY OF RESEARCH
Support open data and methods to enhance research reproducibility

DIGITAL PUBLISHING
Articles designed for optimal readership across devices

FOLLOW US
@frontiersin

IMPACT METRICS
Advanced article metrics track visibility across digital media

EXTENSIVE PROMOTION
Marketing and promotion of impactful research

LOOP RESEARCH NETWORK
Our network increases your article's readership